BioMed Research International

Nanobiotechnology

Guest Editors: Susana N. Diniz, Alejandro Sosnik, Huiling Mu, and Claudete J. Valduga

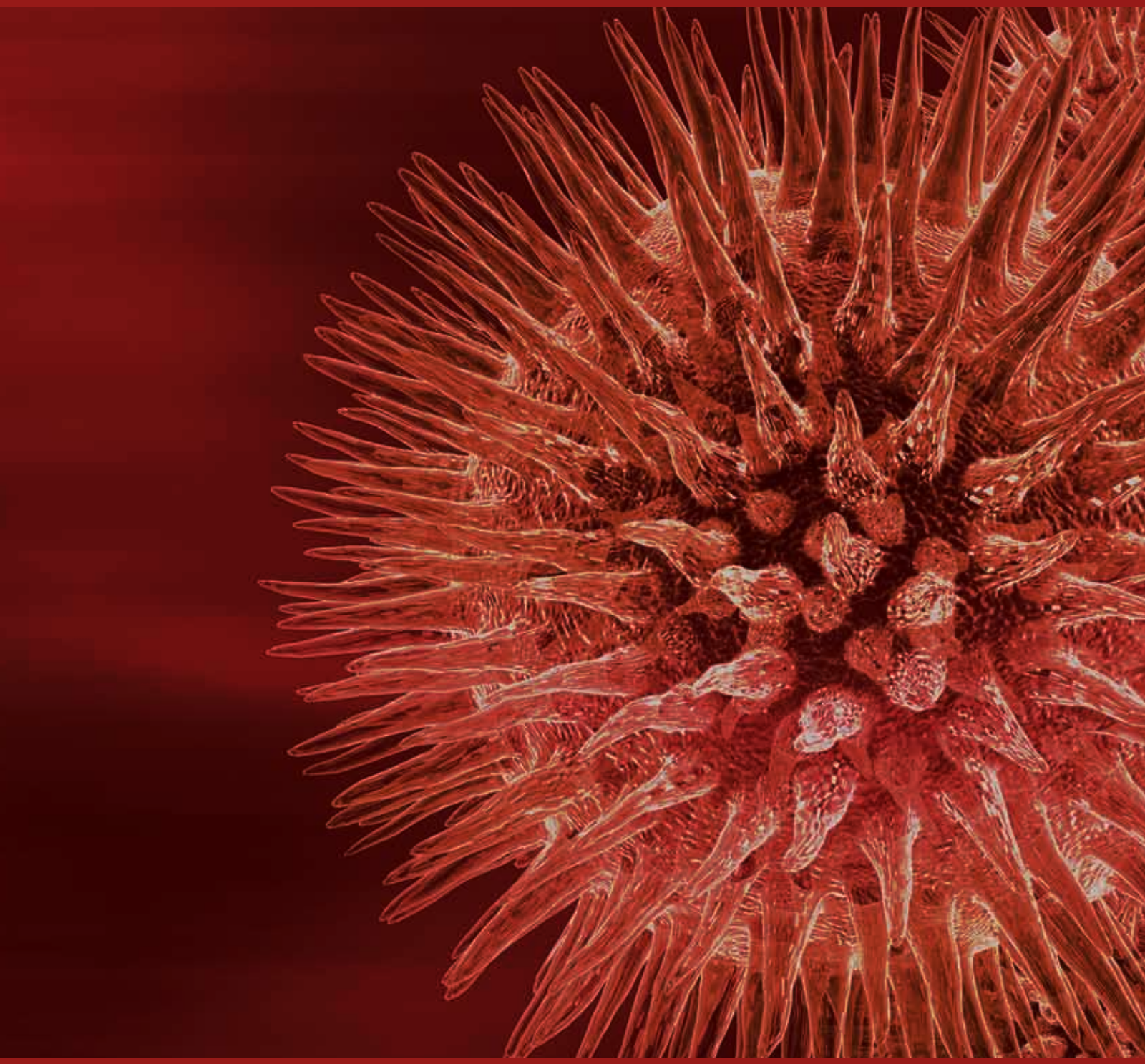

Nanobiotechnology

BioMed Research International

Nanobiotechnology

Guest Editors: Susana N. Diniz, Alejandro Sosnik, Huiling Mu, and Claudete J. Valduga

Contents

Hindawi Publishing Corporation
BioMed Research International
Volume 2013, Article ID 319832, 1 page
http://dx.doi.org/10.1155/2013/319832

Editorial
Nanobiotechnology

Susana N. Diniz,[1] Alejandro Sosnik,[2] Huiling Mu,[3] and Claudete J. Valduga[1]

[1] *Bandeirante Anhanguera University, 02071-013 Sao Paulo, SP, Brazil*
[2] *University of Buenos Aires, 1113 Buenos Aires, Argentina*
[3] *University of Copenhagen, 2100 Copenhagen, Denmark*

Correspondence should be addressed to Claudete J. Valduga; cvalduga@usp.br

Received 25 July 2013; Accepted 25 July 2013

Nanobiotechnology refers to methods and techniques inspired by biology to develop products at the nanometer scale. This modern concept describes the way nanotechnology is used to create devices in order to study biological systems. It is based on the overlapping of multidisciplinary sciences converging to create novel nanostructures that are similar to nature to sense and deliver biomacromolecules. This special issue is compiled with seven articles that explore new approaches on the development of products to address medical/biological problems for diagnosing and treating diseases. Two of them are reviews about the application of nanoparticles in drug delivery and diagnosis.

Biocompatible and biodegradable materials have great potential in nanobiotechnology. The review by A. Shrivastav et al. focuses on nanoparticles based on natural occurring polymeric material, polyhydroxyalkanoates, and their applications in drug delivery.

Diagnosis and treatment of some kinds of cancers can be difficult such as gliomas, which show high resistance to chemotherapy and radiotherapy. The potential of nanobiotechnology for drug delivery, imaging, diagnosis, and therapy was addressed in the review by N. Y. Hernández-Pedro et al.

The development of nanoscale tools for understanding the mechanisms of cellular functions and monitoring the behavior of biomolecules, cell surface interactions, as well as new approaches in drug and gene delivery was the focus of five articles.

The penetration of antineoplastic drugs into solid tumors is a hurdle that can be bypassed by the use of nanodevices, as showed by Y. Liu et al., in which a crosslinked multilamellar liposomal vesicle formulation with a tumor-penetrating peptide, iRGD, is able to improve the delivery of doxorubicin to breast tumor cells *in vitro* and *in vivo*.

D. Shahbazi-Gahrouei et al. illustrate the potential of magnetic nanoparticles for detection and quantification of cell surface antigens in prostate cancer cells. The transfection of RNA by L. Russoa et al., antisense oligonucleotide by J. Xie et al., and plasmid DNA by L. Prossen et al. show the potential of nanobiotechnology for gene therapy and control of antiproliferative diseases.

We are certain that the articles published in this special issue will contribute to the development and application of nanobiotechnology especially as a biological tool for diagnostics and the treatment of diseases.

Susana N. Diniz
Alejandro Sosnik
Huiling Mu
Claudete J. Valduga

Hindawi Publishing Corporation
BioMed Research International
Volume 2013, Article ID 581684, 12 pages
http://dx.doi.org/10.1155/2013/581684

Review Article

Advances in the Applications of Polyhydroxyalkanoate Nanoparticles for Novel Drug Delivery System

Anupama Shrivastav, Hae-Yeong Kim, and Young-Rok Kim

Institute of Life Sciences and Resources & Department of Food Science and Biotechnology, College of Life Sciences, Kyung Hee University, Yongin 446-701, Republic of Korea

Correspondence should be addressed to Young-Rok Kim; youngkim@khu.ac.kr

Received 5 January 2013; Accepted 9 June 2013

Academic Editor: Claudete J. Valduga

Drug delivery technology is emerging as an interdisciplinary science aimed at improving human health. The controlled delivery of pharmacologically active agents to the specific site of action at the therapeutically optimal rate and dose regimen has been a major goal in designing drug delivery systems. Over the past few decades, there has been considerable interest in developing biodegradable drug carriers as effective drug delivery systems. Polymeric materials from natural sources play an important role in controlled release of drug at a particular site. Polyhydroxyalkanoates, due to their origin from natural sources, are given attention as candidates for drug delivery materials. Biodegradable and biocompatible polyhydroxyalkanoates are linear polyesters produced by microorganisms under unbalanced growth conditions, which have emerged as potential polymers for use as biomedical materials for drug delivery due to their unique physiochemical and mechanical properties. This review summarizes many of the key findings in the applications of polyhydroxyalkanoates and polyhydroxyalkanoate nanoparticles for drug delivery system.

1. Introduction

Drug deliveries have become important tools in the medical field and have been extensively investigated because of the strong demand for the controlled delivery of pharmacologically active materials to cells, tissue, and organs. Many drug-delivery methods have been developed using polymers as drug carriers as they can effectively deliver the drug to a target site and thus increase the therapeutic benefit, while minimizing side effects. Because of the flexibility of polymers, it becomes possible to engineer multiple functionalities required for efficient drug delivery, simultaneously maintaining biocompatibility, facile manufacturing, and stable formulation. It is important that the biomaterial should complete the requirement of physical properties, but it is also essential to accomplish its biocompatibility test. Some of the traditionally used polymers like silicone have been suspected to cause cancer [1]. Therefore, there is a need for nontoxic, biodegradable, and biocompatible polymers.

One of the alternatives to conventional polymers is biodegradable plastic or biopolymer. Among the various biodegradable polymers available, there is growing interest in the group of biopolymers known as polyhydroxyalkanoates (PHAs) which are the polyesters of various hydroxyalkanoate monomers accumulating as energy/carbon storage materials by granular inclusions in the cytoplasm of various bacterial cells, usually under unbalanced growth conditions. General structure of PHA is shown in Figure 1. There are approximately 150 different types of hydroxyalkanoic acids at present known as the constituents of these bacterial storage polyesters.

Bacterial PHAs could be bifurcated into two groups depending on the number of carbon atoms in the monomeric units: short-chain-length (SCL) PHAs, which consist of 3–5 carbon atoms, and medium-chain-length (MCL) PHAs, which consist of 6–14 carbon atoms [2]. PHAs are hydrophobic and crystalline in nature. Biologically produced PHAs are composed only of chirally pure (R)-configuration monomers.

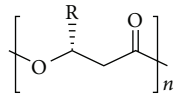

Poly(3-hydroxyalkanoates) [PHA]

R group		
$-CH_3$	Poly(3-hydroxyalkanoates)	PHA
$-CH_2\text{-}CH_3$	Poly(3-hydroxyvalerate)	PHV
$-(CH_2)_2-CH_3$	Poly(3-hydroxyhexanoate)	PHHex
$-(CH_2)_4-CH_3$	Poly(3-hydroxyoctanoate)	PHO
$-(CH_2)_6-CH_3$	Poly(3-hydroxydecanoate)	PHD
$-CH_2-$ 	Poly(3-hydroxy-5-phenylvalerate)	PHPV

Figure 1: General structure of polyhydroxyalkanoates (PHAs) and examples of their structural derivatives.

Beijerinck first observed PHAs as refractile bodies inside bacterial cells in 1888. However, the PHA composition was established by Lemoigne in 1926. Bacterial polyhydroxyalkanoates (PHAs) have attracted much attention as environmentally degradable thermoplastics [3, 4]. They are being viewed as potentially useful for replacing many synthetic polymers in a wide range of agriculture, marine, and medical applications.

The PHA polymers are stored in the bacterial cells as defined granules. These granular particles consist of polyester, proteins, and lipids. The composition was for the first time investigated by Griebel in 1968 for PHB granules of *Bacillus megaterium*, which consist of 97.7% of polyester, 1.87% of proteins, and 0.46% of lipids or phospholipids [5].

Particular attention has been focused on the use of poly(3-hydroxybutyrate) (PHB) and related copolymers, mostly poly(3-hydroxybutyrate-*co*-3-hydroxyvalerate) (PHBV), as carriers for drug delivery or scaffolds in tissue engineering. PHB and PHBV have many advantages when compared to other chemically produced polymers like polyglycolate, polylactate, and poly(lactide-co-glycolide) which include excellent biocompatibility, biodegradability, easier processibility, and the controllable retarding properties which can be modulated by variations in processing and molecular weight of the polymer composition. PHB in combination with other biocompatible and nontoxic polymers would also have an enhanced scope in biomedical applications [6]. The main advantage of using PHA in the medical field is that it is biodegradable and can be inserted into the human body, and it does not have to be removed again. Another distinguished characteristic of PHA is that it is biocompatible, generating a mild foreign-body response to any implant.

PHAs have been in the attention of many companies as biodegradable and biocompatible alternatives to synthetic polymers for a very long time. In 1976, Imperial Chemical Industries (ICI Ltd., UK) recognized the potential applicability of PHB to replace some of the oil-derived synthetic polymers. One of the contributions of PHA to medicine has been in the cardiovascular area. Tepha Inc., based in Cambridge, MA, has been devoted to manufacturing pericardial patches, artery augments, cardiological stents, vascular grafts, heart valves, implants, tablets, sutures, dressings, dusting powders, prodrugs, and microparticulate carriers using PHA. The first PHA-based product approved by FDA for clinical application is the TephaFLEX absorbable suture prepared from P4HB (http://www.tepha.com/). In 2007, the FDA had cleared its marketing in the USA, indicating a bright future for a practical application of PHAs in biomedical areas [7].

2. PHA Biosynthesis

PHAs are synthesized by varieties of Gram-positive and Gram-negative bacteria, and more than 300 different microorganisms are known to synthesize and accumulate PHAs intracellularly including *Azotobacter* sp., *Pseudomonas* sp., *Bacillus* sp., and *Methylobacterium* sp. [8]. These types of microbes are carrying metabolic ability to biosynthesize PHAs molecules and accumulate them in their cytoplasm as carbon and energy sources in the shape of granules under nutrient-limiting conditions with excess carbon [9, 10].

The comprehensive investigation was done for metabolic biosynthetic pathways for PHA synthesis in *Cupriavidus necator* (formerly known as *Ralstonia eutropha*). This pathway is common in a wide range of bacteria. A β-ketothiolase catalyzes the formation of a carbon-carbon bond of two acetyl-CoA moieties. NADPH-dependent acetoacetyl-CoA reductase catalyzes the reduction of acetoacetyl-CoA formed in the first reaction to 3-hydroxybutyryl-CoA (Figure 2) [11]. PHB is synthesized by polymerization of (R)-3-hydroxybutyryl-CoA molecules by the PHB synthase leading to the formation of PHB granules (Figure 3). Two moles of acetyl-CoA are used to form an HB unit of the polymer, while an HV unit is formed by the reaction of acetyl CoA and propionyl-CoA [12].

PHA synthesis is also affected by the ratio of NADH to NAD^+. CoA level in the cells is high during cell growth due to the rapid flux of acetyl-CoA into the tricarboxylic acid (TCA) cycle. When a nutrient, such as the nitrogen source, is exhausted, there is increase in the NADH/NAD^+ ratio which inhibits the enzymes of the TCA cycle. As the flux of acetyl-CoA decreases, CoA levels decrease, removing the inhibition of β-ketothiolase. Acetyl-CoA or propionyl-CoA may enter the PHA biosynthetic pathway to produce 3HB or 3HV monomers [13, 14].

Cupriavidus necator has been the most commonly used strain for the industrial production of poly-(R)-3-hydroxybutyrate (PHB), poly((R)-3-hydroxybutyrate-*co*-4-hydroxybutyrate) (P3HB4HB), and poly((R)-3-hydroxybutyrate-*co*-(R)-3-hydroxyvalerate) (PHBV). Other bacteria including *Alcaligenes latus, Aeromonas hydrophila, Pseudomonas oleovorans, Pseudomonas putida,* and recombinant *Escherichia coli* are also used for PHV and PHBV production.

PHAs can be produced from recombinant *E. coli* by heterologously expressing the required PHB biosynthesis genes while providing appropriate cultivation conditions. PHA production in plants has also been taken into consideration. Recently, native PHA granules and *in vitro* synthesized PHA granules have been increasingly considered for applications

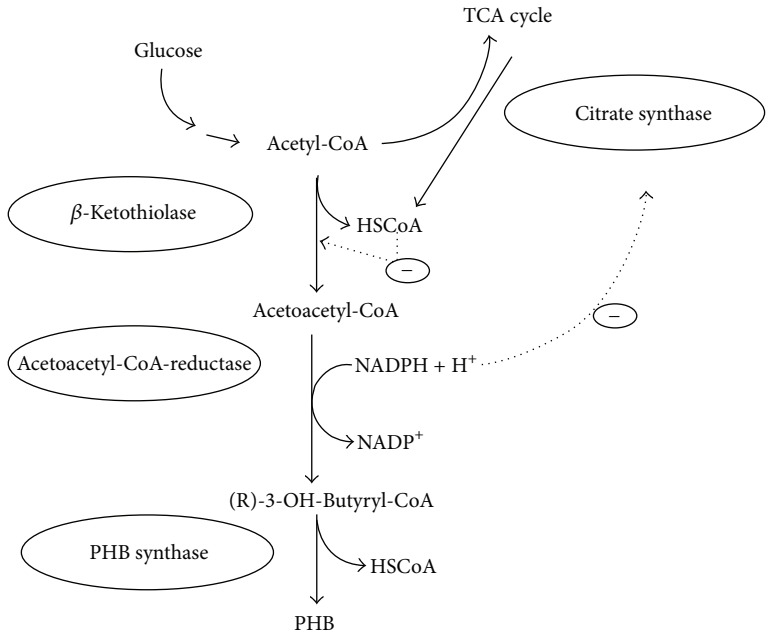

Figure 2: PHB synthesis pathway of *R. eutropha* and regulatory circuits. In the three-step PHB synthesis pathway, two acetyl-CoA molecules are coupled to form acetoacetyl-CoA in a condensation reaction catalysed by β-ketothiolase. The β-ketothiolase is negatively regulated by the product coenzyme A (HSCoA), which is also a product when acetyl-CoA enters the TCA cycle under nonlimited conditions. The product is subsequently and stereoselectively reduced to (R)-3-hydroxybutyryl-CoA in a reaction catalysed by NADPH-dependent acetoacetyl-CoA reductase. High concentration of NADPH and NADH inhibits the citrate synthase of the TCA cycle, which ensures the availability of acetyl-CoA for the β-ketothiolase. Finally, PHB is synthesized by polymerization of (R)-3-hydroxybutyryl-CoA molecules by the PHB synthase. Hatched arrows indicate negative regulatory effects. Reprinted with permission from Kessler and Witholt [11], Copyright (2001), Elsevier.

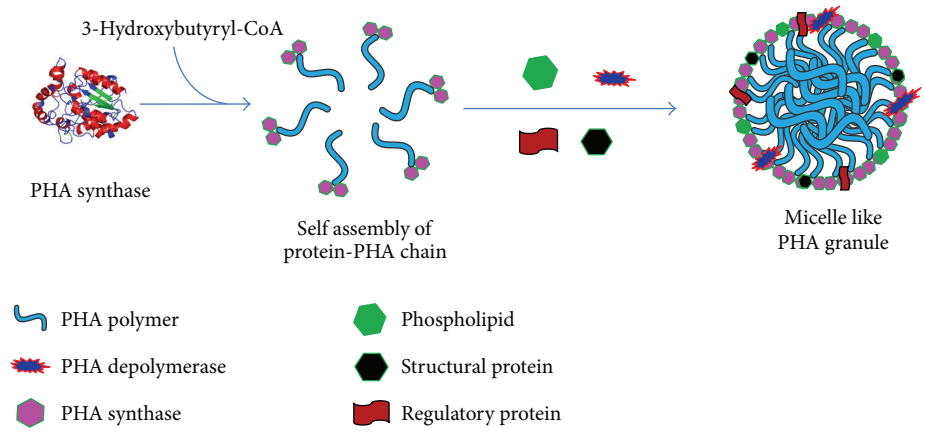

Figure 3: Schematic presentation of PHB granule formation within the cytoplasm of PHB producing microorganism. PHB is synthesized by polymerization of (R)-3-hydroxybutyryl-CoA molecules by PHB synthase leading to the formation of PHB granules. PHB inclusions consist of a hydrophobic core of amorphous PHB surrounded by phospholipid and various proteins.

as functionalized micro- or nanoparticles in biotechnology and biomedicine.

3. Biodegradability of PHA

One of the unique properties of biological PHA materials is their biodegradability in various environments. PHAs are of biological origin; they could be completely broken down in to water and carbon dioxide by microorganisms found in a wide range of environments, such as soil, water, and sewage [16]. A number of microorganisms such as bacteria and fungi in soil, sludge, and sea water excrete extracellular PHA degrading enzymes to hydrolyze solid PHA into water soluble oligomers and monomers and subsequently utilize the resulting products as nutrients within cells. The hydrolytic and enzymatic degradation processes of P(3HB-*co*-4HB) films were studied by monitoring the time-dependent changes in molecular weights and weight loss. P(3HB-co-4HB) films were shown

to be hydrolyzed by both PHA depolymerase and lipase [17–19].

Pişkin reported that the deprivation of PHB *in vivo* is faster than *in vitro* hydrolysis at body temperature, indicating that enzymes existing *in vivo* catalyze the degradation [20]. *In vivo* degradation of P(3HB-*co*-4HB) films in rats was studied wherein P(3HB-*co*-4HB) films were implanted into the intraperitoneal area of rat, and changes in molecular weights were monitored over a period of 4 months. A 20% decrease in the value of Mn was observed with no notable signs of cytotoxicity in the implantation area [19]. PHA implants and other medical devices are degraded at the site of implantation in animals. PHA polymers are degraded by the action of nonspecific lipases and esterases in nature [21]. Löbler et al. detected lipase activities in the rat gastrointestine near the PHA implant, suggesting the involvement of lipases in the metabolism of PHA *in vivo* [22].

Degradation of PHA matrices in the tissues of the host organism offers the possibility of coupling this phenomenon with release of bioactive compounds, such as antibiotic or antitumor drug. If a PHA insert is impregnated with a compound, the degradation over time will release the compound, acting as an automatic dosing agent. The kinetics of dosing of a compound from a PHA matrix can be tuned by altering the polymer properties, along with the use of different types of PHA with different monomer side chains.

4. Biocompatibility of PHA

The suitability of PHA for inclusion in drug delivery or other biomedical applications will depend not only on the biodegradation properties but also on their biocompatibility. For use in medical applications, materials must be biocompatible, which means that they should not cause severe immune reactions when introduced to soft tissues or blood of a host organism during degradation in the body to be considered biocompatible.

PHAs not only appear in microorganisms as storage materials but are also ubiquitous in other natural plants as well as animals, and their metabolism and excretion are both well understood. The monomeric component of P(3HB) and R-3-hydroxybutanoic acid is a product of cell metabolism, produced during fatty acid oxidation in the liver. This hydroxyl acid is a ketone body that is biosynthesized in mitochondria of the liver and is used by the brain as a fuel source. 3-Hydroxybutyric acid is a normal constituent of human blood in concentrations between 0.3 and 1.3 mM [23]. An attractive progress has been made after the finding of the very widespread dispersal of PHB as a low molecular weight oligomer (120–200 monomers) in microorganisms, plants, and animals, including humans. In many cases, this form of PHB is found as a PHB calcium polyphosphate complex in membranes that seems to function as an ion channel through cell membranes [24].

Various medical applications of PHA have been explored extensively in recent years. PHAs have been used to develop devices including nerve repair devices, repair patches, cardiovascular patches, orthopaedic pins, adhesion barriers, guided tissue repair/regeneration devices, nerve guides, tendon repair devices, bone-marrow scaffolds, tissue engineered cardiovascular devices, and wound dressings [25–27]. So far, various tests on animal models have shown polymers, from the PHA family, to be compatible with a range of tissues. Surface properties of PHA films have been shown to be favourable for proliferation and attachment of tissue cells [28, 29], suggesting that PHA is suitable for scaffolding materials in tissue engineering. NIH 3T3 fibroblast cells have been shown to adhere and proliferate on PHA membranes [30]. Also, mesenchymal stem cells were also shown to adhere and proliferate on several PHA substrates, with a terpolymer poly(hydroxybutyrate-*co*-hydroxyvalerate-*co*-hydroxyhexanoate) (P(HB-*co*-HV-*co*-HHx)) [31, 32].

PHA matrices have also been tested for hemocompatibility by inspecting the response of mammalian blood when incubated with polymer films. It was shown that PHB or P (HB-*co*-HV), when in contact with blood, did not affect platelet responses, nor did the polymer activate the complement system. However, the polymer purification procedures had to be followed to significantly reduce the amount of bacterial cell wall material associated with the purified PHA [33, 34].

In evaluating P(3HB) as a potential drug delivery matrix, Korsatko et al. reported no significant differences in cellular growth with mice fibroblasts. Small, low molecular weight, crystalline particles of P(3HB) which represent one of the degradation products are expected to rise *in vivo* from the absorption of P(3HB) [35]. At low concentration, these small P(3HB) particles were found to be well tolerated by macrophages, fibroblasts, Kupffer cells, and hepatocytes. Macrophages, Kupffer cells, and to a lesser extent fibroblasts and osteoblasts were found to phagocytise the small particles of P(3HB) (1–20 μm), and the evidence of biodegradation by macrophages was also found [36].

In vivo and *in vitro* biocompatibility of PHB and P(HBV) copolymers has been studied in which the effects of P(HB-*co*-HV) polymers on the growth of CHO (Chinese hamster ovary) cells in culture were monitored over a 60-hour period. The polymers, used as solvent cast films, did not inhibit growth of cells during this period, thereby suggesting good biocompatibility [37]. Juni and Nakano studied the *in vivo* biocompatibility of PHB by injecting microspheres (100 μm) into the rat thigh muscle [38]. Transient acute inflammation was observed which was terminated 7 days after injection. The microspheres were further reported as being encapsulated by connective tissue during a 4-week postinjection study period.

Despite the initial acute inflammation observed in various *in vivo* studies with P(HB-HV) which is probably in response to the trauma of implantation or injection, P(HB-HV) polymers generally showed good *in vitro* and *in vivo* biocompatibility [39].

5. Polyhydroxyalkanoates in Drug Delivery

Polyhydroxyalkanoates are generally biodegradable and thermoprocessable, making them attractive as biomaterials for

applications in conventional medical devices, drug delivery, and tissue engineering. Biodegradable polymers containing an entrapped drug can be placed in the body, and they are used for localized drug delivery accompanied with the controlled release of a drug over a period of months [40]. Degradation of PHA polymers in the tissues of the host organism offers the possibility of coupling this phenomenon with the release of bioactive compounds, such as antibiotic or antitumor drug.

5.1. PHA Particles as Drug Carriers. PHAs are biocompatible and hydrophobic; they can also be turned into films, porous matrices, microcapsules, microspheres, and nanoparticles. Drugs can be entrapped or microencapsulated in a PHA homopolymer or copolymer. Microsphere- or microcapsule-based delivery systems have been extensively used for the delivery of a number of drugs such as anesthetics, antibiotics, anti-inflammatory agents, anticancer agents, hormones, steroids, and vaccines [41, 42].

Use of PHA microspheres as carriers for steroids was reported by Gangrade and Price [43]. PHB and P(3HB-3HV) were used to prepare microspheres containing progesterone as a model drug. The incorporation of progesterone into the microspheres was very efficient, and over 80% of the theoretical content was incorporated. The *in vitro* release was the slowest from a microsphere prepared from a copolymer containing 9% HV, which was less porous than the microspheres prepared from other polymers.

In the early 1990s, PHAs became candidates for use as drug carriers due to their biodegradability, biocompatibility, and their degradation by surface erosion. The potential use of P(3HB) and P(3HB-*co*-3HV) in drug delivery has been evaluated in a number of studies. PHA may be a potential candidate in treating highly resistant infections, as PHA drug delivery systems showed the ability for provision and maintenance of adequate concentrations of antibiotics at infection sites [44, 45]. PHB, PHBV, and P(3HB-4HB) were shown to be useful in the construction of biodegradable, implantable rods for the local delivery of antibiotics in chronic osteomyelitis therapy [46–48]. When comparing the *in vitro* and *in vivo* releases of the anticancer agent lomustine from PHB and PLA microspheres as potential carriers for drug targeting, it was found that the drug was released faster from the PHB microspheres [49]. Incorporation of ethyl or butyl esters of fatty acids into the PHB microspheres increased the rate of the drug release [50].

Sendil et al. used polyhydroxybutyrate-*co*-hydroxyvalerates (PHBV) of various 3-hydroxyvalerate contents containing antibiotic tetracycline which is known to be effective against many of the periodontal disease-related microorganisms, for the construction of a controlled release system [51]. Tetracycline was loaded in the PHBV microspheres and microcapsules both in its acidic from (TC) and in neutral form (TCN) followed by the analysis of the properties by *in vitro* release studies of the resultant systems. It was observed that release was complete before any signs of degradation were observed.

A study using PHB microspheres demonstrated that release of the antitumor drug rubomycin inhibited proliferative activity of Ehrlich's carcinoma in mice [52]. P(3HB) nanoparticles containing prednisolone were prepared using high-pressure homogenization by Koosha et al. [53]. Biphasic release pattern was observed up to 50% of drug loading, with an initial burst effect followed by slow release of drug, and the completion was achieved in 1 to 2 days. Kawaguchi et al. reported the preparation of microspheres of PHB containing the antitumor drug 2′,3′-diacyl-5-fluoro-2′-deoxyuridine [54]. The PHB sphere showed low toxicity and good compatibility in mice and rats. Recently, the application of PHA as a drug delivery carrier in anticancer study was reported by Lu et al. [55]. A sustained release system of P13 K inhibitor (TGX221) based on PHA nanoparticle was developed and used to block the proliferation of cancer cell lines. TGX221 was gradually released from PHA-based nanoparticles, and the growth of cancer cell lines was significantly slower in cells treated with TGX221 nanoparticles.

Recently, Shah et al. determined the efficacy and bioavailability of cisplatin, a chemotherapeutic agent used against a variety of tumors, in the form of cisplatin-loaded self-assembled amphiphilic copolymer nanoparticles [15]. Novel amorphous amphiphilic block copolymer P(3HV-*co*-4HB)-*b*-mPEG was synthesized from bacterial copolyester poly(3-hydroxyvalerate-*co*-4-hydroxybutyrate) coupled via transesterification reaction using bis(2-ethyl hexanoate) tin catalyst to monomethoxypoly(ethylene glycol). The *in vitro* release profile of cisplatin from the core hydrophobic domain showed a sustained release of the drug. TEM and confocal microscopy examination revealed clearly the internalization of cisplatin-loaded NPs into the tumor cells (Figure 4) and also revealed a suppression effect by the NPs on tumor cell growth, and they also revealed enhancement of apoptotic process of the tumor cells.

5.2. Surface Functionalization of PHA Nanoparticles through Engineered PHA Synthase. In 2005, Peters and Rehm demonstrated that PHA granule formation was not affected by the fusion of GFP with the N-terminus of the PHA synthase [56]. Further studies were carried out to engineer the PHA synthase as a conjugated form with the enzyme β-galactosidase [57]. Conjugated β-galactosidase was stable for several months under various storage conditions. This work showed that protein engineering of the PHA synthase to produce functionalized PHA granules could be a useful tool for developing biological particles for various applications. PHA granules were used as biological template structures for molecular biomimetics by Jahns et al. [58]. The PHA synthase was fused to genetically engineered proteins for inorganic surface (GEPIs) and additionally to the ZZ domain of *Staphylococcus aureus*. PHA granules with a multifunctional surface displaying both specific binding sites for certain inorganic substances (gold or silica) and for IgG were produced (Figure 5). These granules may serve as suitable tools for medical imaging procedures when an antibody-mediated targeted delivery of an inorganic contrast agent is desired.

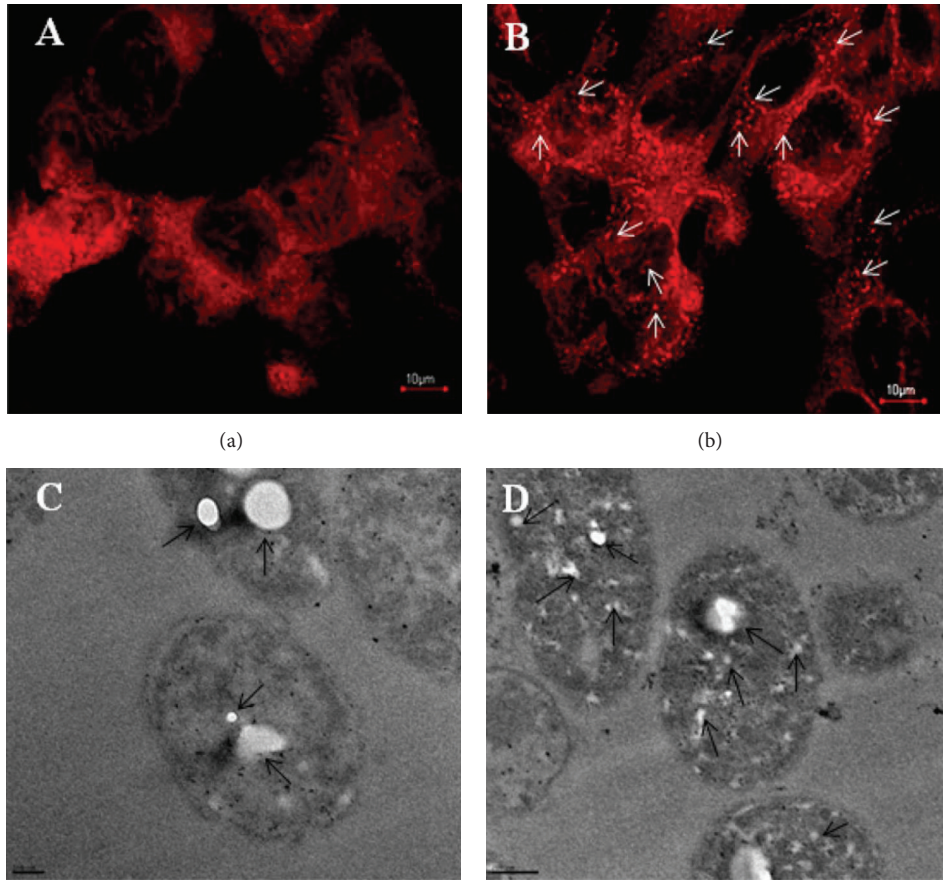

Figure 4: Microscopic study showing the cellular internalization of the P(3HV-*co*-4HB)-*b*-mPEG NPs: (a) CLSM images of the DU145 prostate cancer cells treated with free rhodamine-123 for 12 h; (b) cells treated with rhodamine-loaded NPs for 12 h (scale bar 10 μm); (c) TEM images showing the uptake of NPs in DU145 prostate cancer cells incubated for 6 h (scale bar = 100 nm); (d) cells incubated for 12 h (scale bar = 200 nm). Arrows in the figure represent intracellular localization of NPs. Reprinted with permission from Shah et al. [15], Copyright (2012), Elsevier.

Kim et al. reported a novel system for surface-initiated enzymatic polymerization to modify a solid substrate with biocompatible and biodegradable polymer PHB [59]. Polyhistidine and N-terminus tagged PHA synthase from *Ralstonia eutropha* H16 was used as an initiator for the polymerization through transition metal complexes, Ni^{+2}-nitrilotriacetic acid (Ni-NTA) (Figure 6). This system made it possible to initiate polymerization under physiological conditions and, through the specificity of enzyme, tailor the properties of the surface in a highly controlled manner by catalysing the polymerization in the designated area. The modification of solid substrates with PHB could potentially yield polymer-coated implants or controlled release devices for the applications in drug delivery and tissue engineering. Further work by the same group demonstrated a new approach to end functionalization of PHB using genetically engineered PHA synthase and to modify solid surfaces (Figure 7). Modification of PHA end groups by protein engineering aids in the introduction of various functionalities into PHAs which will allow it to interact with specific ligands or receptors. This new approach will be a useful tool to develop novel classes of block copolymers of which one block is a member of the PHA family with potentially 100 different types of monomers, and the other block is a protein with custom-designed sequences and functionalities. Modification of PHA end groups through protein engineering will provide an effective way of introducing diverse functionalities into the biopolymer, which will further broaden its spectrum to other receptors or ligands of interest for advanced delivery systems [60].

5.3. PHA Nanoparticles-Based Targeted Drug Delivery. Recently, there is a growing interest in the development of novel drug delivery systems using nanotechnology. Nanoparticles represent a promising drug delivery system of controlled and targeted release and have become an important area of research in the field of drug delivery because they have the ability to deliver a wide range of drugs to various areas of the body for sustained periods of time. The surface properties of Nanoparticles can be modified for targeted drug delivery. A wide variety of drugs can be delivered using nanoparticles via a number

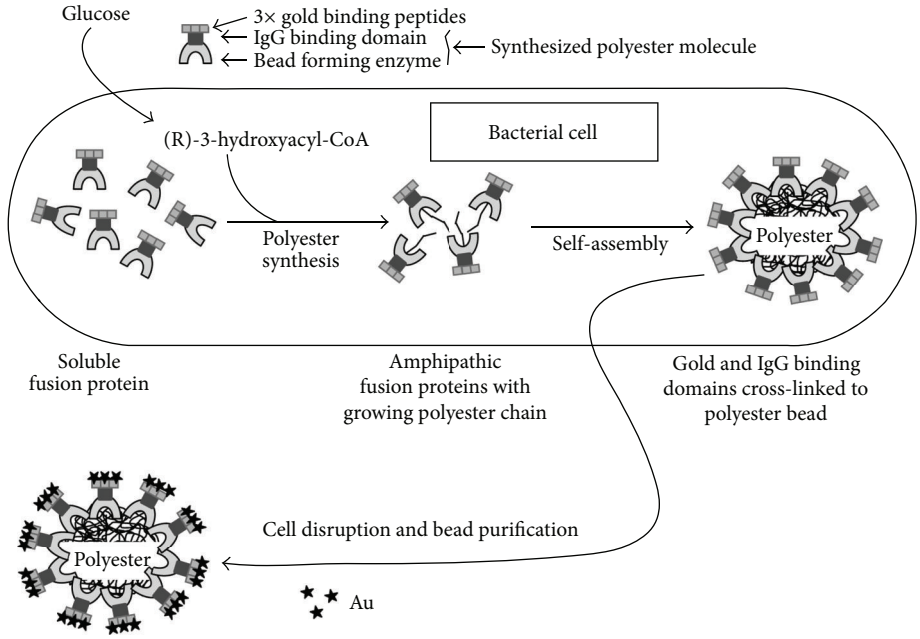

Figure 5: Schematic overview of PHA granules with a multifunctional surface displaying both specific binding sites for certain inorganic substance gold and for IgG. Reprinted with permission from Jahns et al. [58], Copyright (2008), American Chemical Society.

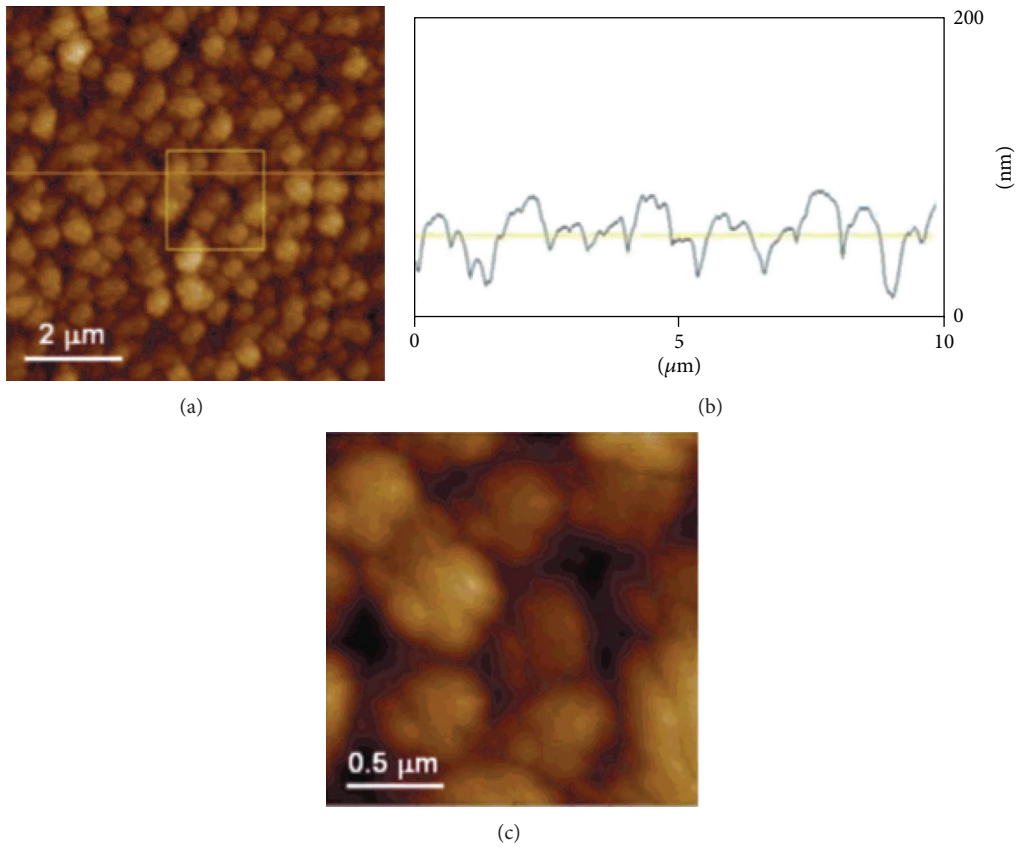

Figure 6: AFM images of the synthesized PHB film on the silicon surface. (a) The cross section (b) taken at the 10 μm horizontal line. Part (c) is the magnified image of the square area (2 μm × 2 μm) in part (a). It shows the microstructure of an individual grain. Reprinted with permission from Kim et al. [59], Copyright (2004), American Chemical Society.

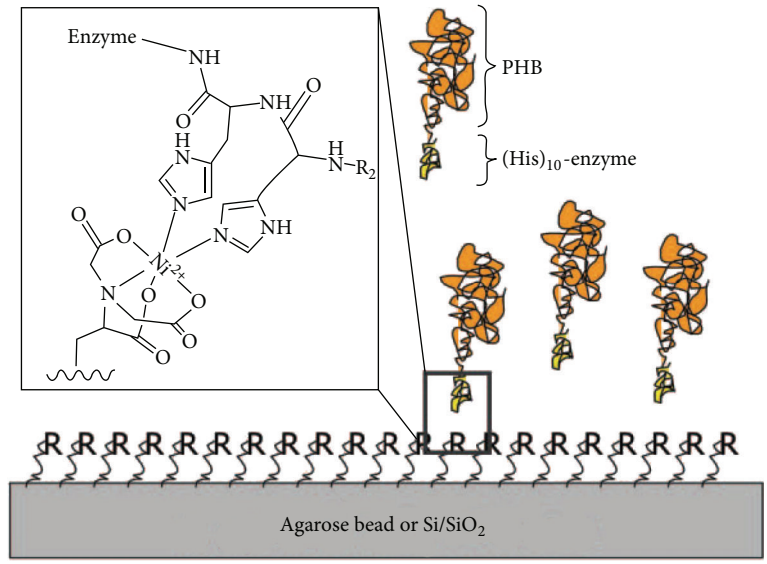

Figure 7: Schematic representation of end-functionalized PHB block copolymers complexing onto an Ni-NTA-derivatized solid surface. The inset shows a part of his-tag complexed with Ni-NTA on the surface. R represents Ni-NTA and R_2 for the rest of histidine units. Paik et al. (2005) [60]. Reproduced by permission of the Royal Society of Chemistry.

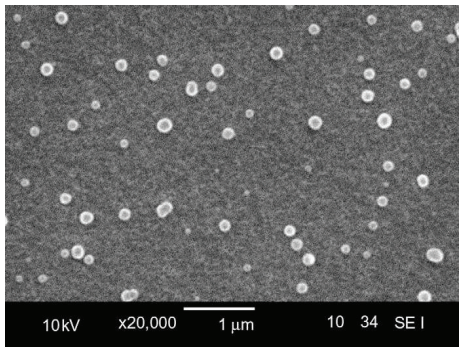

Figure 8: SEM image of RBITC loaded PHA nanoparticles. Reprinted with permission from Yao et al. [61], Copyright (2008), Elsevier.

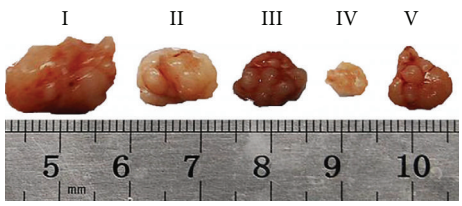

Figure 9: Representative photographs of each group's tumor. I: normal saline; II: free DOX; III: DOX/P(HB-HO) NPs; IV: DOX/FA-PEG-P(HB-HO) NPs; V: DOX/FA-PEG-P(HB-HO) NPs + 1 mM free folic acid. Reprinted with permission from Zhang et al. [62], Copyright (2010), Elsevier.

of routes. Nanoparticles can be used to deliver hydrophilic drugs, hydrophobic drugs, proteins, vaccines, biological macromolecules, and so forth [64].

Targeted drug delivery systems are designed to deliver drugs at the proper dosage for the required amount of time to a specific site of the body where it is needed, thereby preventing any adverse effects drugs may have on other organs or tissues. Targeted delivery assumes great importance particularly in the case of highly toxic drugs such as chemotherapeutic drugs and highly active and fragile biotechnological molecules such as peptides and proteins. It is widely believed that active targeting, through the modification of nanoparticles with ligands, has the potential to enhance the therapeutic efficacy and reduce the side effects relative to conventional therapeutics [65]. In cancer therapy, the presence of targeting ligands can greatly enhance the retention and cellular uptake of nanoparticles via receptor-mediated endocytosis even though tumor accumulation is largely determined by the physicochemical properties of nanoparticles [66]. This can then lead to higher intracellular drug concentration and increase therapeutic activity, which is particularly important for bioactive macromolecules (e.g., DNA and siRNA) that require intracellular delivery for bioactivity [67].

Microspheres of PHB for the targeted delivery of formalinized vaccine of Staphylococcal enterotoxin B, to the gut-associated lymphoid tissues, were reported by Eldridge et al. [68]. Tissue penetration was specific to Peyer's patches for microspheres of 10 μm or less in diameter. In addition, the PHB microspheres exhibited very good absorption.

Yao et al. developed a receptor-mediated drug delivery system in which rhodamine B isothiocyanate (RBITC) model drug was targeted to cancer cells or macrophages by incorporating with P(HB-*co*-HHx) and associating with a recombinant PhaP phasin protein from *C. necator*. SEM image of RBITC-loaded nanoparticles is shown in Figure 8 [61]. These recombinant phasins were fused to ligands

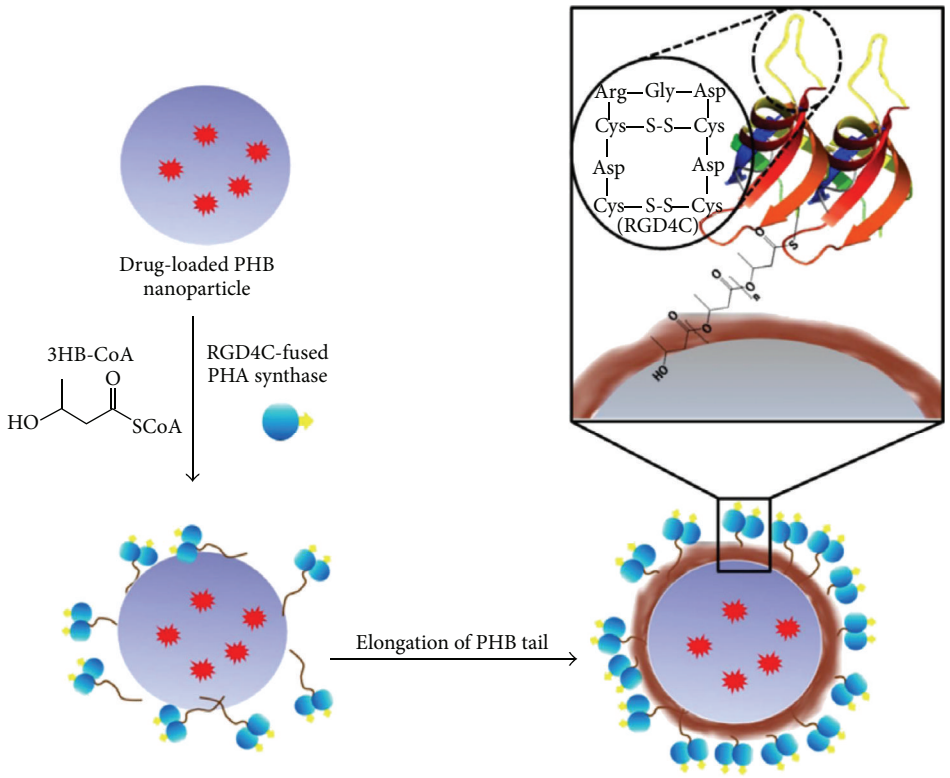

FIGURE 10: Surface functionalization of hydrophobic PHB nanoparticles through enzymatic reaction. Reprinted with permission from Lee et al. [63], Copyright (2011), Elsevier.

mannosylated human α1 acid glycoprotein (hAGP) and human epidermal growth factor (hEGF) for targeting cancer cells or macrophages, respectively. hAGP is recognized by receptors on macrophages, and hEGF is recognized by receptors on hepatocellular carcinoma cells. Proper targeting of PHA/RBITC nanoparticles to each cell line was demonstrated by fluorescence microscopy which showed that the nanoparticles were directed to the correct type of tissue by intake through correct type of cell, proving targeted delivery.

Biopolymer-based nanocarriers with targeting capability for imaging and drug delivery to tumors through molecular recognition of the cancer specific marker, integrin, were developed by Kim et al. [69]. The Arg-Gly-Asp (RGD) motif was used as a ligand to target $\alpha_v\beta_3$ integrins, which have been identified as cell surface receptors that mediate the adhesion of cells to the extracellular matrix and are highly expressed in various cancer cells. PHA synthase was fused to RGD-containing peptide through protein engineering, and further expression in recombinant *E. coli* was done, followed by purification. The engineered enzyme was used to produce an amphiphilic protein-polymer hybrid with a specific end functionality. The resulting block copolymer with RGD peptide at one end was readily self-assembled into a micellar structure in the presence of substrate 3HB-CoA and was successfully used to target tumor cells.

Zhang et al. developed a novel targeting drug delivery system using poly(3-hydroxybutyrate-*co*-3-hydroxyoctanoate) [P(HB-HO)] as the drug carrier, folic acid (FA) as the targeting ligand, and doxorubicin (DOX) as the model anticancer drug [62]. The average size, drug loading capacity, and encapsulation efficiency of the prepared DOX-loaded, folate-mediated P(HB-HO) nanoparticles (DOX/FA-PEG-P(HB-HO) NPs) were found to be around 240 nm, 29.6%, and 83.5%, respectively. The intracellular uptake tests of the nanoparticles (NPs) *in vitro* showed that the DOX/FA-PEG-P(HB-HO) NPs were more efficiently taken up by HeLa cells. In addition, DOX/FA-PEG-P(HB-HO) NPs (IC_{50} = 0.87 μM) showed greater cytotoxicity to HeLa cells than the other treated groups. *In vivo* antitumor activity of the DOX/FA-PEG-P(HB-HO) NPs showed a much better therapeutic efficacy in inhibiting tumor growth, and the final mean tumor volume was 178.91 ± 17.43 mm^3, significantly smaller than normal saline control group (542.58 ± 45.19 mm^3) (Figure 9) which shows that these NPs are effective in selective delivery of anticancer drug to the folate receptor-overexpressed cancer cells.

Recently, Lee et al. demonstrated a new approach to prepare a nanocarrier system with targeting capability for imaging and drug delivery to cancer cells by integrating the unique catalytic characteristics of PHA synthase with simple oil into water emulsion methods (Figure 10) [63]. The effective coupling between the hydrophobic surface of PHB nanoparticle and PHB chain grown from the enzyme fused with a specific ligand provided a simple way of functionalizing nanoparticle with active protein layers in aqueous environment. The surface of nanoparticles was

functionalized with tumor-specific ligand, RGD4C, fused with PHA synthase. The functionalized PHB nanoparticles showed a specific affinity to MDA-MB 231 breast cancer cells indicating that the tumor-specific ligand, RGD4C, was effectively displayed on the surface of PHB nanoparticles through enzymatic modification and confered targeting capability on the drug carrier.

6. Conclusion

Increased interest in the use of PHA for medical applications had arisen the response to the need for the emerging field of drug delivery, where a much wider range of biodegradable and biocompatible polymers are being sought for use as drug carriers. Because of their versatility and wide range of properties, biodegradable PHAs are being used as novel drug delivery systems. In particular, PHA-based drug carrier holds tremendous promise in the areas of cancer therapy and controlled delivery of drugs including steroids, vaccines, and other biological molecules. They can be formulated for targeted drug delivery to tumours or organs. Various successful studies using PHA as a drug carrier have clearly demonstrated that PHA possesses biodegradability and biocompatibility for drug carrier use. PHA has a wide variety of applications, among which the medical applications seem to be the most economically practical area. With the currently increased interest level and the extensive research being carried out in this area, PHAs are potentially emerging as environmentally friendly materials of the next generation with a wide range of applicability.

Acknowledgment

This work was supported by the Basic Science Research Program through the National Research Foundation of Korea (NRF) funded by the Ministry of Education, Science, and Technology (2010-0002963).

References

[1] S. Cammas, M.-M. Béar, L. Moine et al., "Polymers of malic acid and 3-alkylmalic acid as synthetic PHAs in the design of biocompatible hydrolyzable devices," *International Journal of Biological Macromolecules*, vol. 25, no. 1–3, pp. 273–282, 1999.

[2] S. Y. Lee and H. N. Chang, "Production of poly(3-hydroxybutyric acid) by recombinant *Escherichia coli* strains: genetic and fermentation studies," *Canadian Journal of Microbiology*, vol. 41, no. 1, pp. 207–215, 1995.

[3] M. Lemoigne, "Produits de deshydration et de polymerisation de lacide β-oxybutyrique," *Bulletin de la Societe de Chimie Biologique*, vol. 8, pp. 770–782, 1926.

[4] L. L. Madison and G. W. Huisman, "Metabolic engineering of poly(3-hydroxyalkanoates): from DNA to plastic," *Microbiology and Molecular Biology Reviews*, vol. 63, no. 1, pp. 21–53, 1999.

[5] R. Griebel, Z. Smith, and J. M. Merrick, "Metabolism of Poly-β-hydroxybutyrate. I. Purification, composition, and properties of native poly-β-hydroxybutyrate granules from bacillus megaterium," *Biochemistry*, vol. 7, no. 10, pp. 3676–3681, 1968.

[6] C. Errico, C. Bartoli, F. Chiellini, and E. Chiellini, "Poly(hydroxyalkanoates)-based polymeric nanoparticles for drug delivery," *Journal of Biomedicine and Biotechnology*, vol. 2009, Article ID 571702, 10 pages, 2009.

[7] G.-Q. Chen, "A microbial polyhydroxyalkanoates (PHA) based bio- and materials industry," *Chemical Society Reviews*, vol. 38, no. 8, pp. 2434–2446, 2009.

[8] A. Steinbüchel and B. Füchtenbusch, "Bacterial and other biological systems for polyester production," *Trends in Biotechnology*, vol. 16, no. 10, pp. 419–427, 1998.

[9] A. Steinbuchel and H. G. Schlegel, "Physiology and molecular genetics of poly(β-hydroxy-alkanoic acid) synthesis in *Alcaligenes eutrophus*," *Molecular Microbiology*, vol. 5, no. 3, pp. 535–542, 1991.

[10] T. Keshavarz and I. Roy, "Polyhydroxyalkanoates: bioplastics with a green agenda," *Current Opinion in Microbiology*, vol. 13, no. 3, pp. 321–326, 2010.

[11] B. Kessler and B. Witholt, "Factors involved in the regulatory network of polyhydroxyalkanoate metabolism," *Journal of Biotechnology*, vol. 86, no. 2, pp. 97–104, 2001.

[12] Y. Poirier, C. Nawrath, and C. Somerville, "Production of polyhydroxyalkanoates, a family of biodegradable plastics and elastomers, in bacteria and plants," *Bio/Technology*, vol. 13, no. 2, pp. 142–150, 1995.

[13] A. J. Anderson and E. A. Dawes, "Occurrence, metabolism, metabolic role, and industrial uses of bacterial polyhydroxyalkanoates," *Microbiological Reviews*, vol. 54, no. 4, pp. 450–472, 1990.

[14] G. A. R. Nobes, R. H. Marchessault, and D. Maysinger, "Polyhydroxyalkanoates: materials for delivery systems," *Drug Delivery*, vol. 5, no. 3, pp. 167–177, 1998.

[15] M. Shah, N. Ullah, M. H. Choi, M. O. Kim, and S. C. Yoon, "Amorphous amphiphilic P(3HV-co-4HB)-b-mPEG block copolymer synthesized from bacterial copolyester via melt transesterification: nanoparticle preparation, cisplatin-loading for cancer therapy and *in vitro* evaluation," *European Journal of Pharmaceutics and Biopharmaceutics*, vol. 80, no. 3, pp. 518–527, 2012.

[16] D. Byrom, "Polymer synthesis by microorganisms: technology and economics," *Trends in Biotechnology*, vol. 5, no. 9, pp. 246–250, 1987.

[17] Y. Doi, Y. Kanesawa, M. Kunioka, and T. Saito, "Biodegradation of microbial copolyesters: poly(3-hydroxybutyrate-co-3-hydroxyvalerate) and poly(3-hydroxybutyrate-co-4-hydroxybutyrate)," *Macromolecules*, vol. 23, no. 1, pp. 26–31, 1990.

[18] Y. Saito and Y. Doi, "Microbial synthesis and properties of poly(3-hydroxybutyrate-co-4-hydroxybutyrate) in *Comamonas acidovorans*," *International Journal of Biological Macromolecules*, vol. 16, no. 2, pp. 99–104, 1994.

[19] K. Sudesh, H. Abe, and Y. Doi, "Synthesis, structure and properties of polyhydroxyalkanoates: biological polyesters," *Progress in Polymer Science*, vol. 25, no. 10, pp. 1503–1555, 2000.

[20] E. Pişkin, "Biodegradable polymers as biomaterials," *Journal of Biomaterials Science-Polymer*, vol. 6, no. 9, pp. 775–795, 1995.

[21] K. Mukai, Y. Doi, Y. Sema, and K. Tomita, "Substrate specificities in hydrolysis of polyhydroxyalkanoates by microbial esterases," *Biotechnology Letters*, vol. 15, no. 6, pp. 601–604, 1993.

[22] M. Löbler, M. Sass, P. Michel, U. T. Hopt, C. Kunze, and K.-P. Schmitz, "Differential gene expression after implantation of biomaterials into rat gastrointestine," *Journal of Materials Science*, vol. 10, no. 12, pp. 797–799, 1999.

[23] M. Zinn, B. Witholt, and T. Egli, "Occurrence, synthesis and medical application of bacterial polyhydroxyalkanoate," *Advanced Drug Delivery Reviews*, vol. 53, no. 1, pp. 5–21, 2001.

[24] R. N. Reusch, "Poly-β-hydroxybutyrate/calcium polyphosphate complexes in eukaryotic membranes," *Proceedings of the Society for Experimental Biology and Medicine*, vol. 191, no. 4, pp. 377–381, 1989.

[25] G.-Q. Chen and Q. Wu, "The application of polyhydroxyalkanoates as tissue engineering materials," *Biomaterials*, vol. 26, no. 33, pp. 6565–6578, 2005.

[26] S. P. Valappil, S. K. Misra, A. Boccaccini, and I. Roy, "Biomedical applications of polyhydroxyalkanoates, an overview of animal testing and *in vivo* responses," *Expert Review of Medical Devices*, vol. 3, no. 6, pp. 853–868, 2006.

[27] B. Hazer, "Amphiphilic poly(3-hydroxy alkanoate)s: potential candidates for medical applications," *International Journal of Polymer Science*, vol. 2010, Article ID 423460, 8 pages, 2010.

[28] S. K. Misra, S. P. Valappil, I. Roy, and A. R. Boccaccini, "Polyhydroxyalkanoate (PHA)/inorganic phase composites for tissue engineering applications," *Biomacromolecules*, vol. 7, no. 8, pp. 2249–2258, 2006.

[29] Q. Wu, Y. Wang, and G.-Q. Chen, "Medical application of microbial biopolyesters polyhydroxyalkanoates," *Artificial Cells, Blood Substitutes, and Biotechnology*, vol. 37, no. 1, pp. 1–12, 2009.

[30] E. I. Shishatskaya and T. G. Volova, "A comparative investigation of biodegradable polyhydroxyalkanoate films as matrices for *in vitro* cell cultures," *Journal of Materials Science*, vol. 15, no. 8, pp. 915–923, 2004.

[31] X. Wei, Y.-J. Hu, W.-P. Xie, R.-L. Lin, and G.-Q. Chen, "Influence of poly(3-hydroxybutyrate-co-4-hydroxybutyrate-co-3-hydroxyhexanoate) on growth and osteogenic differentiation of human bone marrow-derived mesenchymal stem cells," *Journal of Biomedical Materials Research A*, vol. 90, no. 3, pp. 894–905, 2009.

[32] G.-Z. Ji, X. Wei, and G.-Q. Chen, "Growth of human umbilical cord Wharton's jelly-derived mesenchymal stem cells on the terpolyester poly(3-hydroxybutyrate-co-3-hydroxyvalerate-co-3- hydroxyhexanoate)," *Journal of Biomaterials Science-Polymer*, vol. 20, no. 3, pp. 325–339, 2009.

[33] V. I. Sevastianov, N. V. Perova, E. I. Shishatskaya, G. S. Kalacheva, and T. G. Volova, "Production of purified polyhydroxyalkanoates (PHAs) for applications in contact with blood," *Journal of Biomaterials Science-Polymer*, vol. 14, no. 10, pp. 1029–1042, 2003.

[34] C. J. Brigham and A. J. Sinskey, "Applications of polyhydroxyalkanoates in the medical industry," *International Journal of Biotechnology For Wellness Industries*, vol. 1, no. 1, pp. 53–60, 2012.

[35] W. Korsatko, B. Wabnegg, and H. M. Tillian, "Poly-D-(-)-3-hydroxybutyric acid: a biodegradable carrier for long term medication dosage. II. Comm.: the biodegradation in animal organism and *in-vitro - in-vivo* correlation of the liberation of pharmaceuticals from parenteral matrix retard tablets," *Pharmazeutische Industrie*, vol. 45, no. 10, pp. 1004–1007, 1983.

[36] G. Ciardelli, B. Saad, T. Hirt et al., "Phagocytosis and biodegradation of short-chain poly [(R)-3-hydroxybutyric acid] particles in macrophage cell line," *Journal of Materials Science*, vol. 6, no. 12, pp. 725–730, 1995.

[37] C. W. Pouton and S. Akhtar, "Biosynthetic polyhydroxyalkanoates and their potential in drug delivery," *Advanced Drug Delivery Reviews*, vol. 18, no. 2, pp. 133–162, 1996.

[38] K. Juni and M. Nakano, "Poly(hydroxy acids) in drug delivery," *Critical Reviews in Therapeutic Drug Carrier Systems*, vol. 3, no. 3, pp. 209–232, 1987.

[39] C. W. Pouton, J. E. Kennedy, L. J. Notarianni, and P. L. Gould, "Biocompatibility of polyhydroxy-butyrate and related copolymers," in *Proceedings of the International Symposium on Controlled Release Bioactive Materials*, vol. 15, pp. 179–180, 1988.

[40] R. W. Lenz and R. H. Marchessault, "Bacterial polyesters: biosynthesis, biodegradable plastics and biotechnology," *Biomacromolecules*, vol. 6, no. 1, pp. 1–8, 2005.

[41] G. A. R. Nobes, R. H. Marchessault, and D. Maysinger, "Polyhydroxyalkanoates: materials for delivery systems," *Drug Delivery*, vol. 5, no. 3, pp. 167–177, 1998.

[42] W. J. Orts, G. A. R. Nobes, J. Kawada, S. Nguyen, G.-E. Yu, and F. Ravenelle, "Poly(hydroxyalkanoates): biorefinery polymers with a whole range of applications. The work of Robert H. Marchessault," *Canadian Journal of Chemistry*, vol. 86, no. 6, pp. 628–640, 2008.

[43] N. Gangrade and J. C. Price, "Poly(hydroxybutyrate-hydroxyvalerate) microspheres containing progesterone: preparation, morphology and release properties," *Journal of Microencapsulation*, vol. 8, no. 2, pp. 185–202, 1991.

[44] P. L. Gould, S. J. Holland, and B. J. Tighe, "Polymers for biodegradable medical devices. IV. Hydroxybutyrate-valerate copolymers as non-disintegrating matrices for controlled-release oral dosage forms," *International Journal of Pharmaceutics*, vol. 38, pp. 231–237, 1987.

[45] I. Gursel, F. Yagmurlu, F. Korkusuz, and V. Hasirci, "*In vitro* antibiotic release from poly(3-hydroxybutyrate-co-3-hydroxyvalerate) rods," *Journal of Microencapsulation*, vol. 19, no. 2, pp. 153–164, 2002.

[46] M. F. Yagmurlu, F. Korkusuz, I. Gursel et al., "Sulbactam-cefoperazone polyhydroxybutyrate-co-hydroxyvalerate (PHBV) local antibiotic delivery system: *in vivo* effectiveness and biocompatibility in the treatment of implant-related experimental osteomyelitis," *Journal of Biomedical Materials Research*, vol. 46, no. 4, pp. 494–503, 1999.

[47] F. Türesin, I. Gürsel, and V. Hasirci, "Biodegradable polyhydroxyalkanoate implants for osteomyelitis therapy: *in vitro* antibiotic release," *Journal of Biomaterials Science-Polymer*, vol. 12, no. 2, pp. 195–207, 2001.

[48] I. Gürsel, F. Korkusuz, F. Türesin, N. Gürdal Alaeddinoğlu, and V. Hasirci, "*In vivo* application of biodegradable controlled antibiotic release systems for the treatment of implant-related osteomyelitis," *Biomaterials*, vol. 22, no. 1, pp. 73–80, 2001.

[49] M. C. Bissery, F. A. Valeriote, and C. Thies, "Therapeutic efficacy of CCNU-loaded microspheres prepared from poly (D,L) lactide (PLA) or poly-B-hydroxybutyrate (PHB) against Lewis lung (LL) carcinoma," *Proceedings of the American Association for Cancer Research*, vol. 26, 355 pages, 1985.

[50] M. Kubota, M. Nakano, and K. Juni, "Mechanism of enhancement of the release rate of aclarubicin from poly-β-hydroxybutyric acid microspheres by fatty acid esters," *Chemical and Pharmaceutical Bulletin*, vol. 36, no. 1, pp. 333–337, 1988.

[51] D. Sendil, I. Gürsel, D. L. Wise, and V. Hasirci, "Antibiotic release from biodegradable PHBV microparticles," *Journal of Controlled Release*, vol. 59, no. 2, pp. 207–217, 1999.

[52] E. I. Shishatskaya, A. V. Goreva, O. N. Voinova, E. V. Inzhevatkin, R. G. Khlebopros, and T. G. Volova, "Evaluation of antitumor activity of rubomycin deposited in absorbable polymeric

microparticles," *Bulletin of Experimental Biology and Medicine*, vol. 145, no. 3, pp. 358–361, 2008.

[53] F. Koosha, R. H. Muller, and S. S. Davis, "A continuous flow system for *in vitro* evaluation of drug-loaded biodegradable colloidal barriers," *Journal of Pharmacy and Pharmacology*, vol. 40, 131 pages, 1988.

[54] T. Kawaguchi, A. Tsugane, K. Higashide et al., "Control of drug release with a combination of prodrug and polymer matrix: antitumor activity and release profiles of 2',3'-diacyl-5-fluoro-2'-deoxyuridine from poly(3-hydroxybutyrate) microspheres," *Journal of Pharmaceutical Sciences*, vol. 81, no. 6, pp. 508–512, 1992.

[55] X.-Y. Lu, E. Ciraolo, R. Stefenia, G.-Q. Chen, Y. Zhang, and E. Hirsch, "Sustained release of PI3K inhibitor from PHA nanoparticles and *in vitro* growth inhibition of cancer cell lines," *Applied Microbiology and Biotechnology*, vol. 89, no. 5, pp. 1423–1433, 2011.

[56] V. Peters and B. H. A. Rehm, "*In vivo* monitoring of PHA granule formation using GFP-labeled PHA synthases," *FEMS Microbiology Letters*, vol. 248, no. 1, pp. 93–100, 2005.

[57] V. Peters and B. H. A. Rehm, "*In vivo* enzyme immobilization by use of engineered polyhydroxyalkanoate synthase," *Applied and Environmental Microbiology*, vol. 72, no. 3, pp. 1777–1783, 2006.

[58] A. C. Jahns, R. G. Haverkamp, and B. H. A. Rehm, "Multifunctional inorganic-binding beads self-assembled inside engineered bacteria," *Bioconjugate Chemistry*, vol. 19, no. 10, pp. 2072–2080, 2008.

[59] Y.-R. Kim, H.-J. Paik, C. K. Ober, G. W. Coates, and C. A. Batt, "Enzymatic surface-initiated polymerization: a novel approach for the in situ solid-phase synthesis of biocompatible polymer pol(3-hydroxybutyrate)," *Biomacromolecules*, vol. 5, no. 3, pp. 889–894, 2004.

[60] H.-J. Paik, Y.-R. Kim, R. N. Orth, C. K. Ober, G. W. Coates, and C. A. Batt, "End-functionalization of poly(3-hydroxybutyrate) via genetic engineering for solid surface modification," *Chemical Communications*, no. 15, pp. 1956–1958, 2005.

[61] Y.-C. Yao, X.-Y. Zhan, J. Zhang et al., "A specific drug targeting system based on polyhydroxyalkanoate granule binding protein PhaP fused with targeted cell ligands," *Biomaterials*, vol. 29, no. 36, pp. 4823–4830, 2008.

[62] C. Zhang, L. Q. Zhao, Y. F. Dong, X. Y. Zhang, J. Lin, and Z. Chen, "Folate-mediated poly(3-hydroxybutyrate-co-3-hydroxyoctanoate) nanoparticles for targeting drug delivery," *European Journal of Pharmaceutics and Biopharmaceutics*, vol. 76, no. 1, pp. 10–16, 2010.

[63] J. Lee, S.-G. Jung, C.-S. Park, H.-Y. Kim, C. A. Batt, and Y.-R. Kim, "Tumor-specific hybrid polyhydroxybutyrate nanoparticle: surface modification of nanoparticle by enzymatically synthesized functional block copolymer," *Bioorganic and Medicinal Chemistry Letters*, vol. 21, no. 10, pp. 2941–2944, 2011.

[64] H. Yamamoto, Y. Kuno, S. Sugimoto, H. Takeuchi, and Y. Kawashima, "Surface-modified PLGA nanosphere with chitosan improved pulmonary delivery of calcitonin by mucoadhesion and opening of the intercellular tight junctions," *Journal of Controlled Release*, vol. 102, no. 2, pp. 373–381, 2005.

[65] D. W. Bartlett, H. Su, I. J. Hildebrandt, W. A. Weber, and M. E. Davis, "Impact of tumor-specific targeting on the biodistribution and efficacy of siRNA nanoparticles measured by multimodality *in vivo* imaging," *Proceedings of the National Academy of Sciences of the United States of America*, vol. 104, no. 39, pp. 15549–15554, 2007.

[66] K. F. Pirollo and E. H. Chang, "Does a targeting ligand influence nanoparticle tumor localization or uptake?" *Trends in Biotechnology*, vol. 26, no. 10, pp. 552–558, 2008.

[67] J. Shi, A. R. Votruba, O. C. Farokhzad, and R. Langer, "Nanotechnology in drug delivery and tissue engineering: from discovery to applications," *Nano Letters*, vol. 10, no. 9, pp. 3223–3230, 2010.

[68] J. H. Eldridge, C. J. Hammond, J. A. Meulbroek, J. K. Staas, R. M. Gilley, and T. R. Tice, "Controlled vaccine release in the gut-associated lymphoid tissues. I. Orally administered biodegradable microspheres target the Peyer's patches," *Journal of Controlled Release*, vol. 11, no. 1–3, pp. 205–214, 1990.

[69] H.-N. Kim, J. Lee, H.-Y. Kim, and Y.-R. Kim, "Enzymatic synthesis of a drug delivery system based on polyhydroxyalkanoate-protein block copolymers," *Chemical Communications*, no. 46, pp. 7104–7106, 2009.

Hindawi Publishing Corporation
BioMed Research International
Volume 2013, Article ID 209452, 11 pages
http://dx.doi.org/10.1155/2013/209452

Research Article

Magnetofection: A Reproducible Method for Gene Delivery to Melanoma Cells

Lara Prosen,[1] Sara Prijic,[2] Branka Music,[1] Jaka Lavrencak,[3] Maja Cemazar,[2,4] and Gregor Sersa[2]

[1] *Kolektor Group, Nanotesla Institute Ljubljana, Stegne 29, 1521 Ljubljana, Slovenia*
[2] *Institute of Oncology Ljubljana, Department of Experimental Oncology, Zaloska 2, 1000 Ljubljana, Slovenia*
[3] *Institute of Oncology Ljubljana, Department of Cytopathology, Zaloska 2, 1000 Ljubljana, Slovenia*
[4] *University of Primorska, Faculty of Health Sciences, Polje 42, 6310 Izola, Slovenia*

Correspondence should be addressed to Gregor Sersa; gsersa@onko-i.si

Received 7 December 2012; Revised 7 May 2013; Accepted 9 May 2013

Academic Editor: Alejandro Sosnik

Magnetofection is a nanoparticle-mediated approach for transfection of cells, tissues, and tumors. Specific interest is in using superparamagnetic iron oxide nanoparticles (SPIONs) as delivery system of therapeutic genes. Magnetofection has already been described in some proof-of-principle studies; however, fine tuning of the synthesis of SPIONs is necessary for its broader application. Physicochemical properties of SPIONs, synthesized by the co-precipitation in an alkaline aqueous medium, were tested after varying different parameters of the synthesis procedure. The storage time of iron(II) sulfate salt, the type of purified water, and the synthesis temperature did not affect physicochemical properties of SPIONs. Also, varying the parameters of the synthesis procedure did not influence magnetofection efficacy. However, for the pronounced gene expression encoded by plasmid DNA it was crucial to functionalize poly(acrylic) acid-stabilized SPIONs (SPIONs-PAA) with polyethyleneimine (PEI) without the adjustment of its elementary alkaline pH water solution to the physiological pH. In conclusion, the co-precipitation of iron(II) and iron(III) sulfate salts with subsequent PAA stabilization, PEI functionalization, and plasmid DNA binding is a robust method resulting in a reproducible and efficient magnetofection. To achieve high gene expression is important, however, the pH of PEI water solution for SPIONs-PAA functionalization, which should be in the alkaline range.

1. Introduction

Nanomedicine is one of the several potential applications of nanotechnology that focuses on development of faster diagnosis, enhanced drug delivery, improved imaging, and efficient therapies, particularly in the field of cancer. Cancer nanomedicine utilizes nanoparticles of different origins, structures, shapes, and properties, ranging from 10 to 100 nm in size. Nowadays, especially nanoparticles exhibiting magnetic properties are in development for protein separation and pathogen detection, magnetic resonance imaging (MRI) contrast enhancement, destruction of cancer cells by hyperthermia, and targeted drug delivery [1]. Among all the types of magnetic nanoparticles, biocompatible superparamagnetic iron oxide nanoparticles (SPIONs) with functionalized surface to conjugate therapeutic agent and deliver it to the targeted site are currently very prosperous in research for development of cancer treatment strategies. Furthermore, SPIONs have already demonstrated their potential in cancer gene therapy by magnetofection [2–4]. Magnetofection is based on the utilization of functionalized SPIONs coupled with nucleic acids and guided by an external magnetic field to the targeted cells in order to facilitate the introduction of nucleic acids into the cells [5].

Magnetofection has already proven to be efficient nonviral transfection method *in vitro* and *in vivo* [1, 2, 6–8]. It can be used for transfection of plasmids, small interfering siRNA, short hairpin shRNA, and antisense oligonucleotides [9–11]. In order to obtain sufficient magnetofection efficacy with high cell survival rate, the properties of SPIONs are crucial. The physical and chemical properties of SPIONs largely depend on the type and specific conditions of the

synthesis method. The most widely used methods for SPIONs' synthesis are co-precipitation, precipitation in different types of microemulsions, sol-gel synthesis, hydrothermal synthesis, electrochemical deposition, sonochemical method, and thermal decomposition [12, 13]. All listed SPIONs' synthesis methods have their advantages and disadvantages, but in the terms of magnetofection it is important that synthesis method provides as unique particles as possible with an appropriate shape, size, surface properties, and magnetic core composition [14]. The conditions in SPIONs' synthesis, for example, the iron(II)/iron(III) ratio, the temperature, and the pH of reaction solutions, have been shown to influence the physicochemical properties of SPIONs [15].

Recently we developed *de novo* synthesis of SPIONs on the principle of the Massart co-precipitation method with subsequent surface modification with biocompatible poly(acrylic acid) (PAA) and poly(ethyleneimine) (PEI). The synthesized SPIONs were spherical and 8 ± 1 nm in diameter with iron oxide maghemite magnetic core, superparamagnetic properties, and zeta potential of -24 ± 2 mV at pH 9.5, indicating negative SPIONs' surface charge. After coating of SPIONs with polyanion PAA, diameter of SPIONs-PAA increased to 10 ± 1 nm and zeta potential to -47 ± 2 mV at pH 8.5, indicating good stability of SPIONs-PAA magnetic fluid. Additional functionalization of SPIONs-PAA with polycation PEI shifted negative zeta potential to positive 20 ± 1 mV at pH 8.0. Furthermore, *in vitro* experiments of magnetofection on four different cell lines demonstrated biocompatibility of prepared SPIONs-PAA-PEI-pDNA complexes with 70% cell survival. Magnetofection with SPIONs-PAA-PEI-pDNA complexes proved an effective *in vitro* as well as *in vivo* transfection, comparable to other established and effective non-viral gene delivery methods, that is, electroporation and lipofection [2]. PEI, which was used for functionalization of SPIONs-PAA, has been successfully used as non-viral transfection agent for decades now [16, 17]. Relatively high PEI transfection efficacy was ascribed to his endosomolytic activity [16]; however, its wider use is hindered by high cytotoxicity *in vitro* due to the relatively high molecular weight as well as low and cell type unspecific transfection efficacy *in vivo* [2, 18].

In order to effectively introduce magnetofection into cancer treatment modalities, further research on optimization of SPIONs' synthesis procedure is necessary. With this goal we have investigated the effect of several variables in the steps of SPIONs' synthesis and PEI water solution preparation on physicochemical properties of SPIONs and magnetofection efficacy in murine B16F1 melanoma cell line *in vitro*. An extensive study was conducted demonstrating the robustness of the synthesis method resulting in reproducible magnetofection efficacy of prepared SPIONs-PAA-PEI-pDNA complexes *in vitro* regardless of the variability in the synthesis conditions. However, only the pH of PEI water solution had significant effect on the magnetofection efficacy.

2. Materials and Methods

2.1. Synthesis of SPIONs. SPIONs were synthesized by co-precipitation of iron(III) and iron(II) sulfates ($Fe_2(SO_4)_3 \times H_2O$ and $FeSO_4 \times 7H_2O$, 98%; Alfa Aesar, Ward Hill, MA, USA) in an alkaline aqueous medium according to the Massart method [19]. The synthesis procedure was conducted briefly as follows: 250 mL 0.5 M aqueous solution of iron(III) and iron(II) ions in a weight-to-weight (w/w) ratio of 1.5 : 1 was prepared. Then 150 mL of 25% ammonium hydroxide solution (NH_4OH, Sigma-Aldrich, St. Louis, MO, USA) was added during the magnetic stirring at 600 rpm with further stirring for 30 min at room temperature. After SPIONs' precipitation, the alkaline medium was decanted and replaced with an equal amount of purified water. The washing was repeated 3 times.

In SPIONs' synthesis procedure three variables were evaluated: reagents (fresh or more than one year stored (long stored) iron(II) sulfate salt with 20% and 27% of bound water, respectively), purified water for salt dissolution and SPIONs' washing (DEMI water with pH 4.9 and conductivity of 3.2 μS/cm at 25°C or distilled water with pH 5.5 and conductivity of 0.8 μS/cm at 25°C), and synthesis temperature (23 ± 2°C or 60°C). Thus, six different SPIONs' synthesis batches were prepared (Figure 1). All synthesis procedures were repeated three times, and the data pooled together.

2.2. Stabilization of SPIONs with PAA. For stabilization of prepared magnetic fluid SPIONs were coated *in situ* with PAA (poly(acrylic acid, sodium salt) solution, 45% (w/w) in H_2O, average M_w of 8 kDa, Sigma-Aldrich, Steinheim, Germany). 100 mL of magnetic fluid and 100 mL of PAA water solution of equal mass concentrations at 10 mg/mL were mixed under magnetic stirring at 400 rpm for 5 min at room temperature. Thereafter, magnetic fluid of SPIONs coated with PAA (SPIONs-PAA) was sterilized by filtration using 0.22 μm pore size syringe filter (Techno Plastic Products, TPP, Trasadingen, Switzerland). Concentration of iron oxide in SPIONs was determined by thermogravimetric analysis (HB43, Mettler Toledo, Greifensee, Switzerland). For evaluation of physicochemical properties and further experiments stock solution of SPIONs-PAA was diluted either with DEMI or distilled water to a working concentration of 1 mg/mL.

2.3. Characterization of Physicochemical Properties of SPIONs and SPIONs-PAA. The specific surface area (SSA_{BET}) of heat-dried SPIONs was determined by the Brunauer-Emmett-Teller (BET) method (Tistar 3000, Micromertics, Norcross, GA). SPIONs' diameter (d_{BET}) was calculated using the equation $d_{BET} = 6/(SSA_{BET} \times \rho_{THEO})$, where SSA_{BET} is the specific surface area determined by BET method and ρ_{THEO} is a theoretical density of the studied phase ($\rho_{THEO} = 4.9\ g/cm^3$).

The size, shape, and morphology of SPIONs were evaluated using transmission electron microscopy (TEM) (2000 FX with EDS AN10000; JEOL, Tokyo, Japan). For size estimation, ten diameters of SPIONs from representative samples on TEM micrographs were measured.

Characterization of the synthesized SPIONs' phase content was made by X-ray diffractometry (XRD) (Miniflex II, RIGAKU, Tokyo, Japan) measured within the range of a diffraction angle 2θ from 20° to 70° with a step of 0.02 degree.

The hydrodynamic diameter distribution profiles of SPIONs and SPIONs-PAA were determined by dynamic light scattering (DLS) (LB-550V, HORIBA, Kyoto, Japan) in butylene glycol (1,3-Butanediol, 99%, Alfa Aesar GmbH & Co KG, Karlsruhe, Germany). From the data obtained by DLS also polydispersity index (PdI) of SPIONs and SPIONs-PAA was calculated using the equation $\mathrm{PdI} = (\sigma/d)^2$, where σ is a standard deviation and d is a mean diameter.

The zeta potential of magnetic fluids containing SPIONs at pH = 9.5 and SPIONs-PAA at pH = 8.5 was determined by zetameter (Zetasizer Nano ZS; Malvern Instruments, Malvern, UK) measuring electrophoretic mobility at 21°C applied to the Henry equation. The pH value of magnetic fluids containing SPIONs and SPIONs-PAA was measured by pH meter (S47 K; Mettler Toledo, Greifensee, Switzerland).

2.4. Cell Line, Culturing, and Plating for Magnetofection. Murine melanoma cell line B16F1 (American Type Culture Collection, Manassas, VA, USA) was cultured in advanced minimum essential medium (MEM, Gibco by Life Technologies, Grand Island, NY, USA) supplemented with 5% fetal bovine serum (FBS, Gibco), 10 mM L-glutamine (GlutaMAX, Gibco), 100 U/mL penicillin (Grünenthal, Aachen, Germany), and 50 mg/mL gentamicin (Krka, Novo Mesto, Slovenia). For experiments, cells were grown as a monolayer in 15 cm Petri dish (TPP) and maintained in a humidified atmosphere of 5% CO_2 at 37°C until they reached at least 80% confluence. Then, the medium was removed, and cells were washed with phosphate-buffered saline (PBS; Merck Millipore, Darmstadt, Germany) and detached with 0.25% trypsin/EDTA in Hank's buffer (Gibco). For trypsin inactivation an equal volume of MEM with FBS was added, cells were then collected in 50 mL conical falcon tube (TPP), centrifuged and counted in a hemocytometer. 5×10^4 cells per well were plated on a clear-bottomed 24-well test plate (TPP) in 1 mL of MEM; 24 h after plating cells reached 90–95% confluence, and magnetofection was performed.

2.5. Plasmid DNA. For magnetofection the plasmid DNA (pDNA) encoding enhanced green fluorescent protein (eGFP) under the control of the constitutive cytomegalovirus (CMV) promoter (pCMV-EGFP-N1; BD Biosciences Clontech, Palo Alto, CA, USA) was used. pCMV-EGFP-N1 was amplified in a competent *Escherichia coli* (TOP10; Life Technologies, Carlsbad, CA, USA) and purified using Qiagen Maxi-Endo-Free Kit (Qiagen, Hilden, Germany) according to the manufacturer's protocol. The quality and quantity of isolated pDNA were determined using spectrophotometer (Epoch Microplate Spectrophotometer, Take3 Micro-Volume Plate, BioTek, Bad Friedrichshall, Germany) and agarose gel electrophoresis. The working concentration of 1 mg/mL was prepared with endotoxin-free water.

2.6. SPIONs-PAA Complexes Functionalization. For functionalization of SPIONs-PAA complexes, PEI (polyethylenimine—branched, average M_w of 25 kDa, Sigma-Aldrich, Steinheim, Germany) water solution with concentration of 0.1 mg/mL was prepared. In all procedures SPIONs-PAA to PEI mass ratio of 0.6 : 1 was used. In the first part of the study examining the effect of SPIONs' synthesis conditions on magnetofection efficacy, PEI water solution prepared with dissolution of PEI using vortex mixer (Yellowline IKA, TTS 2, Staufen, Germany), pH unadjusted, and filtration through 0.22 μm membrane was used for SPIONs-PAA-PEI-pDNA complexes preparation (Figure 1).

In the second part of the study examining the effect of PEI water solution preparation on magnetofection efficacy, SPIONs synthesized at 23 ± 2°C, using long stored iron(II) sulfate salt and DEMI water for salt dissolution and SPIONs' washing were used for SPIONs-PAA-PEI-pDNA complexes preparation. In the PEI water solution preparation procedure three variables were varied, and their influence on magnetofection efficacy was evaluated. The first one was the comparison of vortex mixer to magnetic stirrer (Rotamix 560MMH, Tehtnica, Zelezniki, Slovenia) for the dissolution of the viscos PEI into an aqueous medium (Topical irrigation solution, Aqua B. Braun, Melsungen, Germany). The second variable was the pH value adjustment after dissolution (pH remained 10.5 or was adjusted to 7.4 with 1 M HCl), and lastly we tested the effect of filtration of PEI through 0.22 μm membrane on magnetofection efficacy. Thus, eight different PEI water solutions were prepared (Figure 1). The pH of PEI water solutions was measured by a pH meter (S40 SevenMulti, Mettler Toledo, Greifensee, Switzerland).

2.7. SPIONs-PAA-PEI-pDNA Complexes Preparation for Magnetofection. Functionalized SPIONs-PAA complexes with pDNA were prepared immediately prior to magnetofection. The complexes were prepared by mixing 20 μL of PEI (0.1 mg/mL) with 1.2 μL of SPIONs-PAA (1 mg/mL) and addition of 2 μL pDNA (1 mg/mL). Therefore, the final mass ratio of SPIONs-PAA, PEI, and pDNA was 0.6 : 1 : 1.

2.8. Electrophoretic Examination of the Ability of SPIONs-PAA-PEI Complexes to Bind pDNA. We examined the complex formation of pDNA and SPIONs-PAA-PEI by agarose gel electrophoresis. SPIONs-PAA-PEI-pDNA complexes were prepared using all synthesis batches of SPIONs separately. The pDNA without enzymatic restriction and PEI-pDNA complexes were used as controls. All samples and DNA ladder (MassRuler DNA Ladder, Mix, ready-to-use, Fermentas Thermo Fisher Scientific, Waltham, MA, USA) were administered on an agarose gel (1% (w/v)) stained with SYBR Safe (SYBR Safe DNA Gel Stain, Life Technologies, Grand Island, NY, USA). Electrophoresis was run at 100 V for 45 min. Visualization of the bands was performed under ultraviolet transilluminiscence (GelDoc-It TS 310; Ultra-Violet Products (UVP), Upland, CA, USA).

2.9. Magnetofection. SPIONs-PAA-PEI-pDNA complexes were added to murine B16F1 melanoma cells growing in 1 mL of MEM. The cell culture plate was placed on an array of Nd-Fe-B (surface magnetic flux density of 245 mT and magnetic gradient of 40 T/m; Supermagnete, Uster, Switzerland) permanent magnets for 15 minutes. Thereafter,

the cells were incubated at 37°C in a 5% CO_2 humidified atmosphere for 24 h.

2.10. Magnetofection Efficacy Evaluation. The expression of eGFP in the cells indicating magnetofection efficacy was visualized after 24 h by fluorescence microscopy and quantified by flow cytometry.

The photomicrographs of transfected cells expressing eGFP were recorded with digital camera (Olympus DP50, Hamburg, Germany) attached to fluorescent microscope (Olympus IX70) at 488 nm excitation wavelength and 507 nm emission wavelength.

The percentage of transfected cells expressing eGFP and the median fluorescence intensity of the eGFP expression were determined by flow cytometer (BD FACSCanto II; Becton Dickinson, San Jose, CA, USA). For measurements cells were trypsinized, collected in 15 mL conical falcon tubes (TPP), and centrifuged. The supernatant was removed; cells were resuspended in 1 mL of PBS and transferred to 5 mL polystyrene round-bottom tubes (Becton Dickinson).

2.11. Statistical Analyses. All quantitative data are presented as mean (AM) ± standard error (SEM). The data were beforehand tested for normality of distribution using the Shapiro-Wilk test and statistically processed by SigmaPlot statistical software (version 12.0, Systat Software, London, UK). Differences between two experimental groups were statistically evaluated by Student t-test, and for multiple comparison one-way ANOVA analysis of variance followed by the Holm-Sidak test was used. Alpha level was set to 0.05. A probability level of $P < 0.05$ was considered to be statistically significant.

3. Results

3.1. Variables in the Synthesis of SPIONs. Six different magnetic fluids containing SPIONs were prepared accordingly to the detailed description at the Materials and Methods section. Physicochemical properties of SPIONs and SPIONs-PAA, pDNA binding capacity of SPIONs-PAA-PEI complexes and magnetofection efficacy of SPIONs-PAA-PEI-pDNA complexes in murine B16F1 melanoma cells were evaluated in a relation to specific SPIONs' synthesis condition. Variables evaluated in this work were the storage time of iron(II) sulfate salt, the purified waters, and the temperature of SPIONs' synthesis, being the most critical parameters that could influence the physicochemical properties of the particles (Figure 1).

3.1.1. The Effect of Different SPIONs' Synthesis Conditions on Physicochemical Properties of SPIONs and SPIONs-PAA

(1) *Specific Surface Area of SPIONs.* After SPIONs' synthesis, all magnetic fluids were separately heat-dried and the SSA_{BET} of SPIONs was determined using the BET method. The SSA_{BET} of all SPIONs' synthesis bathes and their calculated d_{BET} are shown in Figure 2(a). The SSA_{BET} of SPIONs ranged from 90.8 ± 4.7 m^2/g to 124.4 ± 7.2 m^2/g and calculated d_{BET} from 9.9 ± 0.6 nm to 13.6 ± 0.7 nm (Figure 2(a)). The SPIONs synthesized at 23 ± 2°C had statistically significantly larger SSA_{BET} and consequently smaller calculated d_{BET} compared to SPIONs synthesized at 60°C. The results indicated that variability in SPIONs' surface was affected by the temperature of SPIONs' synthesis but not by other two tested variables.

The image recorded by TEM confirmed the calculated d_{BET} of SPIONs. SPIONs were approx. 10 nm in diameter, spherical, crystalline, and slightly agglomerated (Figure 2(b)).

(2) *Crystal Structure and Chemical Composition of SPIONs.* The iron oxide chemical composition of SPIONs was verified by the XRD diffraction (Figure 2(c)). Diffraction patterns of all SPIONs' synthesis batches had six diffraction peaks with indices (220), (311), (400), (422), (511), and (440) corresponding to pure iron oxide maghemite and/or magnetite. These results demonstrated that all SPIONs' synthesis batches were of pure iron oxides and that tested variables did not influence the chemical composition of SPIONs.

(3) *Hydrodynamic Diameter and Polydispersity Index of SPIONs and SPIONs-PAA*. For the stabilization of magnetic fluid containing SPIONs and prevention of SPIONs' agglomeration, coating of SPIONs was performed. The coating of SPIONs with PAA markedly increased an average hydrodynamic diameter of the particles from 39.6 ± 1.9 nm to 56.5 ± 1.7 nm in all SPIONs' synthesis batches. PdI of SPIONs and SPIONs-PAA from all SPIONs' synthesis batches were 0.1 or less, indicating a narrow particle size distribution and monodispersity. However, the hydrodynamic diameter distribution profiles and polydispersity index of SPIONs as well as SPIONS-PAA have similar and narrow size distributions irrespective of SPIONs' synthesis conditions (Figures 2(d) and 2(e)).

(4) *Zeta Potential of Magnetic Fluids Containing SPIONs and SPIONs-PAA*. To determine the surface charge of SPIONs and SPIONs-PAA, zeta potential was measured. Zeta potentials of SPIONs ranged from −20.2 ± 1.8 mV to −26.6 ± 1.9 mV at pH 9.5, and no significant differences between different synthesis batches were obtained. After coating SPIONs with PAA zeta potentials increased to the more negative values, ranging from −46.1 ± 1.6 mV to −50.3 ± 1.8 mV at pH 8.5, indicating the more negatively charged surface of SPIONs-PAA than that of SPIONs (Figure 2(f)). This designates that the coating of SPIONs with PAA provides stabilization of magnetic fluid as well as the foundation for the further functionalization of SPIONs-PAA's surface with PEI.

3.1.2. The Effect of Different SPIONs' Synthesis Conditions on the Ability of SPIONs-PAA-PEI Complexes to Bind pDNA. For testing pDNA binding capacity to SPIONs-PAA-PEI complexes prepared from all SPIONs' synthesis batches agarose gel electrophoresis was performed (Figure 2(g)). SPIONs-PAA-PEI-pDNA complexes, PEI-pDNA complexes, and pDNA were loaded onto agarose gel. The electrophoretic mobility of the samples and possible retardation of pDNA were monitored. Gel analysis showed that SPIONs-PAA-PEI stayed in the loading pockets of the agarose gel demonstrating

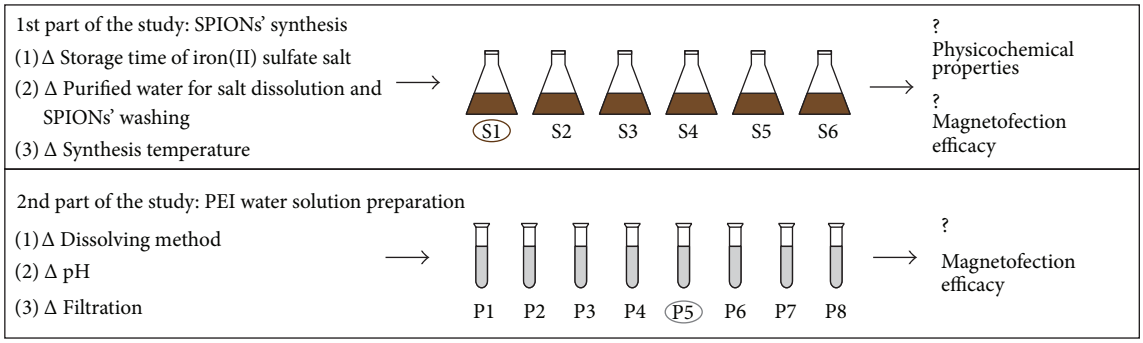

(a)

Variables in the synthesis of SPIONs

SPIONs number	Storage time of iron(II) salts	Purified water	Temperature (°C)
S1	Long stored, 27% of bound water	DEMI	23
S2	Long stored, 27% of bound water	Distilled	23
S3	Fresh, 20% of bound water	DEMI	23
S4	Long stored, 27% of bound water	DEMI	60
S5	Long stored, 27% of bound water	Distilled	60
S6	Fresh, 20% of bound water	DEMI	60

(b)

Variables in the preparation of PEI water solution

PEI number	Dissolving method	pH	Filtration
P1	Vortex	7.4	+
P2	Vortex	7.4	−
P3	Magnetic stirrer	7.4	+
P4	Magnetic stirrer	7.4	−
P5	Vortex	10.5	+
P6	Vortex	10.5	−
P7	Magnetic stirrer	10.5	−
P8	Magnetic stirrer	10.5	+

(c)

Figure 1: Study design scheme (a), variables in the synthesis of SPIONs (b), and preparation of PEI water solution (c). Encircled PEI water solution (P5) was used in the first part of the study examining the effect of SPIONs' synthesis conditions on magnetofection efficacy, whereas SPIONs' synthesis batch (S1) was used in the second part of the study examining the effect of PEI water solution preparation on magnetofection efficacy.

the ability of all SPIONs-PAA-PEI complexes to bind pDNA. Retardation of PEI-pDNA complexes was also noticed in the loading pockets, whereas pDNA moved towards the anode through the agarose gel. These results indicate that all SPIONs' synthesis batches effectively bound pDNA after coating with PAA and functionalization with PEI. Also, pDNA was bound onto PEI *per se*.

3.1.3. The Effect of Different SPIONs' Synthesis Conditions on Magnetofection Efficacy in Murine B16F1 Melanoma Cells. To determine whether SPIONs' synthesis condition can affect efficacy of magnetofection in murine B16F1 melanoma cells, SPIONs-PAA-PEI-pDNA complexes using SPIONs from different synthesis batches were separately added to the cells that were thereafter exposed to Nd-Fe-B magnets for 15 min.

24 h after magnetofection, the expression of eGFP in the cells indicating transfection efficacy was visualized by fluorescence microscopy and quantified by flow cytometry (Figure 3). The images taken under fluorescence epi-illumination indicated that SPIONs-PAA-PEI-pDNA complexes prepared from all SPIONs' synthesis batches successfully transfected cells. eGFP fluorescence reached similar level in exposed group of cells transfected with different SPIONs' synthesis batches. For subsequent quantitative determination of magnetofection efficacy the adherent cells were harvested and analyzed by flow cytometry. The results showed that there were no statistically significant differences in the percentages of fluorescent cells as well as in the median fluorescence intensities between the cells transfected with SPIONs-PAA-PEI-pDNA complexes prepared from different SPIONs' synthesis batches. The magnetofection efficacy was comparable using SPIONs-PAA-PEI-pDNA complexes prepared from all SPIONs' synthesis batches; the percentage of fluorescent cells ranged from 33.5 ± 1.9% to 35.5 ± 0.9% and fluorescence intensity from 3,486 ± 313 a.u. to 4,145 ± 288 a.u.

3.2. The Effect of PEI Water Solution Preparation on Magnetofection Efficacy in Murine B16F1 Melanoma Cells. For testing the effect of PEI water solution preparation on transfection and magnetofection efficacy of pDNA in murine B16F1 melanoma cells, eight different water solutions of branched polymer PEI, required as an enhancer for subsequent binding of pDNA to SPIONs-PAA, with the concentration of 0.1 mg/mL were prepared. Dissolution of PEI in sterile water with vortex mixer or magnetic stirrer, final pH adjustment, and filtration through 0.22 μm membrane were the variables in the preparation. Immediately prior to magnetofection SPIONs-PAA-PEI-pDNA complexes were prepared from SPIONs' synthesis batch S1 using different PEI water solutions (Figure 1). Transfection of cells with PEI-pDNA prepared from all PEI water solutions was used as a control.

The images of murine B16F1 melanoma cells taken 24 h after transfection and magnetofection by fluorescence microscopy and the results of the measurements by flow

SPIONs' synthesis batch number	SSA_{BET} (m^2/g)	d_{BET} (nm)
S1	116.3 ± 5.9	10.7 ± 0.6
S2	124.4 ± 7.2	9.9 ± 0.6
S3	115.2 ± 5.8	10.7 ± 0.5
S4	94.9 ± 3.7	13.0 ± 0.5
S5	90.8 ± 4.7	13.5 ± 0.7
S6	92.9 ± 2.5	13.2 ± 0.4

(a)

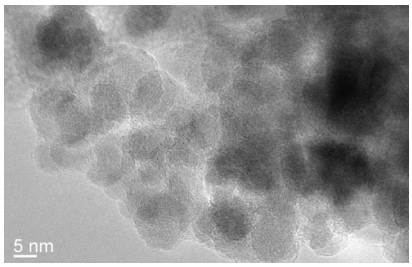

(b)

SPIONs' synthesis batch number	SPIONs (pH = 9.5)	SPIONs-PAA (pH = 8.5)
S1	−26.6 ± 1.9	−47.7 ± 2.6
S2	−24.5 ± 4.4	−46.1 ± 1.6
S3	−20.2 ± 1.8	−48.5 ± 0.6
S4	−21.2 ± 0.3	−50.3 ± 1.8
S5	−24.7 ± 2.1	−49.0 ± 0.5
S6	−23.7 ± 2.1	−46.4 ± 1.0

(f)

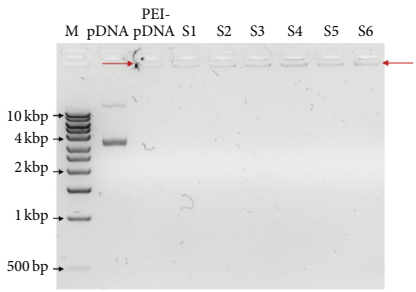

(g)

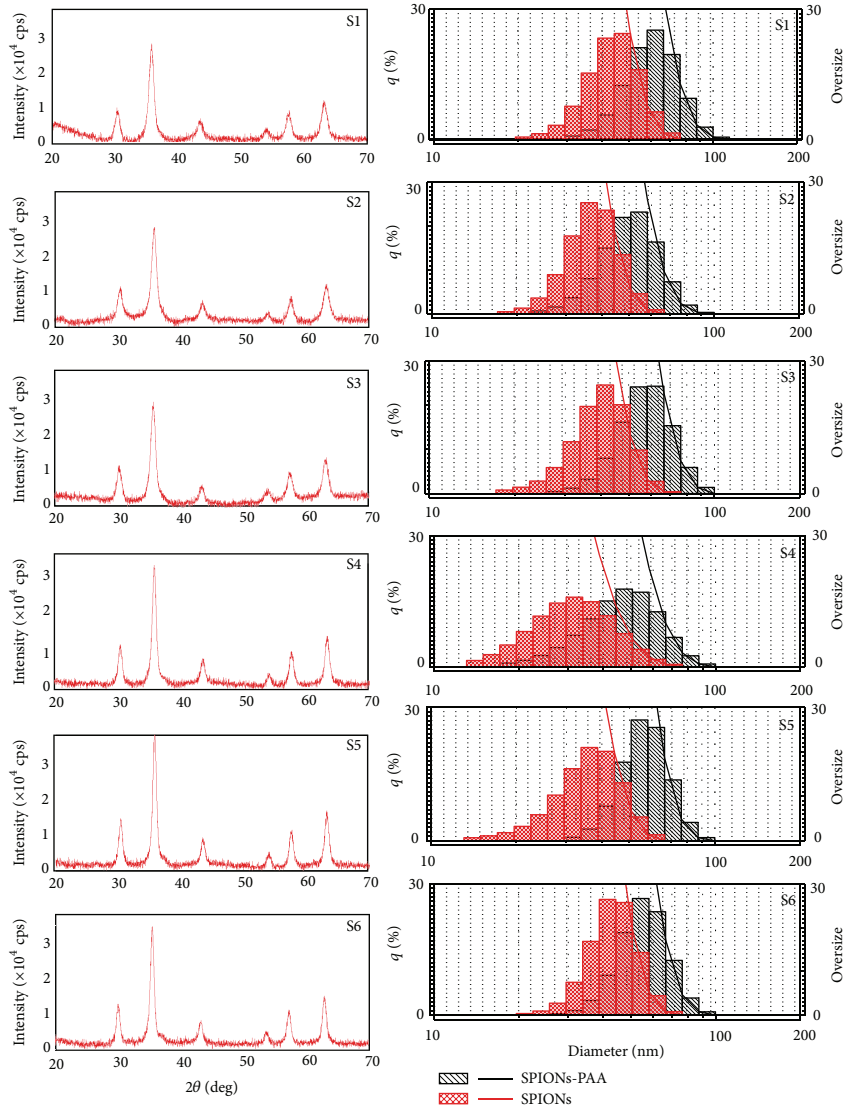

(c) (d)

SPIONs' synthesis batch number	SPIONs		SPIONs-PAA	
	d_{DLS} (nm)	PdI	d_{DLS} (nm)	PdI
S1	41.9 ± 1.2	0.088 ± 0.020	64.4 ± 2.3	0.041 ± 0.005
S2	40.7 ± 1.8	0.070 ± 0.013	55.1 ± 2.3	0.057 ± 0.002
S3	43.7 ± 1.8	0.101 ± 0.041	57.4 ± 0.3	0.050 ± 0.004
S4	32.8 ± 1.6	0.098 ± 0.006	52.3 ± 2.8	0.076 ± 0.017
S5	34.7 ± 5.9	0.056 ± 0.006	54.1 ± 1.8	0.046 ± 0.006
S6	43.5 ± 3.5	0.041 ± 0.001	55.5 ± 3.2	0.054 ± 0.009

(e)

Figure 2: Physicochemical properties of SPIONs, SPIONs-PAA, and the ability of SPIONs-PAA-PEI complexes to bind pDNA. (a) Specific surface area (SSA_{BET}) and calculated diameter (d_{BET}) of SPIONs from all synthesis batches. Data are presented as AM ± SEM from three independent replicates. (b) The TEM micrograph of the representative SPIONs' sample (S1). SPIONs were crystalline, spherical, approx. 10 nm in diameter, and slightly agglomerated. (c) X-ray diffraction patterns of SPIONs from all synthesis batches. All diffractograms exhibit characteristic peaks for iron oxide maghemite and/or magnetite. (d) The hydrodynamic diameter distribution profiles of SPIONs and SPIONs-PAA. Distribution profiles of all the synthesis batches showed related shift in the hydrodynamic diameters after coating SPIONs with PAA. (e) The hydrodynamic diameter (d_{DLS}) and calculated polydispersity index (PdI) of SPIONs and SPIONs-PAA. There were no significant differences in d_{DLS} and PdI of SPIONs and SPIONs-PAA prepared under variable synthesis conditions. (f) Zeta potential (mV) of magnetic fluids containing SPIONs and SPIONs-PAA. After coating SPIONs with PAA zeta potentials increased to the more negative values, indicating the more negatively charged surface of SPIONs-PAA than that of SPIONs. (g) The ability of SPIONs-PAA-PEI complexes to bind pDNA. The samples were loaded onto agarose gel in the following order: DNA size marker (M), pDNA without digestion enzyme restriction (pDNA), PEI-pDNA complexes (PEI-pDNA), and SPIONs-PAA-PEI-pDNA complexes (S1–S6) prepared from all SPIONs' synthesis batches separately. Longer arrows indicate retardation of pDNA bound to either PEI or SPIONs-PAA-PEI from all the synthesis batches. The pDNA alone migrated through the gel towards the anode.

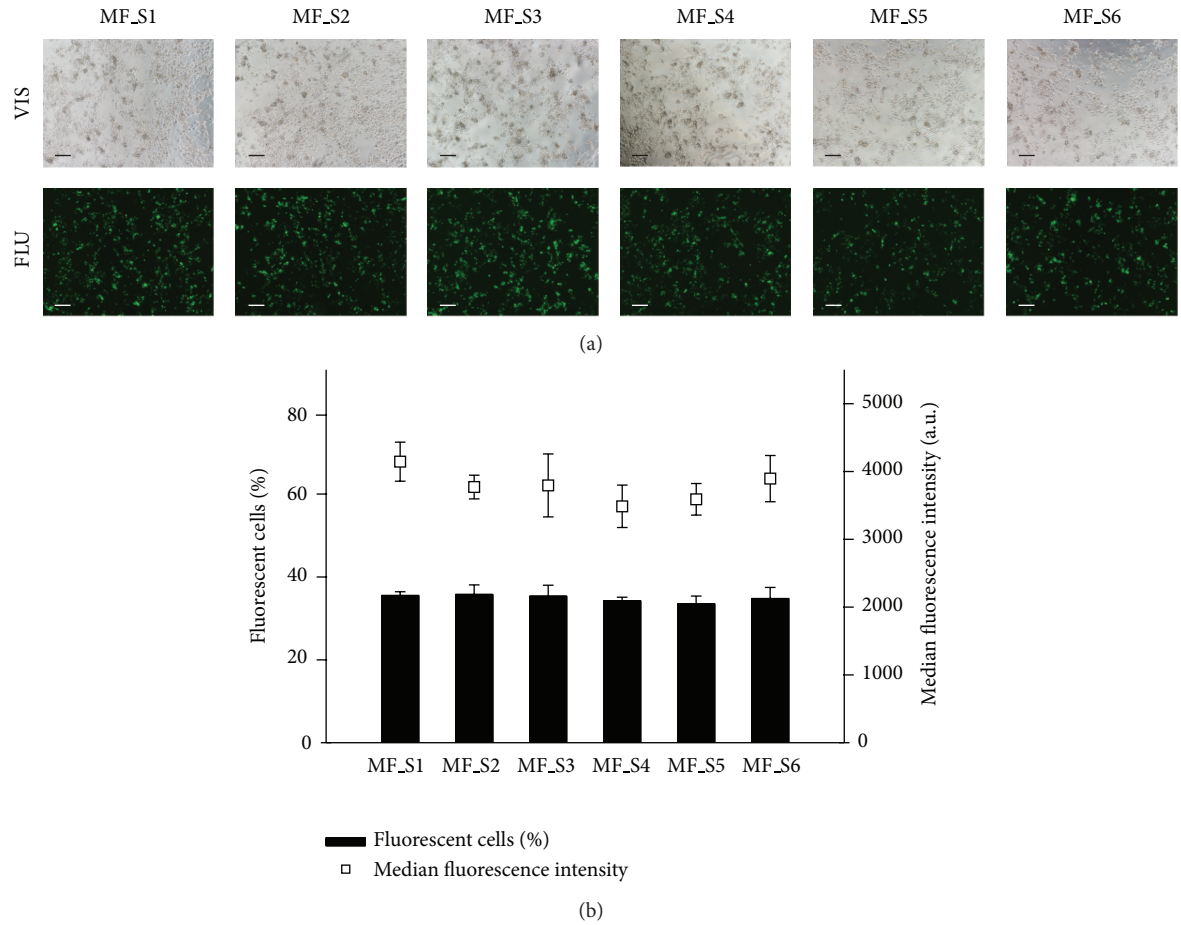

Figure 3: The effect of different SPIONs' synthesis on magnetofection efficacy in murine B16F1 melanoma cells. (a) The expression of eGFP in murine B16F1 melanoma cells visualized by fluorescence microscopy. The images were taken 24 h after magnetofection under ×60 magnification. For magnetofection SPIONs-PAA-PEI-pDNA complexes were prepared using SPIONs from all synthesis batches (from MF_S1 to MF_S6). The first row of images represents cells under visible light (VIS) and the second under fluorescent light (FLU). Scale bar, 200 μm. (b) The expression of eGFP in murine B16F1 melanoma cells quantified by flow cytometry. The results were obtained 24 h after magnetofection with SPIONs-PAA-PEI-pDNA complexes prepared from different SPIONs' synthesis batches (from MF_S1 to MF_S6). Bars and squares represent AM and SEM of the percentage of fluorescent cells and the median fluorescence intensity, respectively.

cytometer demonstrated successful transfection of pDNA into cells either by SPIONs-PAA-PEI-pDNA complexes or using PEI only (Figure 4). Using PEI water solutions prepared by a vortex mixer or magnetic stirrer, with the pH unadjusted (pH = 10.5) and either filtrated through 0.22 μm membrane or not, resulted from 34.8 ± 0.3% to 40.7 ± 1.1% of fluorescent cells and from 3,622 ± 176 a.u. to 4,198 ± 82 a.u. of fluorescence intensity after transfection with PEI-pDNA complexes, and from 38.4 ± 2.9% to 41.7 ± 3.2% of fluorescent cells and from 3,152 ± 168 a.u. to 3,613 ± 417 a.u. of fluorescence intensity after magnetofection. Although an evident difference in the fluorescence intensity among transfection with PEI-pDNA complexes (Figure 4(a), images taken under fluorescent light, from PEI-pDNA_P5 to PEI-pDNA_P8) and magnetofection (Figure 4(a), images taken under fluorescent light, from MF_P5 to MF_P8) can be observed in the images, there were no statistically significant differences between the means of fluorescence intensities and the percentages of fluorescent cells measured by flow cytometer. The pH adjustment of elementary alkaline PEI water solutions to the physiological statistically significantly reduced the expression of eGFP as measured by the decrease of fluorescent cells by approx. 10% and fluorescence intensity by 600 a.u. after transfection with PEI-pDNA complexes and by approx. 17% and 600 a.u. after magnetofection, respectively.

4. Discussion

Our results demonstrate that the described procedure of SPIONs' synthesis by the co-precipitation of iron(II) and iron(III) sulfate salts with subsequent PAA stabilization, PEI functionalization, and pDNA binding is a robust method leading to reproducible magnetofection of murine B16F1 melanoma cells. Synthesis using fresh or long stored iron(II) sulfate salts as a reagent, DEMI or distilled water, and room temperature or 60°C did not significantly affect the physicochemical properties of SPIONs, the ability of binding pDNA,

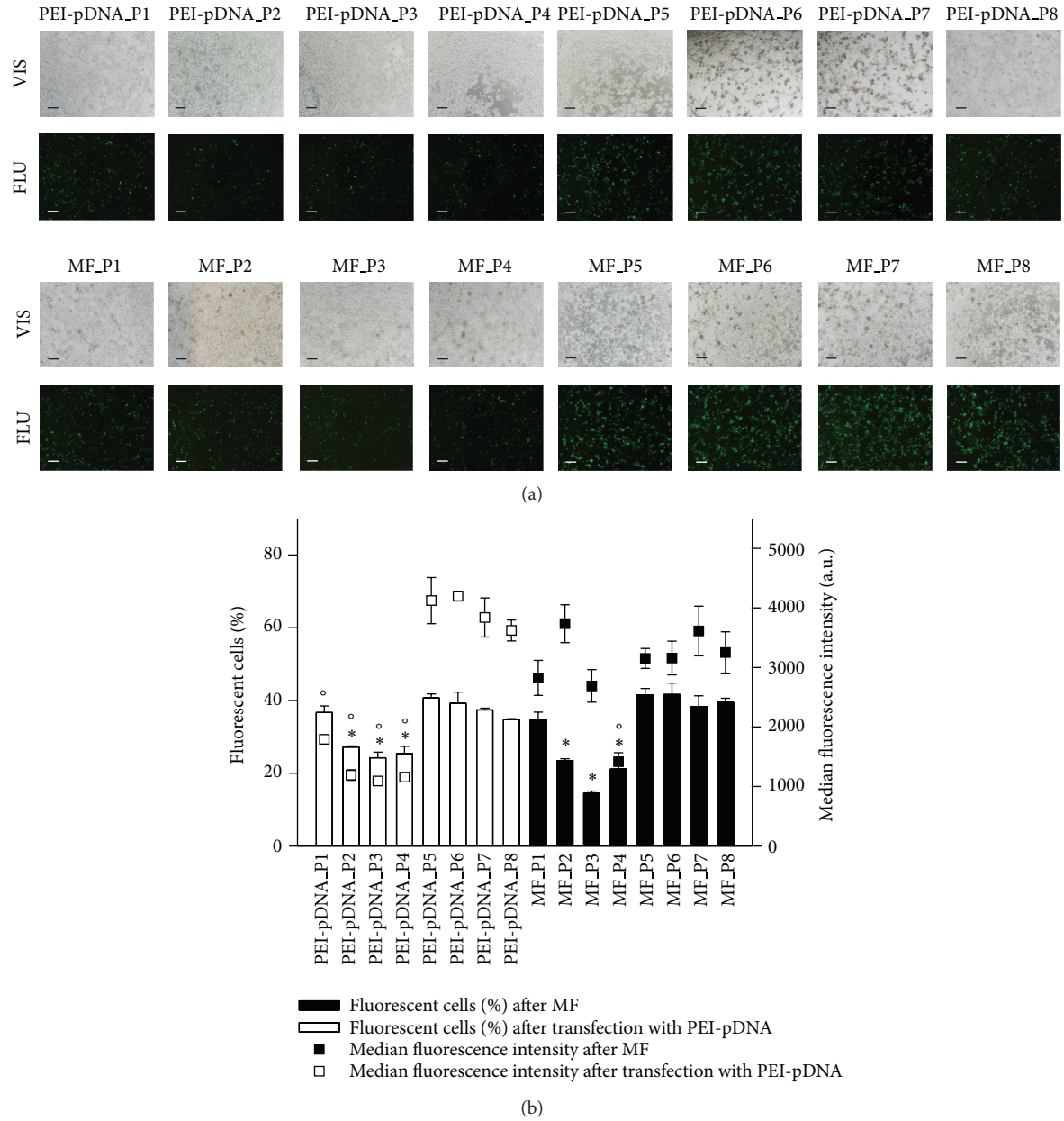

Figure 4: The effect of PEI water solution preparation on magnetofection efficacy in murine B16F1 melanoma cells. (a) The expression of eGFP in murine B16F1 melanoma cells visualized by fluorescence microscopy. The images under ×60 magnification were taken 24 h after transfection with PEI and pDNA complexes (from PEI-pDNA_P1 to PEI-pDNA_P8) and magnetofection (from MF_P1 to MF_P8) using eight different PEI water solutions. The first and the third row of images represent cells under visible light (VIS) and the second and the fourth row represent cells under fluorescent light (FLU). Scale bar, 200 μm. (b) The expression of eGFP in murine B16F1 melanoma cells quantified by flow cytometry. The results were obtained 24 h after transfection with PEI and pDNA complexes (from PEI-pDNA_P1 to PEI-pDNA_P8) and magnetofection (from MF_P1 to MF_P8) using different PEI water solutions. Bars and squares represent AM with SEM of the percentage of fluorescent cells and the median of fluorescence intensity, respectively. Asterisks indicate statistically significant differences between percentages of fluorescent cells after transfection or magnetofection, while circles denote the differences in the median fluorescence intensities after transfection or magnetofection ($^{\circ,*}P < 0.05$).

and magnetofection efficacy. The only factor significantly affecting magnetofection efficacy was the pH of PEI water solution used for functionalization of SPIONs-PAA, which should be in alkaline range in order to obtain pronounced gene expression.

SPIONs' synthesis method and the synthesis conditions vary greatly between different research groups. Iron oxide nanoparticle size distribution, their surface, and magnetic properties can be easily affected through the synthesis procedure [14]. The co-precipitation method is simple and

very effective; however, the main disadvantage is a relatively wide particle size distribution and rather large size of the particles. Our study demonstrates that with the described co-precipitation synthesis method regardless of the variables, such as the storage time of iron(II) sulfate salt, the type of purified water, and the synthesis temperature, we can obtain iron oxide nanoparticles with a narrow size distribution of approx. 10 nm in diameter, spherical in shape, crystalline, and slightly agglomerated. The physicochemical properties of SPIONs' synthesis batch S1, including the size, are the same as physicochemical properties of SPIONs used in our previous study [2], which extrapolates that also magnetic properties of this and all other SPIONs' synthesis batches should be the same, since their size did not alter more than 1–4 nm in diameter [20]. Despite the adequate magnetic properties of SPIONs and SPIONs-PAA the exposure of murine B16F1 melanoma cells *in vitro* to an external magnetic field does not significantly increase transfection efficiency of SPIONs-PAA-PEI-pDNA complexes [2].

The effect of storage time of iron(II) sulfate salt was evaluated in our study. Recently, it was proposed that only fresh iron(II) salt should be used in SPIONs' synthesis, as the use of long stored and oxidized iron(II) salt in the co-precipitation method could lead to insufficient magnetic properties and thus lower magnetofection efficacy [21]. However, the authors did not state the duration of storage time, which in turn could significantly affect the magnetic properties. In our study, we compared the iron(II) sulfate salts with different storage time and percentages of bound water and demonstrated that this is not the critical parameter in the synthesis procedure and that regardless of the storage time magnetofection efficacy is pronounced.

In the previous studies it was demonstrated that higher pH (>11) and ionic strength of reaction solution provide small particles and narrow size distribution [22]. In our study we used ammonium hydroxide as a precipitating reagent resulting in the pH 11 of the obtained magnetic fluid. In addition, our results demonstrate that small changes in the conductivity of water, which could influence ionic strength and the ratio between iron(II) and iron(III) ions do not affect the physicochemical properties of SPIONs as well as the subsequent magnetofection efficacy.

Recently, in the published protocol for SPIONs' synthesis using a co-precipitation method, the temperature used was 90°C [21]; however, the recommended temperature for SPIONs' synthesis via co-precipitation stands in the range from 20°C to 90°C [14]. In order to make the method more simple and robust, we tested two different temperatures, room temperature, and 60°C for SPIONs' synthesis. Our results demonstrate that the synthesis performed at both temperatures lead to the size of SPIONs with approx. 10 nm in diameter; nevertheless at room temperature the size is significantly smaller compared to the size of SPIONs synthesized at 60°C. Furthermore, magnetofection of cells is not affected by this difference of SPIONs' size. Therefore, our results indicate that the synthesis of SPIONs for magnetofection can be effectively performed at room temperature.

In the second part of the study, important parameters for the functionalization of SPIONs and subsequent binding of pDNA were evaluated. PEI is a well-known transfection reagent, and it is also used for the coating and/or functionalization of many different nanoparticles [23–25]. However, its effectiveness and usefulness in transfection greatly depend on the specific steps in the preparation of PEI water solution, such as filtration through 0.22 μm membrane for sterilization and removal of an undissolved PEI, heating for the complete dissolution of PEI, and final pH adjustment to the physiological pH (7.4) [26]. We tested three parameters in PEI water solution preparation: the type of dissolving method (using vortex mixer or magnetic stirrer), pH adjustment to 7.4, and filtration through 0.22 μm membrane in order to examine their effect on the functionalization of SPIONs-PAA's surface with PEI and consequent magnetofection efficacy. In contrast to other studies [27], our results demonstrate that pH is a very important parameter for pronounced magnetofection efficacy. It was shown that low pH in endolysosomes/lysosomes influenced further protonation of amine groups of branched PEI and consequent release of transfection complexes from endolysosomes/lysosomes via proton sponge effect [18]. The results of our study demonstrate that the pH adjustment of PEI water solution from 10.5 to physiological 7.4 significantly reduces transfection efficiency of both, PEI-pDNA, and SPIONs-PAA-PEI-pDNA complexes. In accordance with the study conducted by Thomas and Klibanov [18], we can speculate that at lower pH in our hands, maximum protonation degree of PEI was approached. Therefore, further protonation in endolysosomes/lysosomes was reduced leading to diminished release of pDNA from the endolysosomes/lysosomes via the proton sponge effect and consequently to the lower transfection efficiency.

Generally, SPIONs with different biocompatible coatings have already been used as a drug (chemotherapeutics, therapeutic proteins) or gene (therapeutic pDNA, antisense oligonucleotides) carriers for targeted delivery to specific tissues [11, 28–31]. Physicochemical properties and magnetofection efficacy of SPIONs synthesized in our study are comparable to physicochemical properties and magnetofection efficacy of SPIONs used in our previous study as well as to other non-viral transfection methods, such as lipofection and electroporation [2].

5. Conclusion

Our results demonstrate that physicochemical properties and magnetofection efficacy are not affected by varying specific parameters in the synthesis of SPIONs by the co-precipitation with the synthesis conditions and the reagents we used. In principal the robustness of co-precipitation results in a reproducible and efficient magnetofection. The only factor that significantly affects the magnetofection efficacy is the pH of water solution of PEI, which is used for the functionalization of SPIONs-PAA. It should be in an alkaline range in order to obtain pronounced gene expression. SPIONs used in the present study as well as those described in our previous study exhibit comparable physicochemical properties and magnetofection efficacy [2]. Thus, the results of our study could

lead to the preparation of the guidelines for the synthesis procedure with subsequent broader utilization of SPIONs-PAA-PEI complexes for magnetofection, as we demonstrate the robustness of the co-precipitation of iron(II) and iron(III) sulfate salts and reproducibly pronounced gene expression after magnetofection with SPIONs-PAA-PEI.

Acknowledgments

The authors thank Rajnar N., Urh T., Erjavec J., and Lavric M. for all the work they contributed in this research. Research was conducted in the scope of LEA EBAM (French-Slovenian European Associated Laboratory: Pulsed Electric Fields Applications in Biology and Medicine) and COST Action TD1104. Operation part was financed by the European Union, European Social Fund. Operation was implemented in the framework of the Operational Programme for Human Resources Development for the Period 2007–2013, Priority axis 1: Promoting entrepreneurship and adaptability, Main type of activity 1.1.: Experts and researchers for competitive enterprises.

References

[1] S. Prijic and G. Sersa, "Magnetic nanoparticles as targeted delivery systems in oncology," *Radiology and Oncology*, vol. 45, no. 1, pp. 1–16, 2011.

[2] S. Prijic, L. Prosen, M. Cemazar et al., "Surface modified magnetic nanoparticles for immuno-gene therapy of murine mammary adenocarcinoma," *Biomaterials*, vol. 33, no. 17, pp. 4379–4391, 2012.

[3] C. Hüttinger, J. Hirschberger, A. Jahnke et al., "Neoadjuvant gene delivery of feline granulocyte-macrophage colony-stimulating factor using magnetofection for the treatment of feline fibrosarcomas: a phase I trial," *Journal of Gene Medicine*, vol. 10, no. 6, pp. 655–667, 2008.

[4] A. Jahnke, J. Hirschberger, C. Fischer et al., "Intra-tumoral gene delivery of feIL-2, feIFN-γ and feGM-CSF using magnetofection as a neoadjuvant treatment option for feline fibrosarcomas: a phase-I study," *Journal of Veterinary Medicine A*, vol. 54, no. 10, pp. 599–606, 2007.

[5] C. Plank, F. Scherer, U. Schillinger, C. Bergemann, and M. Anton, "Magnetofection: enhancing and targeting gene delivery with superparamagnetic nanoparticles and magnetic fields," *Journal of Liposome Research*, vol. 13, no. 1, pp. 29–32, 2003.

[6] F. Scherer, M. Anton, U. Schillinger et al., "Magnetofection: enhancing and targeting gene delivery by magnetic force *in vitro* and *in vivo*," *Gene Therapy*, vol. 9, no. 2, pp. 102–109, 2002.

[7] S. Xenariou, U. Griesenbach, S. Ferrari et al., "Using magnetic forces to enhance non-viral gene transfer to airway epithelium *in vivo*," *Gene Therapy*, vol. 13, no. 21, pp. 1545–1552, 2006.

[8] C. Plank, O. Zelphati, and O. Mykhaylyk, "Magnetically enhanced nucleic acid delivery. Ten years of magnetofection-progress and prospects," *Advanced Drug Delivery Reviews*, vol. 63, no. 14-15, pp. 1300–1331, 2011.

[9] O. Mykhaylyk, O. Zelphati, E. Hammerschmid, M. Anton, J. Rosenecker, and C. Plank, "Recent advances in magnetofection and its potential to deliver siRNAs *in vitro*," *Methods in Molecular Biology*, vol. 487, pp. 111–146, 2009.

[10] T. Buerli, C. Pellegrino, K. Baer et al., "Efficient transfection of DNA or shRNA vectors into neurons using magnetofection," *Nature protocols*, vol. 2, no. 12, pp. 3090–3101, 2007.

[11] F. Krötz, C. de Wit, H. Y. Sohn et al., "Magnetofection—a highly efficient tool for antisense oligonucleotide delivery *in vitro* and *in vivo*," *Molecular Therapy*, vol. 7, no. 5, part 1, pp. 700–710, 2003.

[12] S. Prijic, J. Scancar, R. Romih et al., "Increased cellular uptake of biocompatible superparamagnetic iron oxide nanoparticles into malignant cells by an external magnetic field," *Journal of Membrane Biology*, vol. 236, no. 1, pp. 167–179, 2010.

[13] M. Mahmoudi, S. Sant, B. Wang, S. Laurent, and T. Sen, "Superparamagnetic iron oxide nanoparticles (SPIONs): development, surface modification and applications in chemotherapy," *Advanced Drug Delivery Reviews*, vol. 63, no. 1-2, pp. 24–46, 2011.

[14] Wahajuddin and S. Arora, "Superparamagnetic iron oxide nanoparticles: magnetic nanoplatforms as drug carriers," *International Journal of Nanomedicine*, vol. 7, pp. 3445–3471, 2012.

[15] L. Tong, M. Zhao, S. Zhu, and J. Chen, "Synthesis and application of superparamagnetic iron oxide nanoparticles in targeted therapy and imaging of cancer," *Frontiers of Medicine*, vol. 5, no. 4, pp. 379–387, 2011.

[16] O. Boussif, F. LezoualC'h, M. A. Zanta et al., "A versatile vector for gene and oligonucleotide transfer into cells in culture and *in vivo*: polyethylenimine," *Proceedings of the National Academy of Sciences of the United States of America*, vol. 92, no. 16, pp. 7297–7301, 1995.

[17] D. Edinger and E. Wagner, "Bioresponsive polymers for the delivery of therapeutic nucleic acids," *Wiley Interdisciplinary Reviews*, vol. 3, no. 1, pp. 33–46, 2011.

[18] M. Thomas and A. M. Klibanov, "Non-viral gene therapy: polycation-mediated DNA delivery," *Applied Microbiology and Biotechnology*, vol. 62, no. 1, pp. 27–34, 2003.

[19] R. Massart, "Preparation of aqueous magnetic liquids in alkaline and acidic media," *IEEE Transactions on Magnetics*, vol. 17, no. 2, pp. 1247–1248, 1981.

[20] J. Chatterjee, Y. Haik, and C. J. Chen, "Size dependent magnetic properties of iron oxide nanoparticles," *Journal of Magnetism and Magnetic Materials*, vol. 257, no. 1, pp. 113–118, 2003.

[21] O. Mykhaylyk, Y. S. Antequera, D. Vlaskou, and C. Plank, "Generation of magnetic nonviral gene transfer agents and magnetofection *in vitro*," *Nature Protocols*, vol. 2, no. 10, pp. 2391–2411, 2007.

[22] J. Lodhia, G. Mandarano, N. J. Ferris, P. Eu, and S. F. Cowell, "Development and use of iron oxide nanoparticles (Part 1): synthesis of iron oxide nanoparticles for MRI," *Biomedical Imaging and Intervention Journal*, vol. 6, no. 2, article e12, 2010.

[23] Y. Hu, G. Tang, J. Liu et al., "FGF receptor-mediated gene delivery using ligands coupled to PEI-β-CyD," *Journal of Biomedicine and Biotechnology*, vol. 2012, Article ID 989235, 7 pages, 2012.

[24] V. Cebrián, F. Martín-Saavedra, C. Yagüe, M. Arruebo, J. Santamaría, and N. Vilaboa, "Size-dependent transfection efficiency of PEI-coated gold nanoparticles," *Acta Biomaterialia*, vol. 7, no. 10, pp. 3645–3655, 2011.

[25] Y. Zhou, Z. Tang, C. Shi, S. Shi, Z. Qian, and S. Zhou, "Polyethylenimine functionalized magnetic nanoparticles as a potential non-viral vector for gene delivery," *Journal of Material Science*, vol. 23, no. 11, pp. 2697–2708, 2012.

[26] J. R. Toledo, Y. Prieto, N. Oramas, and O. Sánchez, "Polyethylenimine-based transfection method as a simple and effective way to produce recombinant lentiviral vectors," *Applied*

Biochemistry and Biotechnology, vol. 157, no. 3, pp. 538–544, 2009.

[27] W. T. Godbey, K. K. Wu, and M. G. Mikos, "Size matters: molecular weight affects the efficiency of poly(ethylenimine) as a gene delivery vehicle," *Journal of Biomedical Materials Research*, vol. 45, no. 3, pp. 268–275, 1999.

[28] A. Z. Wang, V. Bagalkot, C. C. Vasilliou et al., "Superparamagnetic iron oxide nanoparticle-aptamer bioconjugates for combined prostate cancer imaging and therapy," *ChemMedChem*, vol. 3, no. 9, pp. 1311–1315, 2008.

[29] M. Y. Hua, H. W. Yang, C. K. Chuang et al., "Magnetic-nanoparticle-modified paclitaxel for targeted therapy for prostate cancer," *Biomaterials*, vol. 31, no. 28, pp. 7355–7363, 2010.

[30] F. N. Al-Deen, J. Ho, C. Selomulya, C. Ma, and R. Coppel, "Superparamagnetic nanoparticles for effective delivery of malaria DNA vaccine," *Langmuir*, vol. 27, no. 7, pp. 3703–3712, 2011.

[31] C. G. Hadjipanayis, R. Machaidze, M. Kaluzova et al., "EGFRvIII antibody-conjugated iron oxide nanoparticles for magnetic resonance imaging-guided convection-enhanced delivery and targeted therapy of glioblastoma," *Cancer Research*, vol. 70, no. 15, pp. 6303–6312, 2010.

Hindawi Publishing Corporation
BioMed Research International
Volume 2013, Article ID 710502, 7 pages
http://dx.doi.org/10.1155/2013/710502

Research Article

A Polyethylenimine-Linoleic Acid Conjugate for Antisense Oligonucleotide Delivery

Jing Xie,[1,2] Lesheng Teng,[1,2] Zhaogang Yang,[1] Chenguang Zhou,[2] Yang Liu,[2] Bryant C. Yung,[2] and Robert J. Lee[1,2]

[1] *Institute of Life Sciences, Jilin University, Changchun, Jilin 130023, China*
[2] *Division of Pharmaceutics, College of Pharmacy, The Ohio State University, Columbus, OH 43210, USA*

Correspondence should be addressed to Robert J. Lee; lee.1339@osu.edu

Received 4 January 2013; Revised 28 April 2013; Accepted 5 May 2013

Academic Editor: Susana N. Diniz

A novel antisense oligonucleotide (ASO) carrier, polyethylenimine conjugated to linoleic acid (PEI-LA), was synthesized and evaluated for delivery of LOR-2501 to tumor cells. LOR-2501 is an ASO targeting ribonucleotide reductase R1 subunit (RRM1). In this study, PEI-LA was synthesized by reacting PEI (Mw ~ 800) with linoleoyl chloride. Gel retardation assay showed complete complexation between PEI-LA and LOR-2501 at N/P ratio above 8. No significant cytotoxicity was observed with these complexes at the tested dosage levels. Interestingly, at N/P ratio of >6, levels of cellular uptake of PEI-LA/LOR-2501 were double that of PEI/LOR-2501 complexes of the same N/P ratio. PEI-LA/LOR-2501 induced downregulation of 64% and 70% of RRM1 at mRNA and protein levels, respectively. The highest transfection activity was shown by PEI-LA/LOR-2501 complexes at N/P ratio of 10. Finally, using pathway specific inhibitors, clathrin-mediated endocytosis was shown to be the principle mechanism of cellular internalization of these complexes. In conclusion, PEI-LA is a promising agent for the delivery of ASOs and warrants further investigation.

1. Introduction

Antisense oligonucleotide (ASO) therapy is an emerging therapeutic modality for the treatment of human diseases, including cancer [1–3]. An ASO targets a specific mRNA sequence, reducing its expression [4–6]. A number of ASOs have entered clinical trial [7–9]. However, clinical success for ASO has been very limited, possibly due to the lack of an effective delivery system [10–12]. LOR-2501 is a 20-mer phosphorothioate ASO targeting the R1 subunit of ribonucleotide reductase [13], an enzyme associated with drug resistance. LOR-2501 has shown potent antitumor activities in murine xenograft tumors of the lung, the liver, the ovary, the brain, the breast, and the pancreas. LOR-2501 has been studied in a phase I clinical trial in 2006 for the treatment of prostate cancer [13, 14]. The efficacy of LOR-2501 is dependent on its successful delivery to the cytoplasm. Polyethylenimine (PEI) is a homopolymer with high positive charge density and endosomolytic activity [15–17]. High molecular weight (25 kDa) PEI has frequently been used for gene delivery [18–20]. However, it is fairly cytotoxic [21–23]. Low molecular weight (~800 Da) PEI demonstrates much lower cytotoxicity but is much less active in transfection [22, 24, 25]. Previous studies have shown that conjugating PEI to a lipophilic moiety greatly improved its transfection activity [26, 27]. In the present study, a novel conjugate, PEI-LA was synthesized and evaluated as a carrier for ASO. PEI-LA/LOR-2501 was evaluated in KB cells for biological activity. The mechanism of cellular internalization was also investigated.

2. Materials and Methods

2.1. Materials. PEI-800 (polyethylenimine 800 Da), triethylamine, and linoleoyl chloride were purchased from Sigma-Aldrich (St. Louis, MO, USA). Sucrose and anhydrous diethylether were purchased from Fisher Scientific (Pittsburgh, PA, USA). CellTiter 96 AQueous One Solution Cell Proliferation Assay System (MTS Assay Kit) was purchased from Promega (Madison, WI, USA). LOR-2501 (5′-CTC TAG CGT CTT AAA GCC GA-3′, fully phosphorothioate substituted) was purchased from Alpha DNA.

2.2. Synthesis and Characterization of PEI-LA Conjugate. PEI-LA was synthesized by N-acylation of PEI-800. Briefly, 32 mg PEI-800 was dissolved in 2.5 mL dichloromethane. Triethylamine (50 μL) and then 48 mg linoleoyl chloride, dissolved in 2.5 mL dichloromethane, were slowly added to the stirring solution of PEI. The reaction proceeded for 12 h at room temperature. An excess of diethylether was used to precipitate and then wash the product PEI-LA. Finally, the product was dried under vacuum for 2 h. The product was then analyzed by ^{1}H NMR (300 MHz, $CDCl_3$). The characteristic proton chemical shifts are in PEI, $-NCH_2-CH_2N-$, $\delta \sim 2.50$–3.50 ppm (m, 40H); in LA, δ 0.87 ppm (t, 3H, terminal $-CH_3$), 1.25 ppm (m, 16H, $-(CH_2)_3CH_3$ and $-(CH_2)_5-$), 1.75 ppm (b, 2H, $-(CH_2)_5CH_2CO-$), 2.01 ppm (m, 4H, $-CH_2CHCHCH_2CHCHCH_2-$), 2.25 ppm (b, 2H, $=CHCH_2CH=$), and 5.74 ppm (b, 4H, $-CH=CHCH_2CH=$ CH–).

2.3. Determination of PEI-LA/ASO Complex Formation. An agarose gel retardation assay was conducted to determine the capacity of PEI-LA to form an electrostatic complex with ASO. ASO LOR-2501 was combined with PEI-LA to form complexes at N/P ratios of 1–10. The samples were maintained at room temperature for 30 min and then loaded onto a 1% (w/v) agarose gel containing 0.5 μg/mL ethidium bromide. Electrophoresis was conducted at 100 V for 20 min. The gel was imaged under UV light on an ImageMaster VDS (Pharmacia, Sweden).

2.4. Particle Size and Zeta Potential Analysis. Particle size of PEI-LA/ASO complexes was determined by dynamic light scattering (DLS) on an NICOMP submicron particle sizer 370 (Santa Barbara, CA, USA) under the volume-weighted setting. The zeta potential of PEI-LA was determined on a ZetaPALS instrument (Brookhaven Instruments Corp., Worcestershire, NY, USA) after dilution to a volume of 1.4 mL in 0.1X PBS.

2.5. Cell Culture. KB cells (a subline of HeLa) were grown in Dulbecco's Modified Eagle Medium (DMEM) (Invitrogen, Grand Island, NY, USA) supplemented with 10% fetal bovine serum (FBS) and 1% penicillin/streptomycin. The cells were maintained at 37°C under a humidified atmosphere containing 5% CO_2.

2.6. Cytotoxicity Assay. KB cells were seeded at a density of 1×10^4 cells/cm^2 in a 96-well plate 24 h prior to transfection. Cells were washed three times with serum-free media and incubated with PEI-LA/LOR-2501 with varying N/P ratios. Transfection media was removed after 4 h. Fresh culture media was then added, and the cells were incubated at 37°C for an additional 44 h. Then, cell viability was analyzed by MTS assay per the manufacturer's instructions. Briefly, 20 μL MTS solution was added to each well, and the plate was incubated for 1 h at 37°C. Optical density at 490 nm was determined on a standard plate reader. Cell survival was reported as a percentage of the untreated control.

2.7. Confocal Microscopy. KB cells were seeded in a chambered cover glass slide overnight and treated with either fluorescent Cy3-LOR-2501 or PEI-LA/Cy3-LOR-2501 for 1 h at 37°C. Cellular nuclei were stained with Hoechst 33342 (Invitrogen, Grand Island, NY, USA) for 5 min at room temperature. Internalization of free or complexed Cy3-LOR-2501 was observed by an Olympus FV1000 confocal microscope (Olympus Optical Co., Tokyo, Japan).

2.8. Flow Cytometry. KB cells were seeded in a 24-well plate at a density of 5×10^4 cells/well. After 24 h of incubation at 37°C, cells were washed with serum-free media and treated with PEI-LA/LOR-2501, free LOR-2501, or PEI/LOR-2501 in serum-free media for 1 h. Following treatment, cells were washed with DMEM, harvested, fixed in 4% formalin, and analyzed on an EPIC XL flow cytometer (Beckman Coulter Inc., CA, USA).

2.9. Quantitative Analysis of mRNA by RT-PCR. The effect of LOR-2501 complexes on R1 mRNA level was determined by RT-PCR. KB cells were seeded in a 6-well plate at a density of 1×10^4 cells/cm^2 overnight at 37°C. Cells were treated with PEI-LA/LOR-2501 with varying N/P ratios, free LOR-2501, or PEI/LOR-2501 in serum-free media for 4 h. After treatment, cells were washed three times with 1X PBS, and fresh media was added. Cells were incubated for an additional 44 h. After incubation, media was removed and cells were treated with 1 mL TRIzol reagent per well. RNA was then extracted and purified according to the manufacturer's protocol. RNA was quantified on a NanoDrop 2000 spectrophotometer by measuring OD at 260 nm (Thermo Scientific, Waltham, MA, USA) and converted to cDNA by SuperScript III first-strand synthesis system (Invitrogen, Grand Island, NY, USA) according to the manufacturer's instruction. A PHC-3 thermal cycler (Bio-RAD, Hercules, CA, USA) was used to amplify the cDNA which was then combined with SYBR Green and the appropriate primers for amplification by real-time PCR. R1 mRNA was normalized against β-actin.

2.10. Determination of R1 Protein Expression by Western Blot. Western blot was used to determine the effect of LOR-2501 on R1 protein expression. KB cells, treated as described in the section above, were lysed with a lysis buffer (150 mM NaCl, 50 mM Tris-HCl pH 7.4, 1% v/v NP40) containing a protease inhibitor cocktail (Roche). Protein was quantified by BCA assay (Pierce, Rockford, IL, USA). Then, 20 μg protein samples were loaded onto a 10% SDS-PAGE gel for electrophoresis. Proteins were then transferred to a nitrocellulose membrane. Transferred blots were blocked with 5% nonfat milk in Tris-buffered saline/Tween-20 for 1 h and immunoblotted against the primary antibodies, either goat anti-human R1 (Dako, Carpinteria, CA, USA) or rabbit anti-human GAPDH antibody (Santa Cruz, Santa Cruz, CA, USA), at 4°C overnight. This was followed by incubation with horseradish peroxidase-conjugated rabbit anti-goat IgG (Pierce, Rockford, IL, USA) or goat anti-rabbit IgG (Amersham Biosciences, Piscataway, NJ, USA) for 1 h at room temperature. Blots were developed on an enhanced

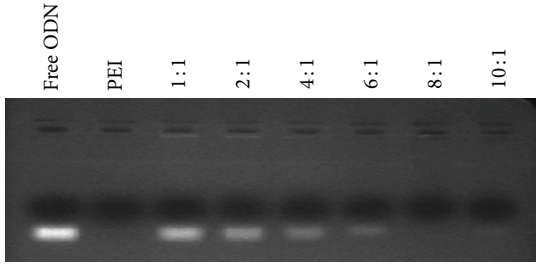

Figure 1: Agarose gel analysis of PEI-LA/LOR-2501 complexes. A series of PEI-LA/LOR-2501 complexes were prepared at varying N/P ratios and analyzed on a 1% agarose gel, as described in Section 2.3.

chemiluminescence (ECL) detection system (GE Healthcare, Waukesha, WI, USA) [28, 29].

2.11. Treatment with Endocytosis Inhibitors. KB cells were seeded in a 24-well plate at a density of 5×10^4 cells/well. After 24 h of incubation at 37°C, cells were washed with serum-free media and treated with media containing wortmannin (10 μM), filipin (1 μM), or sucrose (1 M) for 1 h. Wortmannin, filipin, and sucrose are specific inhibitors of macropinocytosis, caveolae/lipid raft-mediated endocytosis, and clathrin-mediated endocytosis respectively. After removing the inhibitor solution, cells were treated with FAM-LOR-2501 or PEI-LA/Cy3-LOR-2501 for 1 h. Cells were then washed twice with PBS and fixed in 4% formalin. Cellular uptake was analyzed on an EPICS XL flow cytometer.

3. Results

3.1. Characterization of PEI-LA/LOR-2501 Complexes. Degree of complexation between PEI-LA and LOR-2501 was measured by an agarose gel retardation assay. As shown in Figure 1, PEI-LA was able to completely retard LOR-2501 at N/P above 8. The results of particle size and zeta potential analyses are shown in Figure 2. The data showed that increasing the concentration of PEI-LA induced a reversal of zeta potential from negative to positive. Particle size measurement by dynamic light scattering revealed the successful formation of PEI-LA/LOR-2501 particles of under 200 nm in diameter at N/P above 8.

3.2. Cytotoxicity of PEI-LA/LOR-2501 Complexes. The cytotoxicity of PEI-LA/LOR-2501 complexes was measured in KB cells by MTS assay. As shown in Figure 3, cell viability was maintained at over 90% across all PEI-LA/LOR-2501 complexes ($P > 0.05$).

3.3. Confocal Microscopy. In order to investigate the uptake of PEI-LA/LOR-2501 by KB cells, confocal microscopy was employed (Figure 4). The results showed extensive internalization of fluorescently labeled Cy3-LOR-2501 (red, Figure 4(b)) and trafficking to the cytosol. Blue Hoechst 33342 stain was used for observation of the cellular nuclei (Figure 4(a)). A phase contrast image (Figure 4(c)) and an overlay of fluorescent images (Figure 4(d)) are shown as well.

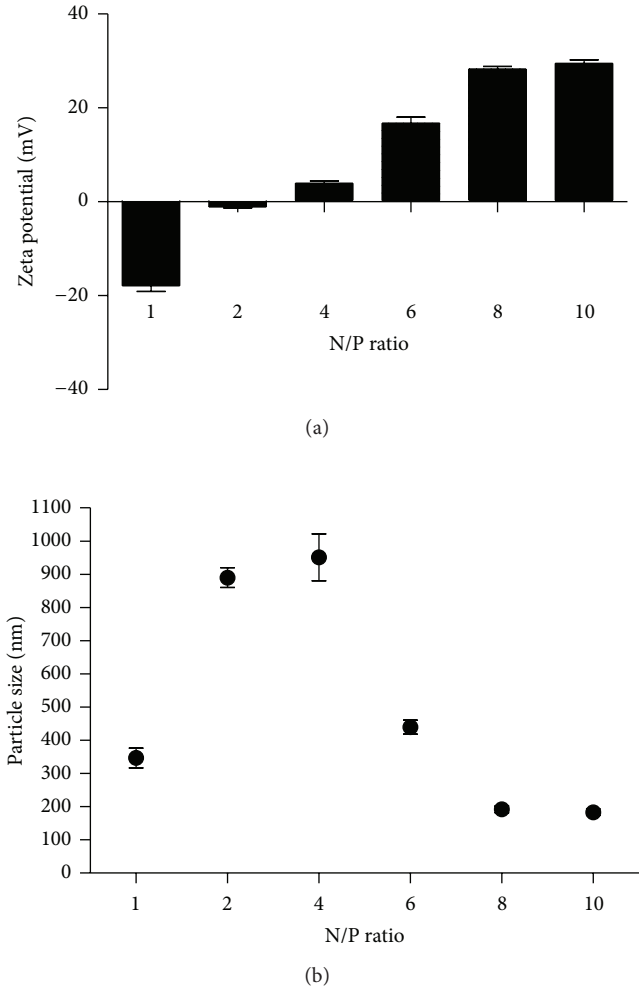

Figure 2: Zeta potential of PEI-LA/LOR-2501 complexes. A series of PEI-LA/LOR-2501 complexes were prepared at varying N/P ratios. Zeta potential and particle size were then measured, as described in Section 2.4.

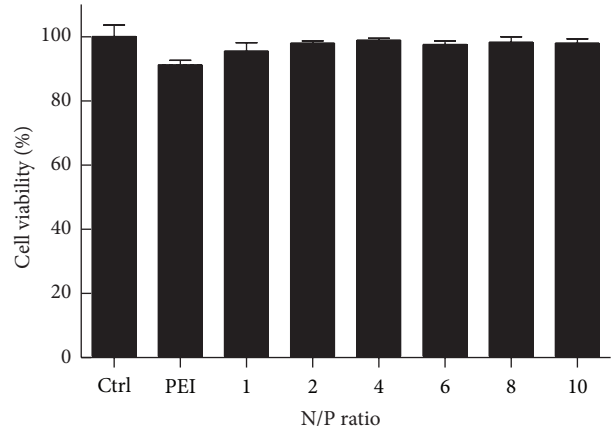

Figure 3: Cytotoxicity of PEI-LA/LOR-2501 complexes. A series of PEI-LA/LOR-2501 complexes were prepared at varying N/P ratios and then added to KB cells. Cell viability was determined by MTS assay at 44 h after transfection.

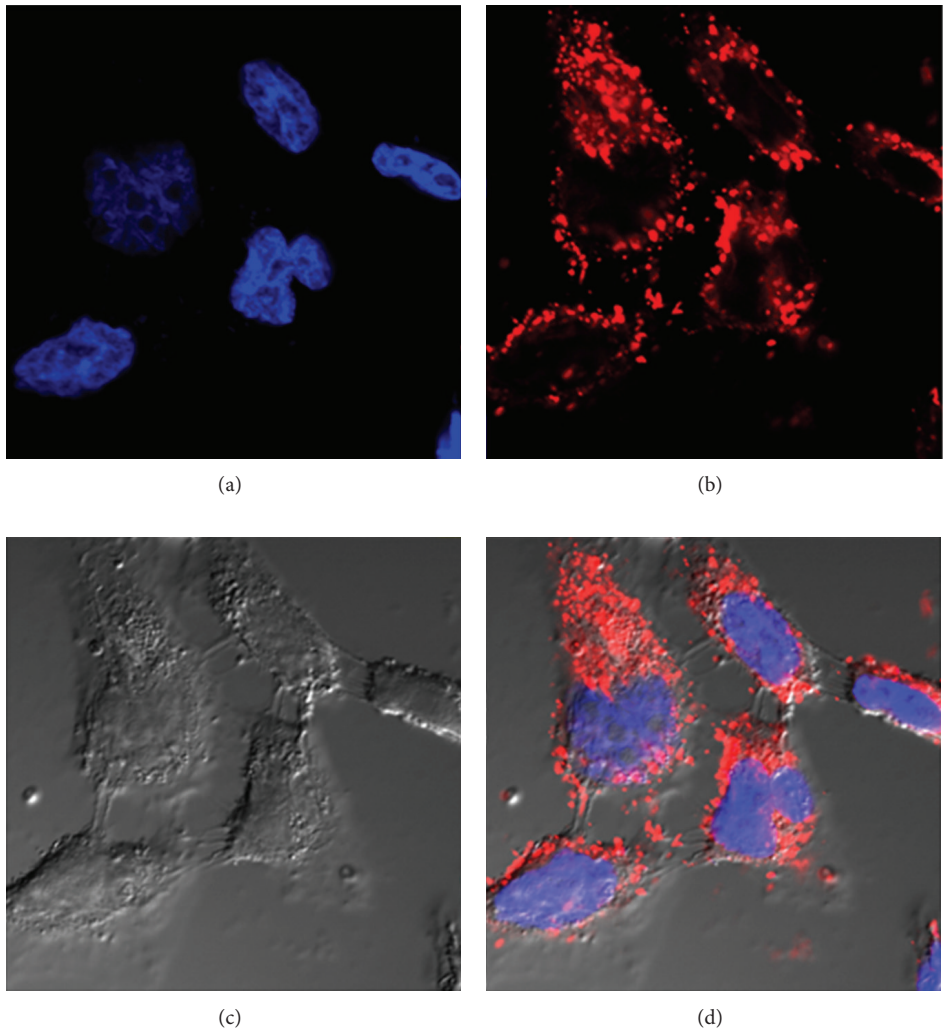

Figure 4: Intracellular localization of PEI-LA/LOR-2501 complexes. KB cells were incubated with PEI-LA complexed to Cy3-labeled LOR-2501 and then evaluated by confocal microscopy. Cy3 fluorescence is shown in red with Hoechst 33342 nuclear stain shown in blue.

3.4. Flow Cytometry. Similarly, flow cytometry was used to study the uptake of the PEI-LA/LOR-2501 complexes by KB cells. As shown in Figure 5(a), when the N/P ratio of PEI-LA/LOR-2501 complexes was 8, the cells exhibited markedly increased fluorescence intensity relative to those treated with fluorescent-free ASO. Moreover, PEI-LA/LOR-2501 was shown to have higher delivery efficiency than PEI-800 (Figure 5(b)).

3.5. Determination of R1 mRNA Expression by Quantitative RT-PCR. Functional delivery of LOR-2501 with PEI-LA was confirmed by real-time RT-PCR analysis (Figure 6). It was shown that PEI-LA/LOR-2501 induced downregulation of R1 mRNA expression. Greater downregulation was observed at higher N/P ratio. With the control PEI/ASO complexes, mRNA decreased by only 20%. Much greater downregulation of 51% to 64% was encountered for PEI-LA/LOR-2501 complexes at N/P ratios of 6 and 10, respectively. Free LOR-2501 showed only a slight capacity for mRNA downregulation.

3.6. Determination of R1 Protein Expression by Western Blot. Western blot analysis was conducted to determine the effect of PEI-LA/LOR-2501 on R1 protein level. As shown in Figure 7, free ASO and PEI/LOR-2501 exhibited minimal decreases in R1 protein levels. At higher N/P ratios, the PEI-LA/LOR-2501 complexes showed significant downregulation activity. From N/P 6 to 10, protein downregulation increased from 59% to 70%.

3.7. Treatment with Inhibitors. Mechanistic study (Figure 8) of the cellular uptake and trafficking mechanisms is critical to the understanding of the relationship between nanoparticle design and transfection efficiency [30, 31]. Inhibition by filipin, a lipid raft/caveolae-mediated endocytosis inhibitor, reduced uptake by 10%. Inhibition by sucrose, a clathrin-mediated endocytosis inhibitor, reduced uptake by 81%. Inhibition by wortmannin, a macropinocytosis inhibitor, reduced uptake by 52%. Taken together, it is apparent that PEI-LA utilizes all three modes of endocytic transport, with

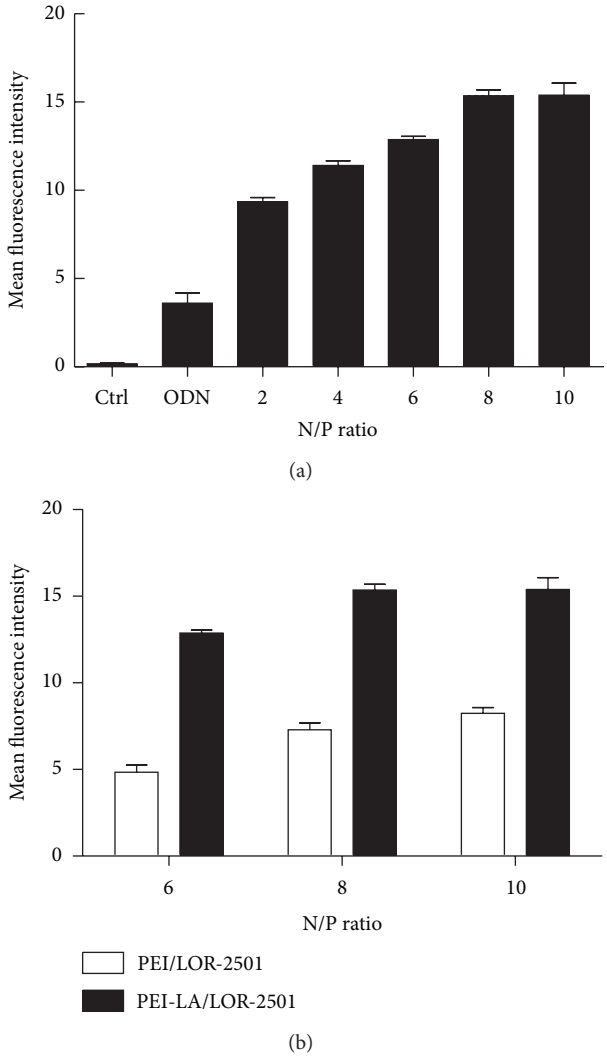

Figure 5: Effect of N/P ratio on cellular uptake of ODN complexes. (a) Cellular uptake of PEI-LA/Cy3-LOR-2501. (b) Cellular uptake of PEI-LA/ASO and of PEI/ASO. A series of PEI or PEI-LA/LOR-2501 complexes were prepared at varying N/P ratios. Cellular uptake was determined by mean fluorescence intensity by flow cytometry.

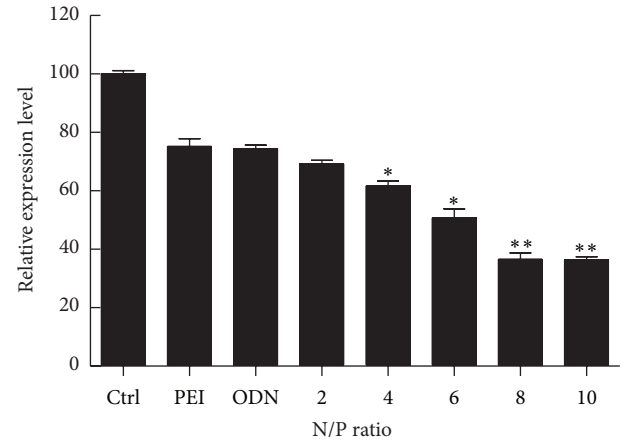

Figure 6: Downregulation of R1 mRNA in KB cells. A series of PEI-LA/LOR-2501 complexes were prepared at varying N/P ratios. R1 mRNA levels were determined by qRT-PCR, relative to β-actin, as described in Section 2.9.

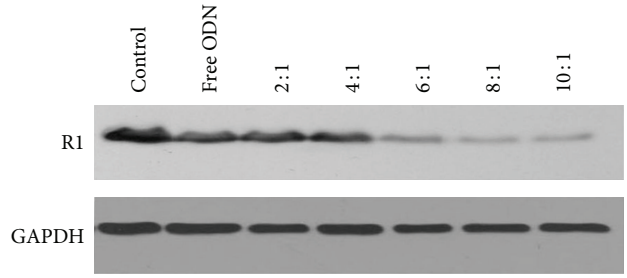

Figure 7: Downregulation of R1 protein in KB cells. A series of PEI-LA/LOR-2501 complexes were prepared at varying N/P ratios. R1 protein and GAPDH levels were determined by Western blot, as described in Section 2.10.

clathrin-mediated endocytosis taking on a leading role in PEI-LA/LOR-2501 delivery.

4. Discussion

Clinical translation of ASO-based therapies has been limited by inefficient delivery of oligonucleotides [32, 33]. In this study, a novel carrier, PEI-LA, was designed and synthesized for use as a delivery agent. PEI-LA has demonstrated excellent properties as a transfection agent. Gel retardation demonstrated total complexation between PEI-LA and LOR-2501 at N/P of 8. Further, no significant cytotoxicity was observed with formulations at the tested dosage levels.

Surface charge of PEI-LA/ASO is an important factor in determining efficiency of cellular uptake. At the N/P ratio >8 (Figure 2), zeta potentials of PEI-LA/ASO increased and then plateaued at between +25 and +35 mV. PEI-LA/ASO complexes bearing a positive surface potential should facilitate efficient interaction with a negatively charged cell surface [34, 35].

We evaluated the uptake of PEI-LA/ASO in KB cells and found that PEI-LA/ASO generated outstanding transfection activities compared to free ASO. In fact, as we increased PEI-LA/ASO N/P ratio to greater than 6, the cellular uptake of PEI-LA/ASO reached double that of PEI-800 complexes at the same N/P ratio. In addition, PEI-LA/ASO showed much higher transfection efficiency relative to unconjugated low molecular weight PEI as shown by the relative increases in mRNA and protein downregulation. This is consistent with previous reports on hydrophobically modified PEI by Kim et al. and by Teng et al. [26, 27]. The most potent transfection activity was shown with the PEI-LA/LOR-2501 formulation at N/P of 10. The LA moiety has two cis-double bonds, whereas in the previously reported PEI-oleic acid conjugate [27], oleic acid contained a single cis-double bond. The superior transfection activity of PEI-LA is possibly due to the polyunsaturated characteristic of the LA moieties, which may promote bilayer disruption and increased endosomal escape of the ASO following internalization by endocytosis.

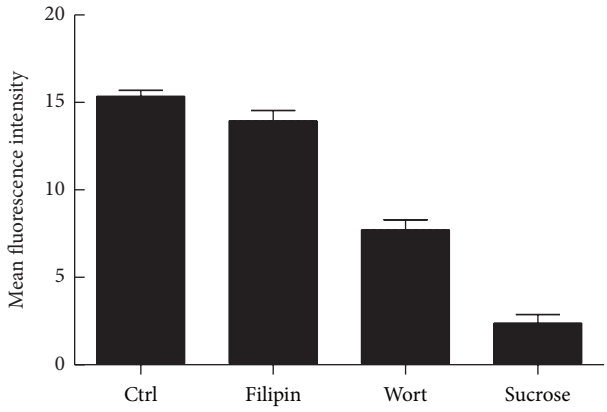

Figure 8: The effect of inhibitor treatment on PEI-LA/Cy3-LOR-2501 uptake. KB cells were treated with various pathway specific endocytosis inhibitors and incubated with PEI-LA/Cy3-LOR-2501 complexes. Cellular uptake was determined by flow cytometry, as described in Section 2.11.

The PEI-LA/LOR-2501 complexes showed increased cellular uptake compared to the control PEI/LOR-2501 complexes and greater target downregulatory activities. This may be due to the stabilization of the complexes due to the hydrophobic interactions between the LA moieties. It is interesting that some uptakes were observed with free Cy3-labeled oligos. This may be due to nonspecific cellular uptake due to the use of serum-free media. The observed downregulation was modest. It is worth noting that free LOR-2501 has shown potent antitumor activities in the absence of delivery agent *in vivo* [13], which suggests that it may have some capacity for cellular entry on its own.

Observations by confocal microscopy and data from flow cytometry showed successful delivery of ASO into the cell. Subcellular distribution of the PEI-LA/ASO, as shown in Figure 4, indicated that ASO (red) was localized in the cytoplasm but not in the nucleus (blue). Finally, experiments using internalization inhibitors showed that clathrin-mediated endocytosis was the principle mechanism of entry. Identification of these trafficking mechanisms will be beneficial to further optimization of the formulation.

5. Conclusion

PEI-LA is a promising novel agent for the delivery of ASO. The addition of LA to low molecular weight PEI increases delivery efficiency without introducing vehicle-related cytotoxicity. PEI-LA/LOR-2501 was able to efficiently downregulate R1 mRNA and protein levels and, therefore, is a promising candidate for further development. Future studies will evaluate PEI-LA/LOR-2501 in *in vivo* models to evaluate its therapeutic potential.

Authors' Contribution

Jing Xie and Lesheng Teng contributed equally to this work.

Acknowledgments

This work was supported in part by Grant CA135243 to Robert J. Lee.

References

[1] D. A. Braasch and D. R. Corey, "Novel antisense and peptide nucleic acid strategies for controlling gene expression," *Biochemistry*, vol. 41, no. 14, pp. 4503–4510, 2002.

[2] K. T. Flaherty, J. P. Stevenson, and P. J. O'Dwyer, "Antisense therapeutics: lessons from early clinical trials," *Current Opinion in Oncology*, vol. 13, no. 6, pp. 499–505, 2001.

[3] J. B. Opalinska and A. M. Gewirtz, "Nucleic-acid therapeutics: basic principles and recent applications," *Nature Reviews Drug Discovery*, vol. 1, no. 7, pp. 503–514, 2002.

[4] T. Aboul-Fadl, "Antisense oligonucleotides: the state of the art," *Current Medicinal Chemistry*, vol. 12, no. 19, pp. 2193–2214, 2005.

[5] B. L. Davidson and P. B. McCray, "Current prospects for RNA interference-based therapies," *Nature Reviews Genetics*, vol. 12, no. 5, pp. 329–340, 2011.

[6] C. A. Stein and Y. C. Cheng, "Antisense oligonucleotides as therapeutic agents—is the bullet really magical?" *Science*, vol. 261, no. 5124, pp. 1004–1012, 1993.

[7] S. Mani, C. M. Rudin, K. Kunkel et al., "Phase I clinical and pharmacokinetic study of protein kinase C-α antisense oligonucleotide ISIS 3521 administered in combination with 5-fluorouracil and leucovorin in patients with advanced cancer," *Clinical Cancer Research*, vol. 8, no. 4, pp. 1042–1048, 2002.

[8] G. Monteleone, M. C. Fantini, S. Onali et al., "Phase I clinical trial of Smad7 knockdown using antisense oligonucleotide in patients with active Crohn's disease," *Molecular Therapy*, vol. 20, no. 4, pp. 870–876, 2012.

[9] C. S. Zent, B. J. Smith, Z. K. Ballas et al., "Phase I clinical trial of CpG oligonucleotide 7909 (PF-03512676) in patients with previously treated chronic lymphocytic leukemia," *Leukemia & Lymphoma*, vol. 53, no. 2, pp. 211–217, 2012.

[10] E. Fattal and G. Barratt, "Nanotechnologies and controlled release systems for the delivery of antisense oligonucleotides and small interfering RNA," *British Journal of Pharmacology*, vol. 157, no. 2, pp. 179–194, 2009.

[11] G. de Rosa and M. I. La Rotonda, "Nano and microtechnologies for the delivery of oligonucleotides with gene silencing properties," *Molecules*, vol. 14, no. 8, pp. 2801–2823, 2009.

[12] S. Agrawal, J. Temsamani, W. Galbraith, and J. Tang, "Pharmacokinetics of antisense oligonucleotides," *Clinical Pharmacokinetics*, vol. 28, no. 1, pp. 7–16, 1995.

[13] Y. Lee, A. Vassilakos, N. Feng et al., "GTI-2501, an antisense agent targeting R1, the large subunit of human ribonucleotide reductase, shows potent anti-tumor activity against a variety of tumors," *International Journal of Oncology*, vol. 28, no. 2, pp. 469–478, 2006.

[14] Y. Ko, S. North, S. R. Berry et al., "Dose escalation phase of a phase I/II study of GTI-2501, an antisense to the R1 subunit of ribonucleotide reductase (RNR) and docetaxel in patients with metastatic hormone-refractory prostate cancer," *Journal of Clinical Oncology*, vol. 24, no. 18, p. 98S, 2006.

[15] A. Akinc, M. Thomas, A. M. Klibanov, and R. Langer, "Exploring polyethylenimine-mediated DNA transfection and the proton sponge hypothesis," *Journal of Gene Medicine*, vol. 7, no. 5, pp. 657–663, 2005.

[16] O. Boussif, M. A. Zanta, and J. P. Behr, "Optimized galenics improve in vitro gene transfer with cationic molecules up to 1000-fold," *Gene Therapy*, vol. 3, no. 12, pp. 1074–1080, 1996.

[17] R. Kircheis, L. Wightman, A. Schreiber et al., "Polyethylenimine/DNA complexes shielded by transferrin target gene expression to tumors after systemic application," *Gene Therapy*, vol. 8, no. 1, pp. 28–40, 2001.

[18] O. Boussif, F. Lezoualc'h, M. A. Zanta et al., "A versatile vector for gene and oligonucleotide transfer into cells in culture and in vivo: polyethylenimine," *Proceedings of the National Academy of Sciences of the United States of America*, vol. 92, no. 16, pp. 7297–7301, 1995.

[19] R. Deng, Y. Yue, F. Jin et al., "Revisit the complexation of PEI and DNA—how to make low cytotoxic and highly efficient PEI gene transfection non-viral vectors with a controllable chain length and structure?" *Journal of Controlled Release*, vol. 140, no. 1, pp. 40–46, 2009.

[20] H. Tian, W. Xiong, J. Wei et al., "Gene transfection of hyperbranched PEI grafted by hydrophobic amino acid segment PBLG," *Biomaterials*, vol. 28, no. 18, pp. 2899–2907, 2007.

[21] S. Boeckle, K. von Gersdorff, S. van der Piepen, C. Culmsee, E. Wagner, and M. Ogris, "Purification of polyethylenimine polyplexes highlights the role of free polycations in gene transfer," *Journal of Gene Medicine*, vol. 6, no. 10, pp. 1102–1111, 2004.

[22] M. Thomas, Q. Ge, J. J. Lu, J. Chen, and A. M. Klibanov, "Cross-linked small polyethylenimines: while still nontoxic, deliver DNA efficiently to mammalian cells in vitro and in vivo," *Pharmaceutical Research*, vol. 22, no. 3, pp. 373–380, 2005.

[23] M. L. Forrest, J. T. Koerber, and D. W. Pack, "A degradable polyethylenimine derivative with low toxicity for highly efficient gene delivery," *Bioconjugate Chemistry*, vol. 14, no. 5, pp. 934–940, 2003.

[24] G. P. Tang, Z. Yang, and J. Zhou, "Poly(ethylenimine)-grafted-poly[(aspartic acid)-co-lysine], a potential non-viral vector for DNA delivery," *Journal of Biomaterials Science, Polymer Edition*, vol. 17, no. 4, pp. 461–480, 2006.

[25] H. Gharwan, L. Wightman, R. Kircheis, E. Wagner, and K. Zatloukal, "Nonviral gene transfer into fetal mouse livers (a comparison between the cationic polymer PEI and naked DNA)," *Gene Therapy*, vol. 10, no. 9, pp. 810–817, 2003.

[26] S. Kim, J. S. Choi, H. S. Jang, H. Suh, and J. Park, "Hydrophobic modification of polyethyleneimine for gene transfectants," *Bulletin of the Korean Chemical Society*, vol. 22, no. 10, pp. 1069–1075, 2001.

[27] L. S. Teng, J. Xie, L. R. Teng, and R. J. Lee, "Enhanced siRNA delivery using oleic acid derivative of polyethylenimine," *Anticancer Research*, vol. 32, no. 4, pp. 1267–1271, 2012.

[28] Z. Yang, W. Sun, and K. Hu, "Adenosine A1 receptors selectively target protein kinase C isoforms to the caveolin-rich plasma membrane in cardiac myocytes," *Biochimica et Biophysica Acta*, vol. 1793, no. 12, pp. 1868–1875, 2009.

[29] Z. Yang, W. Sun, and K. Hu, "Molecular mechanism underlying adenosine receptor-mediated mitochondrial targeting of protein kinase C," *Biochimica et Biophysica Acta*, vol. 1823, no. 4, pp. 950–958, 2012.

[30] T. I. Kim, J. U. Baek, J. K. Yoon, J. S. Choi, K. Kim, and J. S. Park, "Synthesis and characterization of a novel arginine-grafted dendritic block copolymer for gene delivery and study of its cellular uptake pathway leading to transfection," *Bioconjugate Chemistry*, vol. 18, no. 2, pp. 309–317, 2007.

[31] M. A. E. M. van der Aa, U. S. Huth, S. Y. Häfele et al., "Cellular uptake of cationic polymer-DNA complexes via caveolae plays a pivotal role in gene transfection in COS-7 cells," *Pharmaceutical Research*, vol. 24, no. 8, pp. 1590–1598, 2007.

[32] C. Zhang, J. T. Newsome, R. Mewani, J. Pei, P. C. Gokhale, and U. N. Kasid, "Systemic delivery and pre-clinical evaluation of nanoparticles containing antisense oligonucleotides and siRNAs," *Methods in Molecular Biology*, vol. 480, pp. 65–83, 2009.

[33] B. Yu, X. Zhao, J. L. Lee, and R. J. Lee, "Targeted delivery systems for oligonucleotide therapeutics," *AAPS Journal*, vol. 11, no. 1, pp. 195–203, 2009.

[34] W. Li and F. C. Szoka Jr., "Lipid-based nanoparticles for nucleic acid delivery," *Pharmaceutical Research*, vol. 24, no. 3, pp. 438–449, 2007.

[35] P. P. Karmali and A. Chaudhuri, "Cationic liposomes as non-viral carriers of gene medicines: resolved issues, open questions, and future promises," *Medicinal Research Reviews*, vol. 27, no. 5, pp. 696–722, 2007.

Hindawi Publishing Corporation
BioMed Research International
Volume 2013, Article ID 734596, 6 pages
http://dx.doi.org/10.1155/2013/734596

Research Article

Delivery of RNA and Its Intracellular Translation into Protein Mediated by SDS-CTAB Vesicles: Potential Use in Nanobiotechnology

Laura Russo,[1] Valerio Berardi,[1,2] Franco Tardani,[3] Camillo La Mesa,[3] and Gianfranco Risuleo[1]

[1] *Dipartimento di Biologia e Biotecnologie "Charles Darwin," Sapienza Università di Roma, Piazzale Aldo Moro 5, 00185 Roma, Italy*
[2] *SUNY Downstate Medical Center, 450 Clarkson Avenue, Brooklyn, NY 11203, USA*
[3] *Dipartimento di Chimica "Stanislao Cannizzaro," Sapienza Università di Roma, Piazzale Aldo Moro 5, 00185 Roma, Italy*

Correspondence should be addressed to Gianfranco Risuleo; gianfranco.risuleo@uniroma1.it

Received 18 October 2012; Revised 2 May 2013; Accepted 5 May 2013

Academic Editor: Susana N. Diniz

Catanionic vesicles are supramolecular aggregates spontaneously forming in water by electrostatic attraction between two surfactants mixed in nonstoichiometric ratios. The outer surface charges allow adsorption to the biomembrane by electrostatic interactions. The lipoplex thus obtained penetrates the cell by endocytosis or membrane fusion. We examined the possible cytotoxic effects and evaluated the transfection efficiency of one vesicle type as compared to known commercial carriers. We show that the individual components of two different vesicles types, CTAB (cetyltrimethylammonium bromide) and DDAB (didodecyldimethylammonium bromide) are detrimental for cell survival. We also assayed the cytotoxicity of SDS-DDAB vesicles and showed dose and time dependency, with the DDAB component being *per se* extremely cytotoxic. The transfection efficiency of exogenous RNA mediated by SDS-CTAB increases if vesicles assemble in the presence of the reporter RNA; finally, freezing abrogates the transfection ability. The results of our experimental strategy suggest that catanionic vesicles may be adopted in gene therapy and control of antiproliferative diseases.

1. Introduction

Catanionic vesicles are supramolecular aggregates formed by mixing in non-stoichiometric ratios cationic and anionic surfactant species [1]. Surfactants of opposite charge tend to aggregate in polar solvents, such as water. The electrostatic interactions between the polar heads and hydrophobic tails favor the formation of self-assembled and organized supramolecular structures [2]. The occurrence of this phenomenon depends upon the so-called "critical micellar concentration" (CMC) which represents the concentration where the surfactants in solution aggregate to form spontaneously micelles with different morphologies. In addition, the diverse shapes depend on the geometry of the individual surfactant molecule. The relationship between molecular geometry of the surfactant and the morphology of the self-organized structures can be determined by the packing parameter P, originally introduced by Israelachvili and coworkers [3]. This parameter is defined as the ratio between the volume of the hydrophobic tract (V) and the area of the polar head (a) multiplied by the length of the chain (L) being part of the same surfactant ($P = V/aL$). The modulus of P is suggestive of the type of structure/shape that surfactants tend to assume upon aggregation. The formation of vesicles is, therefore, possible when the packing parameter reaches an optimal value thus leading to the formation of a double layer [4].

Previous work from our laboratory, where the phase diagram was presented, indicated that to form quasispherical vesicles, it is necessary to mix the surfactants at nonequimolar concentrations since at stoichiometric ratio the two components precipitate [1].

Concerning the potential use of these complexes in biotechnological and biomedical applications, it should be

pointed out that the interaction of vesicles with other molecules, such as DNA, RNA, or other biopolymers, results in the formation of the above mentioned lipoplex. This represents a potential tool to deliver genetic material across the cell membrane via plasma-membrane fusion and/or endocytosis. As a matter of fact, previous work from our laboratory showed that it is possible to form complexes between DNA and vesicles with an excess positive charge at the surface, which could be potentially delivered within the cell [5, 6]. However, vesicles may show a cytotoxic effect, which is directly related to time of exposure and dose of administration. The literature focused on this specific aspect is not very abundant [7, 8], even though recent work from our laboratory showed that tumor cells exhibit a higher sensitivity to treatment with SDS-CTAB vesicles as compared to normal mouse fibroblasts [9]. However, in spite of their cytotoxicity, it is possible to adjust the experimental conditions such as time and dose of treatment to allow a successful vesicle-mediated transfection with subsequent expression of exogenous genetic material [9–11]. In addition, pilot studies indicate that catanionic vesicles may be utilized in anticancer therapy [11].

In the present work, we report on the cytotoxic action of both the individual surfactants and vesicles formed by the same ones, on HEK-293 cultured cells. In addition, we quantitatively evaluated the transfection, mediated by SDS-CTAB vesicles, of an exogenous RNA and measured the level of translation of the reporter protein. Strictly speaking, in fact, one should talk in terms of messenger RNA translation rather than gene expression. The data discussed here clearly indicate that after transfection, the nucleic acid is translated into protein with the correct structure and at abundant level. The novelty of the data discussed here consists of the fact that naked RNA, a very vulnerable biomacromolecule, is protected by the interaction with vesicles. Finally, these data add further evidence that vesicles may find a use in biotechnology and gene therapy.

2. Experimental Section

2.1. Vesicle Preparation and Characterization. Vesicles were prepared and characterized as previously published and extensively discussed [5, 6, 9]. Briefly, the micellar solutions of SDS and DDAB were mixed in water, The individual concentrations for each surfactant were 0,02133 g (SDS) and 0,01607 g (CTAB or DDAB) in 10.00 g of H_2O. Purification was made by dissolving the individual species in hot ethyl alcohol, under stirring with subsequent precipitation and filtering the surfactant solution by cold acetone. The salts were recovered and vacuum-dried at 70°C. Their purity was determined by conductivity methods in water at 25.0°C. Mixtures of the single species were prepared in conductivity water (χ close to $1 * 10^{-7}\ \Omega^{-1}\ cm^{-1}$, at room temperature) and heated above the respective Krafft points of each surfactant [12]. Thereafter, the solutions were mixed together. The dynamic light scattering (DLS) unit determining vesicle size is a Malvern Zeta Nanosizer, working at 632.8 nm in back scattering mode.

2.2. Cell Cultures and In Vivo Translation. Cells were maintained according to standard cell culture protocols. Transfection experiments *in vivo* were done in a Human Embryonal Kidney cell line (HEK-293). In general, 1×10^5 cells per well were seeded on 12 well polylysine-treated plates without antibiotics. Cells were allowed to reach at least 80% confluence prior to transfection. We used Plasmid pOT.CAT-A98 to generate CAT-A98 mRNAs. The RNAs used for transfection were transcribed *in vitro* using a commercial kit (RiboMax) and were phenol-chloroform-extracted (5 : 1 v/v at pH 4.7), ethanol-precipitated, and further purified on Sephadex G-50 or G-25 columns (GE Healthcare); CAT-A98 mRNAs were $5'$-capped and polyadenylated. As control, CAT-A98 mRNAs were transfected using Lipofectamine 2000 (Invitrogen) in Opti-MEM culture medium (Invitrogen). Briefly, transfections were performed with RNA and Lipofectamine at a ratio of 1 : 2.5 as previously published [13]. CAT was transfected at different molar concentrations (as indicated in the captions of the figures). Where appropriate, CAT mRNA was added before the formation of vesicles, or alternatively to preformed ones. Cells were exposed to the RNA/transfection mixture for 4 hours. Subsequently, this was replaced with fresh, serum-containing medium, and incubation was continued for 3 hours. Cells were collected, lysed, and probed for CAT protein using a CAT-ELISA Kit (Roche). ELISA data were normalized to total protein concentrations of cells assessed by the Bradford assay [14].

2.3. Evaluation of Cell Viability. Cell viability was evaluated by the colorimetric Mosmann assay [15] on both HEK-293 and 3T6 cells (see also legends of the figures). This quantitative method has been extensively illustrated in previous works, for instance see [9]. In any case, absorbance values measured at 570 nm can be directly converted into number of vital cells.

2.4. Statistics. All experiments and measurements were independently replicated 3 times. Statistical analysis was done by one-way ANOVA test [12] followed by comparative LSDs (Least Significant Differences) test. Results were considered significant when $P < 0.05$.

3. Results and Discussion

3.1. Estimates of Vesicle Size and Charge Density. The vesicular mixtures were prepared as previously reported [1, 5, 6, 9]. The shelf life of these dispersions is up to four months long, and we could not observe any tendency to phase separation over a three-month period. The thermodynamic stability of the vesicles is controlled by several parameters such as the overlapping of curvature elasticity, bending energy, and electrostatic terms [16–19]. The surface charge density is governed by the partition of the two surfactants between the bilayer and the bulk and is therefore controlled by Gibbs energy of transfer for the two species [17, 18]. DLS gives relevant information on vesicle size and polydispersity. In our case, the average hydrodynamic value is centered on 300 nm (Figure 1(c)). A single population is evident with a unimodal

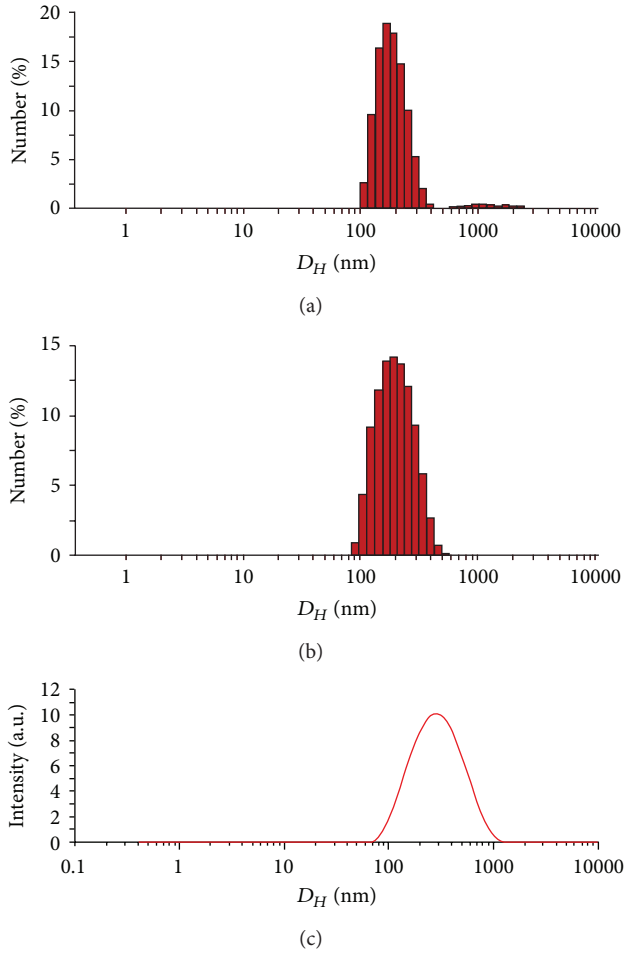

FIGURE 1: Estimation of the vesicle size by DLS. Size distribution of the SDS-DDAB vesicle monitored prior (a) and after filtration (b). (c) Integration of the data reported in panel (b). Concentration of the vesicle was 3.8 mmol kg^{-1}; the total surfactant concentration was 4.05 mmol kg^{-1}. The pore size of the filter was 450 nm.

distribution function, which is comparable to other vesicular dispersions of the catanionic family [9, 20–24]. The negligible peak observed in Figure 1(a) is attributable to a very small fraction of aggregated vesicles which, as a matter of fact, is eliminated by filtration (Figure 1(b)).

3.2. Cytotoxicity of Individual Surfactants and Vesicles. In this work, we compared the cytotoxic action of the individual surfactants SDS, CTAB, and DDAB on HEK-293 cells. Treatment time was four hours at increasing vesicle concentrations. The four-hour treatment time was chosen since this is required in the subsequent transfection experiments. In any case, it is worth noting that the CTAB component is more toxic than SDS (Figure 2(a)). Moreover, the mortality rate is directly proportional to the concentration for both surfactants. DDAB *per se* exhibited a dramatically higher toxicity than CTAB (not shown).

In a second series of experiments, we have compared the toxic effects of two different vesicles, SDS-CTAB and SDS-DDAB, after four hours of exposure and in the same range of

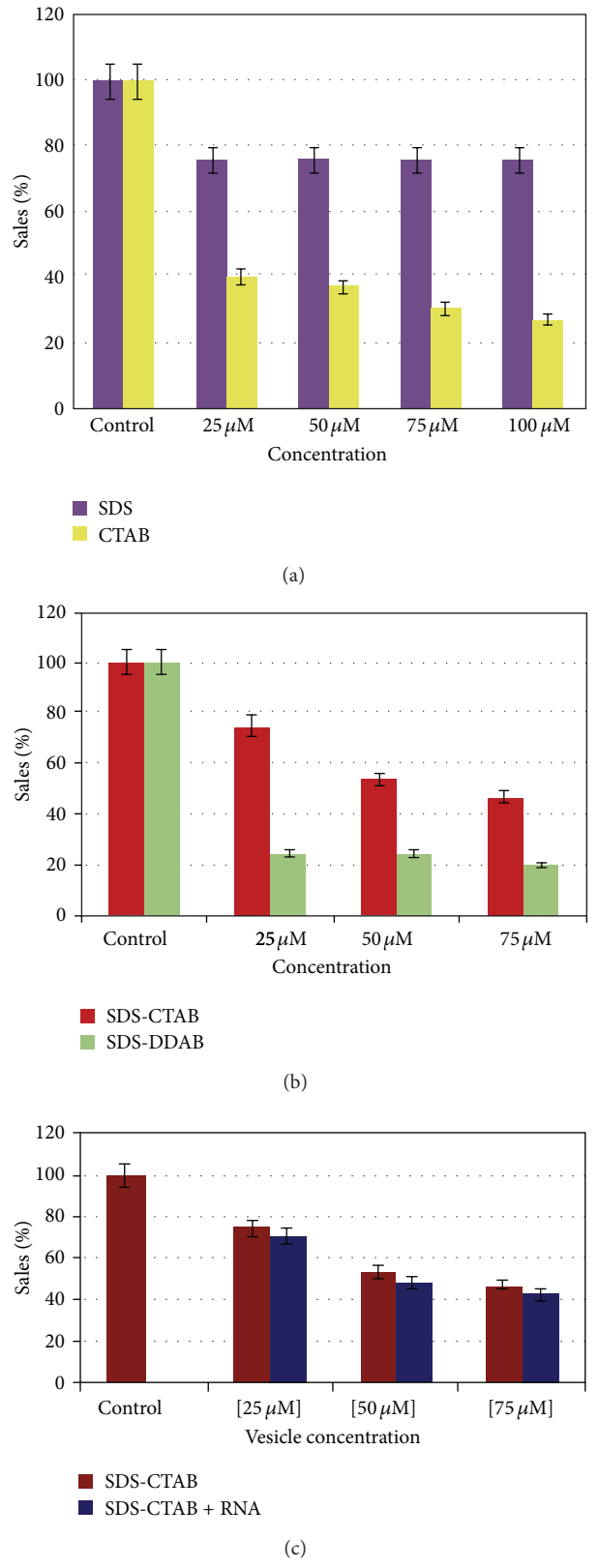

FIGURE 2: Effect of the separate surfactants and vesicles on the viability of HEK-293 cells. (a) Purple bars show the effect of SDS, while yellow bars show the toxicity of CTAB. (b) Compared cytotoxicity of SDS-CTAB (red bars) and SDS-DDAB (green bars). (c) Cytotoxicity of vesicle/RNA lipoplexes.

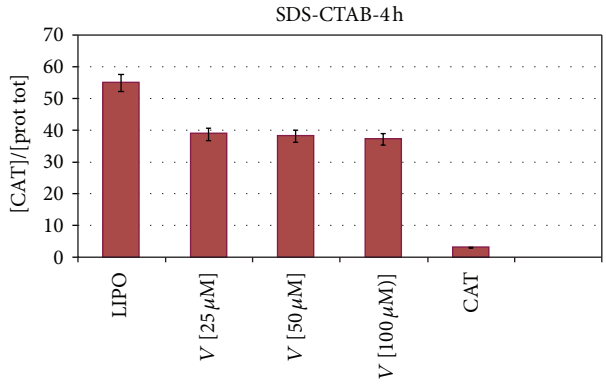

Figure 3: Transfection efficiency of mRNA-CAT. In this experiment, the RNA was added to preformed vesicles. The intracellular level of CAT is lower in the case of SDS-CTAB vesicles as compared to a commercial transfection system (Lipofectamine). See text for further details. LIPO (Lipofectamine); $V[25\,\mu M]$ ($25\,\mu M$ vesicle concentration); $V[50\,\mu M]$ ($50\,\mu M$ vesicle concentration); $V[100\,\mu M]$ ($100\,\mu M$ vesicle concentration); CAT (naked CAT mRNA).

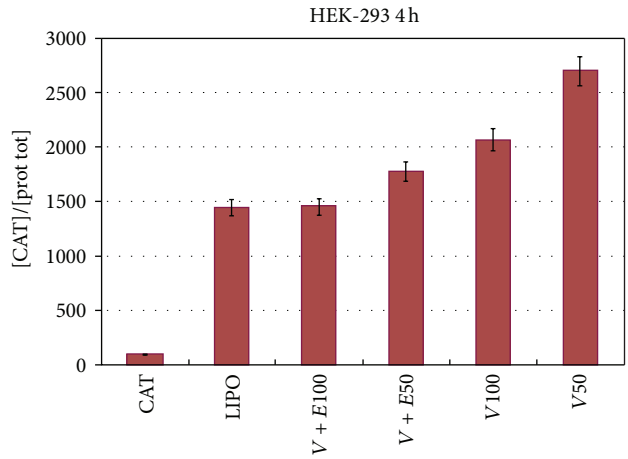

Figure 4: Transfection efficiency of mRNA CAT after treatment with RNase. In this experiment, the mRNA CAT was added to the surfactant mixture prior to the vesicle formation. This result strongly suggests that the RNA is internalized within the vesicle aqueous space and is thus protected by the nucleolytic attack. Panel (A): vesicles not treated with RNase (last two bars to the right) exhibit a higher efficiency than Lipofectamine. Panel (B): comparison between RNase untreated and treated vesicles. The numbers at the bottom of the bar indicate the vesicle concentration (μM).

concentrations used in the previous experiments. As shown in Figure 2(b), the SDS-DDAB vesicles are far more toxic than the SDS-CTAB ones. This validates the former results obtained with the individual surfactants (Figure 2(a)) and suggests that the higher cytotoxic effect is mainly due to the DDAB component forming the vesicular aggregate. This is the rational for the use of SDA-CTAB vesicles in all subsequent experiments. Cytotoxicity of vesicles with bound RNA was also investigated (Figure 2(c)). Results show a slight increase in cell mortality which may be ascribed to the toxic effect of free RNA present in the mixture.

3.3. RNase Protection Assay: Transfection of Chloramphenicol-Acetyltransferase Reporter mRNA. Chloramphenicol-Acetyltransferase (CAT) is a bacterial enzyme whose messenger RNA (mRNA) can be translated into active protein in eukaryotic cells. We transfected the CAT mRNA into HEK-293 cells using SDS-CTAB vesicles. The rationale of these experiments is that CAT is not normally present in higher cells; therefore, the detection of this enzyme is the diagnostic sign that the CAT mRNA has been successfully transferred across the plasma membrane by the vesicles and, subsequently, translated into protein within the cytoplasm matrix. We quantified the intracellular concentration of enzyme by the immunoenzymatic assay ELISA; finally, the level of CAT was normalized to the total protein content of the cells.

We compared the efficiency of RNA intracellular delivery of our vesicles with Lipofectamine, a commercially available liposome transfection system. Transfection of naked CAT mRNA represented the negative control and, evidently, is almost totally hydrolyzed by the RNases normally present in the cytoplasm. As matter of fact, messenger RNA exists in a quasilinear molecular configuration which is easily hydrolyzed by the resident RNases. In the first experiments, we added the CAT mRNA to preformed vesicle. One can expect that in this case, the RNA is anchored via electrostatic interactions to the surface of the vesicles. The results of Figure 3 show that the immunoreaction between the CAT protein and anti-CAT antibody is, as expected, almost absent in the case of the transfection with naked CAT mRNA (bar to the right); this is consistent with the idea that the RNA is demolished by the RNases present in the cytoplasm and therefore becomes unavailable to be translated into protein. The transfection efficiency at the indicated concentrations of SDS-CTAB is indeed lower than the one exhibited by Lipofectamine (bar to the left) but is in any case quite satisfactory. One way to explain this lower efficiency is that the RNA located partly or totally on the external surface of the RNA is, again, attacked and inactivated by the cell RNases. Therefore, in the next experiments, we formed the vesicle in the presence of CAT mRNA: the assumption is that in this case the RNA would be included in the aqueous space internal to the vesicles. We treated these lipoplexes with RNase and subsequently transfected the cells as reported above. The results of Figure 4 show an improved transfecting performance of the vesicles, and Figure 4 demonstrates that in this case the RNA is protected by the nucleolytic attack. Actually, the efficiency increases with the concentration and becomes almost twice higher (at 100 μM vesicles) with respect to Lipofectamine used as control (last bar to the left and first to the right, resp.). This strongly suggests that actually the RNA molecule is internalized and protected within the vesicle. Subsequently to transfection, the CAT mRNA is released in the cytoplasm where it can be translated into protein. In the last set of experiments discussed here, we probed the role of the storage temperature; as a matter of fact, previous evidence from our laboratory [1, 8] suggests that vesicles are quite stable in a temperature range of 15–25°C. To test the idea

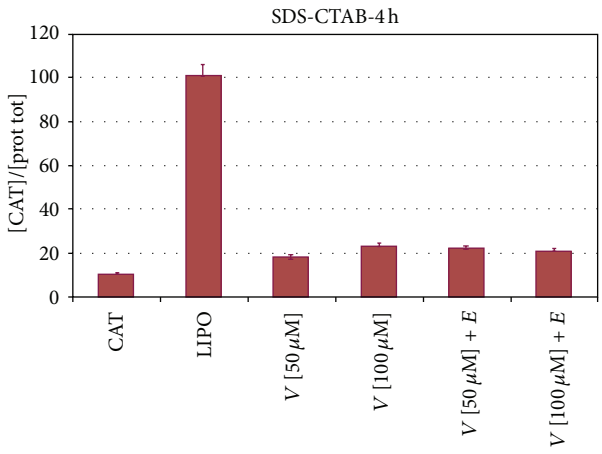

Figure 5: Effect of freezing on the transfection efficiency. Vesicles were formed in the presence of mRNA CAT and kept frozen at −20°C for 24 hours. After thawing, the aggregates were treated with RNase and transfected into HEK-293 cells. Data clearly indicate that the RNase treatment almost abolishes the translation of CAT mRNA into protein. LIPO (Lipofectamine); V[25 μM] (25 μM vesicle concentration); V[50 μM] (50 μM vesicle concentration); V[100 μM] (100 μM vesicle concentration); CAT (naked CAT mRNA).

that freezing damages, or abolishes, the transfecting efficiency of the vesicles, we froze and kept them at a temperature of −25°C for about 24 hours. Data reported in Figure 5 clearly show that freezing almost abolishes the transfection capacity of the SDS-CTAB vesicles. The data of this ELISA assay demonstrate, in fact, that after freezing, the translation of the CAT mRNA drops almost to the same level as the one exhibited by the naked RNA (first bar to the left). Therefore, it is plausible to assume that freezing alters the supramolecular organization of the vesicles and consequently abrogates their activity of potential molecular biomachines for the delivery of bioactive polymers. As a matter of fact, from these data, we can infer that also other bio-macromolecules may be transferred inside the cells. One interesting aspect, yet to be investigated, is the mode of cell death. Previous evidence from our laboratory indicates that administration of vesicles to cultured cells causes apoptosis [9]. This is a multistep and very complex mode for a cell to die. Therefore, the elucidation of the key step in the process of cell death may help to set up the best experimental condition which, to minimal cell mortality, corresponds to an optimal delivery of the cargo macromolecule (or also small molecules) of biotechnological interest. Finally, a very important and original result shown in this work is that the interaction of CAT mRNA with the vesicles causes it to internalize within the supramolecular aggregate. To our knowledge, this is the first example of an mRNA being delivered within a cell and translated into a protein with a properly folded conformation as shown by the data obtained with the experiment of RNA protection. The ELISA approach in fact evidences the interaction of antigen/antibody (CAT protein/antiCAT-antibody) only if the antigen is found in the proper and very likely active molecular structure.

4. Conclusions

In conclusion, the data discussed in this work evidence that it is possible to define an experimental situation where the cell mortality caused by the exposure to the vesicles is minimal. This is a crucial aspect to maximize the transfection efficiency of catanionic vesicles. The formation of vesicles in the presence of the molecule to be delivered inside the cell is of crucial importance for its internalization within the inner aqueous medium. Furthermore, the vesicles are stable at room temperature and have a relatively long shelf life. They must be stored at room temperature and should not be frozen since this would disrupt their supramolecular structure thus abolishing their capacity of molecular delivery. Catanionic vesicles efficiently deliver genetic material across the cell membrane. Transfection efficiency increases if vesicles are formed in the presence of RNA. Treatment with RNase suggests the internal localization of RNA the nucleic acid.

Abbreviations

CAT:	Chloramphenicol-acetyltransferase
DLS:	Dynamic light scattering
ELISA:	E-linked immunosorbent assay
HEK-293:	Human Embryonal Kidney cells
SDS-CTAB:	Sodium dodecylsulfate/cetyltrimethylammonium bromide
SDS-DDAB:	Didodecyldimethylammonium bromide.

Conflict of Interests

The authors declare that no conflict of interests exists. They do not have a direct financial relation with commercial identities that might lead to a conflict of interests.

Acknowledgments

This work was a partial fulfillment of the doctoral thesis of L. Russo. The authors thank the Foundation Institute Pasteur Cenci-Bolognetti for granting a postdoctoral fellowship to V. Berardi. Partial funding by the Italian Ministry of Education is also acknowledged, grant to C. La Mesa.

References

[1] C. Letizia, P. Andreozzi, A. Scipioni, C. La Mesa, A. Boninconto, and E. Spigone, "Protein binding onto surfactant-based synthetic vesicles," *Journal of Physical Chemistry B*, vol. 111, no. 4, pp. 898–908, 2007.

[2] G. Gaucher, M. H. Dufresne, V. P. Sant, N. Kang, D. Maysinger, and J. C. Leroux, "Block copolymer micelles: preparation, characterization and application in drug delivery," *Journal of Controlled Release*, vol. 109, no. 1–3, pp. 169–188, 2005.

[3] J. N. Israelachvili, D. J. Mitchell, and B. W. Ninham, "Theory of self-assembly of lipid bilayers and vesicles," *Biochimica et Biophysica Acta*, vol. 470, no. 2, pp. 185–201, 1977.

[4] S. Segota and D. Tezak, "Spontaneous formation of vesicles," *Advances in Colloid and Interface Science*, vol. 121, no. 1–3, pp. 51–75, 2006.

[5] A. Bonincontro, M. Falivene, C. La Mesa, G. Risuleo, and M. R. Peña, "Dynamics of DNA adsorption on and release from SDS-DDAB Cat—anionic vesicles: a multitechnique study," *Langmuir*, vol. 24, no. 5, pp. 1973–1978, 2008.

[6] A. Bonincontro, C. La Mesa, C. Proietti, and G. Risuleo, "A biophysical investigation on the binding and controlled DNA release in a cetyltrimethylammonium bromide-sodium octyl sulfate cat-anionic vesicle system," *Biomacromolecules*, vol. 8, pp. 1824–1829, 2008.

[7] J. H. S. Kuo, M. S. Jan, C. H. Chang, H. W. Chiu, and C. T. Li, "Cytotoxicity characterization of catanionic vesicles in RAW 264.7 murine macrophage-like cells," *Colloids and Surfaces B*, vol. 41, no. 2-3, pp. 189–196, 2005.

[8] N. Lozano, L. Pérez, R. Pons, and A. Pinazo, "Diacyl glycerol arginine-based surfactants: biological and physicochemical properties of catanionic formulations," *Amino Acids*, vol. 40, no. 2, pp. 721–729, 2011.

[9] C. Aiello, P. Andreozzi, C. La Mesa, and G. Risuleo, "Biological activity of SDS-CTAB cat-anionic vesicles in cultured cells and assessment of their cytotoxicity ending in apoptosis," *Colloids and Surfaces B*, vol. 78, no. 2, pp. 149–154, 2010.

[10] M. Wang and M. Thanou, "Targeting nanoparticles to cancer," *Pharmacological Research*, vol. 60, pp. 90–99, 2010.

[11] P. Guo, "A special issue on bionanotechnology," *Journal of Nanoscience and Nanotechnology*, vol. 5, no. 12, pp. i–iii, 2005.

[12] D. F. Evans and H. Wennerstroem, *The Colloidal Domain: Where Physics, Chemistry, Biology and Technology Meet*, chapt I, VCH, New York, NY, USA, 1st edition, 1994.

[13] A. V. Kondrashov, M. Kiefmann, K. Ebnet, T. Khanam, R. S. Muddashetty, and J. Brosius, "Inhibitory effect of naked neural BC1 RNA or BC200 RNA on eukaryotic in vitro translation systems is reversed by poly(A)-binding protein (PABP)," *Journal of Molecular Biology*, vol. 353, no. 1, pp. 88–103, 2005.

[14] M. M. Bradford, "A rapid and sensitive method for the quantitation of microgram quantities of protein utilizing the principle of protein-dye binding," *Analytical Biochemistry*, vol. 72, pp. 248–254, 1976.

[15] T. Mosmann, "Rapid colorimetric assay for cellular growth and survival: application to proliferation and cytotoxicity assays," *Journal of Immunological Methods*, vol. 65, no. 1-2, pp. 55–63, 1983.

[16] H. T. Jung, B. Coldren, J. A. Zasadzinski, D. J. Iampietro, and E. W. Kaler, "The origins of stability of spontaneous vesicles," *Proceedings of the National Academy of Sciences of the United States of America*, vol. 98, no. 4, pp. 1353–1357, 2001.

[17] H. T. Jung, S. Y. Lee, E. W. Kaler, B. Coldren, and J. A. Zasadzinski, "Gaussian curvature and the equilibrium among bilayer cylinders, spheres, and discs," *Proceedings of the National Academy of Sciences of the United States of America*, vol. 99, no. 24, pp. 15318–15322, 2002.

[18] E. W. Khaler, K. L. Herrington, D. J. Iampietro, B. Coldren, H. T. Jung, and J. A. Zasadzinski, "Phase behavior and microstructure in aqueous mixtures of cationic and anionic surfactants," in *Mixed Surfactant Systems*, M. Abe and J. Scamehorn, Eds., pp. 298–338, Dekker, New York, NY, USA, 2005.

[19] R. Nagarajan, "Molecular packing parameter and surfactant self-assembly: the neglected role of the surfactant tail," *Langmuir*, vol. 18, no. 1, pp. 31–38, 2002.

[20] S. A. Safran, P. A. Pincus, D. Andelman, and F. C. MacKintosh, "Stability and phase behavior of mixed surfactant vesicles," *Physical Review A*, vol. 43, no. 2, pp. 1071–1078, 1991.

[21] M. T. Yatcilla, K. L. Herrington, L. L. Brasher, E. W. Kaler, S. Chiruvolu, and J. A. Zasadzinski, "Phase behavior of aqueous mixtures of cetyltrimethylammonium bromide (CTAB) and Sodium Octyl Sulfate (SOS)," *Journal of Physical Chemistry*, vol. 100, no. 14, pp. 5874–5879, 1996.

[22] S. M. Mel'nikov, R. Dias, Y. S. Mel'nikova, E. F. Marques, M. G. Miguel, and B. Lindman, "DNA conformational dynamics in the presence of catanionic mixtures," *FEBS Letters*, vol. 453, no. 1-2, pp. 113–118, 1999.

[23] R. O. Brito, E. F. Marques, S. G. Silva et al., "Physicochemical and toxicological properties of novel amino acid-based amphiphiles and their spontaneously formed catanionic vesicles," *Colloids and Surfaces B*, vol. 72, no. 1, pp. 80–87, 2009.

[24] N. Lozano, A. Pinazo, C. La Mesa, L. Perez, P. Andreozzi, and R. Pons, "Catanionic vesicles formed with arginine-based surfactants and 1,2-dipalmitoyl-sn-glycero-3-phosphate monosodium salt," *Journal of Physical Chemistry B*, vol. 113, no. 18, pp. 6321–6327, 2009.

Hindawi Publishing Corporation
BioMed Research International
Volume 2013, Article ID 351031, 20 pages
http://dx.doi.org/10.1155/2013/351031

Review Article

Application of Nanoparticles on Diagnosis and Therapy in Gliomas

Norma Y. Hernández-Pedro,[1] Edgar Rangel-López,[2] Roxana Magaña-Maldonado,[1] Verónica Pérez de la Cruz,[2] Abel Santamaría del Angel,[2] Benjamín Pineda,[1] and Julio Sotelo[1]

[1] *Neuroimmunology and Neuro-Oncology Unit, National Institute of Neurology and Neurosurgery, 14269 Mexico City, DF, Mexico*
[2] *Excitatory Amino Acids Laboratory, National Institute of Neurology and Neurosurgery, 3877 Mexico City, DF, Mexico*

Correspondence should be addressed to Benjamín Pineda; benpio76@hotmail.com

Received 5 January 2013; Accepted 13 March 2013

Academic Editor: Alejandro Sosnik

Glioblastoma multiforme (GBM) is one of the most deadly diseases that affect humans, and it is characterized by high resistance to chemotherapy and radiotherapy. Its median survival is only fourteen months, and this dramatic prognosis has stilled without changes during the last two decades; consequently GBM remains as an unsolved clinical problem. Therefore, alternative diagnostic and therapeutic approaches are needed for gliomas. Nanoparticles represent an innovative tool in research and therapies in GBM due to their capacity of self-assembly, small size, increased stability, biocompatibility, tumor-specific targeting using antibodies or ligands, encapsulation and delivery of antineoplastic drugs, and increasing the contact surface between cells and nanomaterials. The active targeting of nanoparticles through conjugation with cell surface markers could enhance the efficacy of nanoparticles for delivering several agents into the tumoral area while significantly reducing toxicity in living systems. Nanoparticles can exploit some biological pathways to achieve specific delivery to cellular and intracellular targets, including transport across the blood-brain barrier, which many anticancer drugs cannot bypass. This review addresses the advancements of nanoparticles in drug delivery, imaging, diagnosis, and therapy in gliomas. The mechanisms of action, potential effects, and therapeutic results of these systems and their future applications in GBM are discussed.

1. Introduction

Cancer is the most common cause of death in many countries. Central nervous system (CNS) tumors are an important cause of morbidity and mortality worldwide. It was estimated that 22,340 new cases of primary malignant brain and CNS tumors were diagnosed in the United States in 2011. Approximately 3,000 of them were new cases in childhood whereas about half of all CNS tumors were malignant in adults [1]. The distribution of CNS tumors shows that approximately 60% of these tumors have the typical glioblastoma histopathology [2]. Glioblastoma multiforme (GBM) comprises a heterogeneous group of neoplasms that differ in their location within the CNS; it is responsible for the 51% of all primary gliomas in adults and represents the second cause of cancer death in adults less than 35 years old [3]. Despite advances in diagnosis and treatment of GBM, their prognosis, incidence, and mortality rates remain poor.

Conventional treatment for malignant gliomas includes the use of chemotherapeutic drugs, radiotherapy, and interventional surgery [4]. However, both chemotherapy and radiotherapy give inconsistent results in terms of prolonging survival and response to treatment [5]. The median survival for GBM in patients subjected to the conventional multimodal therapies is 14.6 months, and the progression-free survival for recurrent GBM is less than 24 weeks [6, 7]. The conventional treatment for GBM shows some drawbacks that limit its potential use in therapy such as neurotoxicity, lack of specificity, poor drug accumulation in tumors, and severe side effects. Also, the blood-brain barrier (BBB) plays an

important role limiting strategies of therapy, because several drugs have little or no solubility to cross this physical barrier.

Many approaches have been used to treat gliomas; however all of them have failed in modifying the prognostic and quality of life of patients suffering this devastating disease in the last decade. As the nanotechnology has expanded its application to biomedicine and biomedical areas, nanotoxicology has emerged to elucidate the relationship of the physical and chemical properties (size, shape, surface chemistry, composition, and aggregation) of nanostructures with induction of toxic biological responses [8]. Because these structures are small sized (less 100 nm), simple performed, fast and cheap in cost, they have been widely used in cytotoxic *in vitro* studies [9, 10]. Recently, nanotechnology is considered as a new tool for its application in diagnosis and treatment of malignant gliomas. Nanotechnology has revolutionized the conventional way in which gliomas therapy, diagnosis, and treatment are achieved mainly due to recent advances in material engineering, drug availability, and the advantage of targeting cancer cells, simply due to being accumulated and entrapped in cancer cells. This review is therefore primarily devoted to the current approaches used in imaging and treatment of gliomas. In addition, we present a brief description of the most common materials used in the design, composition, structure, and drug delivery systems by nanoparticles.

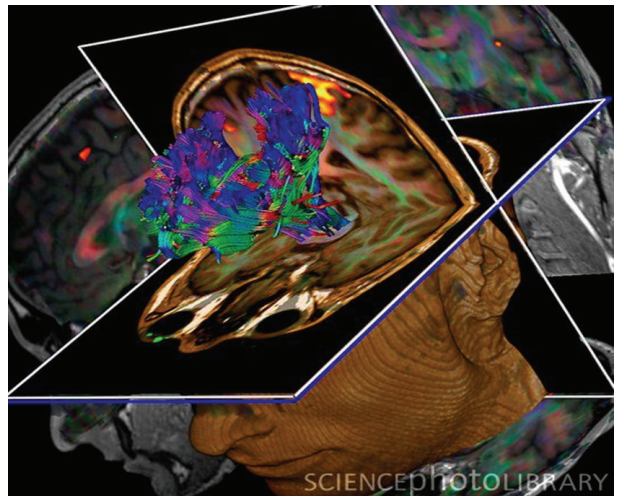

Figure 1: Brain tumour. Coloured 3D diffusion tensor imaging (DTI) and magnetic resonance imaging (MRI) scans of the brain of a 29-year-old with a low-grade glioma in the left frontal lobe. A DTI scan shows the bundles of white matter nerve fibers and is being used here for presurgical planning. The fibers transmit nerve signals between brain regions and between the brain and the spinal cord. A glioma arises from glial cells; nervous system supports cells. DTI scans show the diffusion of water along white matter fibers, allowing their orientations and the connections between brain regions to be mapped.

2. Use of Nanoparticles in Gliomas Diagnosis

In the imaging field, the development of nanoparticles as contrast agents has allowed obtaining detailed cellular and molecular imaging, monitoring drug delivery specifically to tumoral areas, and providing data for efficient surgical removal of solid tumors [11, 12].

Positron Emission Tomography (PET) is a well-established imaging modality that uses signals emitted by positron-emitting radiotracers to construct images about the distribution of the tracer *in vivo* [13, 14]. PET has provided valuable biophysiological information on various central nervous system disorders. In brain tumors, different radiotracers have been applied in PET studies to evaluate tumor blood flow and metabolism, as well as to detect tumors. Radiotracers such as 18F-labeled fluorodeoxyglucose ([18F]-α-methyl-tyrosine, L- and D-S-(3-[18F] fluoropropyl) homocysteine have been used for the PET imaging of tumors, but L- and D-S-(3-[18F] fluoropropyl)homocysteine biodegradation products generate a high background signal in the tissues [15]. In contrast, [2-18F]-2-deoxy-fluoro-D-glucose (FDG) has been the most frequently used marker for the evaluation of glucose metabolism in brain tumors. However, the utility of FDG-PET imaging for detection of brain cancer is controversial due to the small differences in rate of glucose utilization between normal brain and brain malignance (the FDG uptake is usually similar to that in normal white matter), and FDG-PET is effective in differentiating recurrent tumor from radiation necrosis for high-grade tumors, but it has limited value in defining the extent of tumor involvement and recurrence of low-grade lesions [16, 17].

On the other hand, magnetic resonance imaging (MRI) is a widely accepted modality for providing anatomical information and high spatial-resolution anatomic images primarily based on contrast derived from the tissue-relaxation parameters T(1)- and T(2)*-weighted sequences. MRI is capable of visualizing various intracranial lesions and detecting the correlation between the major white matter fiber bundle and glioma lesions. The biggest advantage of a brain MRI is that it provides a good anatomical background without bone artifacts, and it is also capable of exhibiting the panorama and three-dimensional location of the tumor [18]. Nowadays, a novel neuroimaging modality has been developed for patients with brain tumors named functional magnetic resonance imaging (fMRI), which allows to obtain not only noninvasive measurements, localization, and lateralization of specific brain activation areas, but also the possibility to evaluate motor and speech functions, helping in the selection of the most appropriate, sparing treatment, and function-preserving surgery. However, fMRI cannot be considered as a fully established modality of diagnostic neuroimaging due to the lack of guidelines of the responsible medical associations as well as the lack of medical certification of important hardware and software components [19] (Figure 1).

To overcome these limitations, there are significant efforts in developing alternative imaging methods that are capable of enhancing the signal or generating bright and positive contrast [20, 21]. Some nanoparticles such as liposomal

conjugates are known to accumulate in tumors due to the enhanced permeability of tumor blood vessels and the retention effect [22]. However, it still may not be possible to accurately localize an area of increased activity using PET images alone because of the absence of identifiable anatomic structures in nonrigid tissues, such as abdomen or brain [23, 24]. The greatest advantage of performing combined MRI compatible with PET scanners (PET/MRI) not only is to reduce radiation exposure, but also should theoretically be possible to obtain "perfect" spatial records of molecular/functional PET and anatomic/functional MRI studies [25, 26].

The use of macromolecular agents based on dendrigraft poly-L-lysines (DGLs), using chlorotoxin (CTx) as a tumor-specific ligand, has been explored with promising results in the field of clinical diagnosis of brain tumors using MRI studies, where it has been showed that the signal enhancement of mice treated with CTx-modified contrast reached peak level at 5 min for both glioma and liver tumor, significantly higher than unmodified counterpart. Most importantly, the signal enhancement of CTx-modified contrast agent is maintained much longer when it was compared to controls [27]. Recently, Veiseh et al. developed a nanovector comprised of a superparamagnetic iron oxide nanoparticle core coated with polyethylene-glycol- (PEG-)grafted chitosan and polyethylenimine (PEI). The functionality of the construct was achieved with short interfering RNA (siRNA) and the tumor-targeting peptide, chlorotoxin (CTx), to improve tumor specificity and potency. Receptor-mediated cellular internalization of nanovectors and the consequent gene knockdown through targeted siRNA delivery and the specific contrast of brain tumor cells were confirmed by flow cytometry, quantitative RT-PCR, fluorescence microscopy, and MRI studies [28]. This finding is especially important for tumors such as glioma which is known hard to be diagnosed due to the presence of BBB.

Magnetic nanoparticles (MNPs) represent a promising nanomaterial for the targeted therapy and imaging of malignant brain tumors. Conjugation of peptides or antibodies to the surface of MNPs allows direct targeting of the tumor cell surface and potential disruption of active signaling pathways present in tumoral cells [29]. It is known that magnetic nanoparticles also exhibit a higher longitudinal relaxivity, providing intrinsic signal enhancement on T1-weighted images [30]. Varieties of magnetic nanoparticles have been introduced as contrast agents for MRI and molecular imaging probes because of their super ability in shortening transverse relaxation times in T1- and $T(2)^*$-weighted images, which leads to a strong decrease in signal intensity of target organs or so-called "negative contrast" on conventional $T(2)^*$-weighted images.

The arginine-glycine-aspartic acid (RGD) sequence is currently the basic module for a variety of RGD-containing peptides which display preferential binding to α and β_3 integrins, which play a key role in tumor angiogenesis and metastasis and were not detectable in normal blood vessels [31]. This probe could detect the tumor location with fluorescence imaging and assess the tumor-targeting efficacy of probe with radioactive analysis [32]. It has been proposed that the imaging techniques PET and MRI will greatly benefit from the use of bifunctional nanoprobe conjugates, such as polyaspartic-acid- (PASP-) coated iron oxide (IO) nanoparticles conjugated with cyclic RGD peptides and the macrocyclic chelating agent 1,4,7,10-tetraazacyclododecane-N, N', N'', N'''-tetraacetic acid (DOTA) for integrin $\alpha_v\beta_3$ recognition. A displacement competitive binding assay indicates that DOTA-IO-RGD conjugates bound specifically to integrin $\alpha_v\beta_3$ *in vitro*. Small-animal PET and T2-weighted MRI showed integrin-specific delivery of conjugated RGD-PASP-IO nanoparticles and prominent reticuloendothelial system uptake. This bifunctional imaging approach may allow for earlier tumor detection with a high degree of accuracy [33–35].

2.1. Iron Magnetic Nanoparticles Auxiliary on Diagnosis. Over the past two decades, magnetic iron oxide nanoparticles (MPIOs) have been subject of extensive studies as an important class of MRI contrast agents for medical imaging [36, 37]. An MPIO, in general, is composed of maghemite (Fe_2O_3, γ-Fe_2O_3) or magnetite crystals less than 20 nm in diameter. These nanocrystals contain thousands of Fe atoms and approach saturation magnetization under a magnetic field typical for MRI [38]. In some *in vivo* studies it has been reported that absorption of these particles can occur through interactions with biological components such as proteins and cells; afterwards, they can distribute into various organs where they may remain in the same nanostructure or become metabolized [39]. It is known that MPIOs causes toxicity through the production of an excess of reactive oxygen species (ROS), including free radicals such as the superoxide anion, hydroxyl radicals, and the nonradical hydrogen peroxide. High ROS levels can damage cells by peroxidizing lipids, disrupting DNA, modulating gene transcription, altering proteins, and resulting in decline of physiological function and cell apoptosis/death [40] (Figure 2).

Superparamagnetic iron oxide particles (SPIOs) enhance contrast in MRI, which allows clinicians to monitor anatomical, physiological, and molecular changes during the evolution of a disease or treatment. Following intravenous injection, these nanoparticles accumulate in macrophages residing in the liver, bone marrow, and spleen, as well as tumors and sites of inflammation [41]. These particles are rapidly internalized by the mononuclear phagocytic system; consequently, they have been used in models of cell migration and homing in C6 models *in vivo* [42]. However the current applications for SPIO nanoparticles are limited because they have an average diameter of 80 nm in size, and it has shown relatively low toxicity in some *in vivo* applications [43–46]. Because SPIOs have a better resolution in MRI than conventional imaging, some changes in their structure has been developed to improve their diameter and diminish the adverse effects. Recently, these particles have been modified in ultrasmall superparamagnetic iron oxide (USPIO) particles which have diameters less than 50 nm and a longer half-life in the circulation system, allowing inclusively the labeling of macrophages migrating to remote areas [47].

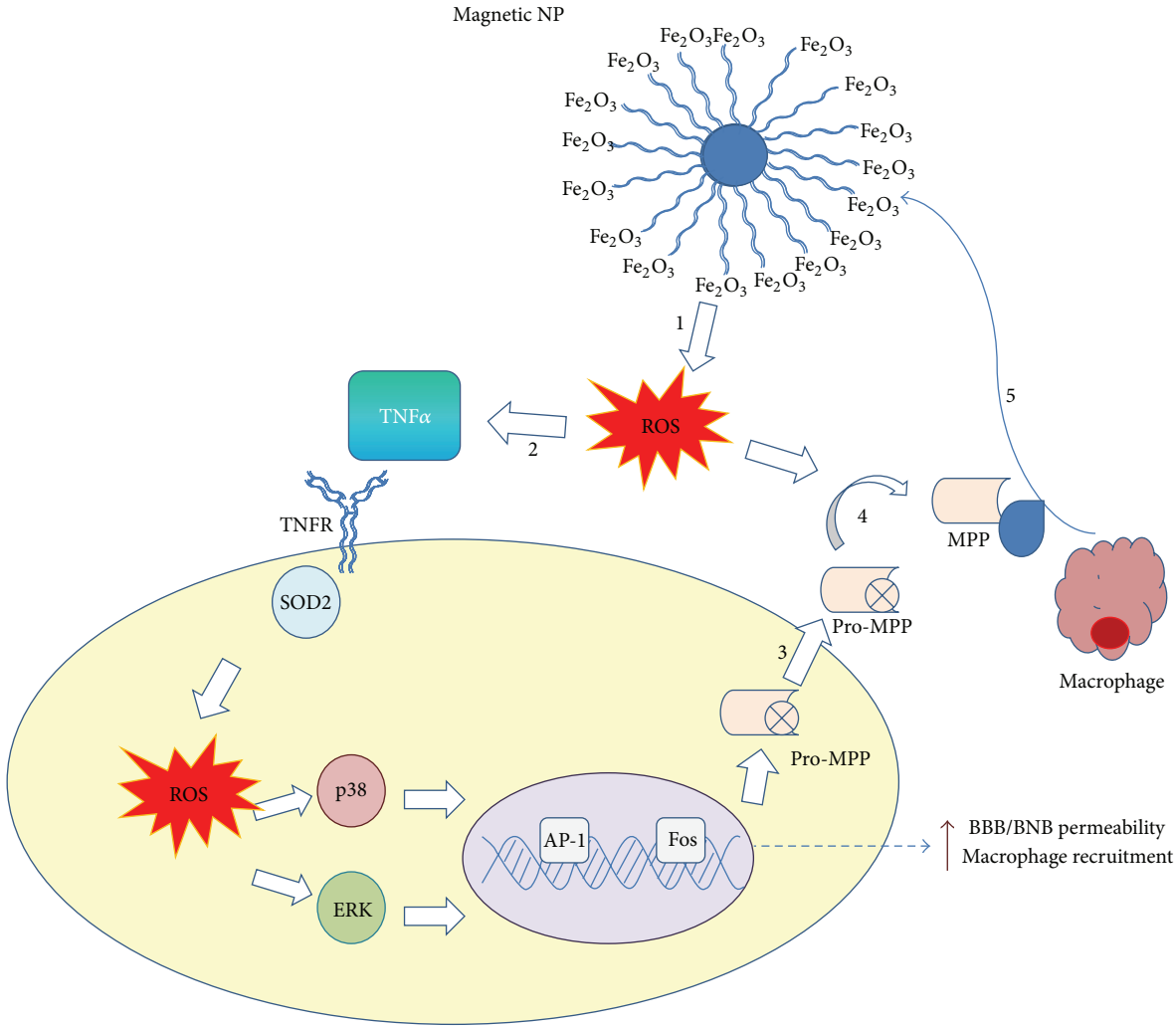

Figure 2: Proposed mechanism by Shubayev et al. [40] for MNP-induced macrophage recruitment into neuronal tissues. (1) Exposure to cytotoxic MNPs stimulated the formation of ROS in resident cells. (2) ROS promotes expression and release of proinflammatory cytokines, such as TNF-α. Through its two receptors (TNFR), TNF-α activates p38 and ERK mitogen-activated protein kinases pathways to (3) induce the expression of matrix metalloproteinases (MMPs) in its inactive, pro-MMP form. In addition, (4) ROS can directly promote MMP activation from proform. MMPs are the only enzymes in the body capable of degrading blood-brain and blood-nerve barriers (BBB/BNB), which (5) promotes infiltration of circulating macrophages (mΦ) into neuronal tissues. MNP size and surface chemistry determine the mechanisms and the target cells of MNP internalization, as well as extent of neurotoxicity of MNPs (the figure is taken and modified from [40]).

Other nanoparticles composed of iron are the monocrystalline iron oxide nanoparticles (MIONs), which are nanoconjugates that permit accurate delineation of tumor margins which lead to an increase long-lasting signal of the tumor in T1-weighted sequences. In animal models, they constitute a contrast agent that is taken up by endocytosis by malignant glioma cells [48, 49]. The use of MIONs is a promising strategy to avoid surgically induced intracranial contrast enhancement, which is known to be a potential source of error in intraoperative MRI imaging of patients [50]. Currently, they have been used in animal models.

Manganese oxide nanoparticles have shown a prominent MRI T1 contrast using a U87MG glioblastoma xenograft model, and it has been confirmed that the particles can accumulate efficiently in tumor area to induce effective T1 signal alteration [51]. Additionally, pH-sensitive poly(lactic-co-glycolic acid) (PLGA)-encapsulated manganese oxide (MnO) nanocrystals have shown an excellent bright contrast on MRI following endocytosis of nanoparticles into the low pH compartments within the cells. Subsequently, these particles are degraded, and MnO dissolves to release Mn^{2+} causing the cells to appear bright on MRI. The magnitude of the change in MRI properties is as high as 35-fold, making it the most dynamic MRI contrast agent reported. Possible applications of these MnO particles include slow release of Mn^{2+}, tumor targeting, and confirmation of cell uptake [52].

Gadolinium $[Gd(H_2O)_8]^{3+}$ is the contrast agent mainly used in magnetic resonance imaging. However, it is known

that high levels of gadolinium *in vivo* cause toxicity; therefore it requires the metal to be complexed by strong organic chelators. Gadolinium III (Gd III) is a highly paramagnetic complex with seven unpaired electrons, which have a strong impact on the relaxation of influenced water protons. Advances in colloidal nanocrystal synthesis have led to the development of ultrasmall crystals of gadolinium oxide (US-Gd_2O_3), with 2-3 nm in diameter, the smallest and the densest of all Gd-containing nanoparticles. Each nanocrystal can generate signal contrast of several orders of magnitude higher than a gadolinium chelate. Currently, US-Gd_2O_3 has been successfully used to label glioma cells GL-261 from localization and visualization *in vivo* using MRI. Because very high amounts of Gd are efficiently internalized and retained into the cells, it has been possible to detect the bright in T1-weighted MRI images [53]. The properties of the gadolinium-based particles give promising opening to a particle-assisted in imaging field.

Ultrashort echo time (UTE) imaging is able to track materials with extremely short T(2)*-weighted and very fast signal decay [54, 55]. With very short echo time (TE), typically below 0.1 milliseconds, UTE imaging allows signal acquisition with little T(2)*-weighted influence. The use of UTE imaging has allowed obtaining positive contrast imaging of U87MG human glioblastoma cells targeted with iron nanoparticles (IONPs) conjugated with a small RGD sequence, which has a high affinity to bound to cells over-expressing $\alpha_v\beta_3$ integrin such as ovarian carcinomas, breast carcinomas, gliomas, and other solid tumors [56–59]. A high concentration of RGD-containing probes must accumulate to overcome the limited sensitivity for the detection of contrast media. Therefore, UTE imaging may open the opportunity for the applications of magnetic nanoparticles with a strong T1 effect but also extremely short T(2)*-weighted [60].

Besides PET and MRI, fluorophores have been used in imaging applications. However, their use has been limited by poor quantum yield, poor tissue penetration of the excitatory light, and excessive tissue autofluorescence. The use of inorganic fluorescent particles that offer a high quantum yield is frequently limited due in part to the toxicity of the particles.

2.2. Nanoshells and Quantum Dots. Metal nanoshells and quantum dots are complexes that have shown good resolution in glioma imaging. Metal nanoshells are composed of a silica core surrounded by a thin metal shell or ultrathin coating of silver or gold [61]. These nanoparticles can be produced to absorb or scatter light, depending on the relative dimensions of the core size and shell thickness [62, 63]. Nanoshells have been used most commonly to treat murine gliomas. However, gold nanoshells have been used as contrast agents in optical imaging [64, 65], showing that these agents can both increase the surrounding water proton signals in the T1-weighted image and reduce the signal in T2-weighted images. Also, these nanoparticles exhibit strong absorption in the range of 600–800 nm, and their optical properties are strongly dependent upon the thickness of the gold-silver alloy shell. The intravenous administration of gold nanoshells has resulted in limited tumor accumulation, which represents a major challenge for contrast agents in optical imaging [64, 65]. Thus, these nanoshells have the potential to be utilized for tumor cell ablation due to physical characteristics (i.e., size, structure, and core), which when they are irradiated using laser light, they produce localized heat sufficient to damage tumor cells, ensuring a minimal thermal injury to the healthy tissue surrounding [66, 67].

Other nanoparticles which are now under extensive research are nanoshell conjugates of luminescent rare-earth-doped sodium ytterium fluoride ($NaYF_4$), which are nanocrystalline infrared-to-visible upconversion phosphors, ytterbium (Yb), and erbium (Er) codoped $NaYF_4$. These nanoparticles could be complexed with human serum albumin to originate water-dispersible nanoparticles, which could act as promising upconverting fluorescence labels when they are conjugated with cyclic arginine-glycine-aspartic acid (cRGD) sequence, specifically targeting both human glioblastoma cell lines and melanoma cells overexpressing $\alpha_v\beta_3$ integrin receptors. These characteristics offer an appropriate tool for targeted imaging of focal diseases [68, 69]. Rare-earth-doped nanoparticles utilize near-infrared upconversion, and they have been used to overcome the optical limitations of traditional fluorophores, but currently they are not typically suitable for biological application due to their insolubility in aqueous solution, lack of functional surface groups for conjugation with certain biomolecules, and potential cytotoxicity.

Quantum dots (QDs) are based on semiconductor compounds consisting of a cadmium-based core surrounded by an inert layer of metallic shell [70, 71]. Similar to gold nanoshells, quantum dots have excellent optical properties that are dependent on particle size. The tunable optical properties of these agents have primarily been used in preclinical optical imaging for a variety of cancer applications, including cellular and molecular imaging of brain tumors, including gliomas [72–74].

Near-infrared QDs composed of Cd(NO3)2, Hg(NO3)2, NaHTe (CdHgTe, CdTeSe/CdS), and a thiol group as stabilizer in gelatin solution are newly emerged as inorganic fluorescent probes. They provide several advantages over organic fluorophores for biological imaging, including broad excitation spectra coupled with narrow, tunable emission spectra and high resistance to photobleaching [75]. Lately, QDs have been used as excellent alternatives of traditional dyes in many fluorescence-based bioanalytical techniques [69, 76]. They exhibited strong fluorescence ranging from 580 to 800 nm that could be tuned by molar ratios of Hg^{2++} and gelatin. Compared with bare CdHgTe QDs, the photostability of this compact complex nanostructure is remarkably improved. The fluorescence of CdHgTe/gelatin nanospheres was much more resistant to the interference from certain endogenous biomolecules such as human serum albumin, transferrin, and hemoglobin [77].

In glioma cell cultures, nanospheres were small enough to be taken up by cells, and the fluorescence of QDs was not quenched inside the cells. Moreover, no morphological change of the cells was observed, indicating that the nanospheres were biocompatible. Some *in vivo* studies have

shown that the CdHgTe/gelatin nanospheres are immediately distributed to all over the vessels by blood circulation after injection. A network of blood vessels could be distinguished in fluorescence images, and the dynamic changes of nanospheres in the superficial vessels were clearly observed [78]. Although, these particles could be used as promising nanocarriers for proteins, DNA, and small molecules in the research of *in situ*, real time monitoring of drug release and therapy studies in the near future.

In Table 1 are summarized some of the most applied nanoparticles in diagnosis of gliomas.

3. Nanoparticles as Therapeutics for Brain Tumors

Despite considerable advancements in therapy of malignant gliomas in the last years, treatment outcomes are mostly unsatisfactory. A promising way to bypass these impairments and to elicit the specific delivering of drugs to treat tumors within the CNS is the employment of biodegradable polymeric NPs, which can be loaded with different chemotherapeutic drugs to induce selective toxicity, and additionally, modulate cellular and humoral immune responses when looking for a specific immune response against tumoral cells [79]. A wide variety of NPs have been designed, each one with particular properties (certain size, shape, and composition) in a scale of strategies such as conjugated antigens, which are recognized by specific receptors [80]; antigens encapsulated within NPs, which offer the ability to protect the antigen from degradation; labeled NPs, which are also recognized by specific receptors and allow an effective tracking of their migration; and the use of NPs as vehicles for specific delivery of chemotherapeutic drugs [81, 82]. Some of the more representative nanoparticles used as carriers in the treatment of gliomas are described below.

3.1. Lipid Carriers. Liposomes are concentric bilayered vesicles surrounded by a phospholipid membrane. They are related to micelles which are generally composed by hydrophilic and hydrophobic regions. The amphiphilic nature of liposomes, their facility of surface modification, and a good biocompatibility profile make them an appealing solution for increasing the circulating half-life of proteins and peptides. They may contain hydrophilic compounds, which remain encapsulated in the aqueous interior, which may escape encapsulation through diffusion out of the phospholipid membrane. Liposomes can be designed to adhere to cellular membranes to deliver a drug payload or simply transfer drugs through endocytosis [83–86]. *In vitro* and *in vivo* experiments have indicated that the activity of a range of drugs or their active metabolites may be enhanced by their encapsulation in liposomes [87–89].

Paclitaxel is a chemotherapeutic that inhibits cell division through promotion of the assembly and stabilization of microtubules. Unfortunately, paclitaxel is highly hydrophobic, and its absorption across the BBB is also poor. To overcome this limitation, paclitaxel has been conjugated to liposomes [90]. Recently, Xin et al. determined the potential of Angiopep-conjugated PEG-PCL nanoparticles loaded with paclitaxel as a dual-targeting drug delivery system in the treatment of glioma. Nanoparticles were conjugated to Angiopep (ANG-NP) for enhanced delivery across the BBB as well as for targeting the tumor via lipoprotein receptor-related protein-mediated endocytosis. Treatment with paclitaxel-loaded ANG-NP resulted in enhanced inhibitory effects in both the antiproliferative and cell apoptosis assay on U87 MG glioma cells. Also, the transport ratios across the BBB model *in vitro* using transwell membrane were significantly increased, and the cell viability of U87 MG glioma cells after crossing the BBB was significantly decreased by ANG-NP-paclitaxel [91]. Additionally, paclitaxel has been attached to an amphiphilic block copolymer of PEG-poly(lactic acid) (PLA) to form a polymer-drug conjugate. Due to the amphiphilicity of this conjugate, after self-assembling in aqueous medium, the paclitaxel molecule was trapped in the core part of the micelles formed and gets well protected, and the PEG segments constitute the upper part of the micelles, and they remain soluble in water [92]. The PEG-PLA-paclitaxel micelles displayed enhanced inhibition ability to tumor growth as shown by the body weight change, survival time, and tumor image size. This improved therapeutic effect was ascribed to the enhanced permeation and retention effect of the PEG-PLA-paclitaxel micelles. Fluorescent imaging of the brain slice further confirmed that rats treated with blank PEG-PLA micelles and PEG-PLA-paclitaxel micelles can pass the BBB and remain in the brain, which displayed higher cell uptake and stronger inhibition and apoptosis toward glioma cells [91].

Curcumin is a polyphenolic compound derived from the Indian spice turmeric. It has been shown to exert antitumor effects in many different cancer cell lines and animal models either by proapoptotic, antiangiogenic, anti-inflammatory, immunomodulatory, and antimitogenic effects [93–95]. Some potential molecular targets for curcumin include insulin-like growth factor (IGF), serine threonine protein kinase (Akt), mitogen-activated protein kinase (MAPK), signal transducer, the activator of transcription 3 (STAT3), nuclear factor kappa β (NF$\kappa\beta$), and Notch [96, 97]. These pathways are all thought to be active in malignant brain tumors, raising the possibility that curcumin could be effective in treating these diseases [98, 99]. Lim et al. used nanoparticle-encapsulated curcumin to treat medulloblastoma and glioblastoma cells, causing a dose-dependent decrease in growth of multiple brain tumor cell cultures. The reduction in viable neoplastic cells was associated with a combination of G2/M arrest and apoptotic induction [100]. Also, curcumin has been used in a spherical core-shell nanostructure formed by amphiphilic methoxy polyethylene glycol-poly(caprolactone) (mPEG-PCL) block copolymers and was effectively transported and delivered into C6 glioma cells through endocytosis of the nanoparticles and localized around the nuclei in the cytoplasm. *In vitro* studies proved that the cytotoxicity of these nanoconjugates would be result of a pro-apoptotic effect against rat C6 glioma cell line in a dose-dependent manner [101].

Celecoxib, a cyclo-oxygenase- (COX-) 2 inhibitor, has been reported to mediate growth inhibitory effects and to

Table 1: Some nanoparticles used in diagnosis of glioblastoma multiforme.

Nanoparticle composition	Size/sharp	Function	Figure
Polyaspartic-acid-(PASP-) coated iron oxide	200–700 nm forming rounded flakes	Specific recognition of tumor angiogenic cells due to be conjugated to RGD[*1] peptides and fluorescent probes	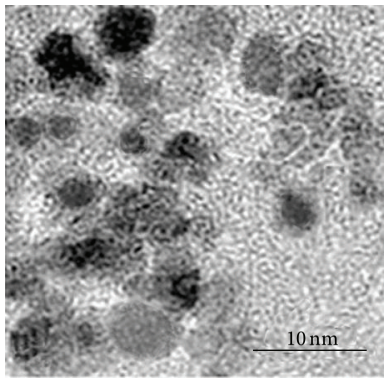
Magnetic iron oxide nanoparticles (MPIOs)	Less than 20 nm in size with crystalline cores of magnetite surrounded by a shell of dextran	The high Fe atoms content allows these nanomaterials intracellular interactions due to the magnetic field generated for MRI[*2] studies	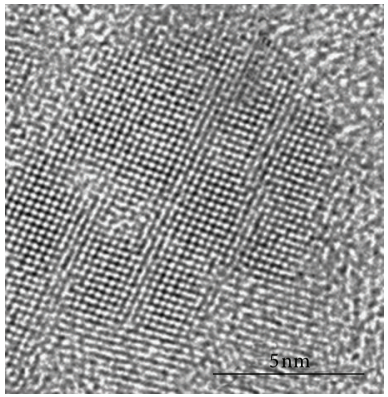
Monocrystalline iron oxide nanoparticles (MIONs)	4.7 nm as average size for these ultrafine almost spherical particles	When they are complexed to bioconjugates such as antibodies or fluorescent labels, they delimit tumor margins eliciting surgical resection of tumors	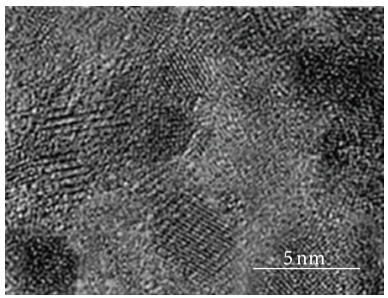

Table 1: Continued.

Nanoparticle composition	Size/sharp	Function	Figure
Ultrasmall gadolinium oxide (US-Gd_2O_3) nanocrystals	The core is 2-3 nm in size. These nanoparticles can be conjugated to target peptides or antibodies generating a diversity of structures	The very small size and superior density of these nanomaterials produce higher signal contrast than other gadolinium-containing particles	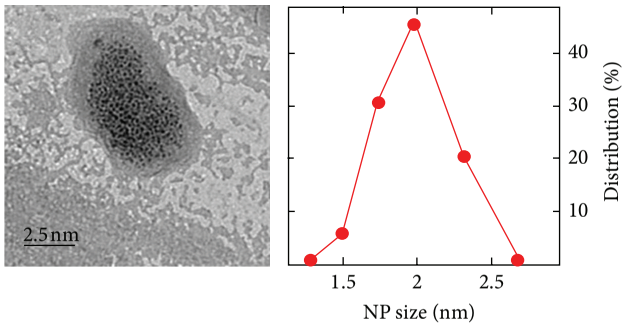 (a) (b)
Nanoshells of crystalline metals	Diameter size 50–100 nm with single or double walls covering nanoparticles	During engaged reaction metal, nanoparticles (i.e., gold) are covered with mono- or multiple layers of another metal (i.e., silver) increasing contrast in optical imaging. Also, they could be conjugated with luminescent labels	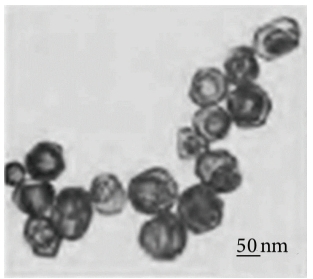
Quantum dots (QDs) cadmium-based complexed to inert metals	The high diversity of sizes (10–20 nm) allows to use these nanomaterials in multicolor assays	The relationship between physical size of QDs and the wavelength of emitted fluorescence is referred to as "tunability"; therefore one wavelength can produce different colours depending of the size of QDs	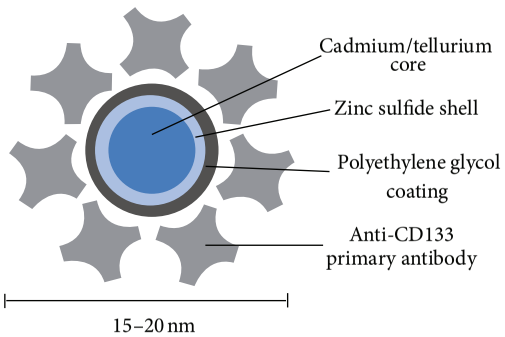

*[1]RGD: arginine-glycine-aspartic acid sequence.
*[2]MRI: magnetic resonance imaging.

induce apoptosis in various cancer cell lines [102]. Celecoxib has been conjugated to poly-D,L-lactide-co-glycolide (PLGA) and tested in glioma finding that the celecoxib recovered in the nanoparticles showed similar antitumor activity against U87MG cells and C6 cells in a dose-dependent manner. These results show that PLGA nanoparticles incorporating celecoxib are promising candidates for antitumor drug delivery [103].

Although doxorubicin (DOX) has not been used as treatment in brain tumors, because it has poor distribution and limited penetration, it is one of the most likely candidates for CNS chemotherapy [104]. Here, we describe some studies where liposomes were used as carriers of DOX. The liposomal encapsulation of DOX using polyethylene glycol (PEG) liposomes has shown a long circulation time in plasma, reduced cardiac toxicity, and improved penetration of DOX across the BBB by leading to increased efficacy of the distribution and accumulation into tumors [105]. The first studies compared the accumulation between free doxorubicin and PEG-liposome encapsulated in glioma C6 cells models, showing an increase in their uptake and accumulation by glioma cells compared to conventional liposomes or free doxorubicin. Also, the incorporation of PEG into this liposome membrane allowed a long circulating half-life, slow plasma clearance, and a reduced volume of distribution [106].

Nanoconjugates coupled with liposomes could be a new treatment of gliomas, because they increase both the uptake of and specificity to glioma cells. The chlorotoxin (CTx) is a scorpion-derived peptide, which binds with high specificity to glioma cell surface as a specific chloride channel and matrix metalloproteinase-2 blocker. It was firstly applied to establish the CTx-modified doxorubicin- (DOX-)loaded liposome delivery system for targeting brain glioma and improving the anticancer efficacy. Recently, it has been developed in BALB/c mice-bearing U87 tumor xenografts, a novel liposome system with a uniform distribution, high encapsulation efficiency, and adequate loading capacity of both fluorescent probe and DOX. The biodistribution of DOX-loaded liposomes by body imaging and antiglioma pharmacodynamics were studied finding that CTx-modified liposomes were drastically accumulated in subcutaneous and intracranial tumors, showing higher tumor growth inhibition and lower blood toxicity in the armpit tumor model. *In vivo* results exhibited good correlation of glioma targeting of the CTx-modified liposomes, with the CTx as the targeting ligand [107].

In order to increase the uptake of these nanoparticles, specific ligands were coupled to the distal ends of the PEG chains to increase their uptake through receptor-mediated targeting while maintaining PEG stability. The membrane transferrin receptor (Tr) mediated endocytosis or internalization of the complex of transferrin bound iron, and the transferrin receptor is the major route of cellular iron uptake. This efficient cellular uptake pathway has been exploited for the site-specific delivery not only of anticancer drugs and proteins but also of therapeutic genes into proliferating malignant cells that overexpress the transferrin receptors [108, 109]. Studies have shown that PEG liposomes coupled to transferrin are able to achieve preferential receptor-mediated targeting of C6 glioma *in vitro* [110, 111]. On the other hand, lactoferrin (Lf) and the procationic liposomes (PCLs) have been conjugated to develop DOX-loaded Lf-PCL (DOX-Lf-PCL) nanoparticles. In primary culture and glioma cell C6 model, DOX-Lf-PCLs showed significantly higher uptake, and their *in vivo* systemic administration increases the accumulation of Lf-PCLs in the brain [87]. These studies suggested that nanoconjugates and Lf-PCLs were available for brain drug delivery representing potential future clinical application.

4. Nanocrystals

Nanocrystals are aggregates of molecules that can be combined into a crystalline form of the drug surrounded by a thin coating of surfactant. They have extensive uses in materials research, chemical engineering, and as quantum dots for biological imaging; there is no carrier material as in polymeric nanoparticles [112–114]. Nanocrystalline species may be prepared from a hydrophobic compound and coated with a thin amphiphilic layer. It has been demonstrated that the size and shape of nanocrystals play an important role in their biological activity [115].

Some nanocrystals have shown to inhibit the proliferation in different cancer cells lines [116]. Silver nanoparticles (AgNPs) have recently been the focus of intense research due to their capacity to induce the expression of genes associated with cell cycle progression, DNA damage, and apoptosis in human cells at noncytotoxic doses [117]. The toxicity of starch-coated AgNPs have been studied in normal human lung fibroblast cells (IMR-90) and human glioblastoma cells (U251); uptake of AgNPs is predominantly done by endocytosis and partly adhered to membranous surfaces. Once inside, AgNPs show a uniform intracellular distribution of both cytoplasm and nucleus. The accumulation of these particles causes DNA damage and reduces cellular ATP content, causing damages in mitochondria and increasing the production of reactive oxygen species (ROS) in a dose-dependent manner in glioma cells. Also, it has been proposed that AgNPs can induce DNA damage leading to cell cycle arrested in G2/M phase and enhancing the apoptosis rate of cancer cells [118–121].

The combination of AgNPs with magnetic nanoparticles hyperthermia (MNPH) treatment has been used as treatment in glioma model. AgNPs had significant effect on enhancing thermoinduced killing *in vitro*. In the glioma-bearing rat model, AgNPs combined with MNPH enhance Bax (Bcl-2–associated X protein) expression in cancer cells, which was correlated with cell apoptosis induction. The mechanism of thermosensitization by AgNPs might be related to the release of Ag^+ cation from the silver nanostructures inside cells. Ag^+ cation has the ability to capture electrons and thus functions as an oxidative agent [18, 122].

Based on thermodynamic constraints, metallic Ag cores have been modified with (in)organic ligands allowing the synthesis of protein-conjugated Ag_2S nanoparticles that increase physical and chemical stability [123]. Recently, Wang et al. observed cell death that might result from the interaction between mitochondria proteins and Ag^+ released from

nanocrystals, which were predominantly endocytosed, and partly adhered to the membrane surface [78]. Even when high dosages can be achieved with nanocrystals and poorly soluble drugs can be formulated to increase their bioavailability via treatment with an appropriate coating layer, studies about the stability of nanocrystals and the cytotoxicity of these nanoparticles, with respect to their size and shape, are needed in order to advance in nanotechnology for tumor treatment, cure and to predict the possible toxic side effects on the body [18, 78].

4.1. Nanotubes. Self-assembling sheets of atoms arranged in tubes are defined as nanotubes. They may be organic or inorganic in composition and can be produced as single- or multiwalled structures. They have large internal volumes, and the external surface can be easily functionalized. While they are potentially promising for pharmaceutical applications, human tolerance of these compounds remains unknown, toxicity reports are conflicting, and extensive researches regarding the biocompatibility and toxicity of nanotubes are needed [124]. Carbon nanotubes (CNTs) are formed by rolling sheets of graphite-like carbon with hollow tubes. They are categorized based on the number of carbon layers assembled together: single-walled (SW), double-walled (DW), and multiwalled (MW). The diameters vary according to the number of layers: 0.4–2 nm for SWNTs, 1–3.5 nm for DWNTs, and 2–100 nm for MWCNTs [125]. The length of these tubes can be extended to tens of micrometers and is dependent on the method of production.

As in nanovectors, CNTs have the advantage of providing a versatile, biodegradable, and nonimmunogenic delivery alternative to viral vectors for molecular therapy or immunotherapy as direct delivery of antigens to antigen presenting cells (APCs) or microglia in the central nervous system [126]. Kateb et al. evaluated the efficacy of multiwalled carbon nanotubes (MWCNTs) as potential nanovectors for delivery of macromolecules into microglia (MG) using the cell line BV2 (a microglia cell line) to determine the capacity to uptake MWCNTs by BV2 cells *in vitro*, demonstrating the ability of BV2 cells to more efficiently internalize MWCNTs as compared to glioma cells without any significant signs of cytotoxicity. They were able to visualize ingestion of MWCNTs into MG, cytotoxicity, and loading capacity of MWCNTs under normal culture conditions, suggesting that MWCNTs could be used as a novel, nontoxic, and biodegradable nanovehicles for targeted therapy in brain tumors.

On the other hand, this group also analyzed the internalization of these nanotubes in an intracranial glioma model and characterized some changes in tumor cytokine production following intratumoral injection of MWCNTs in GL261 murine glioma model. Authors demonstrated that MWCNTs were preferentially detected in tumor macrophages (MPs), and to a lesser extent in MG. In addition to MG and MP, a small fraction of glioma cells, which are not typically capable of phagocytosis, also became positive for MWCNTs; FACS and quantitative RT-PCR were performed to analyze the inflammatory response and cytokine profile. A transient influx of MP was seen in both normal brain and GL261 gliomas in response to MWCNTs; whereas no significant change in cytokine expression was noted in normal group [127]. They concluded that CNTs can potentially be used as a nanovector delivery system to modulate MP function in tumors.

4.2. Inorganic Nanoparticles. Ceramic nanoparticles are typically composed of inorganic compounds such as silica or alumina. Originally used with silica-based materials [128], this approach was extended to organosilicates [129], transition metal oxides [130], metalloid [131], and metal sulfides [132] to produce a myriad of nanostructures with a characteristic size, shape, and porosity. Generally, inorganic nanoparticles may be engineered to evade the reticuloendothelial system by varying their size and surface composition. Moreover, the nanoparticle structure is porous, and it provides a physical encasement to protect an entrapped molecular payload from degradation or denaturation. Mesoporous silica materials contain a complex "worm-like" network of channels throughout the interior of the solid nanoparticles. It is relatively easy to modify the surfaces of these particles with unique functionalities via a variety of chemical transformations. Several functional groups can be introduced onto the surface of inorganic nanoparticles, ranging from saturated and unsaturated hydrocarbons to carboxylic acids, thiols, amines, and alcohols. Inorganic nanoparticles are relatively stable over broad ranges of temperature and pH, yet their lack of biodegradation and slow dissolution raises safety questions, especially for long term administration [133, 134].

4.3. Dendrimers. Dendrimers are polymer-based macromolecules formed from monomeric or oligomeric units, such that each layer of branching units doubles or triples the number of peripheral groups. These structures are considered as one of the most promising polymer architectures in biomedical applications in recent years [135, 136]. Such structures are highly branched, multigenerational nanoparticles consisting of exterior end groups that can be functionalized [137–139]. Examples included the encapsulation of therapeutic agents inside the dendrimers and attachment of drugs, targeting moieties and functional groups on the surface of them by covalent bounding or physical absorbing, which afforded the possibility to produce the desired multifunctional nanocarriers for drug delivery.

The avoid area within dendrimer and the extent of its branching, the size control, and its facility of modification and preparation offer great potential for drug delivery. Generally, they have a symmetrical structure, with the potential to create an isolated "active site" core area through chemical functionalization. The modification of the degree of branching may allow for encapsulation of a molecule within this structure [140]. For instance, a dendrimer may become water soluble when its end groups are functionalized with hydrophilic groups, such as carboxylic acids. Thus, water-soluble dendrimers may be designed with internal hydrophobicity, suitable for the incorporation of a hydrophobic drug. The frequently used genetic transfection agent *polyfect* consists of dendrimer molecules radiating from a central core. Amino

groups at the terminal ends of the dendrimer branches are positively charged at physiological pH, therefore interacting with the negatively charged phosphate groups of nucleic acids [141]. However, dendrimers require further improvements in cytotoxicity profiles, biocompatibility, and biodistribution into the body.

Drug carriers such as dendrimers have been used for therapeutic purposes in the treatment of gliomas. These nanomaterials were conjugated to D-glucosamine as the ligand for enhancing their permeability across BBB and tumor targeting. The efficacy of methotrexate- (MTX-)loaded dendrimers was established against U87 MG and U343 MGa cells. Permeability of rhodamine-labeled dendrimers and MTX-loaded dendrimers across an *in vitro* BBB model and their distribution into vascular human glioma tumor spheroids were also studied. Glycosylated dendrimers were found to be endocytosed in significantly higher amounts than nonglucosylated dendrimers by the cell lines mentioned above. These MTX-loaded dendrimers were also able to kill even MTX-resistant cells highlighting their ability to overcome MTX resistance. In addition, the amount of MTX transported across BBB was three to five times more after loading in the dendrimers. Glycosylation further increased the cumulative permeation of dendrimers across BBB and hence increased the amount of MTX available across it. These results shown that glucosamine not only can be used as an effective ligand for targeting glial tumors but also enhanced their permeability across BBB [142].

Furthermore, the poly(amidoamine) (PAMAM) dendrimer was employed as a carrier to codeliver antisense-miR-21 oligonucleotide (as-miR-21) and 5-fluorouracil (5-FU) to achieve delivery of as-miR-21 to human glioblastoma cells and enhance the cytotoxicity of 5-FU antisense therapy. PAMAM could be simultaneously loaded with 5-FU and as-miR-21, forming a complex smaller than 100 nm in diameter. Both the chemotherapeutant and as-miR-21 could be efficiently introduced into tumor cells. The codelivery of as-miR-21 significantly improved the cytotoxicity of 5-FU and dramatically increased the apoptosis of U251 cells, while the migration ability of the tumor cells was decreased. These results suggest that the codelivery system may have important clinical applications in the treatment of miR-21-overexpressing glioblastoma [143].

5. Antibodies Conjugated to Nanoparticles

Tumor-specific targeting using achievements of nanotechnology is a mainstay of increasing efficacy of antitumor drugs. One of the most significant advances in tumor-targeted therapy is the surface modification of nanoparticles with monoclonal antibodies (mAbs) alone or in combination with antineoplastic drugs in cancer therapy [144]. Another important advantage of this technology is the possibility of masking the unfavorable physicochemical characteristics of the incorporated molecule. In particular, the treatment of brain tumors takes advantage of this characteristics due to efficient and specific brain delivery of the anticancer drugs [145]. These different strategies can be exploited for a variety of biomedical applications such as cancer immunotherapy that manipulate the immune system for therapeutic benefits and minimize adverse effects [146].

In order to improve direct tumor targeting and to avoid the damage of nontumor cells Fujita et al. [147] synthesized a new polycefin variant conjugated to two monoclonal antibodies of different specificities in a promising drug carrier poly(β-l-malic acid) (PMLA) polymer, natural product of *Physarum polycephalum* [148] that is used as a carrier matrix of biopharmaceuticals with some advantages such as lack of toxicity *in vitro* and *in vivo*, nonimmunogenicity, biodegradability, stability in the bloodstream, and easy cellular uptake [149–152]. Also, they studied the drug accumulation in glioma-bearing animals finding that the polycefin variant with the combination of mouse anti-TfR [153, 154] and human tumor-specific antibody 2C5 [155, 156] provides the most efficient drug delivery route through mouse endothelial system and into implanted human brain tumor cells. It was not achieved by variants with single mAbs or devoid of antibodies. The presence of two or more different antibodies at the same time on drug delivery systems, especially on polycefin variants, may be important for future specific drug delivery and therapeutic efficacy in tumor treatment.

Another interesting approach is the use of immunoliposomes, which are antibodies conjugated to the liposomes using the antibody motif of protein A (ZZ) as an adaptor. Feng et al. [157] used the immunoliposomes to deliver sodium borocaptate (BSH) encapsulated in liposomes composed of nickel lipid (a lipid derivatized with a nickel-chelating head group) and antiepidermal growth factor receptor (EGFR); antibodies were conjugated to the liposomes using the antibody affinity motif of protein A (ZZ) as an adaptor into EGFR-overexpressing glioma cells. Immunohistochemical analysis using an anti-BSH monoclonal antibody revealed that BSH was delivered effectively into the cells but not into EGFR-deficient glioma or primary astrocytes. In an animal model of brain tumors, both the liposomes and the BSH were only observed in the tumor. Moreover, enriched boron or ^{10}B conjugated with anti-EGFR antibodies by ZZ-His provides a selective delivery system into glioma cells, and this was confirmed by inductively coupled plasma-atomic emission spectrometry (ICP-AES) both *in vitro* and *in vivo* [157].

5.1. Solid Lipid Nanoparticles. Solid lipid nanoparticles are lipid-based submicron colloidal carriers. They were initially designed in the early 1990s as a pharmaceutical alternative to liposomes and emulsions. In general, they are more stable than liposomes in biological systems due to their relatively rigid core consisting of hydrophobic lipids that are solid at room and body temperatures, surrounded by a monolayer of phospholipids [158]. These aggregates are further stabilized by the inclusion of high levels of surfactants. Because of their facility of biodegradation, they are less toxic than polymer or ceramic nanoparticles. Also, they have controllable pharmacokinetic parameters and can be engineered with three types of hydrophobic core designs: a homogenous matrix, a drug-enriched shell, or a drug-enriched core. It has been demonstrated that the compound payload can leave the

hydrophobic core at warmer temperatures. Conversely, the compound payload enters the hydrophobic core at lower temperatures. These principles are used to load and unload solid lipid nanoparticles for the delivery of therapeutic agents, taking advantage of recent techniques to selectively produce hypo- and hyperthermia. These nanoparticles can be used to deliver drugs orally, topically, or via inhalation.

Recently, Kuo and Liang used innovative catanionic solid lipid nanoparticles (CASLNs) prepared in microemulsions carrying carmustine (BCNU) (BCNU-CASLNs) that were grafted with antiepithelial growth factor receptor (EGFR) (anti-EGFR/BCNU-CASLNs) and applied to inhibit the propagation of human brain malignant glioblastomas cells due to gliomas normally express certain types of growth factor receptor. The catanionic surfactants (1 Mm) yielded the smallest particle size of BCNUCASLNs and the largest entrapment efficiency of BCNU with a moderate toxicity to human brain-microvascular endothelial cell and a tolerable expression of TNF-α. Thereby, anti-EGFR/BCNU-CASLNs could have a potential use in anticancer chemotherapy for clinical application [159].

These nanoparticles could be loaded with others types of chemotherapeutics such as doxorubicin (DOX). The use of CASLNs loaded with DOX and grafted with antiepithelial growth factor receptor (EGFR) (anti-EGFR/DOX-CASLNs) suppressed the propagation of malignant U87MG cells. At 1 mM concentrations of these catanionic surfactants conjugated with hexadecyltrimethylammonium bromide and sodium anionic sodium dodecylsulfate, CASLNs entrapped the largest quantity of DOX, concluding that catanionic surfactants at 1 mM and 100% of cacao butter (CB) could be satisfactory conditions for preparing anti-EGFR/DOX-CASLNs to inhibit proliferation of malignant U87MG cells, and the grafted anti-EGFR could substantially enhance the delivery efficiency of DOX to U87MG cells [160].

Above all, these nanoparticles are not used yet in clinical trials against glioblastoma or others types of brain tumors, but this innovative approach can be an effective delivery system with high targeting efficacy against brain tumors due to the great capacity to deliver chemotherapeutic agents and to reduce toxicity.

In Table 2 we are summarized some of the most applied nanoparticles for treatment of gliomas.

6. Special Considerations

While it is important to achieve an increased uptake of functional targeting nanoparticles by GBM cells, it is also important to consider the biodistribution of the nanoparticles in blood circulation and liver accumulation, highlighting the importance of controlling ligand loading in order to achieve optimal performance for therapeutic and imaging applications for multivalent nanoparticle-based systems [161].

7. Perspectives

Nowadays, several research groups are actively trying to combine a variety of functions into NPs as platforms for targeting different immune and tumoral cells and to develop diverse strategies to modulate specific treatments. A major effort toward successful NP-based therapeutics will be needed to avoid extensive and nonspecific immunostimulatory or immunosuppressive reactions to the nanomaterials, once they have been administered into the body, in order to find a right balance between any remaining potential damage and the health and quality of life of patients. This implies the future development of new or adapted methods appropriate to assess new medicinal tools involving NPs. Although many questions still require extensive investigation, the available data suggest that a variety of NPs can be engineered to become part of the next generation of immunomodulatory platforms and treatments [80].

Nanoparticles exploit biological pathways to achieve payload delivery to cellular and intracellular targets, including transport across the BBB. The central nervous system is protected by this barrier which maintains its homeostasis. However, many potential drugs for the treatment of diseases of the central nervous system (CNS) cannot reach the brain in high concentrations. This physical barrier limits the brain uptake of the vast majority of neurotherapeutics and neuroimaging contrast agents [7, 17]. One possibility to deliver drugs to the CNS is the employment of polymeric nanoparticles. Modification of the nanoparticle surface with covalently attached targeting ligands or by coating with certain surfactants had enabled the adsorption of specific plasma proteins. The ability of these carriers to overcome BBB appears to be receptor-mediated endocytosis in brain capillary endothelial cells. The possibility to employ nanoparticles for delivery of proteins and other macromolecules across the BBB suggests that this technology holds great promises for noninvasive therapy of the CNS diseases. Recently, some studies have shown the distribution, pharmacokinetics, and drugs delivery into the brain in rodents and found that nanoparticles greater than approximately 100–150 nm in diameter will tend to accumulate in tumors due to their higher extravasation in comparison with normal vasculature [16, 162]. Rapid advances and emerging technologies in nanoparticles have shown a profound impact on cancer diagnosis, treatment, and monitoring. Now, the interest of researchers is defining physical and chemical characteristics to provide an effective therapy without side effects.

8. Conclusion

Studies on the biological composition, administrations, and adverse events of new nanomaterials suited for biomedical applications are important for therapeutic drug delivery and the development of innovative and better treatments [163]. Furthermore, the engineering of the particle backbone structure, size, shape of the nanoparticle surface, and the core itself provides yet another dimension of physical control that can be directed toward an increased strength, increased chemical specificity, or heat resistance. Most polymeric nanoparticles are biodegradable and biocompatible and have been adopted as a preferred method for drug delivery. Since nanoparticles come into direct contact with cellular membranes,

Table 2: Nanoparticles proposed as candidates for the treatment of glioblastoma multiforme.

Nanoparticle	Structure	Function	Figure
Liposomes	Bilayered vesicles conjugated with some proteins or drugs (i.e., anfotericine) for recognition and/or lists of cancer cells	Due to their amphiphilic structure, it is feasible to manipulate surface modification and/or conjugate them with biomolecules to increase the circulating half-life and deliver antineoplastic drugs in tumoral areas	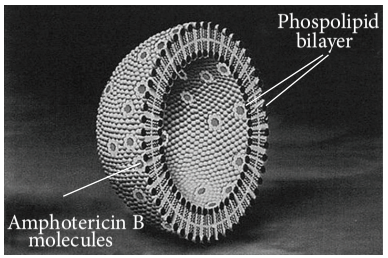
Solid lipid nanoparticles	Submicron colloidal carriers that could be loaded with others types of chemotherapeutics or specific antibodies	Currently, these particles are under research, but they could deliver chemotherapeutic agents into neoplastic cells due to their biocompatible and fusionable membranes	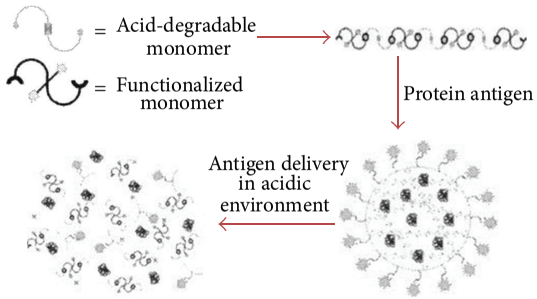
Drugs or toxin conjugated nanoparticles	The satisfactory size of nanoparticles allows to encapsulate anti-neoplastic drugs, toxins, or specific antibodies directed to membrane-bound antigens in cancer cells	These nanoconjugates deliver their drug load to increase local levels of apoptotic molecules near tumors or to accumulate in focal areas to exert their cytotoxic effect	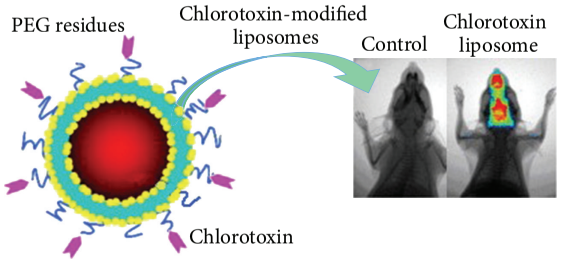

Table 2: Continued.

Nanoparticle	Structure	Function	Figure
Nanocrystals	Crystalline aggregates of hydrophobic molecules coated with a thin hydrophilic layer	Depending of the size of crystals several protein-metal conjugates can originate nanorods or nanowires which could enhance thermosensitivity of cancer cells	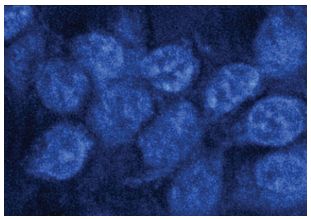
Nanotubes	Single or multilayered sheets of self-assembling organic or inorganic atoms	Due to their large inner volume and great external surface could be drug-loaded and may induce cellular death	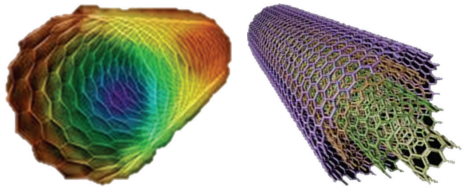
Dendrimers	Monomeric or oligomeric multibranched structures whose exterior-end groups can be conjugated to drugs, antibodies, or metal atoms	These symmetrical particles may encapsulate drugs, targeting moieties, antibodies, and functional groups to carry and deliver them inside tumor	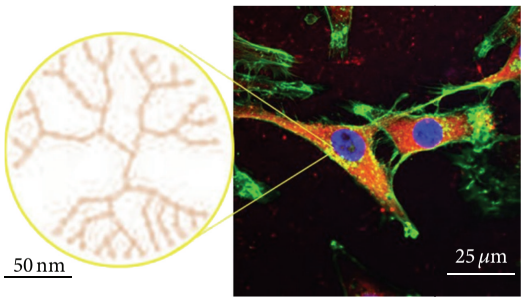

their surface properties may determine the mechanism of internalization and intracellular localization [164]. They also exhibit a good potential for surface modification via chemical transformations, provide excellent pharmacokinetic control, and are suitable for the entrapment and delivery of a wide range of therapeutic agents.

The use of nanoparticles could be a good option in diagnosis and treatment of gliomas. Studies suggest that a variety of NPs can be engineered to become part of the next generation of agents delivery and specific treatment on gliomas. The use of a biocompatible system of NPs, conjugates should reduce the toxicity and side effects of systemic drugs administration and therefore improve the quality of life in cancer patients. However, several studies conducted largely on mice have shown undesired side effects such as inflammatory response including substantial lung neutrophil influx and mortality at high doses. In addition, NPs may feasibly represent a useful imaging tool to diagnosis and followup; also, it to be used to assess/monitor efficacy of antiangiogenic or other antitumour treatments, thus improving the clinical management of brain tumours. Nevertheless, additional research is required in multifunctional NPs based drug delivery systems to overcome the problems and understand how nanoparticles interact with biological systems and the environment for effective therapy.

References

[1] D. C. Adamson, B. A. Rasheed, R. E. McLendon, and D. D. Bigner, "Central nervous system," *Cancer Biomarkers*, vol. 9, no. 1–6, pp. 193–210, 2011.

[2] National Cancer Institute, *Central Brain Tumor Registry of the United States*, 2011.

[3] E. Allard, C. Passirani, and J. P. Benoit, "Convection-enhanced delivery of nanocarriers for the treatment of brain tumors," *Biomaterials*, vol. 30, no. 12, pp. 2302–2318, 2009.

[4] R. Stupp, M. E. Hegi, M. R. Gilbert, and A. Chakravarti, "Chemoradiotherapy in malignant glioma: standard of care and future directions," *Journal of Clinical Oncology*, vol. 25, no. 26, pp. 4127–4136, 2007.

[5] I. F. Parney and S. M. Chang, "Current chemotherapy for glioblastoma," *Cancer Journal*, vol. 9, no. 3, pp. 149–156, 2003.

[6] D. A. Reardon, A. Desjardins, K. B. Peters et al., "Phase 2 study of carboplatin, irinotecan, and bevacizumab for recurrent glioblastoma after progression on bevacizumab therapy," *Cancer*, vol. 117, no. 23, pp. 5351–5358, 2011.

[7] R. Stupp, M. E. Hegi, W. P. Mason et al., "Effects of radiotherapy with concomitant and adjuvant temozolomide versus radiotherapy alone on survival in glioblastoma in a randomised phase III study: 5-year analysis of the EORTC-NCIC trial," *The Lancet Oncology*, vol. 10, no. 5, pp. 459–466, 2009.

[8] I. Lynch, K. A. Dawson, and S. Linse, "Detecting cryptic epitopes created by nanoparticles," *Science's STKE*, vol. 2006, no. 327, p. pe14, 2006.

[9] V. L. Colvin, "The potential environmental impact of engineered nanomaterials," *Nature Biotechnology*, vol. 21, no. 10, pp. 1166–1170, 2003.

[10] L. K. Adams, D. Y. Lyon, and P. J. J. Alvarez, "Comparative ecotoxicity of nanoscale TiO_2, SiO_2, and ZnO water suspensions," *Water Research*, vol. 40, no. 19, pp. 3527–3532, 2006.

[11] S. P. Leary, C. Y. Liu, and M. L. J. Apuzzo, "Toward the emergence of nanoneurosurgery: Part II—Nanomedicine: diagnostics and imaging at the nanoscale level," *Neurosurgery*, vol. 58, no. 5, pp. 805–822, 2006.

[12] J. R. McCarthy and R. Weissleder, "Multifunctional magnetic nanoparticles for targeted imaging and therapy," *Advanced Drug Delivery Reviews*, vol. 60, no. 11, pp. 1241–1251, 2008.

[13] S. S. Gambhir, "Molecular imaging of cancer with positron emission tomography," *Nature Reviews Cancer*, vol. 2, no. 9, pp. 683–693, 2002.

[14] W. A. Weber, "Use of PET for monitoring cancer therapy and for predicting outcome," *Journal of Nuclear Medicine*, vol. 46, no. 6, pp. 983–995, 2005.

[15] A. Chopra, "L- and D-*S*-(3-[^{18}F]fluoropropyl)homocysteine," in *Molecular Imaging and Contrast Agent Database (MICAD)*, National Library of Medicine, NIH, Bethesda, Md, USA, 2004–2013.

[16] F. Bénard, J. Romsa, and R. Hustinx, "Imaging gliomas with positron emission tomography and single-photon emission computed tomography," *Seminars in Nuclear Medicine*, vol. 33, no. 2, pp. 148–162, 2003.

[17] A. Takeda, H. Tamano, and N. Oku, "Alteration of zinc concentrations in the brain implanted with C6 glioma," *Brain Research*, vol. 965, no. 1-2, pp. 170–173, 2003.

[18] L. Liu, F. Ni, J. Zhang et al., "Silver nanocrystals sensitize magnetic-nanoparticle-mediated thermo-induced killing of cancer cells," *Acta Biochimica et Biophysica Sinica*, vol. 43, no. 4, pp. 316–323, 2011.

[19] C. Stippich, "Presurgical functional magnetic resonance imaging," *Radiologe*, vol. 50, no. 2, pp. 110–122, 2010.

[20] C. H. Cunningham, T. Arai, P. C. Yang, M. V. McConnell, J. M. Pauly, and S. M. Conolly, "Positive contrast magnetic resonance imaging of cells labeled with magnetic nanoparticles," *Magnetic Resonance in Medicine*, vol. 53, no. 5, pp. 999–1005, 2005.

[21] P. Balchandani, M. Yamada, J. Pauly, P. Yang, and D. Spielman, "Self-refocused spatial-spectral pulse for positive contrast imaging of cells labeled with SPIO nanoparticles," *Magnetic Resonance in Medicine*, vol. 62, no. 1, pp. 183–192, 2009.

[22] H. Maeda, G. Y. Bharate, and J. Daruwalla, "Polymeric drugs for efficient tumor-targeted drug delivery based on EPR-effect," *European Journal of Pharmaceutics and Biopharmaceutics*, vol. 71, no. 3, pp. 409–419, 2009.

[23] H. K. Pannu, C. Cohade, R. E. Bristow, E. K. Fishman, and R. L. Wahl, "PET-CT detection of abdominal recurrence of ovarian cancer: radiologic-surgical correlation," *Abdominal Imaging*, vol. 29, no. 3, pp. 398–403, 2004.

[24] J. Ruf, E. L. Hänninen, H. Oettle et al., "Detection of recurrent pancreatic cancer: comparison of FDG-PET with CT/MRI," *Pancreatology*, vol. 5, no. 2-3, pp. 266–272, 2005.

[25] R. Myers, "The application of PET-MR image registration in the brain," *British Journal of Radiology*, vol. 75, pp. S31–S35, 2002.

[26] J. Čížek, K. Herholz, S. Vollmar, R. Schrader, J. Klein, and W. D. Heiss, "Fast and robust registration of PET and MR images of human brain," *NeuroImage*, vol. 22, no. 1, pp. 434–442, 2004.

[27] R. Huang, L. Han, J. Li et al., "Chlorotoxin-modified macromolecular contrast agent for MRI tumor diagnosis," *Biomaterials*, vol. 32, no. 22, pp. 5177–5186, 2011.

[28] O. Veiseh, F. M. Kievit, C. Fang et al., "Chlorotoxin bound magnetic nanovector tailored for cancer cell targeting, imaging, and siRNA delivery," *Biomaterials*, vol. 31, no. 31, pp. 8032–8042, 2010.

[29] B. Chertok, B. A. Moffat, A. E. David et al., "Iron oxide nanoparticles as a drug delivery vehicle for MRI monitored magnetic targeting of brain tumors," *Biomaterials*, vol. 29, no. 4, pp. 487–496, 2008.

[30] F. D. Knollmann, J. C. Böck, K. Rautenberg, J. Beier, W. Ebert, and R. Felix, "Differences in predominant enhancement mechanisms of superparamagnetic iron oxide and ultrasmall superparamagnetic iron oxide for contrast-enhanced portal magnetic resonance angiography: preliminary results of an animal study original investigation," *Investigative Radiology*, vol. 33, no. 9, pp. 637–643, 1998.

[31] K. Temming, R. M. Schiffelers, G. Molema, and R. J. Kok, "RGD-based strategies for selective delivery of therapeutics and imaging agents to the tumour vasculature," *Drug Resistance Updates*, vol. 8, no. 6, pp. 381–402, 2005.

[32] Z. Li, G. Zhang, H. Shen, L. Zhang, and Y. Wang, "Synthesis and cell uptake of a novel dualmodality 188Re-HGRGD (D) F-CdTe QDs probe," *Talanta*, vol. 85, no. 2, pp. 936–942, 2011.

[33] W. Cai, J. Rao, S. S. Gambhir, and X. Chen, "How molecular imaging is speeding up antiangiogenic drug development," *Molecular Cancer Therapeutics*, vol. 5, no. 11, pp. 2624–2633, 2006.

[34] H. Y. Lee, Z. Li, K. Chen et al., "PET/MRI dual-modality tumor imaging using arginine-glycine-aspartic (RGD)-conjugated radiolabeled iron oxide nanoparticles," *Journal of Nuclear Medicine*, vol. 49, no. 8, pp. 1371–1379, 2008.

[35] E. V. Rosca, R. J. Gillies, and M. R. Caplan, "Glioblastoma targeting via integrins is concentration dependent," *Biotechnology and Bioengineering*, vol. 104, no. 2, pp. 408–417, 2009.

[36] A. Bjornerud, M. F. Wendland, L. Johansson, H. K. Ahlstrom, C. B. Higgins, and A. Øksendal, "Use of intravascular contrast agents in MRI," *Academic Radiology*, vol. 5, supplement 1, pp. S223–S225, 1998.

[37] Y. X. J. Wang, S. M. Hussain, and G. P. Krestin, "Superparamagnetic iron oxide contrast agents: physicochemical characteristics and applications in MR imaging," *European Radiology*, vol. 11, no. 11, pp. 2319–2331, 2001.

[38] Y. Gossuin, P. Gillis, A. Hocq, Q. L. Vuong, and A. Roch, "Magnetic resonance relaxation properties of superparamagnetic particles," *Wiley Interdisciplinary Reviews*, vol. 1, no. 3, pp. 299–310, 2009.

[39] Y. Anzai, C. W. Piccoli, E. K. Outwater et al., "Evaluation of neck and body metastases to nodes with ferumoxtran 10-enhanced MR imaging: Phase III safety and efficacy study," *Radiology*, vol. 228, no. 3, pp. 777–788, 2003.

[40] V. I. Shubayev, T. R. Pisanic II, and S. Jin, "Magnetic nanoparticles for theragnostics," *Advanced Drug Delivery Reviews*, vol. 61, no. 6, pp. 467–477, 2009.

[41] D. L. J. Thorek, A. K. Chen, J. Czupryna, and A. Tsourkas, "Superparamagnetic iron oxide nanoparticle probes for molecular imaging," *Annals of Biomedical Engineering*, vol. 34, no. 1, pp. 23–38, 2006.

[42] E. Gultepe, F. J. Reynoso, A. Jhaveri et al., "Monitoring of magnetic targeting to tumor vasculature through MRI and biodistribution," *Nanomedicine*, vol. 5, no. 8, pp. 1173–1182, 2010.

[43] P. M. Winter, A. M. Morawski, S. D. Caruthers et al., "Molecular imaging of angiogenesis in early-stage atherosclerosis with $\alpha v\beta 3$-integrin-targeted nanoparticles," *Circulation*, vol. 108, no. 18, pp. 2270–2274, 2003.

[44] X. Montet, K. Montet-Abou, F. Reynolds, R. Weissleder, and L. Josephson, "Nanoparticle imaging of integrins on tumor cells," *Neoplasia*, vol. 8, no. 3, pp. 214–222, 2006.

[45] M. Nahrendorf, F. A. Jaffer, K. A. Kelly et al., "Noninvasive vascular cell adhesion molecule-1 imaging identifies inflammatory activation of cells in atherosclerosis," *Circulation*, vol. 114, no. 14, pp. 1504–1511, 2006.

[46] J. H. Lee, Y.-M. Huh, Y.-W. Jun et al., "Artificially engineered magnetic nanoparticles for ultra-sensitive molecular imaging," *Nature Medicine*, vol. 13, no. 1, pp. 95–99, 2007.

[47] M. Di Marco, C. Sadun, M. Port et al., "Physicochemical characterization of ultrasmall superparamagnetic iron oxide particles (USPIO) for biomedical application as MRI contrast agents," *International Journal of Nanomedicine*, vol. 2, no. 4, pp. 609–622, 2007.

[48] T. Egelhof, N. Delbeck, M. Hartmann et al., "Can superparamagnetic contrast media improve MRI-tomographic images of experimental gliomas?" *Radiologe*, vol. 38, no. 11, pp. 943–947, 1998.

[49] W. S. Enochs, G. Harsh, F. Hochberg, and R. Weissleder, "Improved delineation of human brain tumors on MR images using a long-circulating, superparamagnetic iron oxide agent," *Journal of Magnetic Resonance Imaging*, vol. 9, no. 2, pp. 228–232, 1999.

[50] M. Knauth, T. Egelhof, S. U. Roth, C. R. Wirtz, and K. Sartor, "Monocrystalline iron oxide nanoparticles: possible solution to the problem of surgically induced intracranial contrast enhancement in intraoperative MR imaging," *American Journal of Neuroradiology*, vol. 22, no. 1, pp. 99–102, 2001.

[51] J. Huang, J. Xie, K. Chen et al., "HSA coated MnO nanoparticles with prominent MRI contrast for tumor imaging," *Chemical Communications*, vol. 46, no. 36, pp. 6684–6686, 2010.

[52] M. F. Bennewitz, T. L. Lobo, M. K. Nkansah et al., "Biocompatible and pH-sensitive PLGA encapsulated MnO nanocrystals for molecular and cellular MRI," *ACS Nano*, vol. 5, no. 5, pp. 3438–3446, 2011.

[53] L. Faucher, L. Faucher, A. A. Guay-Bégin et al., "Ultra-small gadolinium oxide nanoparticles to image brain cancer cells in vivo with MRI," *Contrast Media & Molecular Imaging*, vol. 6, no. 4, pp. 209–218, 2011.

[54] M. D. Robson and G. M. Bydder, "Clinical ultrashort echo time imaging of bone and other connective tissues," *NMR in Biomedicine*, vol. 19, no. 7, pp. 765–780, 2006.

[55] J. Rahmer, P. Börnert, and S. P. M. Dries, "Assessment of anterior cruciate ligament reconstruction using 3D ultrashort echo-time MR imaging," *Journal of Magnetic Resonance Imaging*, vol. 29, no. 2, pp. 443–448, 2009.

[56] X. Chen, Y. Hou, M. Tohme et al., "Pegylated Arg-Gly-Asp peptide: 64Cu labeling and PET imaging of brain tumor $\alpha v\beta 3$-integrin expression," *Journal of Nuclear Medicine*, vol. 45, no. 10, pp. 1776–1783, 2004.

[57] B. Jia, J. Shi, Z. Yang et al., "99mTc-labeled cyclic RGDfK dimer: initial evaluation for SPECT imaging of glioma integrin $\alpha v\beta 3$ expression," *Bioconjugate Chemistry*, vol. 17, no. 4, pp. 1069–1076, 2006.

[58] S. Cruet, C. Salamanca, G. W. E. Mitchell, and N. Auersperg, "$\alpha v\beta 3$ and vitronectin expression by normal ovarian surface epithelial cells: role in cell adhesion and cell proliferation," *Gynecologic Oncology*, vol. 75, no. 2, pp. 254–260, 1999.

[59] I. Dijkgraaf, J. A. W. Kruijtzer, C. Frielink et al., "$\alpha v\beta 3$ integrin-targeting of intraperitoneally growing tumors with a radiolabeled RGD peptide," *International Journal of Cancer*, vol. 120, no. 3, pp. 605–610, 2007.

[60] L. Zhang, X. Zhong, L. Wang et al., "T1-weighted ultrashort echo time method for positive contrast imaging of magnetic nanoparticles and cancer cells bound with the targeted nanoparticles," *Journal of Magnetic Resonance Imaging*, vol. 33, no. 1, pp. 194–202, 2011.

[61] L. R. Hirsch, A. M. Gobin, A. R. Lowery et al., "Metal nanoshells," *Annals of Biomedical Engineering*, vol. 34, no. 1, pp. 15–22, 2006.

[62] C. Loo, L. Hirsch, M. H. Lee et al., "Gold nanoshell bioconjugates for molecular imaging in living cells," *Optics Letters*, vol. 30, no. 9, pp. 1012–1014, 2005.

[63] J. L. West and N. J. Halas, "Engineered nanomaterials for biophotonics applications: improving sensing, imaging, and therapeutics," *Annual Review of Biomedical Engineering*, vol. 5, pp. 285–292, 2003.

[64] A. W. H. Lin, N. A. Lewinski, J. L. West, N. J. Halas, and R. A. Drezek, "Optically tunable nanoparticle contrast agents for early cancer detection: model-based analysis of gold nanoshells," *Journal of Biomedical Optics*, vol. 10, no. 6, Article ID 064035, 2005.

[65] C. E. Talley, J. B. Jackson, C. Oubre et al., "Surface-enhanced Raman scattering from individual Au nanoparticles and nanoparticle dimer substrates," *Nano Letters*, vol. 5, no. 8, pp. 1569–1574, 2005.

[66] D. E. Gheorghe, L. Cui, C. Karmonik et al., "Gold-silver alloy nanoshells: a new candidate for nanotherapeutics and diagnostics," *Nanoscale Research Letters*, vol. 6, article 554, 2011.

[67] A. R. Lowery, A. M. Gobin, E. S. Day, N. J. Halas, and J. L. West, "Immunonanoshells for targeted photothermal ablation of tumor cells," *International Journal of Nanomedicine*, vol. 1, no. 2, pp. 149–154, 2006.

[68] D. J. Naczynski, T. Andelman, D. Pal et al., "Albumin nanoshell encapsulation of near-infrared-excitable rare-earth nanoparticles enhances biocompatibility and enables targeted cell imaging," *Small*, vol. 6, no. 15, pp. 1631–1640, 2010.

[69] W. Cai, D. W. Shin, K. Chen et al., "Peptide-labeled near-infrared quantum dots for imaging tumor vasculature in living subjects," *Nano Letters*, vol. 6, no. 4, pp. 669–676, 2006.

[70] P. Reiss, M. Protière, and L. Li, "Core/shell semiconductor nanocrystals," *Small*, vol. 5, no. 2, pp. 154–168, 2009.

[71] H. Arya, Z. Kaul, R. Wadhwa, K. Taira, T. Hirano, and S. C. Kaul, "Quantum dots in bio-imaging: revolution by the small," *Biochemical and Biophysical Research Communications*, vol. 329, no. 4, pp. 1173–1177, 2005.

[72] A. M. Smith, H. Duan, A. M. Mohs, and S. Nie, "Bioconjugated quantum dots for in vivo molecular and cellular imaging," *Advanced Drug Delivery Reviews*, vol. 60, no. 11, pp. 1226–1240, 2008.

[73] M. A. Popescu and S. A. Toms, "In vivo optical imaging using quantum dots for the management of brain tumors," *Expert Review of Molecular Diagnostics*, vol. 6, no. 6, pp. 879–890, 2006.

[74] H. Jackson, O. Muhammad, H. Daneshvar et al., "Quantum dots are phagocytized by macrophages and colocalize with experimental gliomas," *Neurosurgery*, vol. 60, no. 3, pp. 524–530, 2007.

[75] S. Kim, Y. T. Lim, E. G. Soltesz et al., "Near-infrared fluorescent type II quantum dots for sentinel lymph node mapping," *Nature Biotechnology*, vol. 22, no. 1, pp. 93–97, 2004.

[76] N. Y. Morgan, S. English, W. Chen et al., "Real time in vivo non-invasive optical imaging using near-infrared fluorescent quantum dots," *Academic Radiology*, vol. 12, no. 3, pp. 313–323, 2005.

[77] Y. Wang, C. Ye, L. Wu, and Y. Hu, "Synthesis and characterization of self-assembled CdHgTe/gelatin nanospheres as stable near infrared fluorescent probes in vivo," *Journal of Pharmaceutical and Biomedical Analysis*, vol. 53, no. 3, pp. 235–242, 2010.

[78] H. J. Wang, L. Yang, H. Y. Yang et al., "Antineoplastic activities of protein-conjugated silver sulfide nano-crystals with different shapes," *Journal of Inorganic Biochemistry*, vol. 104, no. 1, pp. 87–91, 2010.

[79] J. Banchereau and A. K. Palucka, "Dendritic cells as therapeutic vaccines against cancer," *Nature Reviews Immunology*, vol. 5, no. 4, pp. 296–306, 2005.

[80] R. Klippstein and D. Pozo, "Nanotechnology-based manipulation of dendritic cells for enhanced immunotherapy strategies," *Nanomedicine*, vol. 6, no. 4, pp. 523–529, 2010.

[81] G. P. Adams and L. M. Weiner, "Monoclonal antibody therapy of cancer," *Nature Biotechnology*, vol. 23, no. 9, pp. 1147–1157, 2005.

[82] D. Schrama, R. A. Reisfeld, and J. C. Becker, "Antibody targeted drugs as cancer therapeutics," *Nature Reviews Drug Discovery*, vol. 5, no. 2, pp. 147–159, 2006.

[83] D. Papahadjopoulos, A. Portis, and W. Pangborn, "Calcium induced lipid phase transitions and membrane fusion," *Annals of the New York Academy of Sciences*, vol. 308, pp. 50–66, 1978.

[84] B. E. Ryman, R. F. Jewkes, and K. Jeyasingh, "Potential application of liposomes to therapy," *Annals of the New York Academy of Sciences*, vol. 308, pp. 281–307, 1978.

[85] D. D. Lasic, P. M. Frederik, M. C. A. Stuart, Y. Barenholz, and T. J. McIntosh, "Gelation of liposome interior. A novel method for drug encapsulation," *FEBS Letters*, vol. 312, no. 2-3, pp. 255–258, 1992.

[86] A. D. Bangham, "Surrogate cells or Trojan horses. The discovery of liposomes," *BioEssays*, vol. 17, no. 12, pp. 1081–1088, 1995.

[87] H. Chen, Y. Qina, Q. Zhang et al., "Lactoferrin modified doxorubicin-loaded procationic liposomes for the treatment of gliomas," *European Journal of Pharmaceutical Sciences*, vol. 44, no. 1-2, pp. 164–173, 2011.

[88] Y. Qin, H. Chena, Q. Zhang et al., "Liposome formulated with TAT-modified cholesterol for improving brain delivery and therapeutic efficacy on brain glioma in animals," *International Journal of Pharmaceutics*, vol. 420, no. 2, pp. 304–312, 2011.

[89] W. Gong, Z. Wang, N. Liu et al., "Improving efficiency of adriamycin crossing blood brain barrier by combination of thermosensitive liposomes and hyperthermia," *Biological and Pharmaceutical Bulletin*, vol. 34, no. 7, pp. 1058–1064, 2011.

[90] S. Fellner, B. Bauer, D. S. Miller et al., "Transport of paclitaxel (taxol) across the blood-brain barrier in vitro and in vivo," *Journal of Clinical Investigation*, vol. 110, no. 9, pp. 1309–1318, 2002.

[91] H. Xin, X. Jiang, J. Gu et al., "Angiopep-conjugated poly(ethylene glycol)-co-poly(ε-caprolactone) nanoparticles as dual-targeting drug delivery system for brain glioma," *Biomaterials*, vol. 32, no. 18, pp. 4293–4305, 2011.

[92] J. Wang, W. Liu, Q. Tu et al., "Folate-decorated hybrid polymeric nanoparticles for chemically and physically combined paclitaxel loading and targeted delivery," *Biomacromolecules*, vol. 12, no. 1, pp. 228–234, 2011.

[93] H. Hatcher, R. Planalp, J. Cho, F. M. Torti, and S. V. Torti, "Curcumin: from ancient medicine to current clinical trials," *Cellular and Molecular Life Sciences*, vol. 65, no. 11, pp. 1631–1652, 2008.

[94] B. B. Aggarwal, A. Kumar, and A. C. Bharti, "Anticancer potential of curcumin: preclinical and clinical studies," *Anticancer Research*, vol. 23, no. 1, pp. 363–398, 2003.

[95] R. K. Maheshwari, A. K. Singh, J. Gaddipati, and R. C. Srimal, "Multiple biological activities of curcumin: a short review," *Life Sciences*, vol. 78, no. 18, pp. 2081–2087, 2006.

[96] A. B. Kunnumakkara, P. Anand, and B. B. Aggarwal, "Curcumin inhibits proliferation, invasion, angiogenesis and metastasis of different cancers through interaction with multiple cell signaling proteins," *Cancer Letters*, vol. 269, no. 2, pp. 199–225, 2008.

[97] J. Ravindran, S. Prasad, and B. B. Aggarwal, "Curcumin and cancer cells: how many ways can curry kill tumor cells selectively?" *AAPS Journal*, vol. 11, no. 3, pp. 495–510, 2009.

[98] G. P. Atkinson, S. E. Nozell, and E. N. Benveniste, "NF-κB and STAT3 signaling in glioma: targets for future therapies," *Expert Review of Neurotherapeutics*, vol. 10, no. 4, pp. 575–586, 2010.

[99] A. L. Schmidt, A. L. Brunetto, G. Schwartsmann, R. Roesler, and A. L. Abujamra, "Recent therapeutic advances for treating medulloblastoma: focus on new molecular targets," *CNS and Neurological Disorders*, vol. 9, no. 3, pp. 335–348, 2010.

[100] K. J. Lim, S. Bisht, E. E. Bar, A. Maitra, and C. G. Eberhart, "A polymeric nanoparticle formulation of curcumin inhibits growth, clonogenicity and stem-like fraction in malignant brain tumors," *Cancer Biology and Therapy*, vol. 11, no. 5, pp. 464–473, 2011.

[101] J. Shao, D. Zheng, Z. Jiang et al., "Curcumin delivery by methoxy polyethylene glycol-poly(caprolactone) nanoparticles inhibits the growth of C6 glioma cells," *Acta Biochimica et Biophysica Sinica*, vol. 43, no. 4, pp. 267–274, 2011.

[102] M. Tsujii, S. Kawano, S. Tsuji, H. Sawaoka, M. Hori, and R. N. DuBois, "Cyclooxygenase regulates angiogenesis induced by colon cancer cells," *Cell*, vol. 93, no. 5, pp. 705–716, 1998.

[103] T. H. Kim, Y. I. Jeong, S. G. Jin et al., "Preparation of polylactide-co-glycolide nanoparticles incorporating celecoxib and their antitumor activity against brain tumor cells," *International Journal of Nanomedicine*, vol. 6, pp. 2621–2631, 2011.

[104] A. J. Primeau, A. Rendon, D. Hedley, L. Lilge, and I. F. Tannock, "The distribution of the anticancer drug doxorubicin in relation to blood vessels in solid tumors," *Clinical Cancer Research*, vol. 11, no. 24, part 1, pp. 8782–8788, 2005.

[105] T. Siegal, A. Horowitz, and A. Gabizon, "Doxorubicin encapsulated in sterically stabilized liposomes for the treatment of a brain tumor model: biodistribution and therapeutic efficacy," *Journal of Neurosurgery*, vol. 83, no. 6, pp. 1029–1037, 1995.

[106] A. Gabizon and F. Martin, "Polyethylene glycol-coated (pegylated) liposomal doxorubicin. Rationale for use in solid tumours," *Drugs*, vol. 54, supplement 4, pp. 15–21, 1997.

[107] B. Kateb, M. Van Handel, L. Zhang, M. J. Bronikowski, H. Manohara, and B. Badie, "Internalization of MWCNTs by microglia: possible application in immunotherapy of brain tumors," *NeuroImage*, vol. 37, supplement 1, pp. S9–S17, 2007.

[108] S. P. Vyas, A. Singh, and V. Sihorkar, "Ligand-receptor-mediated drug delivery: an emerging paradigm in cellular drug targeting," *Critical Reviews in Therapeutic Drug Carrier Systems*, vol. 18, no. 1, pp. 1–76, 2001.

[109] Z. M. Qian, H. Li, H. Sun, and K. Ho, "Targeted drug delivery via the transferrin receptor-mediated endocytosis pathway," *Pharmacological Reviews*, vol. 54, no. 4, pp. 561–587, 2002.

[110] A. Kito, J. Yoshida, N. Kageyama, N. Kojima, and K. Yagi, "Liposomes coupled with monoclonal antibodies against glioma-associated antigen for targeting chemotherapy of glioma," *Journal of Neurosurgery*, vol. 71, no. 3, pp. 382–387, 1989.

[111] D. A. Eavarone, X. Yu, and R. V. Bellamkonda, "Targeted drug delivery to C6 glioma by transferrin-coupled liposomes," *Journal of Biomedical Materials Research*, vol. 51, no. 1, pp. 10–14, 2000.

[112] W. C. W. Chan and S. Nie, "Quantum dot bioconjugates for ultrasensitive nonisotopic detection," *Science*, vol. 281, no. 5385, pp. 2016–2018, 1998.

[113] B. Dubertret, P. Skourides, D. J. Norris, V. Noireaux, A. H. Brivanlou, and A. Libchaber, "In vivo imaging of quantum dots encapsulated in phospholipid micelles," *Science*, vol. 298, no. 5599, pp. 1759–1762, 2002.

[114] X. Gao, Y. Cui, R. M. Levenson, L. W. K. Chung, and S. Nie, "In vivo cancer targeting and imaging with semiconductor quantum dots," *Nature Biotechnology*, vol. 22, no. 8, pp. 969–976, 2004.

[115] Y. Xiang, L. Liang, X. Wang, J. Wang, X. Zhang, and Q. Zhang, "Chloride channel-mediated brain glioma targeting of chlorotoxin-modified doxorubicine-loaded liposomes," *Journal of Controlled Release*, vol. 152, no. 3, pp. 402–410, 2011.

[116] H. Vallhov, S. Gabrielsson, M. Strømme, A. Scheynius, and A. E. Garcia-Bennett, "Mesoporous silica particles induce size dependent effects on human dendritic cells," *Nano Letters*, vol. 7, no. 12, pp. 3576–3582, 2007.

[117] M. Ahamed, M. S. AlSalhi, and M. K. J. Siddiqui, "Silver nanoparticle applications and human health," *Clinica Chimica Acta*, vol. 411, no. 23-24, pp. 1841–1848, 2010.

[118] P. V. AshaRani, G. L. K. Mun, M. P. Hande, and S. Valiyaveettil, "Cytotoxicity and genotoxicity of silver nanoparticles in human cells," *ACS Nano*, vol. 3, no. 2, pp. 279–290, 2009.

[119] S. Kim, J. E. Choi, J. Choi et al., "Oxidative stress-dependent toxicity of silver nanoparticles in human hepatoma cells," *Toxicology in Vitro*, vol. 23, no. 6, pp. 1076–1084, 2009.

[120] C. Carlson, S. M. Hussein, A. M. Schrand et al., "Unique cellular interaction of silver nanoparticles: size-dependent generation of reactive oxygen species," *Journal of Physical Chemistry B*, vol. 112, no. 43, pp. 13608–13619, 2008.

[121] P. V. Asharani, N. Xinyi, M. P. Hande, and S. Valiyaveettil, "DNA damage and p53-mediated growth arrest in human cells treated with platinum nanoparticles," *Nanomedicine*, vol. 5, no. 1, pp. 51–64, 2010.

[122] L. Yang, H. J. Wang, H. Y. Yang et al., "Shape-controlled synthesis of protein-conjugated silver sulfide nanocrystals and study on the inhibition of tumor cell viability," *Chemical Communications*, no. 26, pp. 2995–2997, 2008.

[123] C. Levard, E. M. Hotze, G. V. Lowry, and G. E. Brown Jr., "Environmental transformations of silver nanoparticles: impact on stability and toxicity," *Environmental Science & Technology*, vol. 46, no. 13, pp. 6900–6914, 2012.

[124] J. J. Li and K. D. Zhu, "Spin-based optomechanics with carbon nanotubes," *Scientific Reports*, vol. 2, article 903, 2012.

[125] M. J. Meziani and Y. P. Sun, "Protein-conjugated nanoparticles from rapid expansion of supercritical fluid solution into aqueous solution," *Journal of the American Chemical Society*, vol. 125, no. 26, pp. 8015–8018, 2003.

[126] C. Salvador-Morales, E. Flahaut, E. Sim, J. Sloan, M. L. H. Green, and R. B. Sim, "Complement activation and protein adsorption by carbon nanotubes," *Molecular Immunology*, vol. 43, no. 3, pp. 193–201, 2006.

[127] C. Klumpp, K. Kostarelos, M. Prato, and A. Bianco, "Functionalized carbon nanotubes as emerging nanovectors for the delivery of therapeutics," *Biochimica et Biophysica Acta*, vol. 1758, no. 3, pp. 404–412, 2006.

[128] C. T. Kresge, M. E. Leonowicz, W. J. Roth, J. C. Vartuli, and J. S. Beck, "Ordered mesoporous molecular sieves synthesized by a liquid-crystal template mechanism," *Nature*, vol. 359, no. 6397, pp. 710–712, 1992.

[129] T. Asefa, M. J. MacLachlan, N. Coombs, and G. A. Ozin, "Periodic mesoporous organosilicas with organic groups inside the channel walls," *Nature*, vol. 402, no. 6764, pp. 867–871, 1999.

[130] Z. R. Tian, W. Tong, J. Y. Wang, N. G. Duan, V. V. Krishnan, and S. L. Suib, "Manganese oxide mesoporous structures: mixed-valent semiconducting catalysts," *Science*, vol. 276, no. 5314, pp. 926–930, 1997.

[131] G. S. Armatas and M. G. Kanatzidis, "Mesostructured germanium with cubic pore symmetry," *Nature*, vol. 441, no. 7097, pp. 1122–1125, 2006.

[132] P. N. Trikalitis, K. K. Rangan, T. Bakas, and M. G. Kanatzidis, "Varied pore organization in mesostructured semiconductors based on the $[SnSe4]^{4-}$ anion," *Nature*, vol. 410, no. 6829, pp. 671–675, 2001.

[133] I. Roy, S. Mitra, A. Maitra, and S. Mozumdar, "Calcium phosphate nanoparticles as novel non-viral vectors for targeted gene delivery," *International Journal of Pharmaceutics*, vol. 250, no. 1, pp. 25–33, 2003.

[134] S. H. Wu, C. Y. Mou, and H. P. Lin, "Synthesis of mesoporous silica nanoparticles," *Chemical Society Reviews*, 2013.

[135] R. S. Dhanikula, A. Argaw, J. F. Bouchard, and P. Hildgen, "Methotrexate loaded polyether-copolyester dendrimers for the treatment of gliomas: enhanced efficacy and intratumoral transport capability," *Molecular Pharmaceutics*, vol. 5, no. 1, pp. 105–116, 2008.

[136] Y. Ren, C. S. Kang, X. B. Yuan et al., "Co-delivery of as-miR-21 and 5-FU by poly(amidoamine) dendrimer attenuates human glioma cell growth in vitro," *Journal of Biomaterials Science*, vol. 21, no. 3, pp. 303–314, 2010.

[137] M. Tan, X. Wu, E. K. Jeong, Q. Chen, and Z. R. Lu, "Peptide-targeted nanoglobular Gd-DOTA monoamide conjugates for magnetic resonance cancer molecular imaging," *Biomacromolecules*, vol. 11, no. 3, pp. 754–761, 2010.

[138] E. C. Wiener, M. W. Brechbiel, H. Brothers et al., "Dendrimer-based metal chelates: a new class of magnetic resonance imaging contrast agents," *Magnetic Resonance in Medicine*, vol. 31, no. 1, pp. 1–8, 1994.

[139] Z. Cheng, D. L. J. Thorek, and A. Tsourkas, "Gadolinium-conjugated dendrimer nanoclusters as a tumor-targeted T 1 magnetic resonance imaging contrast agent," *Angewandte Chemie*, vol. 49, no. 2, pp. 346–350, 2010.

[140] C. C. Lee, J. A. MacKay, J. M. J. Fréchet, and F. C. Szoka, "Designing dendrimers for biological applications," *Nature Biotechnology*, vol. 23, no. 12, pp. 1517–1526, 2005.

[141] M. X. Tang, C. T. Redemann, and F. C. Szoka Jr., "In vitro gene delivery by degraded polyamidoamine dendrimers," *Bioconjugate Chemistry*, vol. 7, no. 6, pp. 703–714, 1996.

[142] H. Yan, J. Wang, P. Yi et al., "Imaging brain tumor by dendrimer-based optical/paramagnetic nanoprobe across the blood-brain barrier," *Chemical Communications*, vol. 47, no. 28, pp. 8130–8132, 2011.

[143] S. K. Pulfer, S. L. Ciccotto, and J. M. Gallo, "Distribution of small magnetic particles in brain tumor-bearing rats," *Journal of Neuro-Oncology*, vol. 41, no. 2, pp. 99–105, 1999.

[144] T. Zhang and D. Herlyn, "Combination of active specific immunotherapy or adoptive antibody or lymphocyte immunotherapy with chemotherapy in the treatment of cancer," *Cancer Immunology, Immunotherapy*, vol. 58, no. 4, pp. 475–492, 2009.

[145] J. Kreuter and S. Gelperina, "Use of nanoparticles for cerebral cancer," *Tumori*, vol. 94, no. 2, pp. 271–277, 2008.

[146] D. Pozo, "Immune-based disorders: the challenges for translational immunology," *Journal of Cellular and Molecular Medicine*, vol. 12, no. 4, pp. 1085–1086, 2008.

[147] M. Fujita, B. S. Lee, N. M. Khazenzon et al., "Brain tumor tandem targeting using a combination of monoclonal antibodies attached to biopoly(β-l-malic acid)," *Journal of Controlled Release*, vol. 122, no. 3, pp. 356–363, 2007.

[148] J. Y. Ljubimova, M. Fujita, N. M. Khazenzon et al., "Nanoconjugate based on polymalic acid for tumor targeting," *Chemico-Biological Interactions*, vol. 171, no. 2, pp. 195–203, 2008.

[149] B. Gasslmaier, C. M. Krell, D. Seebach, and E. Holler, "Synthetic substrates and inhibitors of β-poly(L-malate)-hydrolase (polymalatase)," *European Journal of Biochemistry*, vol. 267, no. 16, pp. 5101–5105, 2000.

[150] S. Cammas, M. M. Béar, L. Moine et al., "Polymers of malic acid and 3-alkylmalic acid as synthetic PHAs in the design of biocompatible hydrolyzable devices," *International Journal of Biological Macromolecules*, vol. 25, no. 1–3, pp. 273–282, 1999.

[151] L. Zhang, J. Yao, J. Zhou, T. Wang, and Q. Zhang, "Glycyrrhetinic acid-graft-hyaluronic acid conjugate as a carrier for synergistic targeted delivery of antitumor drugs," *International Journal of Pharmaceutics*, vol. 441, no. 1-2, pp. 654–664, 2013.

[152] B. S. Lee, M. Vert, and E. Holler, "Water-soluble Aliphatic Polyesters: poly(malic acid)s," in *Biopolymers*, Y. Doi and A. Steinbuchel, Eds., vol. 3, pp. 75–103, Wiley-VCH, New York, NY, USA, 2002.

[153] Y. Zhang and W. M. Pardridge, "Delivery of β-galactosidase to mouse brain via the blood-brain barrier transferrin receptor," *Journal of Pharmacology and Experimental Therapeutics*, vol. 313, no. 3, pp. 1075–1081, 2005.

[154] U. Bickel, T. Yoshikawa, and W. M. Pardridge, "Delivery of peptides and proteins through the blood-brain barrier," *Advanced Drug Delivery Reviews*, vol. 46, no. 1–3, pp. 247–279, 2001.

[155] V. P. Torchilin and A. N. Lukyanov, "Peptide and protein drug delivery to and into tumors: challenges and solutions," *Drug Discovery Today*, vol. 8, no. 6, pp. 259–266, 2003.

[156] L. Z. Lakoubov and V. P. Torchilin, "A novel class of antitumor antibodies: nucleosome-restricted antinuclear autoantibodies (ana) from healthy aged nonautoimmune mice," *Oncology Research*, vol. 9, no. 8, pp. 439–446, 1997.

[157] B. Feng, K. Tomizawa, H. Michiue et al., "Delivery of sodium borocaptate to glioma cells using immunoliposome conjugated with anti-EGFR antibodies by ZZ-His," *Biomaterials*, vol. 30, no. 9, pp. 1746–1755, 2009.

[158] R. H. Müller, K. Mäder, and S. Gohla, "Solid lipid nanoparticles (SLN) for controlled drug delivery—a review of the state of the art," *European Journal of Pharmaceutics and Biopharmaceutics*, vol. 50, no. 1, pp. 161–177, 2000.

[159] Y. C. Kuo and C. T. Liang, "Inhibition of human brain malignant glioblastoma cells using carmustine-loaded catanionic solid lipid nanoparticles with surface anti-epithelial growth factor receptor," *Biomaterials*, vol. 32, no. 12, pp. 3340–3350, 2011.

[160] Y. C. Kuo and C. T. Liang, "Catanionic solid lipid nanoparticles carrying doxorubicin for inhibiting the growth of U87MG cells," *Colloids and Surfaces B*, vol. 85, no. 2, pp. 131–137, 2011.

[161] M. Shokeen, E. D. Pressly, A. Hagooly et al., "Evaluation of multivalent, functional polymeric nanoparticles for imaging applications," *ACS Nano*, vol. 5, no. 2, pp. 738–747, 2011.

[162] D. S. Kohane, "Microparticles and nanoparticles for drug delivery," *Biotechnology and Bioengineering*, vol. 96, no. 2, pp. 203–209, 2007.

[163] A. H. Faraji and P. Wipf, "Nanoparticles in cellular drug delivery," *Bioorganic and Medicinal Chemistry*, vol. 17, no. 8, pp. 2950–2962, 2009.

[164] H. Murakami, M. Kobayashi, H. Takeuchi, and Y. Kawashima, "Preparation of poly(DL-lactide-co-glycolide) nanoparticles by modified spontaneous emulsification solvent diffusion method," *International Journal of Pharmaceutics*, vol. 187, no. 2, pp. 143–152, 1999.

Hindawi Publishing Corporation
BioMed Research International
Volume 2013, Article ID 378380, 11 pages
http://dx.doi.org/10.1155/2013/378380

Research Article

Enhanced Therapeutic Efficacy of iRGD-Conjugated Crosslinked Multilayer Liposomes for Drug Delivery

Yarong Liu,[1] Man Ji,[2] Michael K. Wong,[3] Kye-Il Joo,[1] and Pin Wang[1,4,5]

[1] *Mork Family Department of Chemical Engineering and Materials Science, University of Southern California, 3710 McClintock Avenue, RTH509, Los Angeles, CA 90089, USA*
[2] *Department of Biochemistry and Molecular Biology, University of Southern California, Los Angeles, CA 90033, USA*
[3] *Division of Medical Oncology, Norris Comprehensive Cancer Center, Keck School of Medicine, University of Southern California, Los Angeles, CA 90089, USA*
[4] *Department of Biomedical Engineering, University of Southern California, Los Angeles, CA 90089, USA*
[5] *Department of Pharmacology and Pharmaceutical Sciences, University of Southern California, Los Angeles, CA 90089, USA*

Correspondence should be addressed to Kye-Il Joo; kjoo@usc.edu and Pin Wang; pinwang@usc.edu

Received 26 December 2012; Revised 6 March 2013; Accepted 18 March 2013

Academic Editor: Claudete J. Valduga

Targeting nanoparticles by conjugating various specific ligands has shown potential therapeutic efficacy in nanomedicine. However, poor penetration of antitumor drugs into solid tumors remains a major obstacle. Here, we describe a targeting strategy for antitumor drug delivery by conjugating a crosslinked multilamellar liposomal vesicle (cMLV) formulation with a tumor-penetrating peptide, iRGD. The results showed that iRGD peptides could facilitate the binding and cellular uptake of drug-loaded cMLVs and consequently enhance the antitumor efficacy in breast tumor cells, including multidrug-resistant cells. Moreover, colocalization data revealed that iRGD-conjugated cMLVs (iRGD-cMLVs) entered cells via the clathrin-mediated pathway, followed by endosome-lysosome transport for efficient drug delivery. Finally, *in vivo* study indicated that iRGD-cMLVs could deliver anticancer drugs efficiently to mediate significant tumor suppression.

1. Introduction

For optimal anticancer treatment with cytotoxic drugs, it is necessary to sustain antitumor effects over a prolonged period at an efficacious drug concentration without inducing severe systemic toxicity. Therefore, as an alternative to conventional medicine for cancer therapeutics, nanoparticle-based drug delivery systems have been widely evaluated and utilized to modulate the toxicity profile of anticancer drugs and improve drug circulation time [1–3]. Long-circulating liposomes, such as polyethylene-glycol-(PEG-) coated liposomes, have become one of the most popular nanocarriers for delivering therapeutics and have shown the ability to passively accumulate in tumors as a result of enhanced permeability and retention (EPR) effect [4, 5]. Ultimately, however, active targeting to tumor cells via the inclusion of a tumor-targeting molecule on the nanocarriers is expected to provide more effective cancer therapy [1, 6, 7]. Once extravasated in the tumor environment, the targeting molecules will likely foster the active attachment of nanoparticles to tumor cells expressing the specific receptors for elevated antitumor activity.

Scientific investigations have identified diverse tumor-targeting molecules that can be exploited by nanoparticles to actively target cancer cell-specific markers with unique phenotypes in tumors. For example, it has been reported that drug carriers conjugated with targeting ligands, such as anti-Her2 antibody [8], folate [9], or transferrin (Tf) [10], have achieved therapeutic benefit by successfully targeting human epidermal receptors (HER), folate receptors, and transferrin receptor (TfR), respectively, all of which are overexpressed on tumor cells. The cell- or tissue-specific ligand-receptor

interaction contributes to the increased efficacy as a result of enhanced uptake of the complex into tumor cells by receptor-mediated endocytosis. However, a major obstacle against the clinical application of this targeting strategy has been the poor penetration of the targeted payload through the vascular wall and into the tumor parenchyma, especially in solid tumors, which have a high interstitial pressure [11, 12]. Recently, a tumor-penetrating peptide, iRGD (CRGDKGPDC), was identified and reported to increase vascular and tissue penetration in a tumor-specific and neuropilin-1-dependent manner, as compared to conventional RGD peptides [13, 14]. Like conventional RGD peptides, iRGD homes to tumor sites by binding to $\alpha_v\beta_3$ and $\alpha_v\beta_5$ integrins, which are highly expressed in tumor endothelium [13, 15, 16], thus enhancing the therapeutic effect of antitumor drugs on suppressing tumor growth and/or metastasis. After binding, the iRGD peptide is thought to be proteolytically cleaved to produce CRGDK fragment, which favors binding to neuropilin-1 receptor, thus facilitating the penetration of drugs into the tumor [17].

Here, we explored whether the iRGD peptide could enhance cancer drug delivery and antitumor activity when conjugated to liposomal nanoparticles. Our previous studies evaluated nanoparticles based on a crosslinked multilamellar liposomal vesicle (cMLV), and we found that they exhibited remarkable stability, sustained release kinetics of encapsulated doxorubicin, and improved therapeutic efficiency *in vivo* [18]. Therefore, in this study, we tested the hypothesis that cMLV nanoparticles conjugated with iRGD peptides could enhance the delivery of the antitumor drug doxorubicin. We demonstrated that iRGD could increase both binding and uptake of Dox-loaded cMLV in 4T1 tumor cells. Moreover, the colocalization data showed that iRGD peptides could change the intracellular endocytic routes of cMLV particles, which was further confirmed by the drug-inhibition experiment. Data also showed that systemic injection of iRGD-conjugated nanoparticles could more efficiently suppress tumor growth in the breast tumor model. These results confirmed that the tumor-penetrating peptide iRGD could be a promising means of targeted drug delivery to tumor sites.

2. Materials and Methods

2.1. Materials. Mice. Female 6- to 10-week-old BALB/c mice were purchased from Charles River Breeding Laboratories (Wilmington, MA). All mice were held under specific pathogen-reduced conditions in the Animal Facility of the University of Southern California (USA). All experiments were performed in accordance with the guidelines set by the National Institutes of Health and the University of Southern California on the Care and Use of Animals.

Cell Lines, Antibodies, and Reagents. 4T1 tumor cells (ATCC number: CRL-2539) and JC cells (ATCC number: CRL-2116) were maintained in a 5% CO_2 environment with Dulbecco's modified Eagle's medium (Mediatech, Inc., Manassas, VA) supplemented with 10% FBS (Sigma-Aldrich, St. Louis, MO) and 2 mM of L-glutamine (Hyclone Laboratories, Inc., Omaha, NE). The mouse monoclonal antibodies against clathrin, caveolin-1, and EEA1 were purchased from Santa Cruz Biotechnology, Inc. (Santa Cruz, CA). The mouse monoclonal antibody to Lamp-1 was purchased from Abcam (Cambridge, MA). Alexa488-TFP ester and Alexa488-goat anti-mouse immunoglobulin G (IgG) were obtained from Invitrogen (Carlsbad, CA). Chlorpromazine (CPZ) and Filipin were obtained from Sigma-Aldrich (St. Louis, MO) and used at appropriate concentrations according to the manufacturer's protocols.

2.2. Synthesis of iRGD-cMLVs. Preparation of liposomes was based on the conventional dehydration-rehydration method. All lipids were obtained from NOF Corporation (Japan). 1.5 μmol of lipids 1,2-dioleoyl-sn-glycero-3-phosphocholine (DOPC), 1,2-dioleoyl-sn-glycero-3-phospho-(1′-rac-glycerol) (DOPG), and maleimide-headgroup lipid 1,2-dioleoyl-sn-glycero-3-phosphoeth-anolamine-N-[4-(p-maleimidophenyl) butyramide (MPB-PE) were mixed in chloroform to form a lipid composition with a molar ratio of DOPC : DOPG : MPB = 4 : 1 : 5, and the organic solvent in the lipid mixture was evaporated under argon gas, followed by additional drying under vacuum overnight to form dried thin lipid films. The resultant dried film was hydrated in 10 mM Bis-Tris propane at pH 7.0 with doxorubicin at a molar ratio of 0.2 : 1 (drugs : lipids) with vigorous vortexing every 10 min for 1 h and then applied with 4 cycles of 15 s sonication (Misonix Microson XL2000, Farmingdale, NY) on ice at 1 min intervals for each cycle. To induce divalent-triggered vesicle fusion, $MgCl_2$was added to make a final concentration of 10 mM. The resulting multilamellar vesicles were further crosslinked by addition of dithiothreitol (DTT, Sigma-Aldrich) at a final concentration of 1.5 mM for 1 h at 37°C. The resulting vesicles were collected by centrifugation at 14,000 g for 4 min and then washed twice with PBS. For iRGD conjugation to cMLVs, the particles were incubated with 0.5 μmol of iRGD peptides (GenScript, Piscataway, NJ) for 1 h at 37°C. For pegylation of cMLVs, both unconjugated and iRGD-conjugated particles were further incubated with 0.5 μmol of 2 kDa PEG-SH (Laysan Bio Inc., Arab, AL) for 1 h at 37°C. The particles were then centrifuged and washed twice with PBS. The final products were stored in PBS at 4°C.

2.3. Characterization of Physical Properties. The hydrodynamic size and size distribution of iRGD-cMLVs were measured by dynamic light scattering (Wyatt Technology, Santa Barbara, CA).

2.4. In Vitro Drug Encapsulation and Release. To study the loading capacity of Dox, iRGD-cMLV(Dox) nanoparticles were collected and then washed twice with PBS, followed by lipid extraction of vesicles with 1% Triton X-100 treatment. Dox fluorescence (excitation 480 nm, emission 590 nm) was then measured by a Shimadzu RF-5301PC spectrofluorometer (Japan). To obtain the release kinetics of Dox from liposomes, Dox-loaded iRGD-cMLVs were incubated at 37°C in 10% fetal-bovine-serum-(FBS-) containing media, the releasing media were removed from iRGD-cMLVs incubated at 37°C for quantification of Dox fluorescence every day, and

fresh media were replaced for continuous monitoring of drug release.

2.5. In Vitro Cytotoxicity. 4T1 and JC cells were plated at a density of 5×10^3 cells per well in D10 media in 96-well plates and grown for 6 h. The cells were then exposed to a series of concentrations of cMLV(Dox) or iRGD-cMLV(Dox) for 48 h, and the cell viability was assessed using the Cell Proliferation Kit II (XTT assay) from Roche Applied Science (Indianapolis, IN) according to the manufacturer's instructions. Cell viability percentage was determined by subtracting absorbance values obtained from media-only wells from drug-treated wells and then normalizing to the control cells without drugs. The data were analyzed by nonlinear regression to get the IC_{50} value.

2.6. In Vitro Binding and Internalization Study. 4T1 cells were plated at a density of 2×10^5 cells per well in D10 media in 24-well plates and grown overnight. The cells were incubated with two concentrations (0.2 μg/mL and 0.04 μg/mL) of iRGD-cMLV(Dox) or cMLV(Dox) for 30 min at 4°C (for binding assay) or 2 h at 37°C (for internalization assay). After incubation, the cells were washed twice with PBS to remove the unbound nanoparticles. Binding and cellular uptake of particles were determined by measuring doxorubicin fluorescence using flow cytometry.

2.7. Confocal Imaging. Fluorescence images were acquired on a Yokogawa spinning-disk confocal scanner system (Solamere Technology Group, Salt Lake City, UT) using a Nikon eclipse Ti-E microscope equipped with a 60 × /1.49 Apo TIRF oil objective and a Cascade II: 512 EMCCD camera (Photometrics, Tucson, AZ, USA). An AOTF (acousto-optical tunable filter) controlled laser-merge system (Solamere Technology Group Inc.) was used to provide illumination power at each of the following laser lines: 491 nm, 561 nm, and 640 nm solid state lasers (50 mW for each laser).

To label liposomal particles, DiD lipophilic dyes were added to the lipid mixture in chloroform at a ratio of 0.01 : 1 (DiD : lipids), and the organic solvent in the lipid mixture was evaporated under argon gas to incorporate DiD dyes into a lipid bilayer of vesicles. To detect iRGD peptides, both iRGD-cMLV and unconjugated cMLV particles were incubated with 50 nmol of Alexa488-TFP ester (Invitrogen) for 2 h in 0.1 M sodium bicarbonate buffer (pH = 9.3). After 2 h incubation, the reaction was stopped, and unbound dye molecules were removed via buffer exchange into PBS (pH = 7.4) using a Zeba desalting spin column (Fisher Scientific). For the detection of intracellular nanoparticles, DiD-labeled iRGD-cMLV or DiD-labeled unconjugated cMLV were incubated for 30 min at 4°C with HeLa cells that were seeded overnight on polylysine-coated glass bottom dishes (MatTek Corporation, Ashland, MA). Then the samples were incubated at 37°C to initiate particle internalization at the indicated time points. The culture dish was then rinsed, fixed with 4% formaldehyde, permeabilized with 0.1% Triton X-100, and then immunostained with the corresponding antibodies specific to clathrin, caveolin-1, EEA1, or Lamp-1 and counterstained with DAPI (Invitrogen, Carlsbad, CA).

2.8. Uptake Inhibition Assay. HeLa cells (1×10^5 cells) were preincubated with Chlorpromazine (CPZ, 25 μg/mL) or Filipin (10 μg/mL) for 30 min to disrupt the clathrin- or caveolin-mediated pathway. The cells were then incubated with DiD-labeled iRGD-cMLV or unconjugated cMLV for 1 h at 37°C in the presence of CPZ and filipin. The cells were then washed twice with PBS. The cellular uptake of particles was determined by measuring DiD fluorescence using flow cytometry and normalized on the basis of fluorescent intensity acquired from the untreated cells.

2.9. In Vivo Antitumor Activity Study. BALB/c female mice (6–10 weeks old) were inoculated subcutaneously with 0.2×10^6 4T1 breast tumor cells. The tumors were allowed to grow to a volume of ~50 mm^3 before treatment. On day 10, the mice were injected intravenously through tail vein with PBS (control group), cMLV (2 mg/kg Dox), and iRGD-cMLV (2 mg/kg Dox) every three days (five mice per group). Tumor growth and body weight were then monitored until the end of the experiment. The length and width of the tumor masses were measured with a fine caliper every three days after injection. Tumor volume was expressed as $1/2 \times (\text{length} \times \text{width}^2)$.

3. Results

3.1. Preparation of iRGD-cMLV Nanoparticles. The procedure for the preparation of crosslinked multilayer liposomal vesicles (cMLV) was adapted from a recently reported multistep procedure based on the conventional dehydration-rehydration method to form covalent crosslinkers between adjacent lipid bilayers [19], as illustrated in Figure 1(a). This method employed a divalent cation-triggered vesicle fusion to yield a multilamellar structure, from which interbilayer crosslinkers were formed across the opposing sides of lipid bilayers through the reactive headgroups with dithiothreitol (DTT). The iRGD peptides (CRGDKGPDC) were conjugated to the surface of cMLVs through the functional thiol-reactive maleimide headgroups of maleimide-headgroup lipid, 1,2-dioleoyl-sn-glycero-3-phosphoeth-anolamine-N- [4-(p-maleimidophenyl) butyramide](MPB-PE). As a final step, the surface of the iRGD-conjugated cMLV (iRGD-cMLV) was pegylated with thiol-terminated PEG to further improve the blood circulation time of vesicles [5, 20].

The physical properties of synthesized iRGD-cMLV were characterized. The hydrodynamic size of these targeted nanoparticles was measured by dynamic light scattering (DLS), and the result showed the mean diameter of iRGD-cMLV to be ~230 ± 11.23 nm (Figure 1(b)), which was similar to that of unconjugated cMLV (~220 ± 6.98 nm). Moreover, it has been confirmed that doxorubicin-(Dox-) encapsulation efficiency of ~85% can be achieved via this preparation procedure. An *in vitro* drug release assay also showed that iRGD-cMLV exhibited slow and sustained release kinetics (up to 2 weeks) in a serum environment (Figure 1(c)).

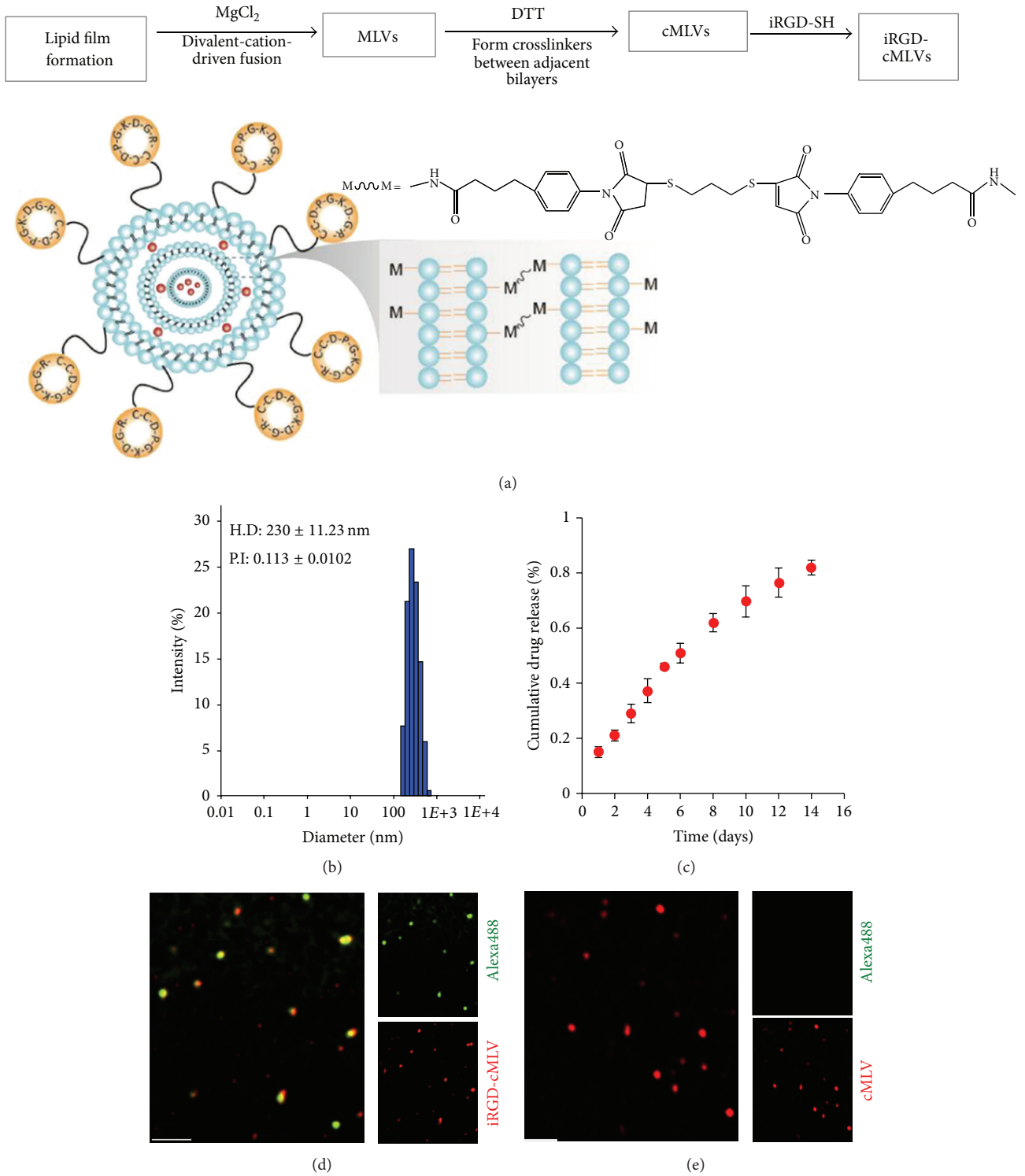

Figure 1: Characterization, release profile, and conjugation of iRGD-cMLVs. (a) Schematic illustration of the synthesis of iRGD-conjugated crosslinked multilamellar vesicle (iRGD-cMLV). (b) The hydrodynamic size distribution of iRGD-cMLVs measured by dynamic light scattering (DLS). Data represented the mean ± SD of at least three experiments with $n = 3$. (c) *In vitro* release kinetics of doxorubicin (Dox) from iRGD-cMLVs. Error bars represent standard error of the mean; $n = 3$ for each formulation. ((d), (e)) Confirmation of the conjugation of iRGD peptides onto the cMLV nanoparticles by confocal imaging. DiD-labeled iRGD-cMLVs (d) and DiD-labeled cMLVs (e) were reacted with Alexa488 dye for 1 h at room temperature followed by confocal imaging. Scale bar represents 5 μm.

Next, we examined whether iRGD peptides were conjugated to the surface of cMLV via the maleimide headgroups. To this end, fluorescent 1,1-dioctadecyl-3,3,3,3-tetramethylindodicarbocyanine-(DiD-) labeled cMLV particles were used to visualize both unconjugated and conjugated particles. In addition, Alexa488 dye was utilized to label iRGD peptides through the amine group of lysine residues on iRGD peptides (CRGD**K**GPDC). The results showed that a significant colocalization of DiD-labeled iRGD-cMLV particles with Alexa488-labeled iRGD peptides was observed (Figure 1(d)), while no Alexa488 signals were detected on unconjugated cMLV particles (Figure 1(e)), suggesting that iRGD peptides were successfully conjugated to cMLV particles.

3.2. Cytotoxicity and Cell Uptake of iRGD-cMLV(Dox). We next determined the effect of iRGD-conjugated cMLV nanoparticles on cytotoxicity levels in cells as compared to unconjugated cMLV nanoparticles. Dox-loaded cMLV (cMLV(Dox)) and Dox-loaded iRGD-cMLV (iRGD-cMLV(Dox)) were incubated with 4T1 or JC cells. JC cells represent a model drug-resistant tumor cell line overexpressing P-glycoprotein and exhibiting drug-resistant phenotype both *in vitro* and *in vivo* [21]. After 48 h incubation, the cytotoxicity of Dox liposomes was measured by a standard XTT assay. *In vitro* cytotoxicity data revealed that iRGD-cMLV showed slightly smaller IC_{50} ($0.011 \pm 0.0037\ \mu$g/mL) in 4T1 cells as compared to cMLV ($0.018 \pm 0.0025\ \mu$g/mL) (Figure 2(a)). A significant difference of cytotoxicity between iRGD-cMLV(Dox) and cMLV(Dox) was observed in JC cells, in which iRGD-cMLV(Dox) showed a lower IC_{50} ($2.01 \pm 0.22\ \mu$g/mL) value than that of cMLV(Dox) ($3.19 \pm 0.32\ \mu$g/mL, $P < 0.05$, Figure 2(b)). The XTT results indicated that delivery of Dox with iRGD-conjugated cMLV was more potent in inhibiting tumor cell proliferation.

To investigate whether the enhanced cell cytotoxicity of iRGD-cMLV resulted from an increased cellular uptake of nanoparticles, the cellular binding and uptake of iRGD-cMLV and cMLV were examined. For the binding assay, cMLV(Dox) or iRGD-cMLV(Dox) was incubated with 4T1 tumor cells at 4°C for 30 min. Then the bound nanoparticles on the cell surface were determined by detecting doxorubicin signals via flow cytometry after removing the unbound nanoparticles. As shown in Figure 2(c), at both concentrations, a significantly higher integrated mean fluorescence intensity (MFI) was observed when the cells were incubated with iRGD-cMLV(Dox), indicating that iRGD-cMLVs can facilitate the attachment of nanoparticles to the cells via the integrin receptor expressed on the surface of tumor cells ($P < 0.01$). Additionally, the cellular accumulation of doxorubicin in 4T1 cells was determined by integrated MFI after the cells were incubated with cMLV(Dox) or iRGD-cMLV(Dox) at 37°C for 2 h. The results showed that a remarkably enhanced cell uptake of doxorubicin was observed when the cells were incubated with iRGD-cMLV(Dox) ($P < 0.01$, Figure 2(d)), suggesting that the increased cellular accumulation of doxorubicin was facilitated by iRGD peptides. Taken together, the iRGD peptides promoted both binding and uptake of drug-loaded nanoparticles in tumor cells, thereby enhancing the drug concentration in cells and improving the cytotoxicity of drugs.

3.3. Internalization and Intracellular Pathways of iRGD-cMLVs. We next investigated the entry mechanism and intracellular process of iRGD-cMLV into tumor cells to determine whether iRGD peptides could change the pathway by which nanoparticles are endocytosed. Endocytosis is known as one of the main entry mechanisms for various nanoscale drug carriers [22, 23]. Several studies have reported the involvement of clathrin- and caveolin-dependent pathways in nanoparticle-mediated endocytosis [24–26]. Therefore, to investigate the role of clathrin- or caveolin-dependent endocytosis of iRGD-cMLVs, we visualized the individual fluorescent DiD-labeled cMLVs or iRGD-cMLVs with endocytic structures (clathrin or caveolin) after 15 min incubation at 37°C. As shown in Figure 3(a), a significant colocalization of unconjugated cMLV particles with caveolin-1 signals was observed, while no colocalization between unconjugated cMLV particles and clathrin structures was detected, indicating that the caveolin pathway may be involved in the endocytosis of cMLVs. However, after 15 min incubation, iRGD-cMLV particles were colocalized with clathrin structures, whereas, no significant colocalization between iRGD-cMLV particles and caveolin-1 signals was observed (Figure 3(b)), suggesting that the endocytosis of iRGD-cMLVs could be clathrin dependent. The quantification of iRGD-cMLVs and cMLVs colocalized with caveolin-1 or clathrin structures by analyzing more than 30 cells confirmed that the clathrin-mediated pathway could be involved in the entry of iRGD-cMLVs, while the endocytosis of cMLVs could be caveolin-1 dependent (Figures 3(c) and 3(d)). The role of clathrin-dependent endocytosis of iRGD-cMLV was further examined by drug-inhibition assays shown in Figure 3(e). Chlorpromazine (CPZ) is known to block clathrin-mediated internalization by inhibiting clathrin polymerization [27], while filipin is a cholesterol-binding reagent that can disrupt caveolin-dependent internalization [28, 29]. As shown in Figure 3(e), CPZ ($10\ \mu$g/mL) significantly decreased the uptake of iRGD-cMLV particles in HeLa cells, while no significant inhibitory effect on their uptake was observed when cells were pretreated with Filipin ($10\ \mu$g/mL). However, pretreatment of cells with Filipin remarkably decreased the uptake of unconjugated cMLV particles ($P < 0.01$), whereas no inhibitory effect on their uptake was observed in CPZ-pretreated cells. Results from the inhibition assay further confirmed that iRGD-cMLV endocytosis is mediated by the clathrin-dependent pathway, while unconjugated cMLV particles enter cells via caveolin-dependent endocytosis.

Once inside the cells, the intracellular fate of the endosomal contents has been considered as an important determinant of successful drug delivery [30]. It was also proposed that nanoparticles might transport to the early endosomes in a GTPase Rb5-dependent manner and also proceed through the conventional endocytic pathway (endosomes/lysosomes) [31–33], probably resulting in enzymatic

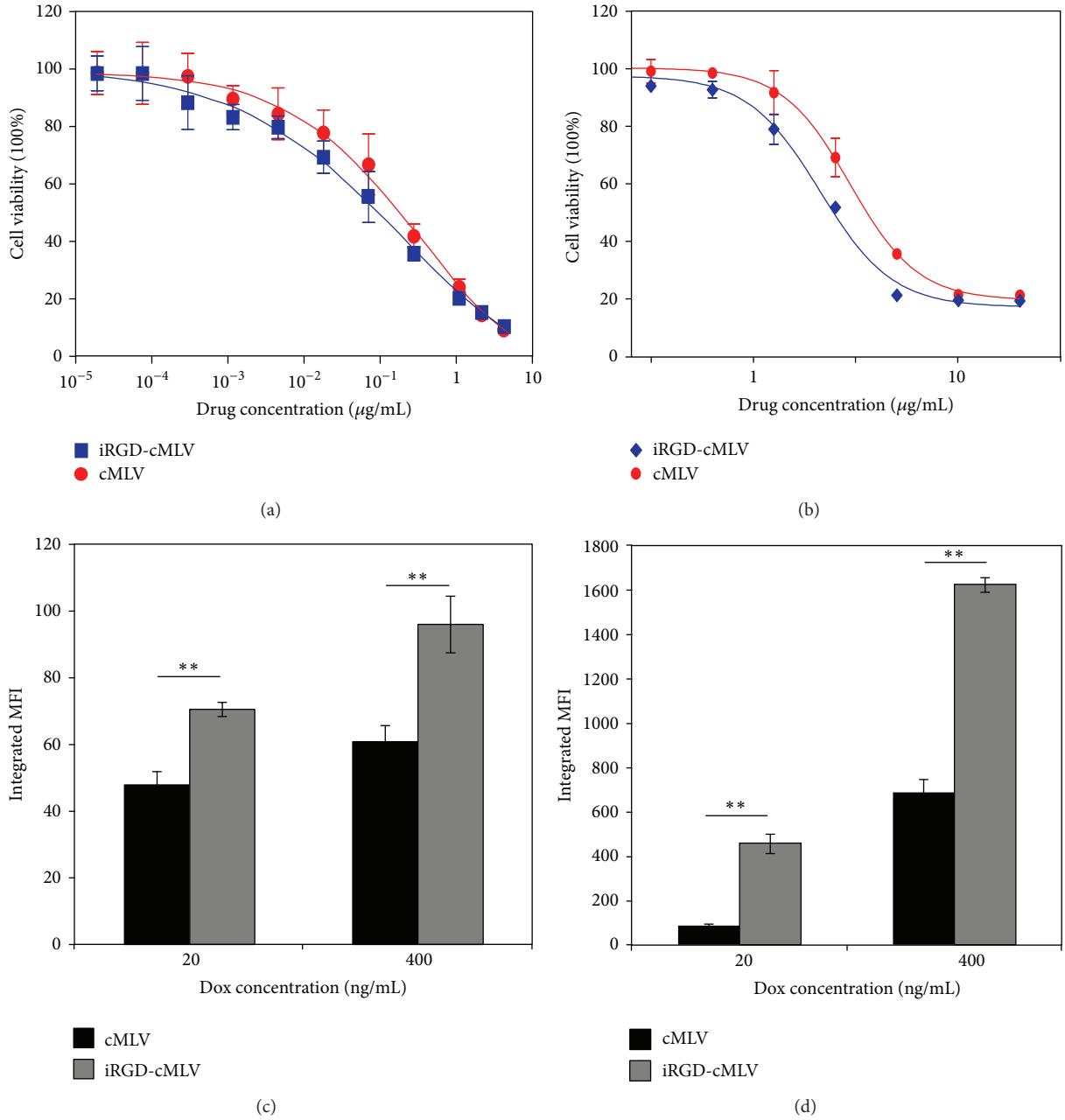

FIGURE 2: *In vitro* cytotoxicity, binding, and internalization of iRGD-cMLVs and cMLVs in tumor cells. ((a), (b)) *In vitro* cytotoxicity of cMLV(Dox) and iRGD-cMLV(Dox) in 4T1 tumor (a) and multidrug-resistant JC cells (b). The cytotoxicity was measured by a standard XTT assay. Error bars represent the standard deviation of the mean from triplicate experiments. ((c), (d)) Binding and internalization of cMLV(Dox) and iRGD-cMLV(Dox) to 4T1 cells. 4T1 cells were incubated with cMLV(Dox) and iRGD-cMLV(Dox) for 30 min at 4°C (c) or 2 h at 37°C (d). Both binding and cellular uptake of nanoparticles were determined by measuring doxorubicin fluorescence using flow cytometry. Statistical analysis was performed with Student's *t*-test. Error bars represent the standard deviation of the mean from triplicate experiments.

destruction of lipid membrane for drug release in lysosomes [30]. To further investigate the subsequent intracellular fate of iRGD-cMLV nanoparticles, DiD-labeled iRGD-cMLV particles were evaluated for their colocalization with the early endosome (EEA-1) [34] and lysosome (Lamp-1) [31] markers at different incubation times at 37°C. As shown in Figure 4(a), most iRGD-cMLV particles were found in the $EEA1^+$ early endosomes after incubation of 30 min, validating the involvement of early endosomes in the intracellular fate of targeted cMLV particles. In addition, after 2 h incubation, a significant colocalization of iRGD-cMLVs with lysosomes was observed, suggesting that iRGD-cMLVs may transport to early endosomes and further travel to lysosomes for possible release of drug from liposomes and endocytic

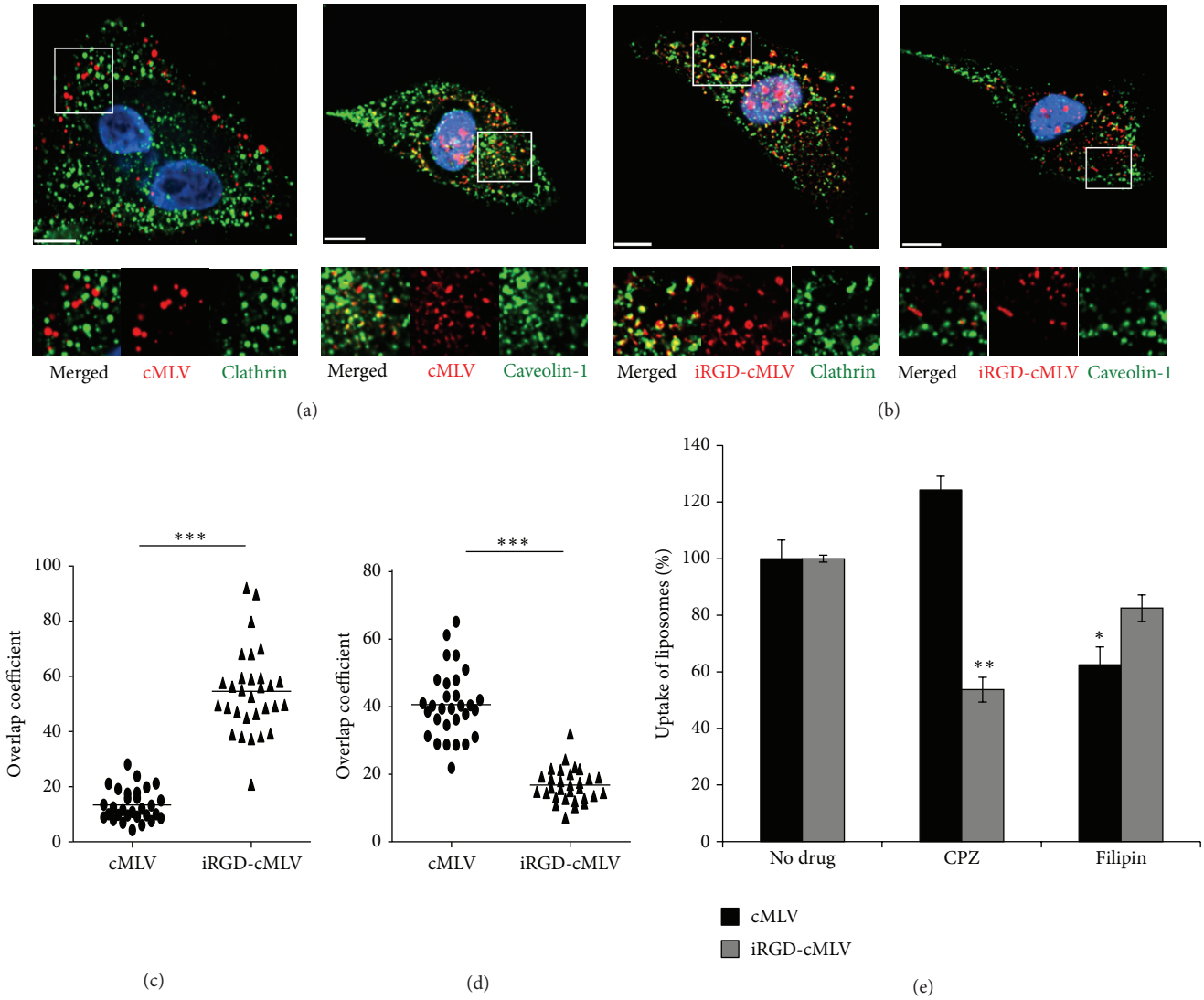

FIGURE 3: Clathrin-mediated internalization of iRGD-cMLVs and caveolin-dependent endocytosis of cMLVs. ((a), (b)) HeLa cells were incubated with DiD-labeled cMLV nanoparticles (red, (a)) or DiD-labeled iRGD-cMLVs particles (red, (b)) for 30 min at 4°C to synchronize internalization. The cells were then incubated at 37°C for 15 min, fixed, permeabilized, and immunostained with anti-clathrin (green) or anti-caveolin-1 antibody (green). The nucleus of cells was counterstained with DAPI. Scale bar represents 10 μm. ((c), (d)) Quantification of cMLV and iRGD-cMLV particles colocalized with clathrin (c) or caveolin-1 signals (d) after 15 min of incubation. Overlap coefficients were calculated using Manders' overlap coefficients by viewing more than 30 cells of each sample using the Nikon NIS-Elements software. Error bars represent the standard deviation of the mean from analysis of multiple images ($^{***}P < 0.005$). (e) Inhibition of clathrin-dependent endocytosis by chlorpromazine (CPZ, 25 μg/mL) and caveolin-dependent internalization by Filipin (10 μg/mL). The uptake of DiD-labeled cMLV and DiD-labeled iRGD-cMLV nanoparticles was determined by measuring DiD fluorescence via flow cytometry. Error bars represent the standard deviation of the mean from triplicate experiments ($^{*}P < 0.05$, $^{**}P < 0.01$).

compartments to cytosol. When taken together, the results showed that iRGD-cMLVs enter tumor cells via clathrin-dependent and receptor-mediated endocytosis, followed by transport through early endosomes and lysosomes.

3.4. Therapeutic Effect of iRGD-cMLV(Dox) in Breast Tumor Animal Model. We have demonstrated that iRGD-conjugated cMLVs can enhance uptake of nanoparticles into cells, resulting in an increased concentration of doxorubicin and *in vitro* cytotoxicity. Here, a breast tumor animal model was used to evaluate the *in vivo* therapeutic efficacy of iRGD-cMLV(Dox), compared with that of cMLV(Dox). At day 0, BALB/c mice were inoculated subcutaneously with 4T1 breast tumor cells. At day 10, mice were injected intravenously with iRGD-cMLV(Dox) or cMLV(Dox) at doses of 2 mg/kg Dox equivalents every three days. Tumor growth and body weight were then monitored until the end of the experiment (Figure 5(a)). As shown in Figure 5(b), mice in the group receiving 2 mg/kg cMLV(Dox) showed a significant tumor inhibition as compared to mice in the untreated group ($P < 0.01$). In addition, a marked

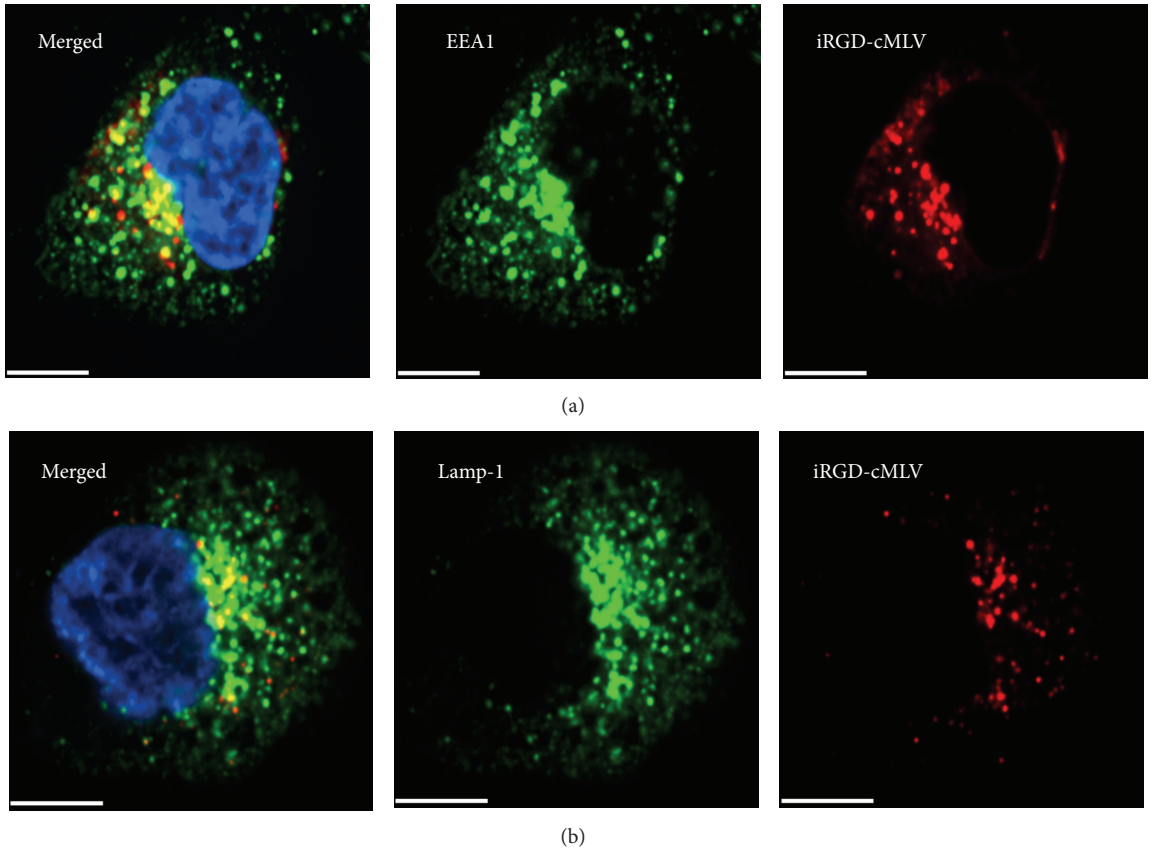

FIGURE 4: Involvement of early endosomes and lysosomes in the intracellular trafficking of iRGD-cMLVs. HeLa cells were incubated with DiD-labeled iRGD-cMLV nanoparticles (red) for 30 min at 4°C to synchronize internalization. The cells were then incubated at 37°C for 45 min and immunostained with anti-EEA1 antibody (green, (a)) or for 2 h and immunostained with anti-Lamp1 antibody (green, (b)). The nucleus of cells was counterstained with DAPI. Scale bar represents 10 μm.

suppression of tumor growth was observed in the group treated by iRGD-cMLV(Dox), suggesting that iRGD peptides could further enhance the therapeutic effect of drug-loaded nanoparticles *in vivo*. During the whole experiment, no weight loss was seen in any of the mice (Figure 5(c)), indicating the absence of systemic toxicity from cMLV and iRGD-cMLV formulations. The enhanced antitumor activity of iRGD-cMLV (Dox) was further confirmed by a significant reduction on tumor weight of mice treated with iRGD-cMLV(Dox), as compared to that treated with cMLV(Dox) (Figure 5(d)).

4. Discussion

Nontargeted, long-circulating liposomes, such as Doxil/Caelyx, have been extensively evaluated to deliver chemotherapeutic drugs to treat cancers via the enhanced permeability and retention mechanism [35–37]. Although significant efforts have been made to enhance their therapeutic activity, the relatively inherent instability of conventional liposomes in the presence of serum component, resulting in rapid drug release profile, has been considered as an obstacle in their development for cancer treatment [38]. In order to develop a liposomal formulation with sustainable release kinetics and improved stability, a cMLV formulation of Dox has been explored as a new nanocarrier platform with promising features of enhanced vesicle stability and reduced systemic toxicity, resulting in improved *in vivo* therapeutic efficiency [18]. Although cMLVs have shown improved antitumor activity, direct delivery of these particles with targeting ligands could potentially further enhance efficacy and minimize toxicity.

Most currently investigated targeting strategies concentrate on directing nanoparticles to tumor cells by utilizing the specific receptor/ligand overexpressed on tumor cells [6, 39, 40]. For instance, RGD (arginine-glycine-aspartate) peptides have been conjugated to drug-loaded nanoparticles to target integrin receptors, which are overexpressed on neovascular endothelial cells [13, 15, 16]. Although the development of targeted payload for anticancer drug delivery has shown potential enhanced therapeutic effect, poor penetration of nanoparticles to tumor cells still thwarts clinical treatment of solid tumor [11, 12]. Therefore, a novel iRGD peptide has been recently identified and reported to increase vascular and tissue penetration in a tumor-specific and neuropilin-1-(NRP-1-) dependent manner [13, 15, 16]. The C-terminal motif CendR of iRGD peptide has been identified as a mediator of cell and tissue penetration through the interaction with

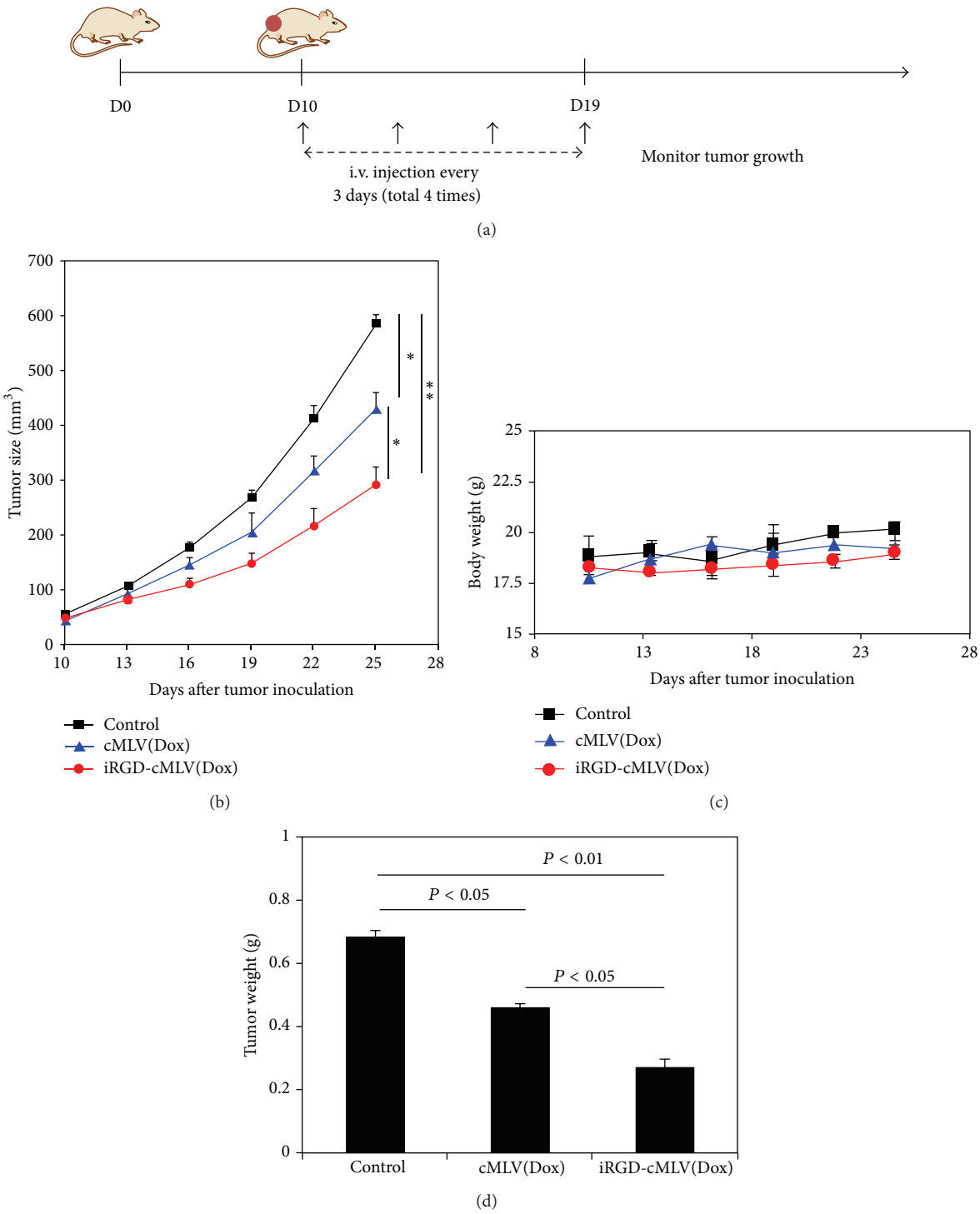

FIGURE 5: Antitumor effect of iRGD-cMLVs and cMLVs in the 4T1 breast tumor model. (a) Schematic diagram of the experimental protocol for the *in vivo* tumor study. (b) Tumor growth was measured after treatment without injection (control), cMLV(Dox), and iRGD-cMLV(Dox) (2 mg/kg Dox equivalents). Error bars represent standard error of the mean; $n = 5$ for each treatment group ($^*P < 0.05$). (c) Average mouse weight loss over the duration of the experiment. (d) Tumor weight of excised tumors from each treatment group at 25 days after tumor inoculation. Error bars represent standard error of the mean; $n = 5$ for each treatment group.

neuropilin-1 receptor, a cell-surface receptor that is involved in the regulation of vascular permeability [41, 42]. For example, it has been reported that the successful infection of many viruses required proteolytic cleavage of capsid proteins to expose the CendR motifs to neuropilin-1 receptor, which could trigger the endocytosis of viral particles into cells [43]. Moreover, several studies have reported that peptides containing CendR motifs could bind to NRP-1 receptor and cause cellular internalization and vascular leakage [44], suggesting that iRGD peptides could have similar effects when covalently coupled to a drug delivery nanocarrier. Previously, we demonstrated the enhanced therapeutic ability of cMLV formulations with reduced systemic toxicity, as compared to that of unilamellar liposome or Doxil-like liposomes [18]. Therefore, in this study, we conjugated iRGD peptides to this relatively stable cMLV particles and evaluated, both *in vitro* and *in vivo*, the effect of these targeted nanoparticles. A similar accumulative drug release profile was observed in iRGD-cMLV formulation as compared to cMLV formulations, due to a similar size distribution and lipid composition of these two formulations. The results showed that iRGD-cMLVs presented superior cytotoxicity resulting from the enhanced binding and uptake of targeted nanoparticles in cells. Moreover, enhanced uptake and penetration of Dox via iRGD-cMLV vesicles enabled the improved *in vivo* therapeutic activity in tumors. iRGD-cMLVs treatment of 4T1 tumors exhibited significant inhibition of tumor growth compared to that treated with cMLVs, further suggesting the potential application of iRGD to drug delivery via nanoparticles.

Furthermore, our imaging study on the entry mechanism of iRGD-cMLVs provided some edifying details about the intracellular fate of these particles. Specifically, the results showed that iRGD-cMLV particles enter cells via clathrin-dependent endocytosis, while the internalization of unconjugated cMLV particles is caveolin-mediated. The different endocytic pathways utilized by iRGD-cMLVs might result from the interaction of nanoparticles with cells via iRGD-integrin binding. The results also suggested that the receptor mediated internalization possibly promoted cell attachment, resulting in an enhanced cellular uptake. Although it has been hypothesized that multiple pathways were involved in endosomal transport [24, 25, 45], our data showed that both iRGD-cMLVs and cMLVs home to early endosomes and further traffic to lysosomes [18]. The involvement of lysosome in the intracellular trafficking routes of both iRGD-cMLVs and cMLVs might facilitate drug release kinetics because enzymes, such as phospholipases, in the endolysosomal compartments can promote disruption of liposomal bilayers [46, 47].

5. Conclusions

This study has evaluated the potential therapeutic effects of a tumor-penetrating peptide, iRGD, by conjugating it with Dox-loaded cMLVs in tumor treatment. We have demonstrated that iRGD-cMLVs can serve as a new targeting strategy to facilitate the penetration of antitumor drugs into tumor cells and further enhance the therapeutic efficacy of drugs both *in vitro* and *in vivo*. In addition, the endocytic pathways involved in the entry of iRGD-cMLVs have been investigated to shed some light on the possible mechanism of enhanced cellular uptake of targeted nanoparticles.

Acknowledgments

The authors thank the USC NanoBiophysics Core Facility. This work was supported by National Institutes of Health grants (R01AI068978 and P01CA132681), a translational acceleration grant from the Joint Center for Translational Medicine, a grant from the Department of Defense Breast Cancer Research Program, and a grant from the Ming Hsieh Institute for Research on Engineering Medicine for Cancer.

References

[1] M. E. Davis, Z. Chen, and D. M. Shin, "Nanoparticle therapeutics: an emerging treatment modality for cancer," *Nature Reviews Drug Discovery*, vol. 7, no. 9, pp. 771–782, 2008.

[2] O. C. Farokhzad and R. Langer, "Impact of nanotechnology on drug delivery," *ACS Nano*, vol. 3, no. 1, pp. 16–20, 2009.

[3] D. Peer, J. M. Karp, S. Hong, O. C. Farokhzad, R. Margalit, and R. Langer, "Nanocarriers as an emerging platform for cancer therapy," *Nature Nanotechnology*, vol. 2, no. 12, pp. 751–760, 2007.

[4] H. Maeda, "The enhanced permeability and retention (EPR) effect in tumor vasculature: the key role of tumor-selective macromolecular drug targeting," *Advances in Enzyme Regulation*, vol. 41, pp. 189–207, 2001.

[5] V. P. Torchilin, "Recent advances with liposomes as pharmaceutical carriers," *Nature Reviews Drug Discovery*, vol. 4, no. 2, pp. 145–160, 2005.

[6] E. Ruoslahti, S. N. Bhatia, and M. J. Sailor, "Targeting of drugs and nanoparticles to tumors," *Journal of Cell Biology*, vol. 188, no. 6, pp. 759–768, 2010.

[7] S. Sengupta, D. Eavarone, I. Capila et al., "Temporal targeting of tumour cells and neovasculature with a nanoscale delivery system," *Nature*, vol. 436, no. 7050, pp. 568–572, 2005.

[8] H. Shmeeda, D. Tzemach, L. Mak, and A. Gabizon, "Her2-targeted pegylated liposomal doxorubicin: retention of target-specific binding and cytotoxicity after *in vivo* passage," *Journal of Controlled Release*, vol. 136, no. 2, pp. 155–160, 2009.

[9] A. R. Hilgenbrink and P. S. Low, "Folate receptor-mediated drug targeting: from therapeutics to diagnostics," *Journal of Pharmaceutical Sciences*, vol. 94, no. 10, pp. 2135–2146, 2005.

[10] L. Xu, K. F. Pirollo, W. H. Tang, A. Rait, and E. H. Chang, "Transferrin-liposome-mediated systemic p53 gene therapy in combination with radiation results in regression of human head and neck cancer xenografts," *Human Gene Therapy*, vol. 10, no. 18, pp. 2941–2952, 1999.

[11] C. H. Heldin, K. Rubin, K. Pietras, and A. Östman, "High interstitial fluid pressure—an obstacle in cancer therapy," *Nature Reviews Cancer*, vol. 4, no. 10, pp. 806–813, 2004.

[12] R. K. Jain, "Transport of molecules, particles, and cells in solid tumors," *Annual Review of Biomedical Engineering*, no. 1, pp. 241–263, 1999.

[13] K. N. Sugahara, T. Teesalu, P. P. Karmali et al., "Tissue-penetrating delivery of compounds and nanoparticles into tumors," *Cancer Cell*, vol. 16, no. 6, pp. 510–520, 2009.

[14] K. N. Sugahara, T. Teesalu, P. P. Karmali et al., "Coadministration of a tumor-penetrating peptide enhances the efficacy of cancer drugs," *Science*, vol. 328, no. 5981, pp. 1031–1035, 2010.

[15] A. Mitra, J. Mulholland, A. Nan, E. McNeill, H. Ghandehari, and B. R. Line, "Targeting tumor angiogenic vasculature using polymer-RGD conjugates," *Journal of Controlled Release*, vol. 102, no. 1, pp. 191–201, 2005.

[16] E. A. Murphy, B. K. Majeti, L. A. Barnes et al., "Nanoparticle-mediated drug delivery to tumor vasculature suppresses metastasis," *Proceedings of the National Academy of Sciences of the United States of America*, vol. 105, no. 27, pp. 9343–9348, 2008.

[17] O. Feron, "Tumor-penetrating peptides: a shift from magic bullets to magic guns," *Science Translational Medicine*, vol. 2, no. 34, Article ID 34ps26, 2010.

[18] K.-I. Joo, L. Xiao, S. Liu et al., "Crosslinked multilamellar liposomes for controlled delivery of anticancer drugs," *Biomaterials*, vol. 34, no. 12, pp. 3098–3109, 2013.

[19] J. J. Moon, H. Suh, A. Bershteyn et al., "Interbilayer-crosslinked multilamellar vesicles as synthetic vaccines for potent humoral and cellular immune responses," *Nature Materials*, vol. 10, no. 3, pp. 243–251, 2011.

[20] N. Dos Santos, C. Allen, A. M. Doppen et al., "Influence of poly(ethylene glycol) grafting density and polymer length on liposomes: relating plasma circulation lifetimes to protein binding," *Biochimica et Biophysica Acta*, vol. 1768, no. 6, pp. 1367–1377, 2007.

[21] B. D. Lee, K. J. French, Y. Zhuang, and C. D. Smith, "Development of a syngeneic *in vivo* tumor model and its use in evaluating a novel P-glycoprotein modulator, PGP-4008," *Oncology Research*, vol. 14, no. 1, pp. 49–60, 2003.

[22] P. D. Dobson and D. B. Kell, "Carrier-mediated cellular uptake of pharmaceutical drugs: an exception or the rule?" *Nature Reviews Drug Discovery*, vol. 7, no. 3, pp. 205–220, 2008.

[23] R. A. Petros and J. M. Desimone, "Strategies in the design of nanoparticles for therapeutic applications," *Nature Reviews Drug Discovery*, vol. 9, no. 8, pp. 615–627, 2010.

[24] S. D. Conner and S. L. Schmid, "Regulated portals of entry into the cell," *Nature*, vol. 422, no. 6927, pp. 37–44, 2003.

[25] C. Le Roy and J. L. Wrana, "Clathrin- and non-clathrin-mediated endocytic regulation of cell signalling," *Nature Reviews Molecular Cell Biology*, vol. 6, no. 2, pp. 112–126, 2005.

[26] L. Pelkmans and A. Helenius, "Endocytosis via caveolae," *Traffic*, vol. 3, no. 5, pp. 311–320, 2002.

[27] L. H. Wang, K. G. Rothberg, and R. G. W. Anderson, "Mis-assembly of clathrin lattices on endosomes reveals a regulatory switch for coated pit formation," *Journal of Cell Biology*, vol. 123, no. 5, pp. 1107–1117, 1993.

[28] E. B. Neufeld, A. M. Cooney, J. Pitha et al., "Intracellular trafficking of cholesterol monitored with a cyclodextrin," *Journal of Biological Chemistry*, vol. 271, no. 35, pp. 21604–21613, 1996.

[29] K. G. Rothberg, J. E. Heuser, W. C. Donzell, Y. S. Ying, J. R. Glenney, and R. G. W. Anderson, "Caveolin, a protein component of caveolae membrane coats," *Cell*, vol. 68, no. 4, pp. 673–682, 1992.

[30] L. M. Bareford and P. W. Swaan, "Endocytic mechanisms for targeted drug delivery," *Advanced Drug Delivery Reviews*, vol. 59, no. 8, pp. 748–758, 2007.

[31] S. R. Carlsson, J. Roth, F. Piller, and M. Fukuda, "Isolation and characterization of human lysosomal membrane glycoproteins, h-lamp-1 and h-lamp-2. Major sialoglycoproteins carrying polylactosaminoglycan," *Journal of Biological Chemistry*, vol. 263, no. 35, pp. 18911–18919, 1988.

[32] S. Christoforidis, H. M. McBride, R. D. Burgoyne, and M. Zerial, "The rab5 effector EEA1 is a core component of endosome docking," *Nature*, vol. 397, no. 6720, pp. 621–625, 1999.

[33] J. P. Luzio, B. Brake, G. Banting, K. E. Howell, P. Braghetta, and K. K. Stanley, "Identification, sequencing and expression of an integral membrane protein of the trans-Golgi network (TGN38)," *Biochemical Journal*, vol. 270, no. 1, pp. 97–102, 1990.

[34] L. Pelkmans, J. Kartenbeck, and A. Helenius, "Caveolar endocytosis of simian virus 40 reveals a new two-step vesicular-transport pathway to the ER," *Nature Cell Biology*, vol. 3, no. 5, pp. 473–483, 2001.

[35] A. A. Gabizon, "Pegylated liposomal doxorubicin: metamorphosis of an old drug into a new form of chemotherapy," *Cancer Investigation*, vol. 19, no. 4, pp. 424–436, 2001.

[36] A. A. Gabizon, "Stealth liposomes and tumor targeting: one step further in the quest for the magic bullet," *Clinical Cancer Research*, vol. 7, no. 2, pp. 223–225, 2001.

[37] J. A. O'Shaughnessy, "Pegylated liposomal doxorubicin in the treatment of breast cancer," *Clinical Breast Cancer*, vol. 4, no. 5, pp. 318–328, 2003.

[38] D. C. Drummond, C. O. Noble, M. E. Hayes, J. W. Park, and D. B. Kirpotin, "Pharmacokinetics and *in vivo* drug release rates in liposomal nanocarrier development," *Journal of Pharmaceutical Sciences*, vol. 97, no. 11, pp. 4696–4740, 2008.

[39] E. Ruoslahti, "Specialization of tumour vasculature," *Nature Reviews Cancer*, vol. 2, no. 2, pp. 83–90, 2002.

[40] G. M. Tozer, C. Kanthou, and B. C. Baguley, "Disrupting tumour blood vessels," *Nature Reviews Cancer*, vol. 5, no. 6, pp. 423–435, 2005.

[41] L. M. Acevedo, S. Barillas, S. M. Weis, J. R. Göthert, and D. A. Cheresh, "Semaphorin 3A suppresses VEGF-mediated angiogenesis yet acts as a vascular permeability factor," *Blood*, vol. 111, no. 5, pp. 2674–2680, 2008.

[42] H. Jia, A. Bagherzadeh, B. Hartzoulakis et al., "Characterization of a bicyclic peptide neuropilin-1 (NP-1) antagonist (EG3287) reveals importance of vascular endothelial growth factor exon 8 for NP-1 binding and role of NP-1 in KDR signaling," *Journal of Biological Chemistry*, vol. 281, no. 19, pp. 13493–13502, 2006.

[43] S. Lambert, M. Bouttier, R. Vassy et al., "HTLV-1 uses HSPG and neuropilin-1 for entry by molecular mimicry of VEGF165," *Blood*, vol. 113, no. 21, pp. 5176–5185, 2009.

[44] T. Teesalu, K. N. Sugahara, V. R. Kotamraju, and E. Ruoslahti, "C-end rule peptides mediate neuropilin-1-dependent cell, vascular, and tissue penetration," *Proceedings of the National Academy of Sciences of the United States of America*, vol. 106, no. 38, pp. 16157–16162, 2009.

[45] A. Verma and F. Stellacci, "Effect of surface properties on nanoparticle-cell interactions," *Small*, vol. 6, no. 1, pp. 12–21, 2010.

[46] T. L. Andresen, S. S. Jensen, and K. Jørgensen, "Advanced strategies in liposomal cancer therapy: problems and prospects of active and tumor specific drug release," *Progress in Lipid Research*, vol. 44, no. 1, pp. 68–97, 2005.

[47] A. Gabizon, H. Shmeeda, and Y. Barenholz, "Pharmacokinetics of pegylated liposomal doxorubicin: review of animal and human studies," *Clinical Pharmacokinetics*, vol. 42, no. 5, pp. 419–436, 2003.

Hindawi Publishing Corporation
BioMed Research International
Volume 2013, Article ID 349408, 9 pages
http://dx.doi.org/10.1155/2013/349408

Research Article

Functionalized Magnetic Nanoparticles for the Detection and Quantitative Analysis of Cell Surface Antigen

Daryoush Shahbazi-Gahrouei,[1] Mohammad Abdolahi,[2] Sayyed Hamid Zarkesh-Esfahani,[3] Sophie Laurent,[4] Corine Sermeus,[4] and Cordula Gruettner[5]

[1] *Department of Medical Physics and Medical Engineering, School of Medicine, Isfahan University of Medical Sciences, Hezar Jerib Street, Isfahan, Iran*
[2] *Department of Medical Physics, School of Medicine, Bushehr University of Medical Sciences, Bushehr, Iran*
[3] *Department of Immunology, Medical School, Isfahan University of Medical Sciences, Hezar Jerib Street, Isfahan, Iran*
[4] *Department of General, Organic, and Biomedical Chemistry, NMR and Molecular Imaging Laboratory, University of Mons, 19 Avenue Maistriau, 7000 Mons, Belgium*
[5] *Micromod Partikletechnologie GmbH, Rostock, Germany*

Correspondence should be addressed to Daryoush Shahbazi-Gahrouei; shahbazi@med.mui.ac.ir

Received 14 September 2012; Accepted 5 December 2012

Academic Editor: Susana N. Diniz

Cell surface antigens as biomarkers offer tremendous potential for early diagnosis, prognosis, and therapeutic response in a variety of diseases such as cancers. In this research, a simple, rapid, accurate, inexpensive, and easily available in vitro assay based on magnetic nanoparticles and magnetic cell separation principle was applied to identify and quantitatively analyze the cell surface antigen expression in the case of prostate cancer cells. Comparing the capability of the assay with flow cytometry as a gold standard method showed similar results. The results showed that the antigen-specific magnetic cell separation with antibody-coated magnetic nanoparticles has high potential for quantitative cell surface antigen detection and analysis.

1. Introduction

The biomarkers as early warning signs for diseases are physiological and pathological changes in expression level or state, which correlate with the progression in a variety of diseases such as cancers [1, 2]. As the biomarkers show a disease state very specifically and sensitively, they can be used for the early diagnosis, differentiation between disease types with higher accuracy, disease monitoring during and after therapy, and as possible therapeutic targets [3–5]. Among the biomarkers, cell surface antigens play a key role in cellular functions and pathomechanism of diseases in a variety of cancers and since many of them are restrictedly produced against a specific tumor, they can act as ideal biomarkers [6]. It is clear that cancer patients would benefit enormously from a better availability of such effective molecular indicators that help in the development of new diagnostic and therapeutic methods [7, 8].

Although the potential applications of cell surface antigens in cancer diseases appear extraordinarily promising idea, the greatest potential for using this type of biomarkers for cancer lies in improving the technology for cancer cells antigen discovery. So, rapid, simple, accurate, and inexpensive detection methods of the relevant marker are very basic and important. Currently, a wide range of technologies are used for detection and characterization of surface antigens; however, the most widely used method is the analysis of cell surface antigens by flow cytometry [9, 10]. Although the flow cytometry is the gold standard method for accurate and automated measurements of cell surface antigens, this technique is not only expensive and only available in specialized centers but also requires sophisticated equipment and reagents as

well as highly trained personnel. Furthermore, in resource-limited countries the access to the technical support and quality assurance programs for flow cytometry is often not readily available [11, 12].

Recently, a new technique has been developed using magnetic nanoparticles coupled to antibodies, as a nonflow cytometric method, which identifies cell surface antigen expression by specific antibody-antigen reaction easier, faster, more efficiently, and at lower cost than the other methods [13]. In addition, the use of magnetic nanoparticles as molecular imaging probes enables noninvasive in vivo studies of antigen expression of diseases in various internal organs [14, 15].

In this work, a rapid and accurate in vitro assay based on magnetic nanoparticles and magnetic cell separation principle was described and developed to discover and quantitatively analyze the cell surface antigen expression of Prostate Specific Membrane Antigen (PSMA). This assay relies on the fact that prostate cancer cells overexpress the PSMA [16, 17].

2. Materials and Methods

2.1. Materials. Sulfo-SMCC cross-linker (Sulfosuccinimidyl-4-(N-maleimidomethyl) cyclohexane-1-carboxylate), Traut's Reagent (2-iminothiolane), and cysteine were purchased from Sigma Chemical Co. (St. Louis, MO, USA). Nanomag-D-spio nanoparticles in suspension (diameter: 20 nm, surface: CLD-NH_2, 5 mg/mL; 2.4 mg Fe/mL) were obtained from micromod Partikeltechnologie GmbH (Rostock, Germany). Midi MACS sorting device, LD, and MS high-gradient magnetic field (HGMF) columns were purchased from Miltenyi Biotec GmbH (Gladbach, Germany). PD-10 columns were purchased from GE Healthcare (Piscataway, NJ). The Bradford reagent was purchased from BioRad (Hercules, CA). Amicon centrifugal filters (0.5 mL capacity, 10 kDa MWCO) were purchased from Millipore (Billerica, MA).

All other chemicals were supplied by Aldrich and used as received. J591 monoclonal antibody was obtained from Professor Neil H. Bander (Cornell University, New York, USA). Cell culture media and fetal bovine serum (FBS) were obtained from GIBCO, Invitrogen Corporation (Carlsbad, CA, USA). Prostate cancer cell lines, DU145 and LNCaP, were purchased from national cell bank of Iran (Pasture Institute, Tehran, Iran) and Cell Lines Service (CLS, Eppelheim, Germany).

2.2. Conjugation of J591 Antibody with Nanoparticles. The monoclonal J591 antibody was thiolated and conjugated to maleimide functionalized nanomag-D-spio nanoparticles (Figure 1). Therefore, the sulfo-SMCC cross-linker was first added to nanomag-D-spio particles with CLD-NH_2 surface to introduce maleimide groups. Specifically, 100 μL of 14.35 μM Sulfo-SMCC solution in DMSO was added to 5 mg of nanoparticles in PBS-EDTA buffer under gentle shaking for 1 h at room temperature. After incubation, the suspension was washed with PBS-EDTA buffer with PD-10 size exclusion columns to remove unreacted sulfo-SMCC. In the next step, primary amines of J591 monoclonal antibodies were modified with 2-iminothiolane to introduce sulfhydryl groups. Typically, 8 μL of 7 mM Traut's reagent solution was added to 400 μL of pure antibody solution in PBS-EDTA buffer (1 mg/mL) and shaken for 1 h at room temperature. To remove unconjugated 2-iminothiolane, the solution was washed three times by 10-kDa cutoff Amicon centrifugal filter units with PBS as an eluent.

The antibody conjugation to SPIO nanoparticles was achieved by addition of the maleimide functionalized particles to the SH-labeled antibody and incubation under gentle shaking for 3 h at room temperature. Remaining functional groups were blocked by addition of 100 μL of 20 mM freshly prepared cysteine solution. Finally, the antibody-labeled SPIO nanoparticles were purified on magnetic columns (MACS separator).

2.3. Characterization. The hydrodynamic particle size and the width of the particle size distribution (polydispersity index) of nanoparticles were obtained via photon correlation spectroscopy (PCS) using a Malvern Nano Series ZS particle size analyzer (Malvern Instruments, Worcestershire, UK). Samples morphology was observed by transmission electron microscopy (TEM) on a Tecnai 10 TEM (FEI Company, USA) operating at 80 kV. To confirm the feasibility and sensitivity as magnetic cell separation nanoprobe, magnetic properties of synthesized nanoprobe were studied by the use of nuclear magnetic resonance dispersion (NMRD) profiles (Spinmaster FFC 2000, STELAR, Italy), in a field strength range extending from 200 μT to 1.2 T. Additional measurements of relaxation rate ($R_{1,2}$) were performed at 20 and 60 MHz on Bruker Minispec system (Bruker, Karlsruhe, Germany).

The binding of antibody molecules to SPIO nanoparticles and the amount of immobilized antibody were determined by the Bradford assay. Briefly, 40 μL of Coomassie Plus reagent concentrate was added to 160 μL of dispersion of nanoparticles, either mAb-coated or noncoated. After 10 min of incubation, the absorbance was measured at 595 nm using a microplate reader (Stat Fax, Awareness Technologies, USA). The results were compared to a standard curve of BSA solution in the concentration range from 10 μg/mL to 150 μg/mL (Figure 3).

The iron concentrations of the samples were measured by relaxometry measurements at 20 MHz after digestion of samples by microwave oven. This was achieved by mineralization of sample in acidic conditions (0.2 mL sample, 0.6 mL HNO_3, and 0.3 mL H_2O_2) by microwave oven (Milestone MLS-1200, Sorisole, Italy). The millimolar iron concentration was determined from the R_1 relaxation rate of samples, using following equation [18, 19]:

$$[\mathrm{Fe}] = \frac{\left(R_1^{\mathrm{obs}} - R_1^{\mathrm{dia}}\right)}{r_1\left(\mathrm{s}^{-1}\,\mathrm{mM}^{-1}\right)}, \quad (1)$$

where R_1^{obs} is the observed longitudinal proton relaxation rate, R_1^{dia} is the relaxation rate of water protons in the absence of the contrast agent, and r_1 is the longitudinal relaxivity

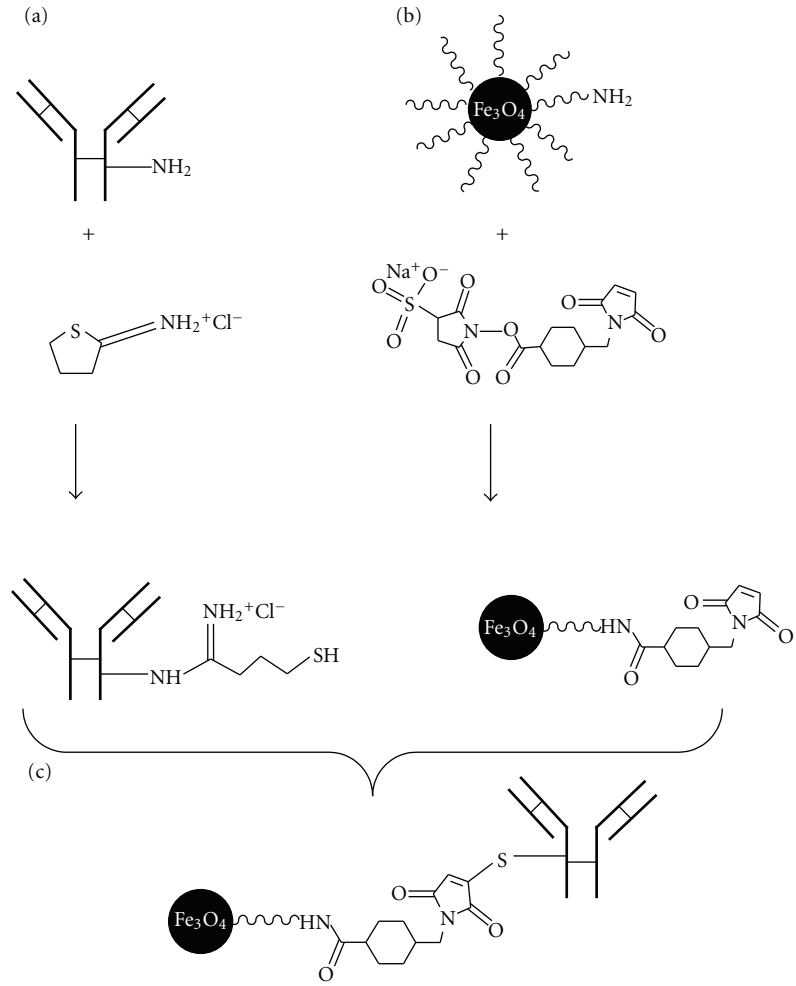

Figure 1: The Scheme of SPIO nanoparticles Conjugation to J591 antibody, (a) functionalization of SPIO-CLD-NH_2 with Sulfo-SMCC, (b) functionalization of antibody with SH groups using Traut's reagent, and (c) conjugation of thiolated antibody to maleimide functionalized SPIO.

defined as the relaxation rates induced by 1 mmol of iron per liter of solution. R_1^{obs} is the relaxation rate which is measured on the solution containing the sample; R_1^{dia} and r_1 were obtained from a standard curve built by measuring the R_1 of various dilutions of mineralized standard sample of iron (ICP standard, Sigma Aldrich) (Figure 4).

2.4. Cell Culture. LNCaP, a PSMA-expressing ($PSMA^+$), and DU145, a PSMA negative ($PSMA^-$) adherent human prostate cancer cell line, were grown in Dulbecco's Modified Eagle Medium supplemented with 2 mM L-glutamine, 1% NEAA, 1 mM sodium pyruvate, 10% fetal bovine serum, and 1% penicillin/streptomycin (Gibco, Grand Island, NY, USA). For DU145, 1.5 g/L sodium bicarbonate and 0.1 mM nonessential amino acids were used. The cells were cultured in 75 cm^2 flasks, at 37°C under a humidified 5% CO_2 atmosphere. For subculture and harvesting the cells, they were washed with PBS followed by treatment with 3 mL TrypLE (Gibco, Grand Island, NY, USA) for 3 min to detach the cells. About 10 mL of culture medium was added to neutralize the TrypLE. The cells were then centrifuged at 3000 RPM for 10 min; the medium was removed and resuspended in complete media and reseeded into new culture flasks.

2.5. In Vitro Cytotoxicity. The cytotoxicity of nanomag-D-spio particles and the corresponding J591-antibody-conjugated nanoparticles against LNCaP and DU145 cells was evaluated by using the 3-(4,5-dimethylthiazol-2-yl)-2,5-diphenyltetrazolium bromide (MTT) assay (Sigma-Aldrich) [20]. Exponentially growing LNCaP and DU145 cells were seeded at a density of 2×10^4 cells/well in 96-well plates (Cell Star, Germany). The plates were incubated for 24 h in a humidified incubator with a CO_2 concentration of 5% to allow adherence of the cells. Once adhered, the cells were incubated with either 0.1 mL of medium containing nanomag-D-spio or SPIO-J591 at iron concentrations ranging from 0.15 to 2.4 mM for 2, 8, and 24 h. The culture medium without any particle was used as the control.

After incubation time 10 μL/well (5 mg/mL), MTT was added and incubation was continued for further 3 h.

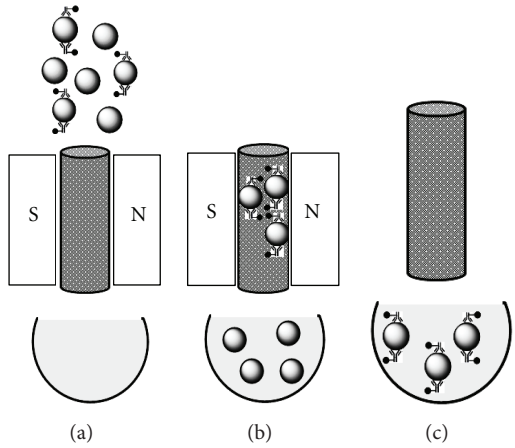

Figure 2: Scheme of the magnetic bead-based cell separation. (a) A mixture of magnetically labeled and nonlabeled cells is applied on a separation column. (b) Specific cell selection using MACS columns. Magnetically labeled cells are retained in the magnetic field of the separation column; unlabeled cells pass through the column as negative fraction. (c) After removal of the column from the magnetic field, the desired cells are eluted as the enriched positive fraction.

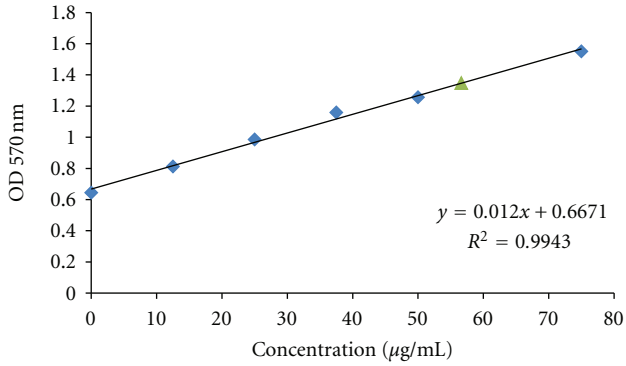

Figure 3: Antibody concentration measurement by Bradford protein assay.

The medium was carefully removed and the formazan crystals (indicating cell viability) were solubilized by adding 100 μL DMSO (Sigma-Aldrich) per well. The absorbance was determined at 570 nm by the Statfax-microplate reader (Awareness Technology, USA). Experiments were performed in triplicate and cell survival was determined as a percentage of viable cells in comparison with control wells. One-way ANOVA and correlation coefficient between viability and iron concentration were used to determine whether the SPIO nanoparticles caused any significant cytotoxicity.

2.6. Fluorescence Microscopy. Fluorescence microscopy was used to qualitatively analyze the cell surface antigen. LNCaP and DU145 cell lines were washed with phosphate buffered saline (PBS), detached by TrypLE, and seeded near confluence (2×10^5 cells/well) on 22 × 22 mm square glass coverslips, which were pretreated with plasminogen in 6-well plates. After attachment, the cells were fixed with 4%

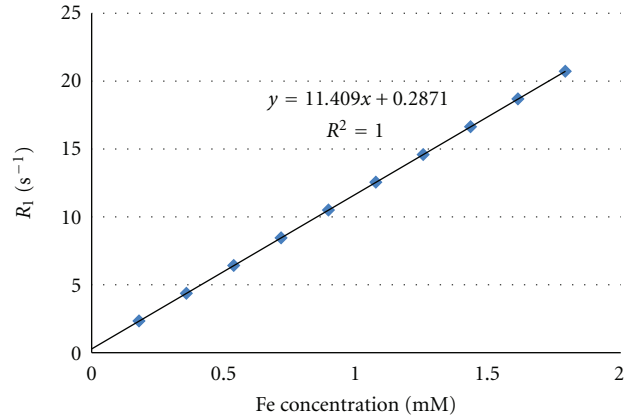

Figure 4: Calibration curve of iron concentration versus relaxation rate at 20 MHz.

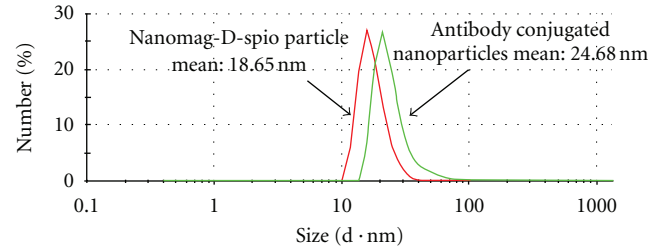

Figure 5: Hydrodynamic diameter of nanomag-D-spio (18.65 nm) and J591-SPIO NPs (24.68 nm).

formaldehyde solution for 15 min, washed with PBS, then treated with Protein-Free Blocking Buffer (PFBB, Perbio Science, Erembodegem, Belgium) for 1 h at room temperature. The cells were washed with PBS and incubated successively with primary J591 anti-PSMA antibody overnight in the dark at 4°C. After washing with PBS, the cells were incubated with goat anti-mouse FITC monoclonal antibody for an additional 1 h at room temperature in the dark. Cells were then washed, and the slides were mounted using diluted 4′,6-diamidino-2-phenylindole (DAPI) (Vector Labconsult, Brussels, Belgium) solution for 5 min at room temperature and rinsed once with PBS and once with water. The cover slips were mounted onto microscope slides and observed on a confocal microscope (Leica Microsystems, Groot Bijgaarden, Belgium). A semiquantitative analysis of the microscope pictures has been performed by using the ImageJ image analysis software (National Institutes of Health).

2.7. Surface Antigen Expression. In a variety of disease, abnormalities concern not only antigen expression but also its intensity, which may have diagnostic or prognostic significance [21, 22]. Quantitative expression of PSMA on the LNCaP and DU145 cell lines was investigated by flow cytometry, as well as by the new proposed method based on magnetic cell separation.

To detect cell-surface expression of PSMA by flow cytometry as a gold standard method, indirect immunofluorescence staining was performed. In brief, cells were trypsynized,

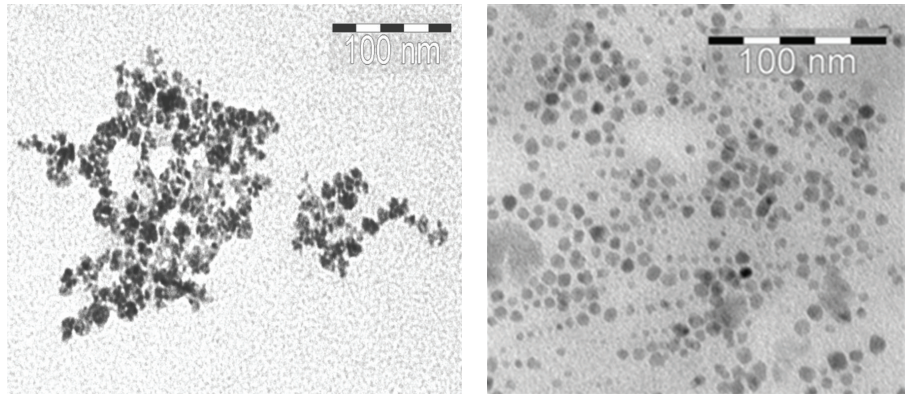

(a) (b)

FIGURE 6: TEM images for plain and antibody conjugated SPIO (a) nanomag-D-spio and (b) SPIO-J591, antibody binding causes a significant reduction of particle agglomeration. The average size of particles estimated from TEM images was about 10–20 nm.

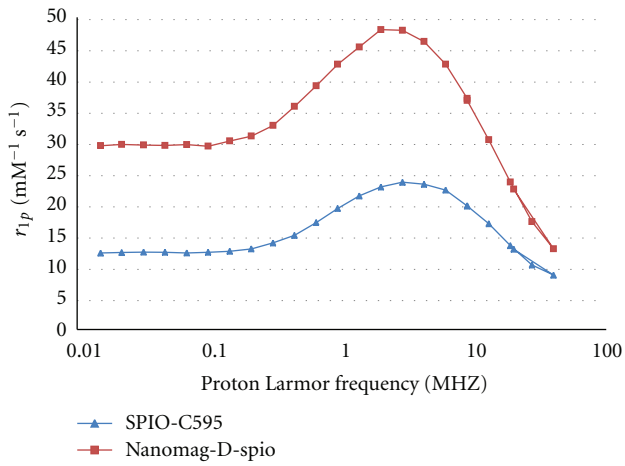

FIGURE 7: NMRD profiles of nanomag-D-spio and synthesized nanoprobes.

washed with PBS containing 0.1% fetal bovine serum (FBS), and 10^6 cells/tube from each cell line were transferred in FACS tubes. The cells were resuspended in 90 μL of washing buffer and were preblocked with FcR Block (human) reagent (Miltenyi) for 10 min at room temperature in the dark. After blocking, primary J591 anti-PSMA antibody (1/150 dilution) was added to each cell tube (one tube of each cell line as a control), incubated for 30 min in the dark at room temperature, and then washed 3 × 5 min using a washing buffer.

After washing, the cells were resuspended and incubated in goat anti-mouse FITC monoclonal antibody for an additional 30 min at room temperature in the dark. Cells were then washed, resuspended in 0.5 mL of PBS plus 0.1% FBS, and analyzed immediately using a CyAN-ADP flow cytometer (Beckman Coulter). All flow cytometry assessments were repeated at least three times at weekly intervals for each sample.

2.8. Magnetic Cell Separation. Immunomagnetic cell selection as a new method for detection and quantitative expression analysis of PSMA antigens on prostate cancer cells, based on magnetic cell separation technique, has been developed and used (Figure 2).

Human prostate cancer LNCaP cells and DU145 cells were detached and washed three times with PBS. A approximately 1-2 × 10^6 cell/tube of each cell type were plated in 15 mL tube and incubated with culture medium containing the synthesized nanoprobe (SPIO-J591) at Fe concentrations of 2 mM. After 2 h incubation at room temperature, cells were washed with PBS three times and resuspended in 1 mL PBS containing 0.1% fetal bovine serum (FBS). The magnetic cell separation was carried out on a midi MACS system. The LS separation column was set in the Midi MACS sorting device, washed twice with 1.0 mL of PBS solution. Then, the cell suspension was added to the separation column, washed three times to obtain the nonmagnetic cells flowing through the sorting column. Finally, the LS separation column was removed from the magnetic field and eluted the double positive cells, and then the $PSMA^+$ cells from the MS separation column. The number of $PSMA^+$ and $PSMA^-$ cells was detected and counted using conventional Trypan blue staining, under an optical microscope. The percentage of PSMA expression on the cell surface was determined using following equation:

$$\text{The percentage of PSMA expression} = \frac{(\text{number of PSMA}^+ \text{ cells})}{(\text{number of PSMA}^+ \text{ cells} + \text{number of PSMA}^- \text{ cells})} \times 100. \quad (2)$$

3. Results and Discussion

3.1. Synthesis. The J591 monoclonal antibody was thiolated with Traut's reagent and conjugated to maleimide functionalized SPIO nanoparticles (Figure 1). The feasibility of

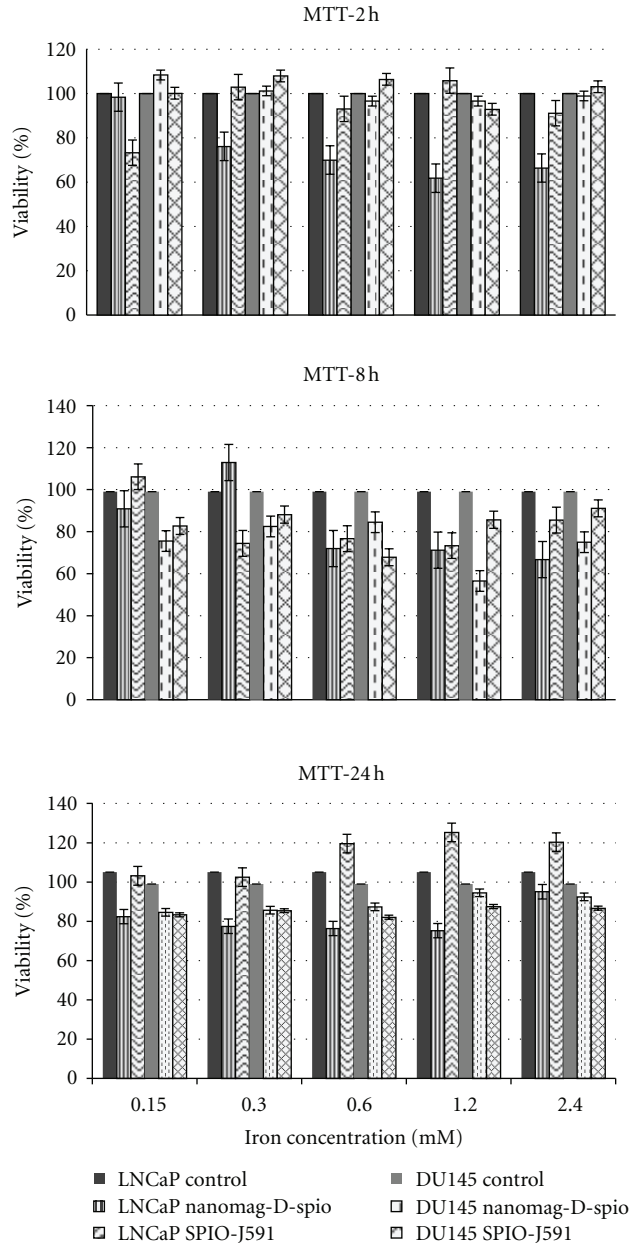

Figure 8: In vitro assessment of cytotoxicity of nanomag-D-spio and SPIO-J591 in LNCaP and DU145 prostate cancer cells by the MTT assay. The cells were incubated with Nanomag-D-SPIO or SPIO-J591 at equivalent iron concentrations ranging from 0.15 to 2.4 mM for 2, 8, and 24 h.

successfully grafting of antibody molecules to SPIO nanoparticles was confirmed by the Bradford assay as well as the measurements of the hydrodynamic size and shape of SPIO nanoparticles by using PCS and TEM. Analyses by Bradford protein assay and spectrophotometric readings show the amount of immobilized antibody of $56 \pm 2\,\mu$g Ab/mL of synthesized nanoprobe (Figure 3). Thanks to a standard curve with a commercially available iron standard solution (ICP standard, Sigma Aldrich), the iron concentration of particles was estimated to be 43.88 ± 1.2 and 24.22 ± 0.9 mM for nanomag-D-spio and J591-SPIO, respectively, by MR relaxometry method (Figure 4).

3.2. Characterization. The particle size distribution of SPIO nanoparticles before and after antibody conjugation was determined by PCS (Figure 5). The hydrodynamic particle diameters are determined to be 18.65 ± 0.21 nm for nanomag-D-spio and 24.68 ± 0.22 nm for J591-SPIO. Figures 6(a) and 6(b) show TEM images for the spherical-shaped plain and antibody-conjugated SPIO, respectively. The average particle size calculated from TEM was 10–20 nm for nanomag-D-spio and J591-SPIO. The morphology study of particles from TEM image suggests that antibody molecules conjugated to SPIO nanoparticle reduce the agglomeration of nanomag-D-spio particles.

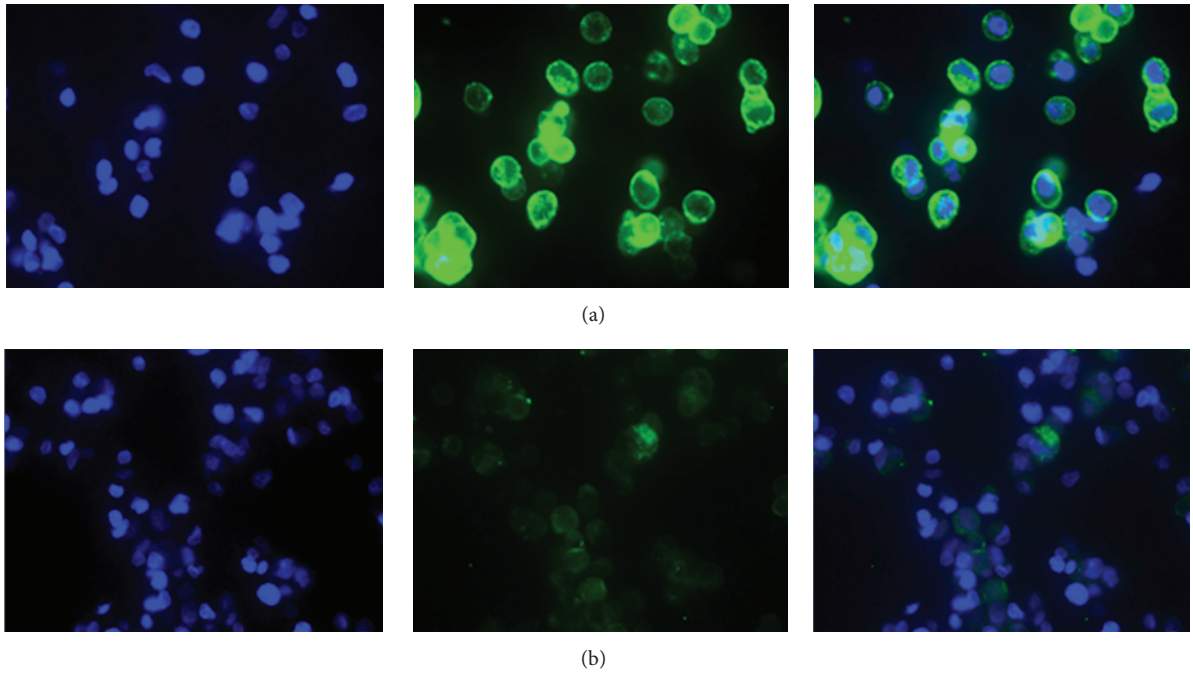

(a)

(b)

Figure 9: Fluorescent microscopy images (×40 magnification) of LNCaP (a) and DU145 (b), prostate cancer cells after overnight incubation with primary J591 anti-PSMA antibody and additional 1 h incubated with goat anti-mouse FITC monoclonal antibody. Blue colour: DAPI-staining of DNA in the nucleus, green colour: goat anti-mouse FITC bonded to primary J591 anti-PSMA antibody.

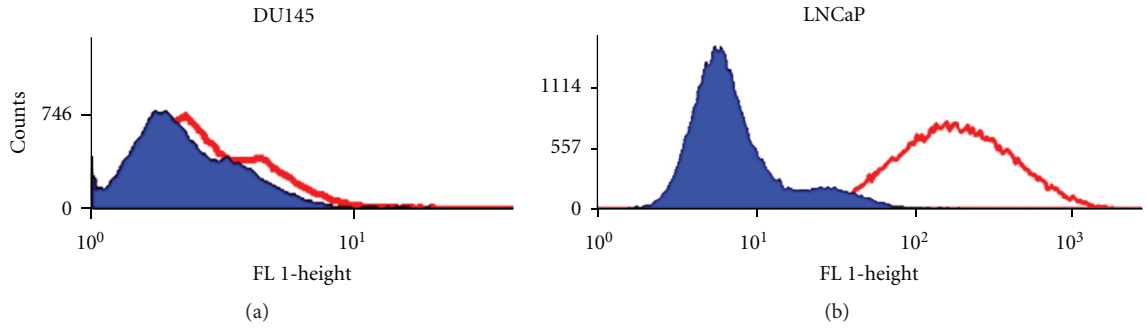

Figure 10: Flow cytometry test shows that DU145 cells lack PSMA expression (a) whereas LNCaP cells express high levels of prostate-specific membrane antigen (PSMA) on their cell surface (b).

NMRD profiles (Spinmaster FFC2000, STELAR, Italy) were used to examine the magnetic properties of SPIO and J591-SPIO nanoparticles under a magnetic field strength between 200 μT and 1.2 T. The magnetic properties of the SPIO nanoparticles did not change significantly by being conjugated to antibody (Figure 7).

R_1 and R_2 relaxation rate measurements of particles were performed on a Bruker Minispec operating at 20 MHz and 60 MHz. A summary of the longitudinal and transversal relaxivity is provided in Table 1.

3.3. In Vitro Cytotoxicity. Each nanoprobe for medical application should show minimal toxicity to the targeted cells. The in vitro cytotoxic effect of nanomag-D-spio and the synthesized nanoprobe was assessed using the standard methyl thiazol tetrazolium bromide (MTT) assay, using LNCaP and DU145 cell lines. The results after different incubation times with different iron concentrations for both cell lines show higher than 60% cell viability in relation to the control sample (Figure 8). The statistical analysis by One-way analysis of variance (ANOVA), followed by Duncan's multiple range test, showed statistically significant evidence of nonfunctionalized or functionalized SPIO toxicity to cells ($P = 0.02$). The P value between 2 and 8 h, 2–24 h, and 8–24 h incubation of DU145 cell line with SPIO-J591 and nanomag-D-spio was 0.007–0.015, 0.03–0.003, and 0.04–0.36, respectively. In comparison to the LNCaP cell line, these values were 0.17–0.21, 0.15–0.02, and 0.48–0.02. As can be seen, the P values are insignificant for most of LNCaP cell line compared to the DU145 cells.

Table 1: Longitudinal and transversal relaxivities (r_1 and r_2) of nanomag-D-spio and synthesized nanoprobe at 20 and 60 MHz at 37°C (Minispec) and the saturation magnetization and size of particles estimated by NMRD profiles data.

Particle	r_1 (s^{-1} mM^{-1})		r_2 (s^{-1} mM^{-1})		r_2/r_1		M_{sat} (Am^2/kg)	r (nm)
	20 MHz	60 MHz	20 MHz	60 MHz	20 MHz	60 MHz		
Nanomag-D-spio	21.6	7.6	112	121.8	5.2	16	36.5	8.25
SPIO-J591	14. 9	7.2	83.7	106.5	5.6	14.8	28	8.05

The results of the MTT assay show a moderate negative correlation ($r = (-0.16)$–(-0.71)) between concentration and viability for most of assays after 2 h and 8 h incubation, but after 24 h incubation a positive correlation ($r = 0.08$–0.73) between the concentration and viability was found.

3.4. Cell Surface Antigen Expression. The qualitative and quantitative expression of PSMA on the LNCaP and DU145 cell lines was investigated by fluorescence microscopy, flow cytometry, and proposed method based on magnetic cell separation.

The qualitative information on the cell surface antigen expression was obtained by fluorescence microscopy. Figures 9(a) and 9(b) show that the cancer cells were defined by DAPI staining (blue), whilst the green fluorescence represents $PSMA^+$ cells. The comparison demonstrates considerably increased fluorescence intensity in the positive LNCaP cells over the negative DU145 cells.

Flow cytometry analysis was performed to confirm the availability and quantitative analysis of desired prostate-specific membrane antigen (PSMA) on cell surface. Immunofluorescent staining of LNCaP and DU145 cell lines showed that LNCaP cells express high levels of PSMA on their cell surface (95 ± 1.2%), whereas DU145 cells lack PSMA expression (3 ± 0.2%) (Figure 10). These results are in good agreement with previously published studies [19, 23].

Immunomagnetic cell selection was used to determine the ability of functionalized SPIO for detection and quantitative analysis of desired antigen expression on the prostate cancer cells surface. Measurements based on magnetic cell separation method as a proposed immunomagnetic cell selection showed a 94 ± 3.4% and a 6 ± 0.8% expression of PSMA on the surface of LNCaP and DU145 cells, respectively. The statistical analysis between the results of antigen expression by two methods was done using Student's paired t-test. Despite statistical significance (P Value of 0.02), the actual difference in mean cell surface antigen expression between the flow cytometry and magnetic cell separation method was quite small.

4. Conclusions

An increasing number of surface antigens have been characterized in mammalian cell systems during the past decade. It has become obvious that these cell surface structures play an enormous role in early diagnosis, characterization, disease monitoring during and following therapy, and as possible therapeutic targets for various illnesses, especially cancers [24, 25]. However, the difficulty and costs of detection, characterization, and validation of new cell surface antigens has held back rapid development in this field. Hence, the development of a more efficient and inexpensive detection methods of the relevant marker is very basic and important.

Here, the detection and quantitative analyses of PSMA on the prostate cancer cells as an example of a cell surface antigen were described. The iron oxide nanoparticles with anti-PSMA monoclonal antibody (mAb J591) were functionalized to serve as a PSMA-specific molecular probe for in vitro detection and separation of $PSMA^+$ prostate cancer cell based on magnetic cell separation technique [26].

Quantitative detection and analysis of desired antigen expression on the cell surface with proposed method was carried out and the results were compared with flow cytometry as a gold standard. Measurements based on the new immunomagnetic cell selection showed an expression of PSMA on the surface of LNCaP and DU145 cells by 94 ± 3.4% and a 6±0.8%, respectively. Whereas using the flow cytometry method, the values of 95 ± 1.2% and 3 ± 0.2%, respectively, have been reported. As the results of both methods are very similar, the magnetic cell separation for the detection and quantitative analysis of the cell surface antigen can be a simple, rapid, accurate, and inexpensive alternative method.

In addition, magnetic separation techniques have several advantages in comparison with traditional techniques for biomarker discovery. It is possible to coat nanoparticles with the ligand of interest, like peptides, aptamers, folic acid, and so forth and use this method to detect and analyze other biomarkers, which is not possible by flow cytometry. Also molecular imaging enables noninvasive in vivo studies of biomarkers of diseases in various internal organs by use of magnetic nanoparticles coupled to targeted reagents [27, 28].

The results obtained from this study prove that use of antibody-coated magnetic beads for isolation of antigen-specific cells is a convenient and simple method for quantitative cell surface antigen detection and analyses.

Acknowledgments

The author thanks Dr. Lhomme Frederic (IMI-Institut d'Immunologie Médicale, Université Libre de Bruxelles (ULB), Brussels, Belgium) for his debonair discussion and meticulous guidance during this work. This work was financially supported by Isfahan University of Medical Science (MUI) (Grant-in-Aid for Scientific Research, no. 19550157), ARC (research contract AUWB-2010-10/15-UMONS-5), FNRS, and ENCITE programs, and it was performed in the framework of COST TD1004 and CM1006.

References

[1] L. Chen, R. Liu, Z. P. Liu, M. Li, and K. Aihara, "Detecting early-warning signals for sudden deterioration of complex diseases by dynamical network biomarkers," *Scientific Reports*, vol. 2, p. 342, 2012.

[2] J. A. Luna-Coronell, P. Syed, K. Sergelen, I. Gyurján, and A. Weinhäusel, "The current status of cancer biomarker research using tumour-associated antigens for minimal invasive and early cancer diagnostics," *Journal of Proteomics*, vol. 76, pp. 102–115, 2012.

[3] H. J. Lee, A. W. Wark, and R. M. Corn, "Microarray methods for protein biomarker detection," *Analyst*, vol. 133, no. 8, pp. 975–983, 2008.

[4] R. Simon, "Genomic biomarkers in predictive medicine: an interim analysis," *EMBO Molecular Medicine*, vol. 3, no. 8, pp. 429–435, 2011.

[5] F. Magni, Y. E. van der Burgt, C. Chinello et al., "Biomarkers discovery by peptide and protein profiling in biological fluids based on functionalized magnetic beads purification and mass spectrometry," *Blood Transfusion*, vol. 8, supplement 3, pp. s92–s97, 2010.

[6] J. C. Hall, L. Casciola-Rosen, and A. Rosen, "Altered structure of autoantigens during apoptosis," *Rheumatic Disease Clinics of North America*, vol. 30, no. 3, pp. 455–471, 2004.

[7] L. Belov, J. Zhou, and R. I. Christopherson, "Cell surface markers in colorectal cancer prognosis," *International Journal of Molecular Sciences*, vol. 12, no. 1, pp. 78–113, 2011.

[8] M. Schrevel, R. Karim, N. T. ter Haar et al., "CXCR7 expression is associated with disease-free and disease-specific survival in cervical cancer patients," *British Journal of Cancer*, vol. 106, no. 9, pp. 1520–1525, 2012.

[9] F. Pagès, J. Galon, M. C. Dieu-Nosjean, E. Tartour, C. Sautès-Fridman, and W. H. Fridman, "Immune infiltration in human tumors: a prognostic factor that should not be ignored," *Oncogene*, vol. 29, no. 8, pp. 1093–1102, 2010.

[10] K. Holmes, L. M. Lantz, B. J. Fowlkes, I. Schmid, and J. V. Giorgi, "Preparation of cells and reagents for flow cytometry," *Current Protocols in Immunology*, vol. 5, p. 5.3, 2001.

[11] L. S. Zijenah, G. Kadzirange, S. Madzime et al., "Affordable flow cytometry for enumeration of absolute $CD4^+$ T-lymphocytes to identify subtype C HIV-1 infected adults requiring antiretroviral therapy (ART) and monitoring response to ART in a resource-limited setting," *Journal of Translational Medicine*, vol. 4, article 33, 2006.

[12] S. Karl, R. P. Wong, T. G. St Pierre, and T. M. Davis, "A comparative study of a flow-cytometry-based assessment of in vitro plasmodium falciparum drug sensitivity," *Malaria Journal*, vol. 8, no. 1, article 294, 2009.

[13] A. Ranzoni, G. Sabatte, L. J. van Ijzendoorn, and M. W. Prins, "One-step homogeneous magnetic nanoparticle immunoassay for biomarker detection directly in blood plasma," *ACS Nano*, vol. 6, no. 4, pp. 3134–3141, 2012.

[14] C. M. Long, H. W. M. Van Laarhoven, J. W. M. Bulte, and H. I. Levitsky, "Magnetovacci nation as a novel method to assess and quantify dendritic cell tumor antigen capture and delivery to lymph nodes," *Cancer Research*, vol. 69, no. 7, pp. 3180–3187, 2009.

[15] R. A. Towner, N. Smith, S. Doblas et al., "In vivo detection of c-Met expression in a rat C6 glioma model," *Journal of Cellular and Molecular Medicine*, vol. 12, no. 1, pp. 174–186, 2008.

[16] U. Elsässer-Beile, P. Bühler, and P. Wolf, "Targeted therapies for prostate cancer against the prostate specific membrane antigen," *Current Drug Targets*, vol. 10, no. 2, pp. 118–125, 2009.

[17] P. Bühler, P. Wolf, and U. Elsässer-Beile, "Targeting the prostate-specific membrane antigen for prostate cancer therapy," *Immunotherapy*, vol. 1, no. 3, pp. 471–481, 2009.

[18] D. Shahbazi-Gahrouei, S. M. Rizvi, M. A. Williams, and B. J. Allen, "In vitro studies of gadolinium-DTPA conjugated with monoclonal antibodies as cancer-specific magnetic resonance imaging contrast agents," *Australasian Physical and Engineering Sciences in Medicine*, vol. 25, no. 1, pp. 31–38, 2002.

[19] M. Abdolahi, D. Shahbazi-Gahrouei, S. Laurent et al., "Synthesis and in vitro evaluation of MR molecular imaging probes using J591 mAb-conjugated SPIONs for specific detection of prostate cancer," *Contrast Media & Molecular Imaging*, vol. 8, no. 2, pp. 175–184, 2013.

[20] T. Mosmann, "Rapid colorimetric assay for cellular growth and survival: application to proliferation and cytotoxicity assays," *Journal of Immunological Methods*, vol. 65, no. 1-2, pp. 55–63, 1983.

[21] J. Woźniak, "Two methods for the quantitative analysis of surface antigen expression in acute myeloid leukemia (AML)," *Folia Histochemica et Cytobiologica*, vol. 42, no. 3, pp. 195–199, 2004.

[22] J. Sikora and J. Zeromski, "Expression of TCR-ζ chain and apoptosis in subpopulations of tumor-associated lymphocytes (TALs) from malignant pleural effusions," *Folia Histochemica et Cytobiologica*, vol. 40, no. 4, pp. 347–351, 2002.

[23] R. E. Serda, N. L. Adolphi, M. Bisoffi, and L. O. Sillerud, "Targeting and cellular trafficking of magnetic nanoparticles for prostate cancer imaging," *Molecular Imaging*, vol. 6, no. 4, pp. 277–288, 2007.

[24] D. Hoelzer, "Novel antibody-based therapies for acute lymphoblastic leukemia," *Hematology/the Education Program of the American Society of Hematology*, pp. 243–249, 2011.

[25] J. Ren, Z. Zhang, F. Wang et al., "MRI of prostate stem cell antigen expression in prostate tumors," *Nanomedicine*, vol. 7, no. 5, pp. 691–703, 2012.

[26] C. S. S. R. Kumar, *Biofunctionalization of Nanomaterials*, Wiley-VCH, Weinheim, Germany, 1st edition, 2005.

[27] K. K. Jain, *The Handbook of Biomarkers*, Springer, New York, NY, USA, 2010.

[28] G. G. Westmeyer, Y. Durocher, and A. Jasanoff, "A secreted enzyme reporter system for MRI," *Angewandte Chemie International Edition*, vol. 49, no. 23, pp. 3909–3911, 2010.